

Formin-2b (Fmn2b) in the development of neural circuits in zebrafish

A thesis
submitted in partial fulfilment of the requirements
for the degree of

Doctor of Philosophy

Dhriti Nagar

20132002



Indian Institute of Science Education and Research, Pune

2021

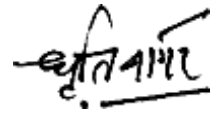
Dedicated to

My Grandmothers

Thank you for enabling me to be a woman in and of science

Declaration

I declare that this written submission represents my ideas in my own words, and where others' ideas have been included; I have adequately cited and referenced the original sources. I also declare that I have adhered to all principles of academic honesty and integrity and have not misrepresented or fabricated or falsified any idea/data/fact/source in my submission. I understand that violation of the above will be cause for disciplinary action by the Institute and can also evoke penal action from the sources that have not been properly cited or from whom proper permission has not been taken when needed.



Date: 18.06.2021

Dhriti Nagar

20132002

Certificate

Certified that the work incorporated in the thesis entitled
“Formin-2b (Fmn2b) in the development of neural circuits in zebrafish”

submitted by

Ms Dhriti Nagar

was carried out by the candidate under my supervision.

The work documented in this thesis or any part of it has not been included in any other
thesis submitted previously for the award of any degree or diploma from any other
University or Institution.

Date: 18.06.2021



Aurnab Ghose

PhD supervisor

Acknowledgements

Science does not happen in isolation. A lot more than reagents, protocols, experiments, and their execution has come together to synthesize this thesis and the work presented herein. People around me have generously granted me their time, help, advice and ideas. I thank you all and promise to spread the kindness that I have received.

Firstly, I thank my mind and body that supported me with all their might during my PhD. Before starting my PhD, I had the good fortune of considerate and thorough mentorship as an Integrated PhD student by Chaitanya Athale, Mukul Rawat and Ankitha Shetty, who prepared me for the years to come. Thank you!

I started my PhD in Aurnab's lab with a promise of adventure, and years later, I get to say, what an adventure indeed. I thank him for his unique style of mentoring, for being interested in my curious attempts with experiments that I knew little about, for being ever so patient and supportive, for the philosophical soliloquies (as promised on the lab wiki) and a smile in the face of adversity. Thank you for not giving up on me and jumping the barriers of academia along with me. The last few years of knowing him have inspired me to be true to my ethos. Thank you, Aurnab!

As the years passed, the thesis took shape with critical inputs from my research advisory committee. I sincerely thank LS Shashidhara, Raghav Rajan, Tressa Jacob and Chinmoy Patra for timely course correction and encouragement. I thank Prof NK Subhedar for inspiring me with his enthusiasm for neuroscience and providing valuable feedback during our lab meetings. A special thanks to Mahendra Sonawane and his lab for help with zebrafish maintenance protocols and sharing transgenic lines.

I thank all the support staff and facility managers at IISER Pune's Biology department, Biostore, IISER Imaging facility, National Facility for Gene Function in Health and Disease (NFGFHD) and BD Biosciences FACS facility without whom this work would not have been possible. The academic office at IISER Pune has always helped guide me through administrative procedures concerning PhD, fellowships and travel grants. Thank you all for your help. Financial support in the form of stipend from IISER Pune in the first two years of the integrated PhD program and CSIR fellowship for the remaining time of my PhD are sincerely acknowledged. I thank Infosys foundation and DBT for travel grants.

The Genome Editing Techniques Initiative (GETIn) internship award by DBT enabled me to learn CRISPR-Cas9 based mutagenesis in zebrafish in the lab of Shawn Burgess at NHGRI, NIH, USA. I thank Shawn, his lab members and NHGRI zebrafish core members for their immense help with the generation of *fmn2b* mutants. I am grateful for Joby Joseph's help with making the behavioural set-up to quantify acoustic startle in zebrafish. The python code for image analysis by tail tracking was developed in collaboration with Tomin K James. Thank you!

The open labs at IISER Pune's Biology department have been instrumental in exchanging ideas, exasperations, excitement, and, most importantly, reagents. I would also like to thank the Physics and Chemistry departments for letting me borrow reagents and instruments critical for my work.

The past and present lab members of the neuronal connectivity lab have been an interesting lot. I thank them for maintaining a professional and friendly work environment and their feedback during lab meetings. I had the most fun working with Shrobona, Ajesh, and Ratnakar. A special thanks to all the rotating students in the lab for increasing my patience and teaching me how to teach. This thesis's foundation was laid by Abhishek, Ketakee, Sampada, Rajan, Ratnakar, Ajesh, Tanushree and Priyanka in characterizing the cellular and molecular function of Formin-2. Thank you all for providing the exciting leads which led to the work in this thesis. I thank Aditi, Devika and Ratnakar for teaching me zebrafish maintenance, breeding and injections.

The camaraderie offered by Sameer, Amogh, Shweta, John, Akanksha, Anshul, Deepak Danish, Harsha, and Anwesh during our theatre interactions and beyond have helped me keep afloat in tough times, teaching me important life lessons. Thank you for being the shiny beacons of hope in despair.

Mayurika, Suhita and Sudha have been the inspiring women in my life and career that every woman in science should have. They have inspired me to be better, stronger and inspire others around me. They have stood by me, heard me, appreciated me and critiqued me as the need arose. I can't thank you enough!

My lifelines during my stay at IISER Pune have been the most amazing batch of Integrated PhD-2013. Joy, adventures, culinary indulgence, drama, trips, we had it all! I have found friends for life in this bunch, and I am forever grateful. Thank you, Deepak, Anshul, Mehak,

Shivani, Aditi, Swati, Akhila, Ron, Sandip, Anish, Neeladri, Jay, Kashyap, Divya, Adarsh, Bharat, Amar, and Harpreet, for being the best batchmates ever. A special thanks to Swati and Mehak for their joyful company during the great lockdown of 2020.

As I was finishing my PhD, I found a mirror in Shivani Bodas, whose love and care filled my soul with joys unknown. Gratitude and love, always!

I am humbled and grateful to be healthy and alive at the moment as the world grapples with the coronavirus pandemic, my commiserations to my friends and loved ones who lost their people fighting Covid.

I thank my family for their encouragement and them crowdfunding my education. Their support enabled me to look ahead without having to worry about what I was leaving behind. My grandparents are the most incredible people of all. Their dedication, love, and commitment towards my well-being and success and the world around them are inspiring. I am grateful to have known their love and to inherit their wisdom and stories. My parents have always loved me the most and enabled me to become the person I am. Thank you, Maa and Papa. My mother's conviction in me has made me the woman she wanted to be. Thank you! I thank my uncles, aunts and cousins for their best wishes and for helping me in all the ways they could. I am grateful for the love my siblings and cousins, all eight of them, shower on me. Thank you!

Around the time I started my PhD, I embarked on another adventure with my fellow explorer Tomin James. It has been seven years since then, and I have come to know him as my partner in life, my confidante, friend, colleague, and mentor. But most importantly, I got to know him as a fellow human, my human. He has imbibed so much goodness, knowledge, humility, and grace. It was my fortune to grow along with him. Tomin, I am grateful that you said yes to accompany me on exploring the world around us and vow to build a better one together. I will always hold you up on this. You stuck with me through thick and thin and made this journey enjoyable. Thank you!

So long, and thanks for all the zebrafish! #

(# Adapted from the books of Douglas Adam)

Contents

Declaration.....	2
Certificate	3
Acknowledgements.....	4
Abstract	12
Synopsis.....	13
Introduction	14
Cytoskeletal remodelling in neuronal development.....	14
Formin-2 in neuronal development and disorders	15
Motivation & Objectives	15
Major findings.....	16
Short latency escape response mediating spiral fiber neurons are affected due to Fmn2b knockdown.	16
Generation of fmn2b mutants and reagents for visualization of specific neuronal populations.....	16
Motor neuron development and the associated motor behaviours are affected in fmn2b mutants.....	16
Preliminary results outlining defects in early embryogenesis and visual circuit neurons in fmn2b mutants.....	17
Conclusions.....	17
References.....	19
1 Introduction	39
1.1 Function follows form	40
1.2 Neuronal morphogenesis	40
1.3 Cytoskeleton and active remodelling in neuronal morphogenesis.....	41

1.4	Neuronal cytoskeleton in Growth cone guidance and axon pathfinding.....	42
1.5	Neuronal cytoskeleton in Axonogenesis, branching and arborization.....	44
1.6	Actin nucleators	46
1.7	Formins	47
1.8	Formin-2.....	49
1.9	Formins in zebrafish neural development.....	53
1.10	Zebrafish neural circuits and behaviour.....	53
2	Role of Fmn2b in the development of spiral fiber neurons and the regulation of short latency escape responses in zebrafish.....	58
2.1	Introduction.....	59
2.2	Results.....	62
2.2.1	Fmn2b, the zebrafish ortholog of Fmn2 has conserved formin homology domains.....	62
2.2.2	Fmn2b is expressed in the zebrafish nervous system.....	62
2.2.3	Morpholino mediated knockdown of Fmn2b.....	64
2.2.4	Assessment of behavioural defects using automated acoustic stimulus delivery and high-speed video recording	64
2.2.5	Fmn2b morphants exhibit a delay in initiating the escape response	69
2.2.6	Fmn2b depletion does not affect the sensory components of the acoustic startle circuit.....	71
2.2.7	The development of Spiral fiber tracts in the hindbrain is regulated by Fmn2b	75
2.2.8	Spiral fiber tracts show outgrowth defects in Fmn2b crispants	77
2.3	Discussion	81
3	Generation and characterization of <i>fmn2b</i> CRISPR mutants	85
3.1	Introduction.....	86
3.2	Results.....	87
3.2.1	Design and validation of sgRNAs	87

3.2.2	Screening potential founder lines with heritable indels	88
3.2.3	Establishing homozygous mutant lines for <i>fmn2b</i>	89
3.2.4	Early developmental phenotypes in <i>fmn2b</i> CRISPR mutants.....	90
3.2.5	Generating reagents to visualize neuronal populations in <i>fmn2b</i> mutants	92
3.3	Discussion	94
4	Motor neuron outgrowth is regulated by <i>Fmn2b</i>	96
4.1	Introduction.....	97
4.1.1	Birth and outgrowth of motor neurons.....	97
4.1.2	Pathway selection by motor neurons.....	98
4.1.3	Cytoskeletal proteins in neuronal morphogenesis and branching	99
4.2	Results.....	101
4.2.1	<i>fmn2b</i> mRNA is expressed in the spinal cord of zebrafish embryos.....	101
4.2.2	<i>fmn2b</i> mutants exhibit defects in Spontaneous Tail Coiling (STC) and Touch Evoked Escape Response (TEER).....	101
4.2.3	<i>fmn2b</i> mRNA is expressed in the motor neurons of zebrafish embryos...	104
4.2.4	CaP motor neuron growth cone translocation is slower in <i>fmn2b</i> mutants	104
4.2.5	Primary motor neuron outgrowth and branching defects in <i>fmn2b</i> mutants	105
4.2.6	Rostral Primary (RoP) motor neuron development is compromised in <i>fmn2b</i> mutants.....	109
4.2.7	The muscle structure is not affected in <i>fmn2b</i> mutants.....	113
4.2.8	Coverage of NMJ synapses in <i>fmn2b</i> mutants	114
4.2.9	Effect of overexpression of <i>Fmn2</i> in motor neurons	116
4.3	Discussion	121
5	Role of <i>Fmn2b</i> in development of visual circuits	126
5.1	Introduction.....	127

5.2	Results.....	130
5.2.1	Expression of <i>fmn2b</i> mRNA in the Retinal Ganglionic Cell layer in zebrafish 130	
5.2.2	<i>fmn2b</i> mutants show thinning of the optic nerve	131
5.2.3	Arborization of Retinal Ganglionic cell (RGC) axons is reduced in the optic tectum of <i>fmn2b</i> mutants	132
5.2.4	The outgrowth of Intertectal neurons (ITNs) is affected in <i>fmn2b</i> mutants 132	
5.3	Discussion	134
6	Future Directions.....	135
6.1	Behavioural characterization of <i>fmn2b</i> mutants	136
6.2	Functional imaging of the neural circuits in <i>fmn2b</i> mutants.....	137
6.3	Molecular mechanisms underlying outgrowth defects due to Fmn2 depletion 138	
6.4	The outgrowth defects could be due to loss of progenitors	139
6.5	Delineating the function of <i>fmn2b</i> in neuronal vs non-neuronal development 140	
6.6	Compensation by other formins.....	142
7	Reagents and Procedures	144
7.1	Zebrafish maintenance and procedures.....	145
7.2	Whole mount in situ hybridization.....	145
7.3	Isolation of motor neurons from transgenic embryos, FACS, RT-PCR	145
7.4	Morpholino and RNA injections	146
7.5	Validation of splice blocking morpholino	147
7.6	sgRNA and Cas9 preparation and injections for crispants and CRISPR mutants 147	
	CRISPR Cas9 based mutagenesis.....	148
7.7	F0 sgRNA injection and analysis in <i>fmn2b</i> crispants	149

7.8	Genotyping fmn2b crispants and CRISPR mutants	149
7.9	Whole mount immunostaining	150
7.10	FM 4-64 labelling	150
7.11	TMR Dextran labelling.....	151
7.12	Neuromuscular junction labelling and quantification	151
7.13	Fluorescence microscopy, live imaging and mounting procedure	151
7.14	Behaviour experiment set up and behaviour analysis.....	151
7.14.1	Automated acoustic startle assay	152
7.14.2	Analysis of tail movement using a custom Python software.....	152
	Spontaneous tail coiling (STC) assay	153
7.14.3	Touch evoked escape response (TEER) assay	153
7.15	Figures and Statistical analysis	153
8	References.....	155

Abstract

The formin family member, Fmn2, is a neuronally enriched cytoskeletal remodelling protein conserved across vertebrates. Recent studies have implicated Fmn2 in neurodevelopmental disorders, including sensory processing dysfunction and intellectual disability in humans. Cellular characterization of Fmn2 in primary neuronal cultures has identified its function in regulating cell-substrate adhesion, microtubule dynamics and consequently growth cone translocation. However, the role of Fmn2 in the development of neural circuits *in vivo* and its impact on associated behaviours remain uncharacterized. As reported in other vertebrates, the zebrafish ortholog of Fmn2, Fmn2b, is also enriched in the developing zebrafish nervous system.

Knockdown of Fmn2b resulted in morphological and behavioural defects underlying locomotor circuits. In a custom-made behavioural assay using high-speed video recording of acoustic startle responses in a closed-loop feedback setup, Fmn2b morphants showed defects in short-latency startle responses. The behavioural defects were caused by defects in the development of an excitatory interneuron, spiral fiber neuron, essential for modulation of the acoustic startle response. However, the knockdown of Fmn2b did not compromise other components of the acoustic startle circuit.

Given the transient nature of morpholinos, CRISPR-Cas9 based mutants were generated for *fmn2b*. Further, transgenic lines in the background of homozygous *fmn2b* mutants were made to examine specific neuronal populations. The *fmn2b* mutants show early developmental defects and phenocopy morphological defects observed in morphants. Behavioural assessment of *fmn2b* mutants revealed abnormal spontaneous tail coiling and touch evoked escape response. The behavioural defects were corroborated by outgrowth and branching defects in the motor neurons of *fmn2b* mutants and were likely due to inadequate innervation of the target myotomes. Preliminary data implicates Fmn2b in the development of visual neural circuits and non-neuronal cytoskeleton regulation during oogenesis and early embryonic development.

Our results indicate that Fmn2 is required for specific regulation of axonal outgrowth and pathfinding *in vivo*, modulating behavioural outputs in larval zebrafish panning different neural circuits. Our findings underscore the importance of Fmn2 in neural development across vertebrate lineages and will eventually aid our understanding of neurodevelopmental disorders using the zebrafish model.

Synopsis

Introduction

Cytoskeletal remodelling in neuronal development

In the developing brain, establishing accurate neuronal connectivity is essential for the organism to perform reliable behavioural output. Neuronal progenitors give rise to newborn neurons in the developing embryo, making intricate neural circuits giving rise to a functional brain. In the lifetime of a neuron, beginning from a spherical cell, it grows to attain specialized structures to make connections with neighbouring cells, including but not limited to neurons (Flynn, 2013; Goodhill et al., 2015; Flynn and Bradke, 2020). In the process of forming neural circuits, neurons extend their axons, and a specialized structure called the growth cone interrogates the environment for suitable guidance cues to traverse their preset trajectories (Tessier-Lavigne and Goodman, 1996; Dickson, 2002; Lowery and Van Vactor, 2009; Kerstein et al., 2015). After reaching their predetermined targets and synapse formation, the connections made by neurons are still vulnerable to experience-dependent plasticity (Gordon-Weeks and Fournier, 2014). The journey of a neuron from birth to its ultimate position in an ensemble where it performs specialized roles in concert with the other neurons in the neural circuit is an impressive feat. Each cellular process governing the guidance and connectivity of the growing neuron needs to be precise. The majority of the cellular processes underlying neuronal development, be it neuritogenesis, axonogenesis, growth cone navigation, synaptogenesis or synaptic plasticity, requires active cytoskeletal remodelling (Dickson, 2002; Lowery and Van Vactor, 2009; Flynn and Bradke, 2020).

Actin and microtubules are the primary cytoskeletal components responsible for neuronal morphogenesis, connectivity and plasticity. Other than the abundantly found actin filaments and microtubules, several cytoskeleton remodelling proteins manipulate the cytoskeleton in response to cues critical for developmental processes. Local rearrangement of actin filaments allows protrusive structures to probe the environment for signals in the form of growth cone filopodia and axonal and dendritic branches. On the other hand, microtubule innervation of these structures provides stability and directionality in addition to aiding axonal transport (Gordon-Weeks and Fournier, 2014; Coles and Bradke, 2015; Lasser et al., 2018; Menon and Gupton, 2018; Kawabata Galbraith and Kengaku, 2019; Flynn and Bradke, 2020; Muñoz-Lasso et al., 2020).

Among the various cytoskeletal remodelling proteins expressed in the nervous system, the focus of this thesis is Formin-2.

Formin-2 in neuronal development and disorders

Formin-2 (Fmn2) is a neuronally enriched actin nucleator and elongator with the characteristic Formin Homology domains (FH1 and FH2) and a unique FSI domain that allows its interaction Spire and is essential for its actin-microtubule crosslinking activity. Formin-2 belongs to the less characterized FMN family of formins (Leader and Leder, 2000; Quinlan et al., 2007; Breitsprecher and Goode, 2013; Roth-Johnson et al., 2014; Yoo et al., 2015; Kawabata Galbraith and Kengaku, 2019; Kundu et al., 2021).

Fmn2 is expressed in the developing and the mature nervous systems of mice, humans and chicken (Leader and Leder, 2000; Katoh and Katoh, 2004; Dutta and Maiti, 2015; Sahasrabudhe et al., 2016). Recent studies have implicated Fmn2 in neurodevelopmental disorders, including sensory processing dysfunction and intellectual disability in humans (Perrone et al., 2012; Almuqbil et al., 2013; Law et al., 2014; Anazi et al., 2017; Marco et al., 2018; Gorukmez et al., 2020). Cellular characterization of Fmn2 in primary neuronal cultures has identified its function in the regulation of cell-substrate adhesion, mechanotransduction, growth cone translocation, axon outgrowth and pathfinding and actin-microtubule crosstalk in growth cone turning (Sahasrabudhe et al., 2016; Ghate et al., 2020; Kundu et al., 2021). Spatiotemporal precision in executing these cellular processes is crucial for achieving accurate neural connectivity in the developing brain.

Motivation & Objectives

The contribution of Fmn2 in cellular processes regulating neuronal development and its ability to regulate both actin and microtubule dynamics makes it an intriguing candidate for further studies. Despite the recent cellular and molecular characterization, the role of Fmn2 in the development of neural circuits in vivo and its impact on associated behaviours remains unexplored. Zebrafish provides an excellent opportunity for genetic manipulation and optical accessibility in a developing organism showing a set of complex behaviours emerging from the underlying neural circuits.

The thesis covers the work done during my PhD to address role of Fmn2 in developing neural circuits in zebrafish. The major findings are summarized below.

Major findings

Short latency escape response mediating spiral fiber neurons are affected due to *Fmn2b* knockdown.

Using automated analysis of behaviour and systematic investigation of the associated circuitry, I uncovered the role of Formin-2 in zebrafish neural circuit development. The zebrafish ortholog, *Fmn2b*, is also enriched in the developing zebrafish nervous system, consistent with reports from other vertebrates. *Fmn2b* was found to be required for the development of an excitatory interneuron pathway. This spiral fiber neuron is an essential circuit component in regulating the short latency Mauthner cell-mediated acoustic startle response. Corroborating the loss of the spiral fiber neurons tracts, high-speed video recording revealed a reduction in the short latency escape events while responsiveness to the stimuli was unaffected. Taken together, this study provides evidence for a circuit-specific requirement of *Fmn2b* in eliciting an essential behaviour in zebrafish.

Generation of *fmn2b* mutants and reagents for visualization of specific neuronal populations

CRISPR-Cas9 based *fmn2b* mutants were made, and two mutant alleles targeting exon 1 of *fmn2b* were characterized. The mutations result in a truncated gene product devoid of the functional domains, FH1, FH2 and FSI. The homozygous mutant alleles were homogenized to carry one copy of each of the two mutant alleles and crossed to transgenic lines labelling motor neurons and retinal ganglionic cells (RGCs). Unlike transient morpholino based knockdown, the *fmn2b* mutants had heritable mutations allowing testing of gene function over generations given that *fmn2b* mRNA is deposited maternally in the zebrafish embryos.

Motor neuron development and the associated motor behaviours are affected in *fmn2b* mutants

Motor behaviours like spontaneous tail coiling and touch evoked escape response were adversely affected in the *fmn2b* mutants. Visualizing developing motor neurons using the *Tg(mnx1:GFP)* in *fmn2b* mutants revealed outgrowth and branching defects despite any changes to myotome integrity. The reduction in arborization and innervation of the myotome by motor neurons explain the motor behaviour defects in *fmn2b* mutants. The

synapse coverage across the axon length in the motor neuron arbor remains unchanged, suggesting that the insufficient activation of the myotome is due to decreased branching as the total number of synapses per unit myotome go down in *fmn2b* mutants. The role of *fmn2b* in regulating motor neuron branching is further strengthened by rescuing branching defects by mouse Fmn2 (mFmn2). The failure in rescuing branching defects in *fmn2b* mutants by the F-actin nucleation dead version, mFmn2-I1226A, highlights the requirement of the F-actin nucleation activity of Fmn2b in axonal branching *in vivo*. Moreover, overexpression of mFmn2 in wildtype zebrafish embryos causes excessive branching of motor neurons, indicating a causal role of Fmn2b in axonal branching. In conclusion, the F-actin nucleation activity of *Fmn2b* is required for motor neuron branching in zebrafish.

Preliminary results outlining defects in early embryogenesis and visual circuit neurons in *fmn2b* mutants

The *fmn2b* mutants also exhibit defects in early embryogenesis manifested as early mortality, morphological defects and abnormal yolk architecture. On the other hand, *fmn2b* mutants have outgrowth and arborization defects in the intertectal neurons (ITNs) and retinal ganglionic cells (RGCs). The preliminary data outlining these defects is presented here and requires careful investigation to substantiate the role of *fmn2b* in oogenesis, embryogenesis in a non-neuronal context and development of neural circuits underlying vision in zebrafish.

Conclusions

The findings presented in this thesis are the first reports of characterization of Formin-2 in the development of neural circuits *in vivo* using zebrafish. Systematic and careful analysis of the neural circuits associated with locomotion and acoustic startle behaviours in *fmn2b* morphants and mutants has highlighted the requirement of Fmn2b in their development. The necessity of F-actin nucleation activity of Fmn2b in motor neuron branching opens up new aspects for investigating the molecular function of Fmn2b *in vivo*. The *fmn2b* mutants generated in this study can be used to test the role of Formin-2 in neural circuits underlying memory, learning, and sensory processing to model the findings from previous studies in mice and human (Perrone et al., 2012; Almuqbil et al., 2013; Law et al., 2014; Anazi et al., 2017; Marco et al., 2018; Gorukmez et al., 2020). The

work presented here underscores the importance of Fmn2 in neural development across vertebrate lineages and highlight zebrafish models in understanding neurodevelopmental disorders.

References

- Agís-Balboa RC et al. (2017) Formin 2 links neuropsychiatric phenotypes at young age to an increased risk for dementia. *EMBO J* 36:2815–2828.
- Ahuja R, Pinyol R, Reichenbach N, Custer L, Klingensmith J, Kessels MM, Qualmann B (2007) Cordon-Bleu Is an Actin Nucleation Factor and Controls Neuronal Morphology. *Cell* 131:337–350.
- Almuqbil M, Hamdan FF, Mathonnet G, Rosenblatt B, Srour M (2013) De novo deletion of FMN2 in a girl with mild non-syndromic intellectual disability. *Eur J Med Genet* 56:686–688.
- Amsterdam A, Burgess S, Golling G, Chen W, Sun Z, Townsend K, Farrington S, Haldi M, Hopkins N (1999) A large-scale insertional mutagenesis screen in zebrafish. *Genes Dev* 13:2713–2724.
- Anazi S et al. (2017) Expanding the genetic heterogeneity of intellectual disability. *Hum Genet* 136:1419–1429.
- Armijo-Weingart L, Gallo G (2017) It takes a village to raise a branch: Cellular mechanisms of the initiation of axon collateral branches. *Mol Cell Neurosci* 84:36–47.
- Atkins M, Gasmi L, Bercier V, Revenu C, Del Bene F, Hazan J, Fassier C (2019) FIGNL1 associates with KIF1B β and BICD1 to restrict dynein transport velocity during axon navigation. *J Cell Biol* 218:3290–3306.
- Avitan L, Pujic Z, Mólter J, Van De Poll M, Sun B, Teng H, Amor R, Scott EK, Goodhill GJ (2017) Spontaneous Activity in the Zebrafish Tectum Reorganizes over Development and Is Influenced by Visual Experience. *Curr Biol* 27:2407-2419.e4.
- Bagnall MW, McLean DL (2014) Modular Organization of Axial Microcircuits in Zebrafish. *Science* (80-) 343:197–200.
- Baier H, Klostermann S, Trowe T, Karlstrom RO, Nüsslein-Volhard C, Bonhoeffer F (1996) Genetic dissection of the retinotectal projection. *Development* 123:415–425.
- Bak M, Fraser SE (2003) Axon fasciculation and differences in midline kinetics between pioneer and follower axons within commissural fascicles. *Development* 130:4999–

5008.

- Balasanyan V, Watanabe K, Dempsey WP, Lewis TL, Trinh LA, Arnold DB (2017) Structure and Function of an Actin-Based Filter in the Proximal Axon. *Cell Rep* 21:2696–2705.
- Beattie CE, Hatta K, Halpern ME, Liu H, Eisen JS, Kimmel CB (1997) Temporal separation in the specification of primary and secondary motoneurons in zebrafish. *Dev Biol* 187:171–182.
- Bello-Rojas S, Istrate AE, Kishore S, McLean DL (2019) Central and peripheral innervation patterns of defined axial motor units in larval zebrafish. *J Comp Neurol* 527:2557–2572.
- Bercier V, Hubbard JM, Fidelin K, Durooure K, Auer TO, Revenu C, Wyart C, Del Bene F (2019) Dynactin1 depletion leads to neuromuscular synapse instability and functional abnormalities. *Mol Neurodegener* 14:1–22.
- Bernhardt RR, Chitnis AB, Lindamer L, Kuwada JY (1990) Identification of spinal neurons in the embryonic and larval zebrafish. *J Comp Neurol* 302:603–616.
- Bill BR, Petzold AM, Clark KJ, Schimmenti L a, Ekker SC (2009) A primer for morpholino use in zebrafish. *Zebrafish* 6:69–77.
- Bonner J, Letko M, Nikolaus OB, Krug L, Cooper A, Chadwick B, Conklin P, Lim A, Chien C Bin, Dorsky RI (2012) Midline crossing is not required for subsequent pathfinding decisions in commissural neurons. *Neural Dev* 7:18.
- Breitsprecher D, Goode BL (2013) Formins at a glance. *J Cell Sci* 126:1–7.
- Bremer J, Granato M (2016) Myosin phosphatase Fine-tunes Zebrafish Motoneuron Position during Axonogenesis. *PLoS Genet* 12:1006440.
- Bresciani E, Broadbridge E, Liu PP (2018) An efficient dissociation protocol for generation of single cell suspension from zebrafish embryos and larvae. *MethodsX* 5:1287–1290.
- Brett M, Stefen H, Djordjevic A, Fok SYY, Chan JW, van Hummel A, van der Hoven J, Przybyla M, Volkerling A, Ke YD, Delerue F, Ittner LM, Fath T (2019) Developmental Expression of Mutant PFN1 in Motor Neurons Impacts Neuronal Growth and Motor Performance of Young and Adult Mice. *Front Mol Neurosci* 12:231.

- Brustein E, Saint-Amant L, Buss RR, Chong M, McDearmid JR, Drapeau P (2003) Steps during the development of the zebrafish locomotor network. *J Physiol Paris* 97:77–86.
- Burgess H a., Granato M (2008) The neurogenetic frontier-lessons from misbehaving zebrafish. *Briefings Funct Genomics Proteomics* 7:474–482.
- Burgess HA, Johnson SL, Granato M (2009) Unidirectional startle responses and disrupted left-right co-ordination of motor behaviors in *robo3* mutant zebrafish. *Genes, Brain Behav* 8:500–511.
- Campellone KG, Welch MD (2010) A nucleator arms race: Cellular control of actin assembly. *Nat Rev Mol Cell Biol* 11:237–251.
- Carrington B, Varshney GK, Burgess SM, Sood R (2015) CRISPR-STAT: An easy and reliable PCR-based method to evaluate target-specific sgRNA activity. *Nucleic Acids Res* 43:e157.
- Chalmers K, Kita EM, Scott EK, Goodhill GJ (2016) Quantitative Analysis of Axonal Branch Dynamics in the Developing Nervous System. *PLoS Comput Biol* 12:1004813.
- Chia PH, Chen B, Li P, Rosen MK, Shen K (2014) Local F-actin network links synapse formation and axon branching. *Cell* 156:208–220.
- Coles CH, Bradke F (2015) Coordinating Neuronal Actin-Microtubule Dynamics. *Curr Biol* 25:R677–R691.
- Colombo A, Palma K, Armijo L, Mione M, Signore IA, Morales C, Guerrero N, Meynard MM, Pérez R, Suazo J, Marcelain K, Briones L, Härtel S, Wilson SW, Concha ML (2013) Daam1a mediates asymmetric habenular morphogenesis by regulating dendritic and axonal outgrowth. *Dev* 140:3997–4007.
- Dahlgaard K, Raposo AASF, Niccoli T, St Johnston D (2007) Capu and Spire Assemble a Cytoplasmic Actin Mesh that Maintains Microtubule Organization in the *Drosophila* Oocyte. *Dev Cell* 13:539–553.
- Das R, Letcher JM, Harris JM, Foldi I, Nanda S, Bobo HM, Mihály J, Ascoli GA, Cox DN (2017) Formin3 regulates dendritic architecture via microtubule stabilization and is required for somatosensory nociceptive behavior. *bioRxiv:227348*.

- Dickson BJ (2002) Molecular mechanisms of axon guidance. *Science* (80-) 298:1959–1964.
- Dumont J, Million K, Sunderland K, Rassinier P, Lim H, Leader B, Verlhac M-H (2007) Formin-2 is required for spindle migration and for the late steps of cytokinesis in mouse oocytes. *Dev Biol* 301:254–265.
- Dutta P, Maiti S (2015) Expression of multiple formins in adult tissues and during developmental stages of mouse brain. *Gene Expr Patterns* 19:52–59.
- Eisen JS (1991) Motoneuronal development in the embryonic zebrafish. In: *Development*, pp 141–147. The Company of Biologists.
- Eisen JS, Myers PZ, Westerfield M (1986) Pathway selection by growth cones of identified motoneurons in live zebra fish embryos. *Nature* 320:269–271.
- Eisen JS, Pike SH, Debu B (1989) The growth cones of identified motoneurons in embryonic zebrafish select appropriate pathways in the absence of specific cellular interactions. *Neuron* 2:1097–1104.
- Eisen JS, Smith JC (2008) Controlling morpholino experiments: don't stop making antisense. *Development* 135:1735–1743.
- Emmons S, Phan H, Calley J, Chen W, James B, Manseau L (1995) cappuccino, a Drosophila maternal effect gene required for polarity of the egg and embryo, is related to the vertebrate limb deformity locus. *Genes Dev* 9:2482–2494.
- Fassier C, Fréal A, Gasmi L, Delphin C, Ten Martin D, De Gois S, Tambalo M, Bosc C, Mailly P, Revenu C, Peris L, Bolte S, Schneider-Maunoury S, Houart C, Nothias F, Larcher J-C, Andrieux A, Hazan J (2018) Motor axon navigation relies on Fidgetin-like 1-driven microtubule plus end dynamics. *J Cell Biol* 217:1719–1738.
- Fassier C, Hutt JA, Scholpp S, Lumsden A, Giros B, Nothias F, Schneider-Maunoury S, Houart C, Hazan J (2010) Zebrafish atlastin controls motility and spinal motor axon architecture via inhibition of the BMP pathway. *Nat Neurosci* 13:1380–1387.
- Fernández-Barrera J, Alonso MA (2018) Coordination of microtubule acetylation and the actin cytoskeleton by formins. *Cell Mol Life Sci* 75:3181–3191.
- Fetcho J, Faber D (1988) Identification of motoneurons and interneurons in the spinal

- network for escapes initiated by the mauthner cell in goldfish. *J Neurosci* 8:4192–4213.
- Fetcho JR (1991) Spinal network of the Mauthner cell. *Brain Behav Evol* 37:298–316.
- Fidelin K, Djenoune L, Stokes C, Prendergast A, Gomez J, Baradel A, Del Bene F, Wyart C (2015) State-dependent modulation of locomotion by GABAergic spinal sensory neurons. *Curr Biol* 25.
- Flynn KC (2013) The cytoskeleton and neurite initiation. *Bioarchitecture* 3:86–109.
- Flynn KC, Bradke F (2020) Role of the cytoskeleton and membrane trafficking in axon–dendrite morphogenesis. In: *Cellular Migration and Formation of Axons and Dendrites*, pp 21–56. Elsevier.
- Funk J, Merino F, Venkova L, Heydenreich L, Kierfeld J, Vargas P, Raunser S, Piel M, Bieling P (2019) Profilin and formin constitute a pacemaker system for robust actin filament growth. *Elife* 8.
- Gallo G (2011) The cytoskeletal and signaling mechanisms of axon collateral branching. *Dev Neurobiol* 71:201–220.
- Gallo G (2016) Coordination of the axonal cytoskeleton during the emergence of axon collateral branches. *Neural Regen Res* 11:709–711.
- Ganguly A, Tang Y, Wang L, Laditka K, Loi J, Dargent B, Leterrier C, Roy S (2015) A dynamic formin-dependent deep F-actin network in axons. *J Cell Biol* 210:401–417.
- Gebhardt C, Auer TO, Henriques PM, Rajan G, Durore K, Bianco IH, Del Bene F (2019) An interhemispheric neural circuit allowing binocular integration in the optic tectum. *Nat Commun* 10:1–12.
- Ghate K, Mutalik SP, Sthanam LK, Sen S, Ghose A (2020) Fmn2 Regulates Growth Cone Motility by Mediating a Molecular Clutch to Generate Traction Forces. *Neuroscience* 448:160–171.
- González-Fraga J, Dipp-Alvarez V, Bardullas U (2019) Quantification of Spontaneous Tail Movement in Zebrafish Embryos Using a Novel Open-Source MATLAB Application. *Zebrafish* 16:214–216.

- Goode BL, Eck MJ (2007) Mechanism and Function of Formins in the Control of Actin Assembly. *Annu Rev Biochem* 76:593–627.
- Goodhill GJ, Faville R a, Sutherland DJ, Bicknell B a, Thompson AW, Pujic Z, Sun B, Kita EM, Scott EK (2015) The dynamics of growth cone morphology. *BMC Biol* 13:1–18.
- Gordon-Weeks PR, Fournier AE (2014) Neuronal cytoskeleton in synaptic plasticity and regeneration. *J Neurochem* 129:206–212.
- Gorukmez O, Gorukmez O, Ekici A (2020) A Novel Nonsense FMN2 Mutation in Nonsyndromic Autosomal Recessive Intellectual Disability Syndrome. *Fetal Pediatr Pathol*.
- Granato M, Nüsslein-Volhard C (1996) Fishing for genes controlling development. *Curr Opin Genet Dev* 6:461–468.
- Granato M, van Eeden FJ, Schach U, Trowe T, Brand M, Furutani-Seiki M, Haffter P, Hammerschmidt M, Heisenberg CP, Jiang YJ, Kane D a, Kelsh RN, Mullins MC, Odenthal J, Nüsslein-Volhard C (1996) Genes controlling and mediating locomotion behavior of the zebrafish embryo and larva. *Development* 123:399–413.
- Gyda M, Wolman M, Lorent K, Granato M (2012) The Tumor Suppressor Gene Retinoblastoma-1 Is Required for Retinotectal Development and Visual Function in Zebrafish Link BA, ed. *PLoS Genet* 8:e1003106.
- Haag N, Schwintzer L, Ahuja R, Koch N, Grimm J, Heuer H, Qualmann B, Kessels MM (2012) The actin nucleator Cobl is crucial for purkinje cell development and works in close conjunction with the F-actin binding protein Abp1. *J Neurosci* 32:17842–17856.
- Haas P, Gilmour D (2006) Chemokine Signaling Mediates Self-Organizing Tissue Migration in the Zebrafish Lateral Line. *Dev Cell* 10:673–680.
- Haddon C, Lewis J (1996) Early ear development in the embryo of the Zebrafish, *Danio rerio*. *J Comp Neurol* 365:113–128.
- Haffter P, Granato M, Brand M, Mullins MC, Hammerschmidt M, Kane D a, Odenthal J, van Eeden FJ, Jiang YJ, Heisenberg CP, Kelsh RN, Furutani-Seiki M, Vogelsang E, Beuchle D, Schach U, Fabian C, Nüsslein-Volhard C (1996) The identification of genes with

- unique and essential functions in the development of the zebrafish, *Danio rerio*. *Development* 123:1–36.
- Hale ME, Katz HR, Peek MY, Fremont RT (2016) Neural circuits that drive startle behavior, with a focus on the Mauthner cells and spiral fiber neurons of fishes. *J Neurogenet* 30.
- Hale ME, Ritter D a., Fetcho JR (2001) A confocal study of spinal interneurons in living larval zebrafish. *J Comp Neurol* 437:1–16.
- Hatta K (1992) Role of the floor plate in axonal patterning in the zebrafish CNS. *Neuron* 9:629–642.
- Hecker A, Schulze W, Oster J, Richter DO, Schuster S (2020) Removing a single neuron in a vertebrate brain forever abolishes an essential behavior. *Proc Natl Acad Sci U S A* 117:3254–3260.
- Higgs DM, Radford CA (2013) The contribution of the lateral line to “hearing” in fish. *J Exp Biol* 216:1484–1490.
- Higgs HN (2005) Formin proteins: A domain-based approach. *Trends Biochem Sci* 30:342–353.
- Ho J, Tumkaya T, Aryal S, Choi H, Claridge-Chang A (2019) Moving beyond P values: data analysis with estimation graphics. *Nat Methods* 16:565–566.
- Hu J, Bai X, Bowen JR, Dolat L, Korobova F, Yu W, Baas PW, Svitkina T, Gallo G, Spiliotis ET (2012) Septin-driven coordination of actin and microtubule remodeling regulates the collateral branching of axons. *Curr Biol* 22:1109–1115.
- Hu M, Easter J (1999) Retinal neurogenesis: The formation of the initial central patch of postmitotic cells. *Dev Biol* 207:309–321.
- Hua JY, Smear MC, Baier H, Smith SJ (2005) Regulation of axon growth in vivo by activity-based competition. *Nature* 434:1022–1026.
- Hubbard JM, Böhm UL, Prendergast A, Tseng P-EB, Newman M, Stokes C, Wyart C (2016) Intraspinal Sensory Neurons Provide Powerful Inhibition to Motor Circuits Ensuring Postural Control during Locomotion. *Curr Biol* 26:2841–2853.

- Hutson LD, Chien C Bin (2002a) Wiring the zebrafish: Axon guidance and synaptogenesis. *Curr Opin Neurobiol* 12:87–92.
- Hutson LD, Chien CB (2002b) Wiring the zebrafish: Axon guidance and synaptogenesis. *Curr Opin Neurobiol* 12:87–92.
- Hwang WY, Fu Y, Reyon D, Maeder ML, Tsai SQ, Sander JD, Peterson RT, Yeh J-RJ, Joung JK (2013) Efficient genome editing in zebrafish using a CRISPR-Cas system. *Nat Biotechnol* 31:227–229.
- Issa F a, O'Brien G, Kettunen P, Sagasti A, Glanzman DL, Papazian DM (2011) Neural circuit activity in freely behaving zebrafish (*Danio rerio*). *J Exp Biol* 214:1028–1038.
- Issa FA, Mock AF, Sagasti A, Papazian DM (2012) Spinocerebellar ataxia type 13 mutation that is associated with disease onset in infancy disrupts axonal pathfinding during neuronal development. *DMM Dis Model Mech* 5:921–929.
- Jabeen S, Thirumalai V (2013) Distribution of the gap junction protein connexin 35 in the central nervous system of developing zebrafish larvae. *Front Neural Circuits* 7.
- Jao LE, Wente SR, Chen W (2013) Efficient multiplex biallelic zebrafish genome editing using a CRISPR nuclease system. *Proc Natl Acad Sci U S A* 110:13904–13909.
- Jontes JD, Buchanan J, Smith SJ (2000) Growth cone and dendrite dynamics in zebrafish embryos: early events in synaptogenesis imaged in vivo. *Nat Neurosci* 3:231–237.
- Kalil K, Dent EW (2014) Branch management: mechanisms of axon branching in the developing vertebrate CNS.
- Kalueff A V et al. (2013) Towards a comprehensive catalog of zebrafish behavior 1.0 and beyond. *Zebrafish* 10:70–86.
- Karlstrom RO, Trowe T, Klostermann S, Baier H, Brand M, Crawford a D, Grunewald B, Haffter P, Hoffmann H, Meyer SU, Müller BK, Richter S, van Eeden FJ, Nüsslein-Volhard C, Bonhoeffer F (1996) Zebrafish mutations affecting retinotectal axon pathfinding. *Development* 123:427–438.
- Katoh M, Katoh M (2004) Characterization of FMN2 gene at human chromosome 1q43. *Int J Mol Med* 14:469–474.

- Kawabata Galbraith K, Kengaku M (2019) Multiple roles of the actin and microtubule-regulating formins in the developing brain. *Neurosci Res* 138:59–69.
- Kerstein PC, Nichol RH, Gomez TM (2015) Mechanochemical regulation of growth cone motility. *Front Cell Neurosci* 9:244.
- Kessels MM, Schwintzer L, Schlobinski D, Qualmann B (2011) Controlling actin cytoskeletal organization and dynamics during neuronal morphogenesis. *Eur J Cell Biol* 90:926–933.
- Ketschek A, Gallo G (2010) Nerve Growth Factor Induces Axonal Filopodia through Localized Microdomains of Phosphoinositide 3-Kinase Activity That Drive the Formation of Cytoskeletal Precursors to Filopodia. *J Neurosci* 30:12185–12197.
- Ketschek A, Jones S, Spillane M, Korobova F, Svitkina T, Gallo G (2015) Nerve growth factor promotes reorganization of the axonal microtubule array at sites of axon collateral branching. *Dev Neurobiol* 75:1441–1461.
- Ketschek A, Spillane M, Dun XP, Hardy H, Chilton J, Gallo G (2016) Drebrin coordinates the actin and microtubule cytoskeleton during the initiation of axon collateral branches. *Dev Neurobiol* 76:1092–1110.
- Kida YS, Sato T, Miyasaka KY, Suto A, Ogura T (2007) Daam1 regulates the endocytosis of EphB during the convergent extension of the zebrafish notochord. *Proc Natl Acad Sci U S A* 104:6708–6713.
- Kimmel CB, Ballard WW, Kimmel SR, Ullmann B, Schilling TF (1995) Stages of embryonic development of the zebrafish. *Dev Dyn* 203:253–310.
- Kinkhabwala A, Riley M, Koyama M, Monen J, Satou C, Kimura Y, Higashijima S-I, Fetcho J (2011) A structural and functional ground plan for neurons in the hindbrain of zebrafish. *Proc Natl Acad Sci U S A* 108:1164–1169.
- Kita EM, Scott EK, Goodhill GJ (2015) Topographic wiring of the retinotectal connection in zebrafish. *Dev Neurobiol* 75:542–556.
- Knafo S, Wyart C (2018) Active mechanosensory feedback during locomotion in the zebrafish spinal cord. *Curr Opin Neurobiol* 52:48–53.
- Kohashi T, Nakata N, Oda Y (2012a) Effective sensory modality activating an escape

- triggering neuron switches during early development in zebrafish. *J Neurosci* 32:5810–5820.
- Kohashi T, Nakata N, Oda Y (2012b) Effective sensory modality activating an escape triggering neuron switches during early development in zebrafish. *J Neurosci* 32:5810–5820.
- Kohashi T, Oda Y (2008) Initiation of Mauthner- or non-Mauthner-mediated fast escape evoked by different modes of sensory input. *J Neurosci* 28:10641–10653.
- Korn H, Faber DS (2005) The Mauthner cell half a century later: A neurobiological model for decision-making? *Neuron* 47:13–28.
- Krainer EC, Ouderkirk JL, Miller EW, Miller MR, Mersich AT, Blystone SD (2013) The multiplicity of human formins: Expression patterns in cells and tissues. *Cytoskeleton* 70:424–438.
- Kundu T, Das SS, Kumar DS, Sewatkar LK, Ghose A (2020) Antagonistic activities of Fmn2 and ADF regulate axonal F-actin patch dynamics and the initiation of collateral branching. *bioRxiv:2020.11.16.384099*.
- Kundu T, Dutta P, Nagar D, Maiti S, Ghose A (2021) Coupling of dynamic microtubules to F-actin by Fmn2 regulates chemotaxis of neuronal growth cones. *J Cell Sci*.
- Kuwada JY (1993) Pathway selection by growth cones in the zebrafish central nervous system. *Perspect Dev Neurobiol* 1:195–203.
- Kuwada JY, Bernhardt RR, Chitnis AB (1990a) Pathfinding by identified growth cones in the spinal cord of zebrafish embryos. *J Neurosci* 10:1299–1308.
- Kuwada JY, Bernhardt RR, Nguyen N (1990b) Development of spinal neurons and tracts in the zebrafish embryo. *J Comp Neurol* 302:617–628.
- Lacoste AMB, Schoppik D, Robson DN, Haesemeyer M, Portugues R, Li JM, Randlett O, Wee CL, Engert F, Schier AF (2014) A Convergent and Essential Interneuron Pathway for Mauthner-Cell-Mediated Escapes. *Curr Biol*:1526–1534.
- Lai S-L, Chan T-H, Lin M-J, Huang W-P, Lou S-W, Lee S-J (2008) Diaphanous-Related Formin 2 and Profilin I Are Required for Gastrulation Cell Movements Heisenberg C-P, ed. *PLoS One* 3:e3439.

- Lam P, Mangos S, Green JM, Reiser J, Huttenlocher A (2015) In Vivo Imaging and Characterization of Actin Microridges Weaver AM, ed. PLoS One 10:e0115639.
- Langebeck-Jensen K, Shahar OD, Schuman EM, Langer JD, Ryu S (2019) Larval Zebrafish Proteome Regulation in Response to an Environmental Challenge. *Proteomics* 19:1900028.
- Lasser M, Tiber J, Lowery LA (2018) The role of the microtubule cytoskeleton in neurodevelopmental disorders. *Front Cell Neurosci* 12:165.
- Law R et al. (2014) Biallelic truncating mutations in FMN2, encoding the actin-regulatory protein formin 2, cause nonsyndromic autosomal-recessive intellectual disability. *Am J Hum Genet* 95:721–728.
- Leader B, Leder P (2000) Formin-2, a novel formin homology protein of the cappuccino subfamily, is highly expressed in the developing and adult central nervous system.
- Leader B, Lim H, Carabatsos MJ, Harrington A, Ecsedy J, Pellman D, Maas R, Leder P (2002) Formin-2, polyploidy, hypofertility and positioning of the meiotic spindle in mouse oocytes. *Nat Cell Biol* 4:921–928.
- Lee RKK, Eaton RC (1991) Identifiable Retidospinal Neurons of the Adult Zebrafish , *Brachydanw rerio*. 3432.
- Lee RKK, Eaton RC, Zottoli SJ (1993) Segmental Arrangement of Reticulospinal Neurons in the Goldfish Hindbrain. 556.
- Lewis TL, Courchet J, Polleux F (2013) Cellular and molecular mechanisms underlying axon formation, growth, and branching. *J Cell Biol* 202:837–848.
- Li M, Zhao L, Page-McCaw PS, Chen W (2016) Zebrafish Genome Engineering Using the CRISPR–Cas9 System. *Trends Genet* 32:815–827.
- Lian G, Dettenhofer M, Lu J, Downing M, Chenn A, Wong T, Sheen V (2016) Filamin A- and formin 2-dependent endocytosis regulates proliferation via the canonical wnt pathway. *Dev* 143:4509–4520.
- Lian G, Sheen VL (2015) Cytoskeletal proteins in cortical development and disease: Actin associated proteins in periventricular heterotopia. *Front Cell Neurosci* 9:1–13.

- Liu K, Petree C, Requena T, Varshney P, Varshney GK (2019) Expanding the CRISPR toolbox in zebrafish for studying development and disease. *Front Cell Dev Biol* 7:13.
- Liu KS, Fetcho JR (1999) Laser ablations reveal functional relationships of segmental hindbrain neurons in zebrafish. *Neuron* 23:325–335.
- Liu LYM, Lin MH, Lai ZY, Jiang JP, Huang YC, Jao LE, Chuang YJ (2016) Motor neuron-derived *Thsd7a* is essential for zebrafish vascular development via the Notch-dll4 signaling pathway. *J Biomed Sci* 23:1–11.
- Liu Y, Halloran MC (2005) Development/Plasticity/Repair Central and Peripheral Axon Branches from One Neuron Are Guided Differentially by Semaphorin3D and Transient Axonal Glycoprotein-1.
- Liu YC, Hale ME (2017) Local Spinal Cord Circuits and Bilateral Mauthner Cell Activity Function Together to Drive Alternative Startle Behaviors. *Curr Biol* 27.
- Lorent K, Liu KS, Fetcho JR, Granato M (2001) The zebrafish space cadet gene controls axonal pathfinding of neurons that modulate fast turning movements. *Development* 128:2131–2142.
- Lowery LA, Van Vactor D (2009) The trip of the tip: understanding the growth cone machinery. *Nat Rev Mol Cell Biol* 10:332–343.
- Luo L (2002) Actin Cytoskeleton regulation in neuronal morphogenesis and structural plasticity. *Annu Rev Cell Dev Biol* 18:601–636.
- Manseau LJ, Schüpbach T (1989) *cappuccino* and *spire*: two unique maternal-effect loci required for both the anteroposterior and dorsoventral patterns of the *Drosophila* embryo. *Genes Dev* 3:1437–1452.
- Marco EJ, Aitken AB, Nair VP, da Gente G, Gerdes MR, Bologlu L, Thomas S, Sherr EH (2018) Burden of de novo mutations and inherited rare single nucleotide variants in children with sensory processing dysfunction. *BMC Med Genomics* 11:50.
- Marín O, Gleeson JG (2011) Function follows form: Understanding brain function from a genetic perspective. *Curr Opin Genet Dev* 21:237–239.
- Marques JC, Lackner S, Félix R, Orger MB (2018) Structure of the Zebrafish Locomotor Repertoire Revealed with Unsupervised Behavioral Clustering. *Curr Biol* 28:181–

195.e5.

- Marsden KC, Jain RA, Wolman MA, Echeverry FA, Nelson JC, Hayer KE, Miltenberg B, Pereda AE, Granato M (2018a) A Cyfip2-Dependent Excitatory Interneuron Pathway Establishes the Innate Startle Threshold. *Cell Rep* 23:878–887.
- Marsden KC, Jain RA, Wolman MA, Miltenberg B, Pereda AE, Correspondence MG, Echeverry FA, Nelson JC, Hayer KE, Granato M, Purpura DP (2018b) A Cyfip2-Dependent Excitatory Interneuron Pathway Establishes the Innate Startle Threshold. *Cell Rep* 23:878–887.
- Matusek T, Gombos R, Szécsényi A, Sánchez-Soriano N, Czibula Á, Pataki C, Gedai A, Prokop A, Raskó I, Mihály J (2008) Formin Proteins of the DAAM Subfamily Play a Role during Axon Growth. *J Neurosci* 28:13310 LP – 13319.
- Mcarthur KL, Chow DM, Fetcho JR (2020) The Zebrafish in Biomedical Research: Biology, Husbandry, Diseases, and Research Applications.
- McLean DL, Fetcho JR (2008) Using imaging and genetics in zebrafish to study developing spinal circuits in vivo. *Dev Neurobiol* 68:817–834.
- Medan V, Preuss T (2014) The Mauthner-cell circuit of fish as a model system for startle plasticity. *J Physiol Paris* 108:129–140.
- Meeker ND, Hutchinson SA, Ho L, Trede NS (2007) Method for isolation of PCR-ready genomic DNA from zebrafish tissues. *Biotechniques* 43:610–614.
- Menelaou E, Svoboda KR (2009) Secondary motoneurons in juvenile and adult zebrafish: Axonal pathfinding errors caused by embryonic nicotine exposure. *J Comp Neurol* 512:305–322.
- Menon S, Gupton S (2018) Recent advances in branching mechanisms underlying neuronal morphogenesis .
- Mogessie B, Schuh M (2017) Actin protects mammalian eggs against chromosome segregation errors. *Science* (80-) 357.
- Moly PK, Hatta K (2011) Early glycinergic axon contact with the Mauthner neuron during zebrafish development. *Neurosci Res* 70:251–259.

- Mumm JS, Williams PR, Godinho L, Koerber A, Pittman AJ, Roeser T, Chien C-B, Baier H, Wong ROL (2006) In vivo imaging reveals dendritic targeting of laminated afferents by zebrafish retinal ganglion cells. *Neuron* 52:609.
- Muñoz-Lasso DC, Romá-Mateo C, Pallardó F V., Gonzalez-Cabo P (2020) Much More Than a Scaffold: Cytoskeletal Proteins in Neurological Disorders. *Cells* 9:358.
- Myers PZ (1985) Spinal motoneurons of the larval zebrafish. *J Comp Neurol* 236:555–561.
- Myers PZ, Eisen JS, Westerfield M (1986) Development and Axonal Outgrowth of Identified Motoneurons in the Zebrafish.
- Nakajima Y (1974) Fine structure of the synaptic endings on the Mauthner cell of the goldfish. *J Comp Neurol* 156:375–402.
- Nakajima Y, Wang DW (1974) Morphology of afferent and efferent synapses in hearing organ of goldfish. *J Comp Neurol* 156:403–416.
- Nakayama H, Oda Y (2004) Common Sensory Inputs and Differential Excitability of Segmentally Homologous Reticulospinal Neurons in the Hindbrain. *J Neurosci* 24:3199–3209.
- Nevin LM, Robles E, Baier H, Scott EK (2010) Focusing on optic tectum circuitry through the lens of genetics. *BMC Biol* 8:126.
- Nicolson T (2017) The genetics of hair-cell function in zebrafish. *J Neurogenet* 31:102–112.
- Nicolson T, Rüsç A, Friedrich RW, Granato M, Ruppertsberg JP, Nüsslein-Volhard C (1998) Genetic analysis of vertebrate sensory hair cell mechanosensation: The zebrafish circler mutants. *Neuron* 20:271–283.
- Nüsslein-Volhard C (2012) The zebrafish issue of *Development*. *Development* 139:4099–4103.
- Odenthal J, Haffter P, Vogelsang E, Brand M, van Eeden FJ, Furutani-Seiki M, Granato M, Hammerschmidt M, Heisenberg CP, Jiang YJ, Kane D a, Kelsh RN, Mullins MC, Warga RM, Allende ML, Weinberg ES, Nüsslein-Volhard C (1996) Mutations affecting the formation of the notochord in the zebrafish, *Danio rerio*. *Development* 123:103–115.

- Pacentine I V, Nicolson T (2019) Subunits of the mechano-electrical transduction channel, *Tmc1/2b*, require *Tmie* to localize in zebrafish sensory hair cells.
- Paul A, Pollard T (2008) The Role of the FH1 Domain and Profilin in Formin-Mediated Actin-Filament Elongation and Nucleation. *Curr Biol* 18:9–19.
- Peleg S, Sananbenesi F, Zovoilis A, Burkhardt S, Bahari-Javan S, Agis-Balboa RC, Cota P, Wittnam JL, Gogol-Doering A, Opitz L, Salinas-Riester G, Dettenhofer M, Kang H, Farinelli L, Chen W, Fischer A (2010) Altered histone acetylation is associated with age-dependent memory impairment in mice. *Science* (80-) 328:753–756.
- Perrone MD, Rocca MS, Bruno I, Faletra F, Pecile V, Gasparini P (2012) De novo 911 Kb interstitial deletion on chromosome 1q43 in a boy with mental retardation and short stature. *Eur J Med Genet* 55:117–119.
- Phng LK, Gebala V, Bentley K, Philippides A, Wacker A, Mathivet T, Sauteur L, Stanchi F, Belting HG, Affolter M, Gerhardt H (2015) Formin-mediated actin polymerization at endothelial junctions is required for vessel lumen formation and stabilization. *Dev Cell* 32:123–132.
- Pike SH, Melancon EF, Eisen JS (1992) Pathfinding by zebrafish motoneurons in the absence of normal pioneer axons. *Development* 114:825–831.
- Pinto CS, Khandekar A, Bhavna R, Kiesel P, Pigo G, Sonawane M (2019) Microridges are apical epithelial projections formed of F-actin networks that organize the glycan layer. *Sci Rep* 9:1–16.
- Ponomareva OY, Holmen IC, Sperry AJ, Eliceiri KW, Halloran MC (2014) Calsyntenin-1 Regulates Axon Branching and Endosomal Trafficking during Sensory Neuron Development & In Vivo; *J Neurosci* 34:9235 LP – 9248.
- Prokop A, Sánchez-Soriano N, Gonçalves-Pimentel C, Molnár I, Kalmár T, Mihály J (2011) DAAM family members leading a novel path into formin research. *Commun Integr Biol* 4:538–542.
- Pruyne D, Evangelista M, Yang C, Bi E, Zigmond S, Bretscher A, Boone C (2002) Role of formins in actin assembly: Nucleation and barbed-end association. *Science* (80-) 297:612–615.

- Quinlan ME, Hilgert S, Bedrossian A, Mullins RD, Kerkhoff E (2007) Regulatory interactions between two actin nucleators, Spire and Cappuccino. *J Cell Biol* 179:117–128.
- Ravanelli AM, Klingensmith J (2011) The actin nucleator Cordon-bleu is required for development of motile cilia in zebrafish. *Dev Biol* 350:101–111.
- Roth-Johnson EA, Vizcarra CL, Bois JS, Quinlan ME (2014) Interaction between microtubules and the drosophila formin cappuccino and its effect on actin assembly. *J Biol Chem* 289:4395–4404.
- Ryley DA, Wu H-H, Leader B, Zimon A, Reindollar RH, Gray MR (2005) Characterization and mutation analysis of the human FORMIN-2 (FMN2) gene in women with unexplained infertility. *Fertil Steril* 83:1363–1371.
- Sahasrabudhe A, Ghatge K, Mutalik S, Jacob A, Ghose A (2015) Formin-2 regulates stabilization of filopodial tip adhesions in growth cones and affects neuronal outgrowth and pathfinding in vivo. *Development:dev*.130104-.
- Sahasrabudhe A, Ghatge K, Mutalik S, Jacob A, Ghose A (2016) Formin 2 regulates the stabilization of filopodial tip adhesions in growth cones and affects neuronal outgrowth and pathfinding in vivo. *Dev* 143:449–460.
- Saint-Amant L, Drapeau P (1998) Time course of the development of motor behaviors in the zebrafish embryo. *J Neurobiol* 37:622–632.
- Santos-Ledo A, Jenny A, Marlow FL (2013) Comparative gene expression analysis of the *fmln* family of formins during zebrafish development and implications for tissue specific functions. *Gene Expr Patterns* 13:30–37.
- Schier a. F, Joyner a. L, Lehmann R, Talbot WS (1996) From screens to genes: Prospects for insertional mutagenesis in zebrafish. *Genes Dev* 10:3077–3080.
- Schönichen A, Geyer M (2010) Fifteen formins for an actin filament: A molecular view on the regulation of human formins. *Biochim Biophys Acta - Mol Cell Res* 1803:152–163.
- Schuh M, Ellenberg J (2008) A New Model for Asymmetric Spindle Positioning in Mouse Oocytes. *Curr Biol* 18:1986–1992.

- Schweitzer J, Becker T, Lefebvre J, Granato M, Schachner M, Becker CG (2005) Tenascin-C is involved in motor axon outgrowth in the trunk of developing zebrafish. *Dev Dyn* 234:550–566.
- Scott EK, Baier H (2009) The cellular architecture of the larval zebrafish tectum, as revealed by Gal4 enhancer trap lines. *Front Neural Circuits* 3:13.
- Scott JW, Zottoli SJ, Beatty NP, Korn H (1994) Origin and function of spiral fibers projecting to the goldfish Mauthner cell. *J Comp Neurol* 339:76–90.
- Severi KE, Portugues R, Marques JC, O'Malley DM, Orger MB, Engert F (2014) Neural Control and Modulation of Swimming Speed in the Larval Zebrafish. *Neuron* 83:692–707.
- Shah AN, Davey CF, Whitebirch AC, Miller AC, Moens CB (2016) Rapid Reverse Genetic Screening Using CRISPR in Zebrafish. *Zebrafish* 13:152–153.
- Sillar KT (2009) Escape Behaviour: Reciprocal Inhibition Ensures Effective Escape Trajectory. *Curr Biol* 19:R697–R699.
- Spillane M, Gallo G (2014) Involvement of Rho-family GTPases in axon branching. *Small GTPases* 5.
- Spillane M, Ketschek A, Jones SL, Korobova F, Marsick B, Lanier L, Svitkina T, Gallo G (2011) The actin nucleating Arp2/3 complex contributes to the formation of axonal filopodia and branches through the regulation of actin patch precursors to filopodia. *Dev Neurobiol* 71:747–758.
- Stainier DYR, Raz E, Lawson ND, Ekker SC, Burdine RD, Eisen JS, Ingham PW, Schulte-Merker S, Yelon D, Weinstein BM, Mullins MC, Wilson SW, Ramakrishnan L, Amacher SL, Neuhauss SCF, Meng A, Mochizuki N, Panula P, Moens CB (2017) Guidelines for morpholino use in zebrafish. *PLoS Genet* 13:e1007000.
- Stewart WJ, Nair A, Jiang H, Mchenry MJ (2014) Prey fish escape by sensing the bow wave of a predator. *1:4328–4336*.
- Stifani N (2014) Motor neurons and the generation of spinal motor neuron diversity. *Front Cell Neurosci* 8:293.
- Stuermer C a (1988) Retinotopic organization of the developing retinotectal projection

- in the zebrafish embryo. *J Neurosci* 8:4513–4530.
- Sullivan L (1896) The tall office building artistically considered. *Lippincott's Mag*:403–409.
- Sun H, Al-Romaih KI, MacRae CA, Pollak MR (2014) Human kidney disease-causing INF2 mutations perturb Rho/Dia signaling in the glomerulus. *EBioMedicine* 1:107–115.
- Swain GP, Snedeker JA, Ayers J, Selzer ME (1993) Cytoarchitecture of Spinal-Projecting Neurons in the Brain of the Larval Sea Lamprey. *J Neurosci* 13:210:194–210.
- Szikora S, Földi I, Tóth K, Migh E, Vig A, Bugyi B, Maléth J, Hegyi P, Kaltenecker P, Sanchez-Soriano N, Mihaly J (2017) The formin DAAM is required for coordination of the actin and microtubule cytoskeleton in axonal growth cones. *J Cell Sci* 130:2506–2519.
- Tanimoto M, Ota Y, Inoue M, Oda Y (2011) Origin of Inner Ear Hair Cells: Morphological and Functional Differentiation from Ciliary Cells into Hair Cells in Zebrafish Inner Ear. *J Neurosci* 31:3784–3794.
- Tessier-Lavigne M, Goodman CS (1996) The molecular biology of axon guidance. *Science* (80-) 274:1123–1133.
- Thisse B, Thisse C (2005) High Throughput Expression Analysis of ZF-Models Consortium Clones. ZFIN Direct Data Submission. High Throughput Expr Anal ZF-Models Consort Clones ZFIN Direct Data Submission Available at: <http://zfin.org>.
- Thisse C, Thisse B (2008) High-resolution in situ hybridization to whole-mount zebrafish embryos. *Nat Protoc* 3:59–69.
- Thurston SF, Kulacz WA, Shaikh S, Lee JM, Copeland JW (2012) The Ability to Induce Microtubule Acetylation Is a General Feature of Formin Proteins. *PLoS One* 7:e48041.
- Umeda K, Shoji W (2017) From neuron to behavior: Sensory-motor coordination of zebrafish turning behavior. *Dev Growth Differ* 59:107–114.
- Varshney GK, Carrington B, Pei W, Bishop K, Chen Z, Fan C, Xu L, Jones M, LaFave MC, Ledin J, Sood R, Burgess SM (2016) A high-throughput functional genomics workflow based on CRISPR/Cas9-mediated targeted mutagenesis in zebrafish. *Nat Protoc* 11:2357–2375.

- Varshney GK, Pei W, Lafave MC, Idol J, Xu L, Gallardo V, Carrington B, Bishop K, Jones M, Li M, Harper U, Huang SC, Prakash A, Chen W, Sood R, Ledin J, Burgess SM (2015) High-throughput gene targeting and phenotyping in zebrafish using CRISPR/Cas9. *Genome Res* 25:1030–1042.
- Vaz R, Hofmeister W, Lindstrand A (2019) Zebrafish models of neurodevelopmental disorders: Limitations and benefits of current tools and techniques. *Int J Mol Sci* 20:1296.
- Westerfield M (1992) Motor axon pathfinding. *2*:28–30.
- Westerfield M, McMurray J V., Eisen JS (1986) Identified motoneurons and their innervation of axial muscles in the zebrafish. *J Neurosci* 6:2267–2277.
- Whitfield TT, Riley BB, Chiang M-Y, Phillips B (2002) Development of the Zebrafish Inner Ear.
- Wills Z, Marr L, Zinn K, Goodman CS, Van Vactor D (1999) Profilin and the Abl tyrosine kinase are required for motor axon outgrowth in the *Drosophila* embryo. *Neuron* 22:291–299.
- Wilson SW, Ross LS, Parrett T, Easter SS (1990) The development of a simple scaffold of axon tracts in the brain of the embryonic zebrafish, *Brachydanio rerio*.
- Wu CH et al. (2012) Mutations in the profilin 1 gene cause familial amyotrophic lateral sclerosis. *Nature* 488:499–503.
- Xiao T, Roeser T, Staub W, Baier H (2005a) A GFP-based genetic screen reveals mutations that disrupt the architecture of the zebrafish retinotectal projection. *Development* 132:2955–2967.
- Xiao T, Roeser T, Staub W, Baier H, Nüsslein-Volhard C, Bonhoeffer F (2005b) A GFP-based genetic screen reveals mutations that disrupt the architecture of the zebrafish retinotectal projection. *Development* 132:2955–2967.
- Xie J, Jusuf PR, Bui B V., Goodbourn PT (2019) Experience-dependent development of visual sensitivity in larval zebrafish. *Sci Rep* 9:1–11.
- Xu M, Liu D, Dong Z, Wang X, Wang X, Liu Y, Baas PW, Liu M (2014) Kinesin-12 influences axonal growth during zebrafish neural development. *Cytoskeleton* 71:555–563.

- Yamada K, Ono M, Bensaddek D, Lamond AI, Rocha S (2013a) FMN2 is a novel regulator of the cyclin-dependent kinase inhibitor p21. *Cell Cycle* 12:2348–2354.
- Yamada K, Ono M, Perkins ND, Rocha S, Lamond AI (2013b) Identification and Functional Characterization of FMN2, a Regulator of the Cyclin-Dependent Kinase Inhibitor p21. *Mol Cell* 49:922–933.
- Yang C, Danielson EW, Qiao T, Metterville J, Brown RH, Landers JE, Xu Z (2016) Mutant PFN1 causes ALS phenotypes and progressive motor neuron degeneration in mice by a gain of toxicity. *Proc Natl Acad Sci U S A* 113:E6209–E6218.
- Yoo H, Roth-Johnson EA, Bor B, Quinlan ME (2015) *Drosophila* Cappuccino alleles provide insight into formin mechanism and role in oogenesis. *Mol Biol Cell* 26:1875–1886.
- Yu J, Lai C, Shim H, Xie C, Sun L, Long CX, Ding J, Li Y, Cai H (2018) Genetic ablation of dynactin p150Glued in postnatal neurons causes preferential degeneration of spinal motor neurons in aged mice. *Mol Neurodegener* 13.
- Zeller J, Granato M (1999) diwanka in motor axon migration.
- Zottoli SJ, Hordes AR, Faber DS (1987) Localization of optic tectal input to the ventral dendrite of the goldfish Mauthner cell. *Brain Res* 401:113–121.

1

Introduction

1.1 Function follows form

To understand the function of the brain, it is essential first to understand how the brain, in all its complexity, is assembled and wired to give rise to its equally complex output, if not more. The phrase “Form follows function” was coined by the American architect Louis Sullivan and adopted by the Bauhaus movement to emphasize that utility directs the structure (Sullivan, 1896). When flipped to “Function follows form”, the phrase can be used in the context of neuroscience to study neuronal function as an emergent property of neuronal anatomy or neural circuits (Marín and Gleeson, 2011).

1.2 Neuronal morphogenesis

To form intricate neural circuits, the fate determined neurons that are primarily spherical need to transform and attain their characteristic neuronal morphologies before making synapses. Neuronal morphogenesis takes place over a series of stages, and the processes are more or less conserved in cultured neurons and in developing organisms. The first stage is the circumferential extension of protrusive structures, lamellipodia and filopodia followed by their engorgement and consolidation, called neuritogenesis. The second stage is the extension of multiple neurites followed by the specification of one of the neurites to become an axon. The process of axon specification is marked by the appearance of a dynamic structure at the growing end, called the growth cone. The third stage is axonogenesis, where the axon elongates while the growth cone navigates the environment in response to appropriate guidance cues. At stage four, the axon development continues in parallel to dendritic and axonal branching and arborization. The fifth and final stage is synaptogenesis, where neurons connect, making synapses and, in the case of some neurons, dendritic spines. The whole process, starting from a spherical cell to the formation of peculiar-looking neurons via specialized and dynamic structural changes, relies heavily on cytoskeletal remodelling. (Luo, 2002; Lowery and Van Vactor, 2009; Kessels et al., 2011; Flynn, 2013; Lewis et al., 2013; Kerstein et al., 2015; Menon and Gupton, 2018; Flynn and Bradke, 2020) *Error! Reference source not found.***Figure 1.1**

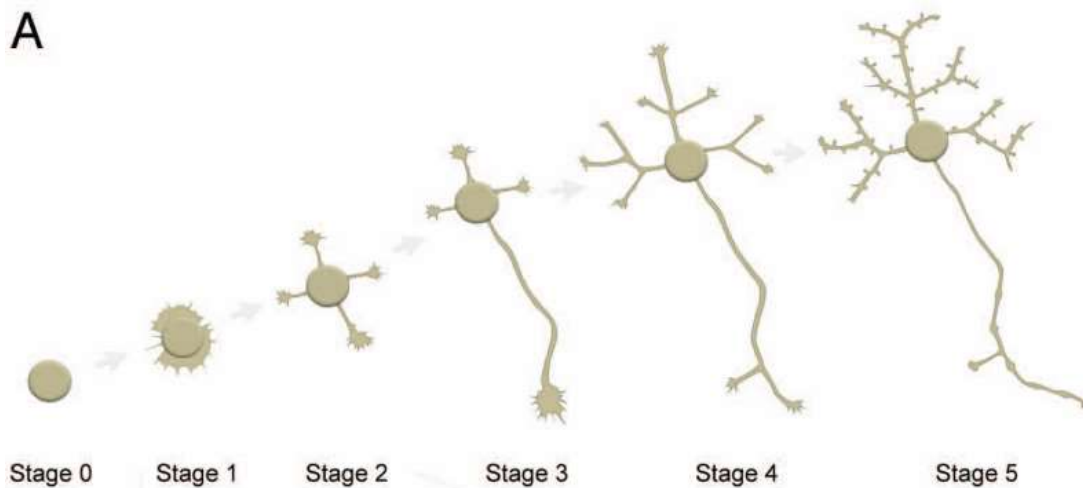


Figure 1.1 Stages of neuronal morphogenesis. The schematic describes the five major stages of neuronal morphogenesis, namely neuritogenesis, axon specification, axonogenesis, growth cone-mediated axon elongation and pathfinding and ultimately synaptogenesis. (Flynn, 2013)

1.3 Cytoskeleton and active remodelling in neuronal morphogenesis

Regulated and adaptive remodelling of the neuronal cytoskeleton is central to almost all aspects of neural development, including neurogenesis, neurite initiation, growth cone-mediated pathfinding and synaptogenesis (Kessels et al., 2011; Flynn, 2013; Lewis et al., 2013; Gordon-Weeks and Fournier, 2014; Flynn and Bradke, 2020; Muñoz-Lasso et al., 2020). A complex interplay mediates the dynamics of the neuronal cytoskeleton between the different cytoskeleton components, each regulated by specific regulators and coordinated by co-regulatory activities. Several actin-binding proteins regulate the dynamic actin cytoskeleton, and mutations in many of these have been associated with neurodevelopmental disorders (Lian and Sheen, 2015; Muñoz-Lasso et al., 2020).

Beginning from the early stages of neuronal morphogenesis, F-actin assembly and drives protrusion during neuritogenesis, followed by microtubule innervation of the protrusive structures to provide stability and direction. The growth cone has a spatially marked arrangement of the actin and microtubule cytoskeleton, and the dynamic interplay of these two major cytoskeletal elements is key to successful navigation of growth cone as discussed in the next section (Coles and Bradke, 2015; Goodhill et al., 2015; Flynn and Bradke, 2020).

1.4 Neuronal cytoskeleton in Growth cone guidance and axon pathfinding

The behavioural repertoire of an organism is a consequence of accurate neural connectivity of the nervous system. During the nervous system development, individual neurons are guided to reach their predetermined targets by environmental cues. For this guidance by extracellular signals, neurons must sense them and react to them with changes in their motility (Lowery and Van Vactor, 2009). Neurons indeed do so by employing a plethora of cytoskeleton remodelling proteins in response to guidance cues (attractive or repellent) to locally and actively rearrange the cytoskeleton at the tip of the growing neuron, called the growth cone. Powered by both actin and microtubules, the growth cone is a dynamic structure at the end of axons and dendrites, enabling the neuron to perform the aforementioned cue-directed motility. Actin rich filopodia extended by the growth cone serve as receivers of the guidance information and are crucial for axon guidance and pathfinding (Tessier-Lavigne and Goodman, 1996; Lowery and Van Vactor, 2009; Goodhill et al., 2015; Muñoz-Lasso et al., 2020). ***Figure 1.2***

Actin and microtubule cytoskeletons interact dynamically to help the growth cone achieve precise neural connectivity. Differential activities of the actin cytoskeleton like F-actin nucleation and polymerization, F-actin bundling, F-actin severing and capping, and actin retrograde flow are required for processes like filopodial protrusions, growth cone motility and retraction (Coles and Bradke, 2015; Muñoz-Lasso et al., 2020). On the other hand, microtubule innervation of sub-structures of growth cone stabilizes the structures strengthening their interaction with the environment. Microtubules also act as railroads for trafficking of metabolites, cargo proteins and mitochondria to the growing end of the neuron and therefore are critical in advance of the growth cone (Coles and Bradke, 2015; Lasser et al., 2018).

The growth cone engages with multiple cues in the environment for efficient navigation and establishing precise neuronal connectivity. While engaging with the cues, the growth cone is in constant interaction with adhesion molecules which serve as a roadmap for the growth and decide the broad trajectory of the growth cone. Further, diffusible guidance cues can be either chemoattractive or chemorepulsive. Major cues include chemotropic molecules like netrin and semaphorins, various morphogens like Shh, Wnt, BMP, growth factors like NGF, BDNF and neurotransmitters (Lowery and Van Vactor, 2009).

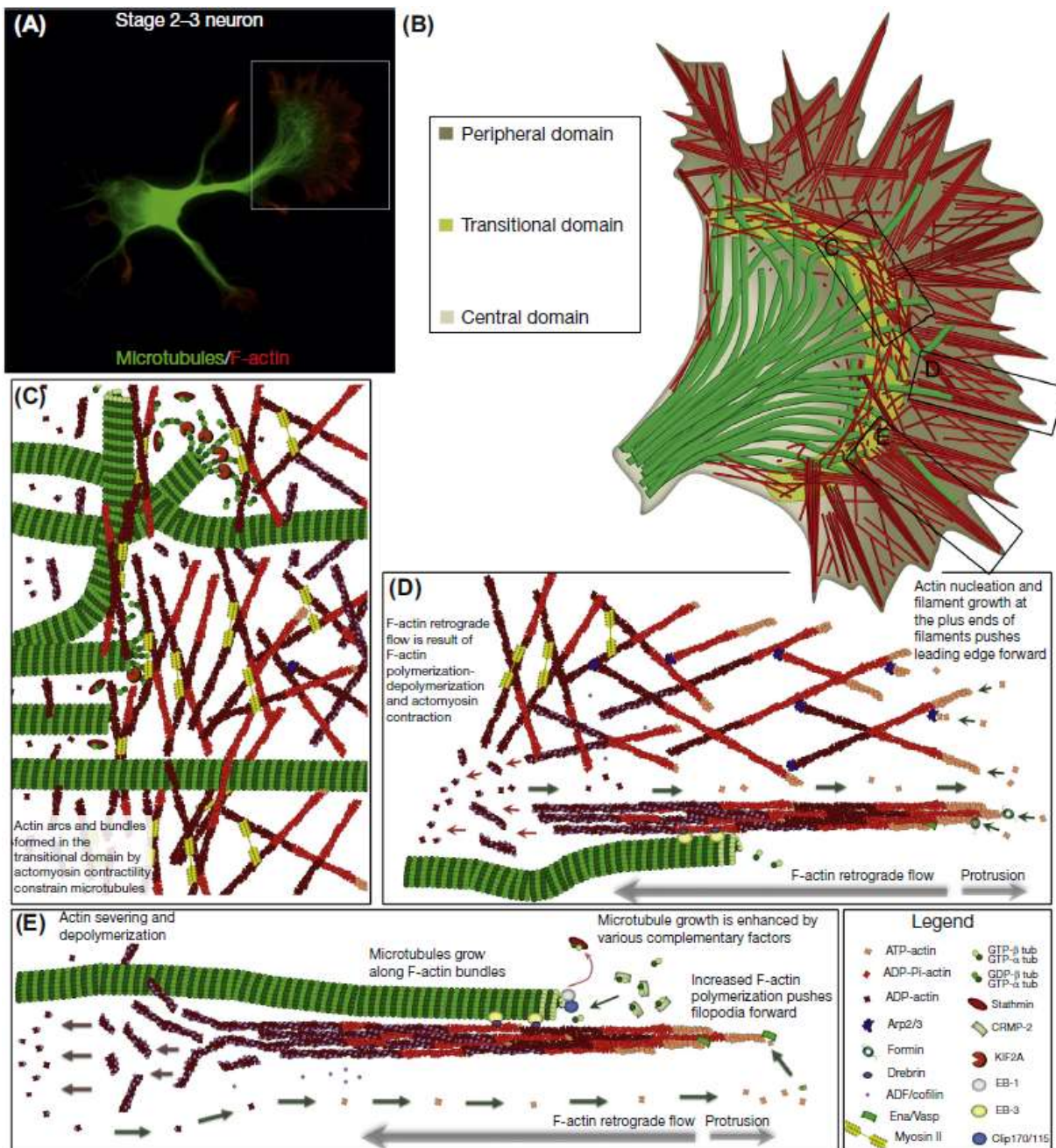


Figure 1.2 Neuronal cytoskeleton in growth cone dynamics. The schematic shows B) Organization of the actin and microtubule cytoskeleton in the growth cone. Actin and microtubule cytoskeleton is arranged in specialized structures in the lamellipodia, filopodia and the transition zones. The leading structures are actin-rich and the axon shaft is rich in microtubule innervation. Actin treadmilling and dynamic instability shown by microtubules are crucial in growth cone dynamics. (Flynn and Bradke, 2020)

The response of the growth cone to these cues is dependent on the collective engagement of the growth cone receptors and signalling inside the growth cone in a context-specific manner that does not remain the same necessarily. Eventually, the proper guidance of the axon led by the growth cone allows pioneer axons to reach their pre-determined

targets (Dickson, 2002; Lowery and Van Vactor, 2009; Bonner et al., 2012; Goodhill et al., 2015; Kerstein et al., 2015) **Figure 1.3.**

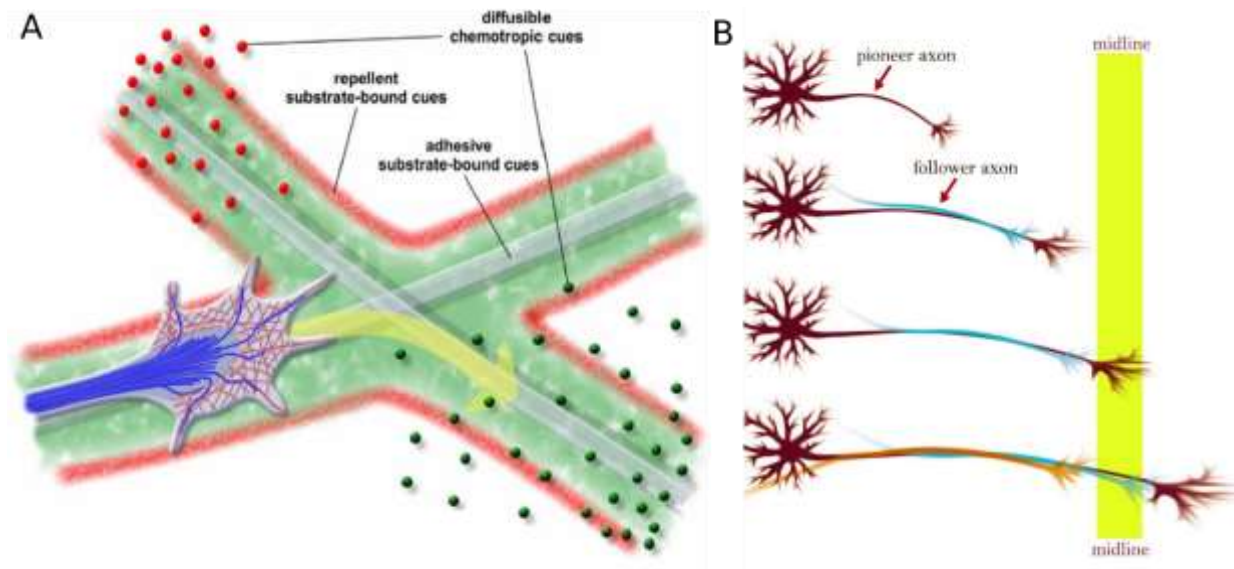


Figure 1.3 Growth cone guidance and pathfinding by pioneer axons. A growth cone deciding to turn towards chemo-attractive cues from the environment. Such processes are crucial for precise axonal pathfinding. B) Guidance cues from the midline help the pioneer axon navigate towards the midline, and the follower neurons follow the same trajectory later. (Bak and Fraser, 2003; Lowery and Van Vactor, 2009)

1.5 Neuronal cytoskeleton in Axonogenesis, branching and arborization

Axonogenesis is an essential process in establishing neural connectivity. After axon specification, the growth cone at the tip of the axon navigates the environment and signal the actin and microtubule machinery. In the case of a chemoattractive cue, the actin and microtubule cytoskeletons are stabilized in the axonal shaft as the axon grows while the growing end remains highly dynamic (Flynn, 2013). Increased F-actin turnover is a hallmark of the advancing growth cone. The active assembly and disassembly of F-actin structures allow the microtubules to extend into the growth cone periphery, further stabilizing the trajectory of the advancing neuron (Flynn and Bradke, 2020). **Figure 1.4**

Axonal branching is an integral part of neural circuit formation. Collateral branches originate perpendicular to the direction of growth the axonal shaft, often at sites marked by growth cone stalling (Lewis et al., 2013). Another modality of axonal branching is growth cone splitting (Armijo-Weingart and Gallo, 2017). Recent studies have highlighted the importance of local cytoskeletal assemblies like actin patches and trails

in axonal branching (Ketschek and Gallo, 2010; Spillane et al., 2011; Hu et al., 2012; Ketschek et al., 2016; Kundu et al., 2020). **Figure 1.5**

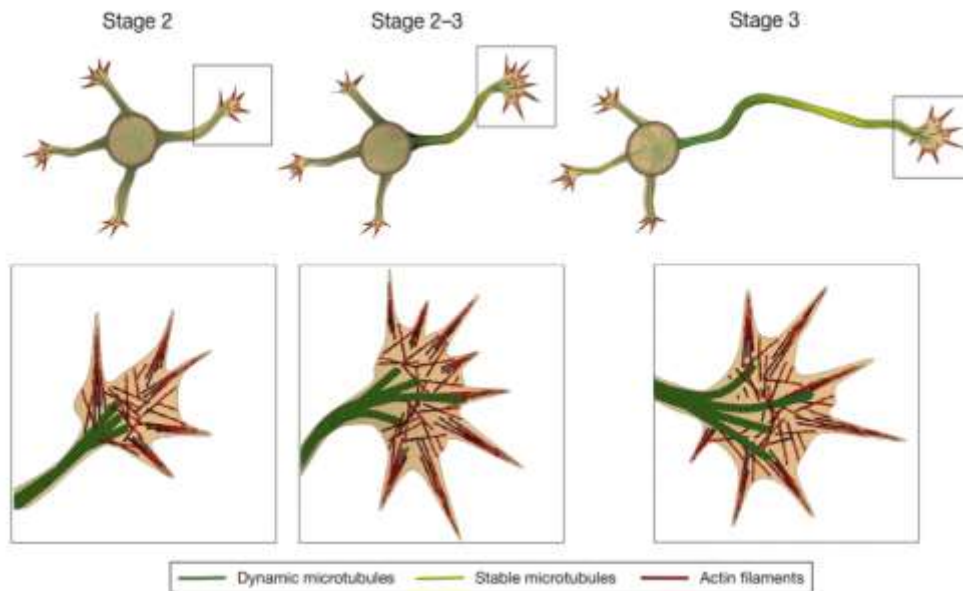


Figure 1.4 Axon elongation and pathfinding requires active cytoskeletal remodelling. (Flynn and Bradke, 2020)

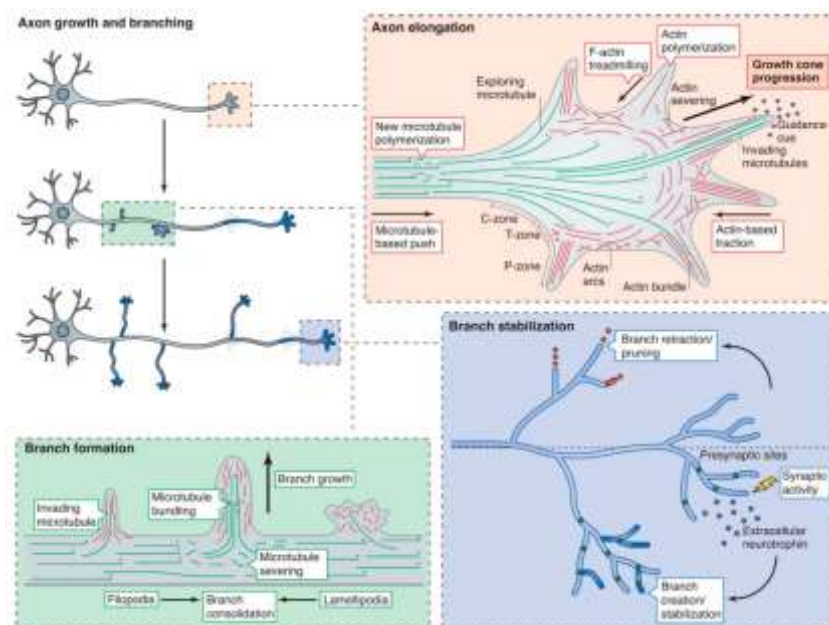


Figure 1.5 Axon branching. Axon elongation is aided by dynamic actin assembly and disassembly that allows microtubule innervation. Along the length of the axon, local changes in the cytoskeleton will enable the formation of actin-rich branching hotspots from where protrusions emerge orthogonally and are further stabilized by microtubules. (Lewis et al., 2013)

1.6 Actin nucleators

Actin nucleators are an important class of actin-binding proteins involved in regulating the seeding of F-actin filaments from monomeric actin and control the architecture of the F-actin network (Campellone and Welch, 2010; Kessels et al., 2011). A variety of actin nucleators are found to be expressed in the developing nervous system. Neuronal cells employ multiple actin nucleators in cytoskeletal remodelling underlying neuronal morphogenesis and circuit formation. Major actin nucleators are the Arp2/3 complex, Formins and WH2 domain containing actin nucleators Cobl and Spire (Goode and Eck, 2007; Campellone and Welch, 2010). **Figure 1.6**

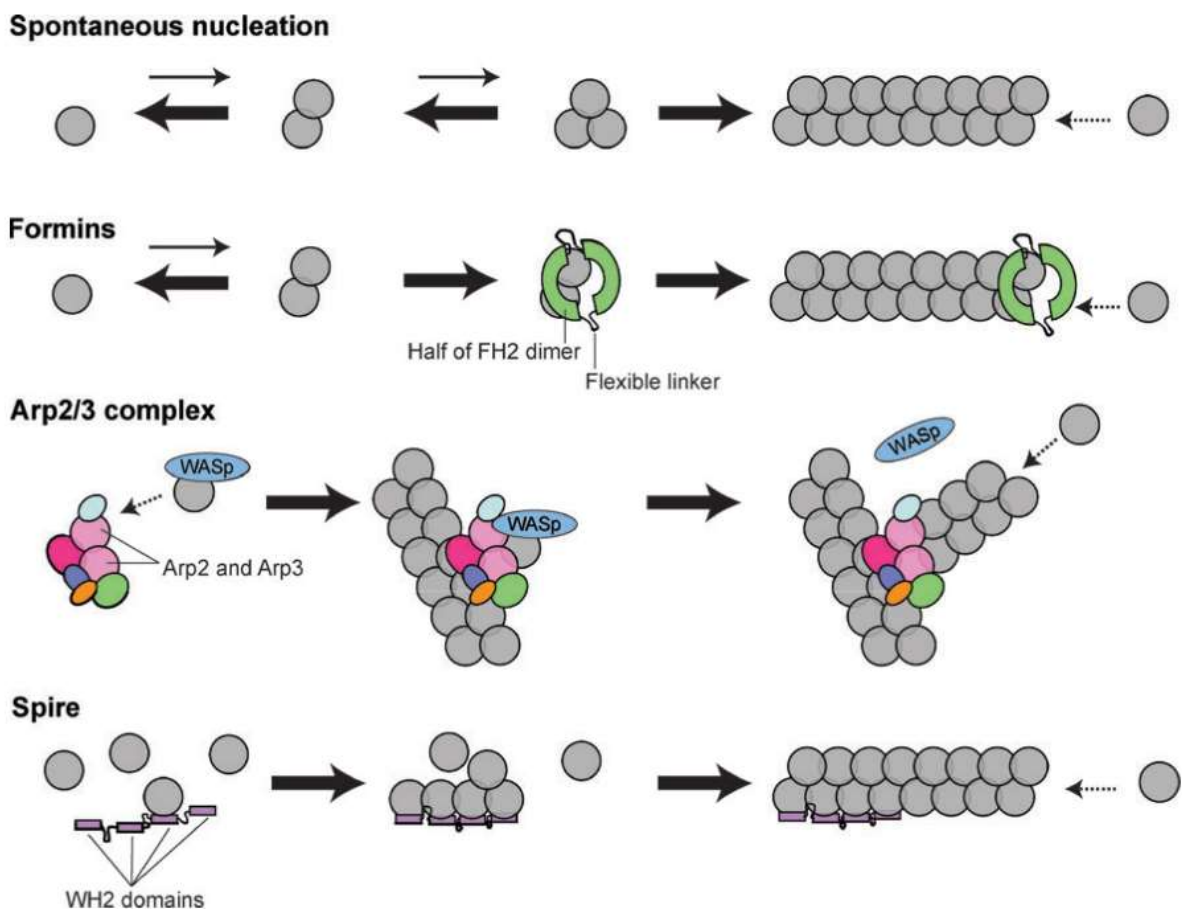


Figure 1.6 Actin nucleators. F-actin nucleation by Formins, Arp2/3 complex and Spire. (Goode and Eck, 2007)

Three classes of actin nucleators have been described previously in zebrafish, Arp2/3 complex, Formin homology domain 2 (FH2) containing family (the Formins) and the WASP homology domain 2 (WH2) containing family of nucleators. Arp2/3 has been shown to regulate actin patches essential for proximal axon specification in zebrafish

motor neurons (Balasanyan et al., 2017) and maintain microridge structure and length on surface epithelial cells in zebrafish (Lam et al., 2015; Pinto et al., 2019). The WH2 domain containing actin nucleator, Cordon bleu (Cobl), is required to develop motile cilia in zebrafish Kupffer's vesicles which in turn maintain laterality in zebrafish (Ravanelli and Klingensmith, 2011).

1.7 Formins

The formin class of actin nucleators have recently been characterized in neuronal development. There are fifteen formins in humans that cluster into eight different subfamilies (Schönichen and Geyer, 2010), and mutations in several formins are associated with various neural disorders (Kawabata Galbraith and Kengaku, 2019). Most formins are conserved across vertebrates and are expressed in various tissues, including the nervous system (Dutta and Maiti, 2015). Varying expression patterns of multiple formins within the same and different tissues is an interesting open question in the field. More research is required to assess the differential functions of formins in neurodevelopment. **Figure 1.7**

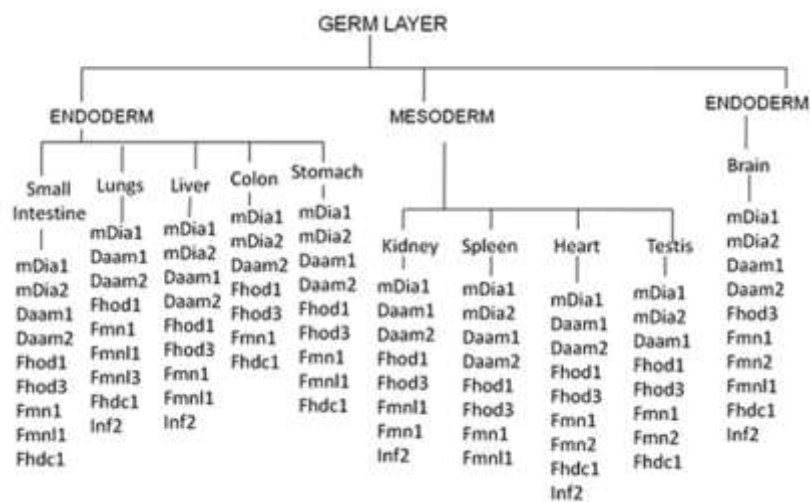


Figure 1.7 Differential expression of formins in various tissues. Multiple formins are expressed in the same tissue pointing towards their functional redundancy. (Dutta and Maiti, 2015)

Formins are well characterized for their ability to regulate actin dynamics by various activities, namely actin nucleation, elongation of unbranched F-actin, capping, bundling, and severing in some cases (Pruyne et al., 2002; Schönichen and Geyer, 2010; Breitsprecher and Goode, 2013). Some formins also mediate microtubule bundling and

stabilization and may not necessarily be dependent on their actin nucleating activities (Thurston et al., 2012; Fernández-Barrera and Alonso, 2018). Formins, therefore, are at an exciting interface in their ability to regulate two significant classes of the cytoskeleton. DAAM and Fmn2 are recently characterized in mediating actin and microtubule cross-talk connecting actin remodelling in growth cone filopodia with microtubule stabilization (Szikora et al., 2017; Kundu et al., 2021).

Formins can broadly be divided into seven families based on the identity of the conserved FH2 domain: DAAM, FHOD, FMN, FMNL, INF, GRID2IP and DIAPH (Breitsprecher and Goode, 2013; Kawabata Galbraith and Kengaku, 2019). The FH2 domain mediates actin nucleation and elongation by a stair-step mechanism at the barbed end of the growing actin filament. The FH1 domain binds to the G-actin-Profilin complex via its poly-Proline stretches and delivers profilin bound actin monomers to the FH2 domain for polymerization (Higgs, 2005; Paul and Pollard, 2008; Breitsprecher and Goode, 2013).

Figure 1.8

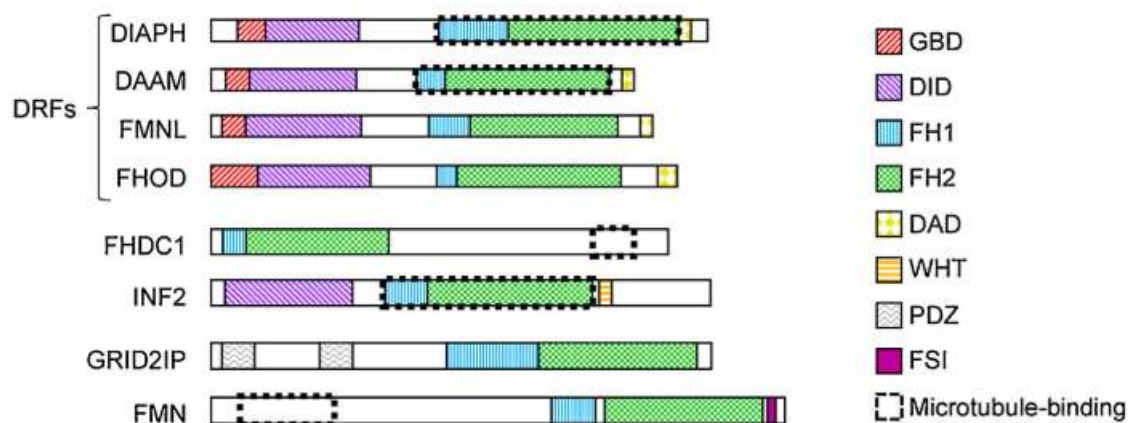


Figure 1.8 Formins. Formins have conserved Formin Homology 1 (FH1) and Formin Homology 2 (FH2) domains. Other regulatory domains are unique to different classes of formins. (Kawabata Galbraith and Kengaku, 2019).

Formins play a vital role in the development and regulation of the nervous system. DIAPH1, DIAPH3 and FMN2 expression levels control spine density, whereas DAPH3 and DAAM1 control the spine length (Kawabata Galbraith and Kengaku, 2019). FMN2 is important in depotentiation and growth cone motility, and mechanotransduction. DIAPH1, FHDC1 and INF2 coordinate organelle dynamics in neurons. DAAM1 is required for dendritogenesis and axonal extension. DIAPH1, DIAPH2 and DAAM are also implicated in growth cone navigation by regulating actin and microtubule cytoskeletons

(Kawabata Galbraith and Kengaku, 2019). Further work needs to be done to estimate the effect of overlapping roles of formins in the nervous system. **Figure 1.9**

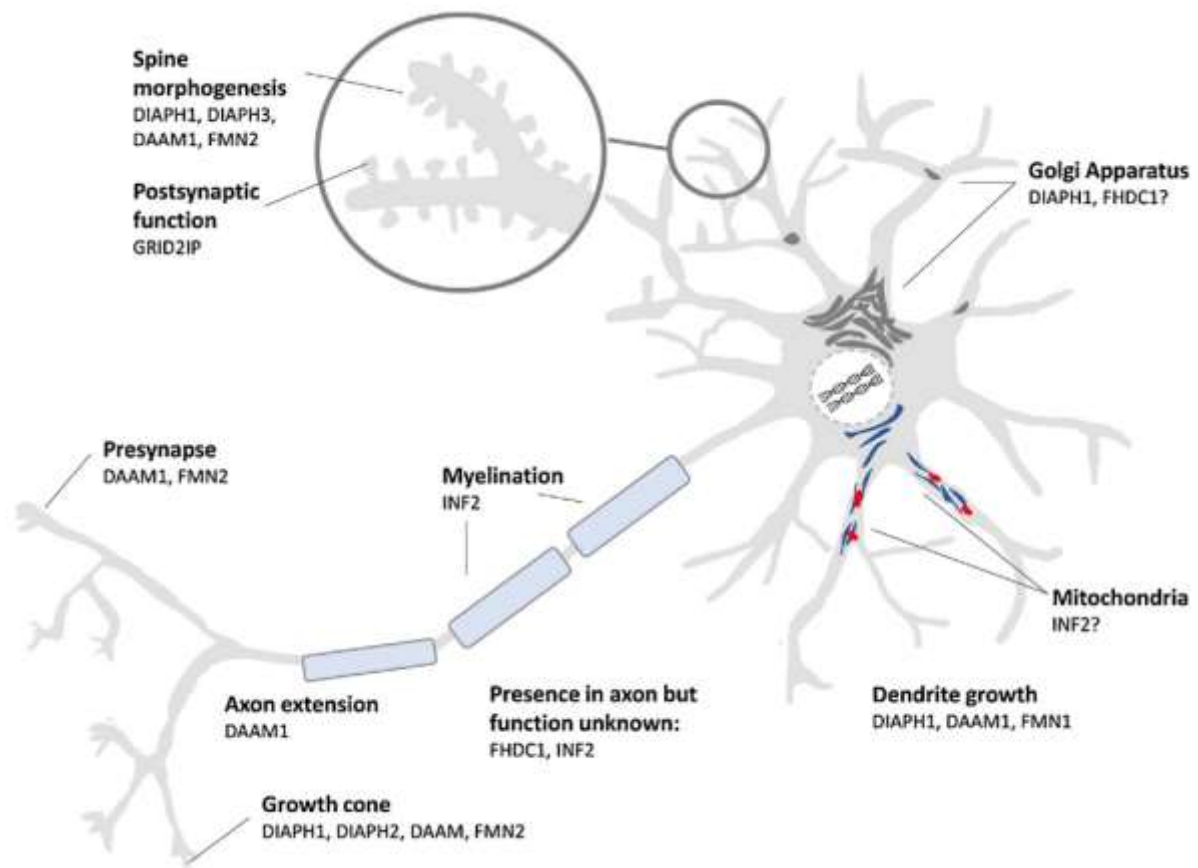


Figure 1.9 Formins in the nervous system. A variety of formins regulate the processes underlying neuronal development. (Kawabata Galbraith and Kengaku, 2019)

1.8 Formin-2

A member of the FMN family, Formin-2 (Fmn2), reported to be enriched in the nervous system in mouse (Leader and Leder, 2000) and chick (Sahasrabudhe et al., 2015), is particularly interesting. After the first report showing the expression of Fmn2 in the nervous system, not much has been done to understand the mechanistic role of Fmn2. Although, other functions were reported underlining the role of mammalian Fmn2 in meiosis and oocyte development (Leader et al., 2002; Ryley et al., 2005; Dumont et al., 2007; Schuh and Ellenberg, 2008; Mogessie and Schuh, 2017). Other studies in humans also indicated that mutations in Fmn2 in humans lead to symptoms of mental retardation, intellectual disabilities (Law et al., 2014), learning deficits (Almuqbil et al., 2013) and unexplained infertility in women (Ryley et al., 2005). **Figure 1.10**

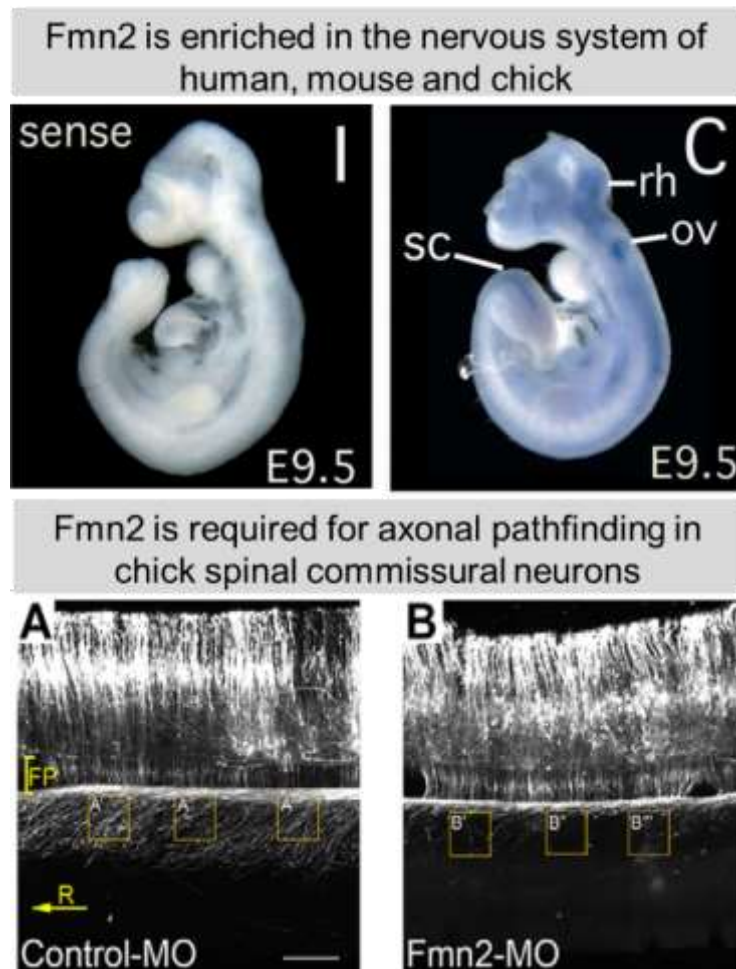


Figure 1.10 Formin-2 in the nervous system. Formin-2 (Fmn2) is expressed in the developing nervous system of mice and is essential for axonal pathfinding in chick spinal cord *in ovo*. (Leader and Leder, 2000; Sahasrabudhe et al., 2016)

Previous studies using chick spinal neuron cultures *in vitro* suggest that Fmn2 is necessary for growth cone structure and filopodial dynamics, processes important in establishing precise neural connectivity during development (Sahasrabudhe et al., 2016; Ghate et al., 2020). Also, *in ovo* studies done in chick show that Fmn2 is necessary for axonal pathfinding by the spinal commissures and, therefore, nail down its importance in establishing neural circuitry (Sahasrabudhe et al., 2016). Further, Fmn2 is shown to be required for generating traction forces by acting as a molecular clutch in the growth cone and stabilizing adhesion sites during migration (Sahasrabudhe et al., 2016; Ghate et al., 2020). **Figure 1.11**

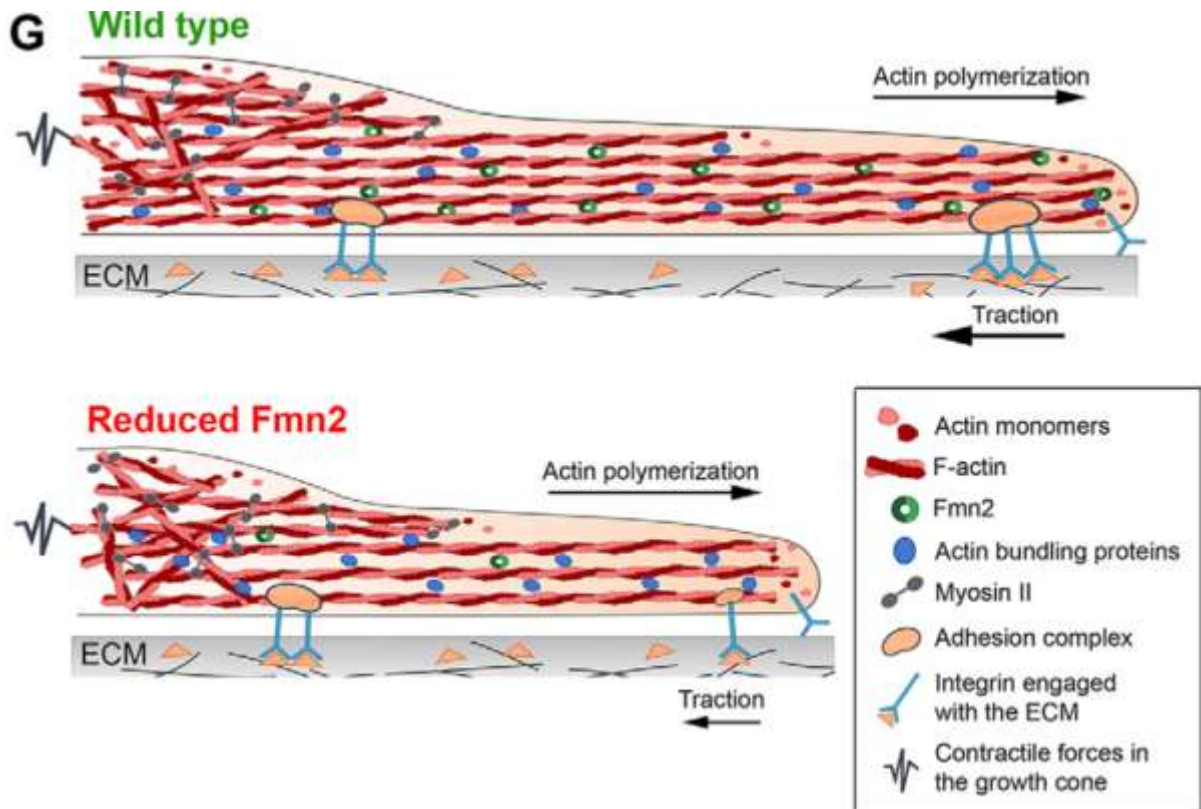


Figure 1.11 Fmn2 regulates substrate adhesion and the consequent generation of traction forces during migration. Knockdown of Fmn2 causes a reduction in strength of point contacts made by the growth cone filopodia causing reduced traction force. (Sahasrabudhe et al., 2016)

Recently, Fmn2 has been implicated in regulating actin-microtubule crosstalk mediated by the FSI domain in cultured spinal neurons and required for growth cone chemotaxis. Fmn2 stabilizes the microtubules in the migrating growth cone to provide directionality in a substrate responsive manner (Kundu et al., 2021). **Figure 1.12**

These reports mainly use cultured primary neurons that have limitations in investigating gene function in assembling neural ensembles giving rise to appropriate behaviour.

Besides the contribution of Formin-2 in nervous system development, it is also implicated in non-neuronal development. Oocytes from Fmn2 null mice have spindle positioning defects and meiotic arrest, causing hypo-fertility in Fmn2 mutants (Leader and Leder, 2000; Mogessie and Schuh, 2017). Fmn2 is reported to be a novel regulator of p21, a cyclin-dependent kinase. Fmn2 promotes cell cycle arrest by inhibiting p21 degradation (Yamada et al., 2013a, 2013b). However, the molecular and regulatory mechanisms of Fmn2 function remain elusive.

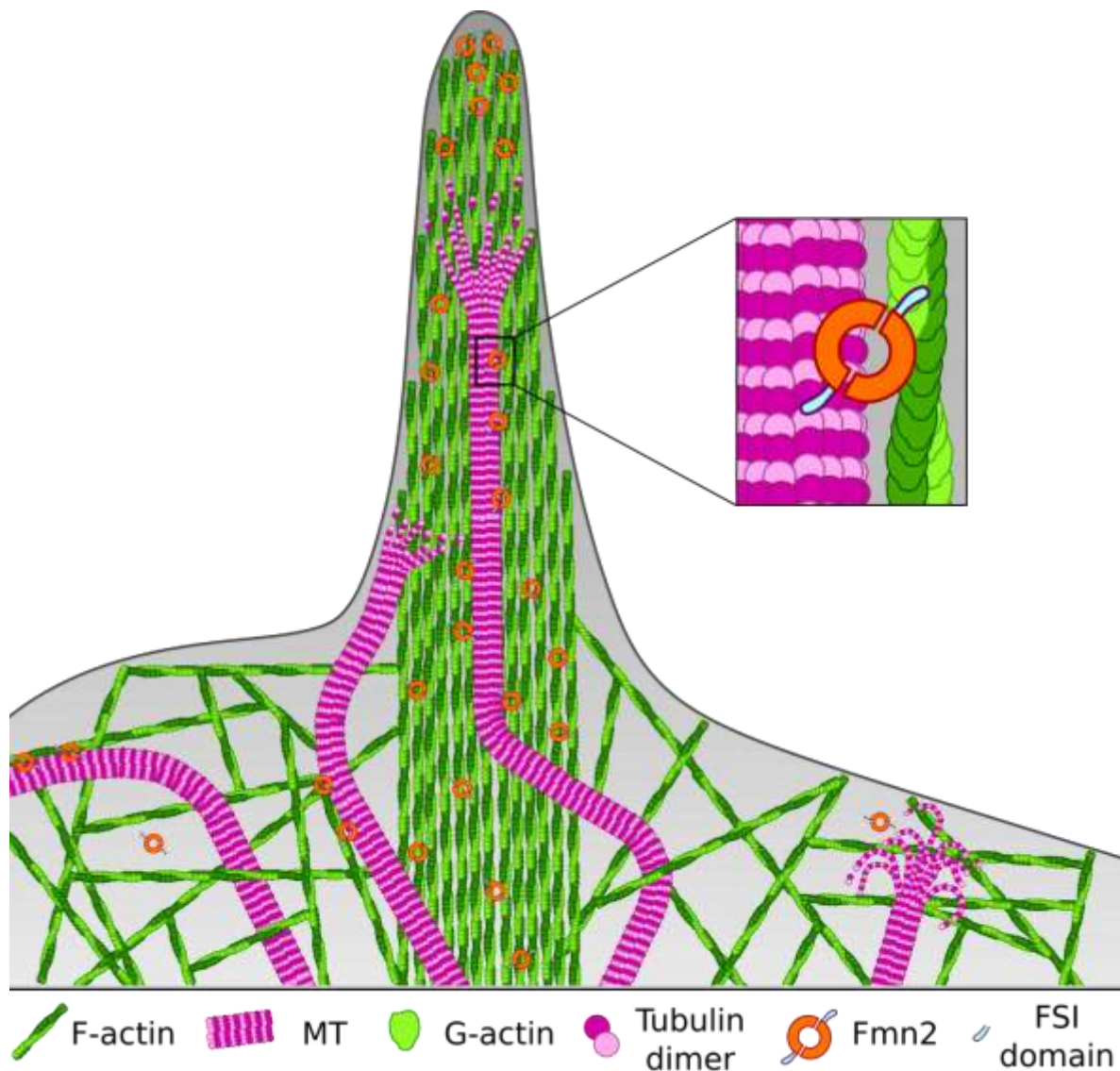


Figure 1.12 Schematic showing actin-microtubule crosstalk in the growth cone and their filipodia. The Formin Spite Interactor (FSI) domain is responsible for cross-linking actin and microtubule polymers in the filopodia of growth cones, presumably due to the presence of multiple positively charged amino acid residues. (Kundu et al., 2021)

In recent years, mutations in Fmn2 have been increasingly associated with neural disorders, including cognitive disabilities and sensory processing dysfunction in humans (Perrone et al., 2012; Almuqbil et al., 2013; Law et al., 2014; Agís-Balboa et al., 2017; Anazi et al., 2017; Marco et al., 2018; Gorukmez et al., 2020). Fmn2 expression was found to be reduced in post mortem brain samples of patients with post-traumatic stress disorder and Alzheimer’s disease (Agís-Balboa et al., 2017). Other reports implicate Fmn2 mutations in corpus callosum agenesis (Perrone et al., 2012; Gorukmez et al., 2020) and microcephaly (Anazi et al., 2017). In rodents, loss of Fmn2 accelerated age-associated memory impairment and amyloid-induced deregulation of gene expression (Peleg et al.,

2010; Agís-Balboa et al., 2017). Despite accumulating evidence, little is known about the function of Fmn2 in the nervous system.

1.9 Formins in zebrafish neural development

The formin family comprises 25 predicted members in zebrafish, out of which 11 are shown to be neuronally enriched (Thisse and Thisse, 2005; Santos-Ledo et al., 2013). A study comparing expression patterns of the formin-like (Fmnl) subfamily of formins shows that the formins, Fmnl1a, Fmnl1b, Fmnl2a, Fmnl2b and Fmnl3 are expressed in the nervous system in a dynamic temporal manner during zebrafish development, in addition to expression in non-neuronal tissues (Santos-Ledo et al., 2013).

However, the role of formins in the development of neural circuits in zebrafish is not well explored despite several studies reporting the enrichment of formins in vertebrate nervous systems (Leader and Leder, 2000; Krainer et al., 2013; Dutta and Maiti, 2015; Sahasrabudhe et al., 2016). The only report available implicates the formin Daam1a in the asymmetric morphogenesis of the zebrafish habenula and the regulation of the dendritic and axonal processes of the dorsal habenular neurons (Colombo et al., 2013). Formin function in non-neuronal tissues has also been sparsely investigated in zebrafish. Daam1a is required for convergent extension and regulates notochord development in zebrafish (Kida et al., 2007), while zDia2, working synergistically with Profilin I, regulates gastrulation (Lai et al., 2008). Fmnl3 has been reported to be involved in blood vessel morphogenesis (Phng et al., 2015). Formins are expressed in several tissue types with rich spatiotemporal diversity in humans (Krainer et al., 2013), mice (Dutta and Maiti, 2015) and zebrafish (Thisse and Thisse, 2005; Kida et al., 2007; Lai et al., 2008; Santos-Ledo et al., 2013; Sun et al., 2014). The conservation of multiple formins with overlapping expression in the nervous system possibly reflects a diversity of distinct regulatory functions, ensuring the highly adaptive yet specific cytoskeleton remodelling necessary for accurate circuit development.

1.10 Zebrafish neural circuits and behaviour

Zebrafish is an excellent vertebrate model to interrogate gene function in establishing neural circuits *in vivo* and associated behaviours (Kalueff et al., 2013; McArthur et al., 2020). Zebrafish larvae have tractable neural circuits responsible for fairly complex

behaviours early in development. It allows us to discover and dissect the contribution of a gene in the development of modular neural ensembles and track changes in behaviour. Zebrafish have been extensively used for reverse and forward genetics studies. ENU and insertional mutagenesis screens have identified a large number of mutants in zebrafish classified based on the affected tissues or function, for example, locomotion, notochord, somite formation, inner ear and development in general (Granato and Nüsslein-Volhard, 1996; Granato et al., 1996; Haddon and Lewis, 1996; Haffter et al., 1996; Odenthal et al., 1996; Schier et al., 1996; Amsterdam et al., 1999; Nusslein-Volhard, 2012). So far, many of these mutants have been mapped to the genes responsible for the phenotypes observed in the mutants, and a lot has been learnt from behavioural genetics using zebrafish mutants (Burgess and Granato, 2008). The space cadet (*spc*) mutant was first phenotypically characterized to have defects in the outgrowth of spiral fiber neurons and Retinal Ganglionic cells (RGCs) and was later mapped to the Retinoblastoma-1 (Rb1) gene (Lorent et al., 2001; Gyda et al., 2012). Mutants with aberrant development of primary motor neurons like *diwanka*, *unplugged*, *stumpys* shed light on the genetic control of outgrowth and pathway selection by motor neurons (Granato et al., 1996; Zeller and Granato, 1999; Hutson and Chien, 2002a; Schweitzer et al., 2005). Differential labelling of the temporal and nasal retinotectal projections by DiI and DiO revealed retinal exit, midline crossing, elongation, pathfinding, topographic innervation errors and arborization phenotypes a variety of mutants (Baier et al., 1996; Karlstrom et al., 1996).

Figure 1.13

On the other hand, a lot of work has been done to identify individual neural circuits in zebrafish and their modular assembly leading to efficient behaviour generation. One of the most studied neural circuits is the Mauthner cell-mediated escape response circuit (Swain et al., 1993; Jontes et al., 2000; Korn and Faber, 2005; Burgess et al., 2009; Sillar, 2009; Issa et al., 2011; Kinkhabwala et al., 2011; Hale et al., 2016; Liu and Hale, 2017). Mauthner mediated escapes are essential to the survival of the zebrafish in the wild environment. The ability to respond in time to evade a predator is equally crucial, if not more, than quickly hunting its prey. Mauthner cells are command neurons for zebrafish locomotion that are under regulation by a variety of neurotransmitters through excitatory and inhibitory interneurons and direct sensory input. Most of the locomotor behaviours require the Mauthner cell activity in response to varying stimuli like tactile, visual or acoustic (Lee and Eaton, 1991; Korn and Faber, 2005; Issa et al., 2011). In

addition to the command Mauthner cell, other neurons and circuit assemblies regulate complex behaviours in zebrafish embryos. Visual information is relayed to the Mauthner cells by the optic tectum (Zottoli et al., 1987). Tactile and acoustic stimulus is received by the Mauthner cell via the peripheral and intraspinal sensory neurons, lateral line system and the inner ear (Kuwada et al., 1990b; Nicolson et al., 1998; Higgs and Radford, 2013; Stewart et al., 2014; Fidelin et al., 2015; Hubbard et al., 2016; Knafo and Wyart, 2018). The Mauthner also received integrated information from sensorimotor integrating nuclei in the brain like the nMLF (Severi et al., 2014). On the other side, the inputs received and processed by the Mauthner cell, and the upstream neural circuits are executed by the motor neurons.

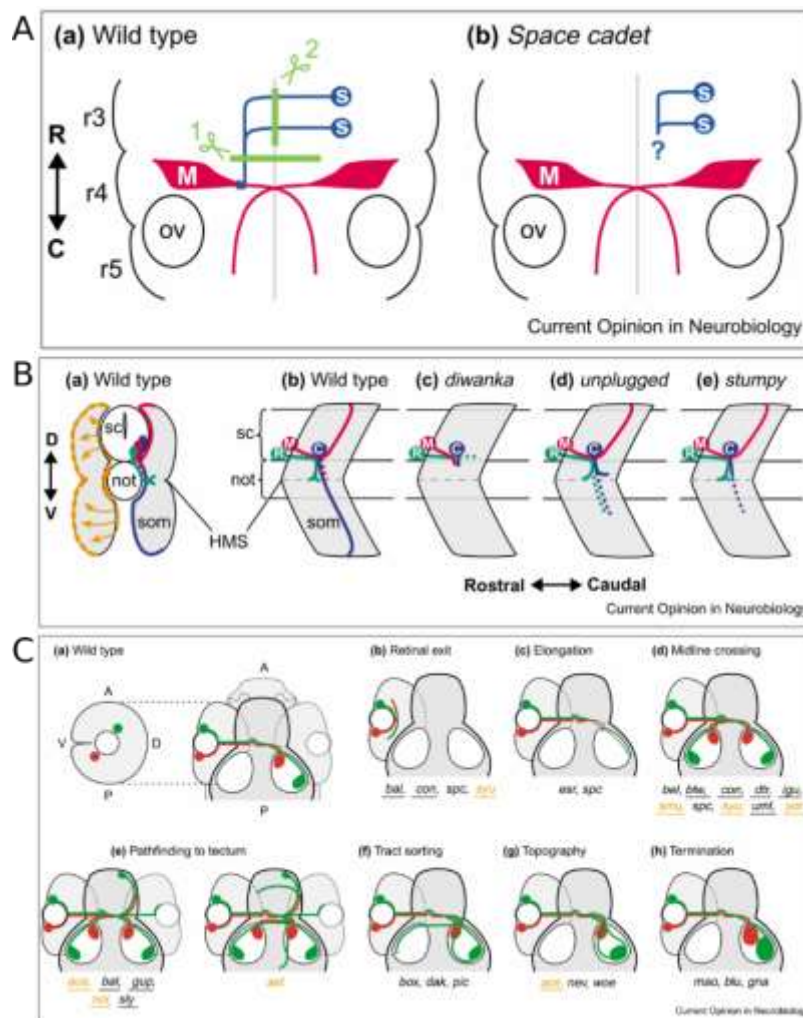


Figure 1.13 Zebrafish mutants uncover axonal outgrowth and pathfinding errors. A) Space Cadet (*spc*) mutant shows the absence of commissural spiral fiber tracts required for fast escape responses. B) Mutants showing outgrowth and pathfinding errors in motor neurons. C)

Erroneous guidance and pathfinding of retinotectal projections in various zebrafish mutants. r3: rhombomere 3, r4: rhombomere 4, r5: rhombomere 5, ov: otic vesicle, M: Mauthner cell, s: spiral fiber neurons. (Hutson and Chien, 2002a)

Zebrafish behaviour can be observed from the early stages of development. Zebrafish embryos start to show muscle activity and spontaneous tail coiling beginning at 17 hpf in response to the firing of the developing motor neurons. Soon after, around 48 hpf, zebrafish embryos start responding to touch by a C-bend escape response. The touch evoked escape response is regulated by reticulospinal and motor neurons in coordination with each other. As the zebrafish embryos undergo a surge in neuronal connectivity, more complex behaviours begin to appear. Around 4 dpf, as the neuromodulatory input kick in, complex locomotor repertoires comprising of multiple locomotory motifs arranged in a temporally regulated sequence and tuned to the environmental stimuli can be observed (Saint-Amant and Drapeau, 1998; Brustein et al., 2003; Kalueff et al., 2013; Marques et al., 2018). **Figure 1.14**

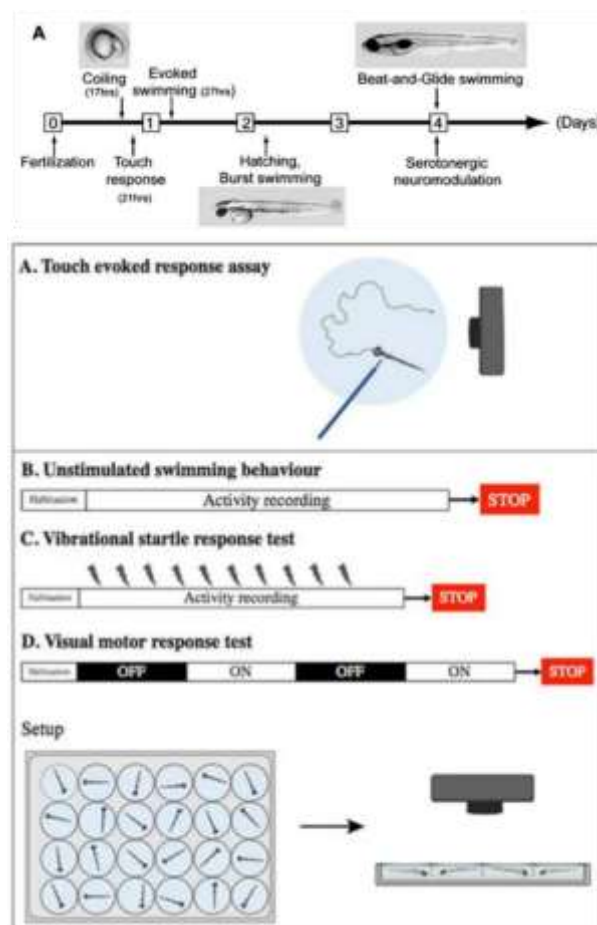


Figure 1.14 Behavioural assays to probe neural circuit function in zebrafish. Locomotor behaviours emerge across development stages in zebrafish. Schematics outlining touch evoked

escape response (TEER) assay, free swimming and acoustic and visual stimulus-evoked swimming assays. (Brustein et al., 2003; Vaz et al., 2019)

Put together, zebrafish provides a unique opportunity to study the role of cytoskeletal remodelling in the developing neurons *in vivo* with the possibility of direct visualization of the subcellular dynamics, tractable neuronal development and behavioural analysis. The genetic and optical amenability makes zebrafish an ideal organism to uncover the function of genes in health and disease.

2

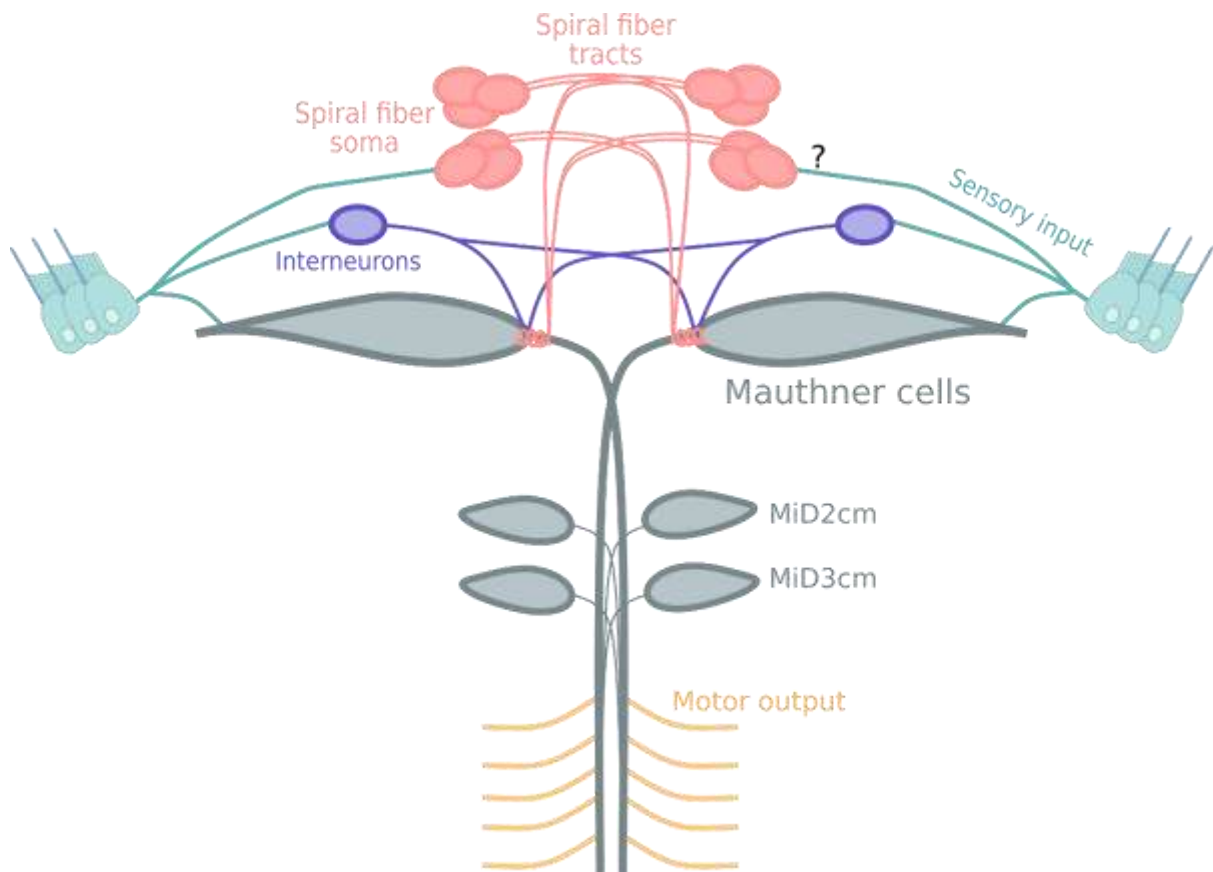
Role of Fmn2b in the
development of spiral fiber
neurons and the regulation
of short latency escape
responses in zebrafish

2.1 Introduction

One of the most studied neural circuits is the Mauthner cell-mediated acoustic startle circuit (Swain et al., 1993; Jontes et al., 2000; Korn and Faber, 2005; Burgess et al., 2009; Sillar, 2009; Issa et al., 2011; Kinkhabwala et al., 2011; Hale et al., 2016; Liu and Hale, 2017; Hecker et al., 2020). Acoustic and tactile stimuli from the environment are processed by the Mauthner cells (M-cells) aided by regulatory excitatory and inhibitory interneuron module and relayed to the motor neurons downstream (Korn and Faber, 2005). Mauthner mediated escapes are essential to the survival of the zebrafish in the wild environment. The acoustic startle circuit comprising sensory inputs to the M-cells and regulatory interneurons imparts the ability to respond in time to evade a predator.

M-cells and two segmental homologs, MiD2cm and MiD3cm, are needed for eliciting a coordinated escape response by a zebrafish larva tuned to the severity of the received stimulus. (Liu and Fetcho, 1999; Kohashi and Oda, 2008). M-cell and its homologs receive a common auditory input but can generate different outputs, evident by their different spiking properties, to downstream neurons to control adaptive escape behaviours. MiD2cm and MiD3cm mediate escapes with longer latencies as compared to the M-cell (Nakayama and Oda, 2004; Kohashi et al., 2012a; Lacoste et al., 2014). The M-cell homologs ensure that an escape response is elicited in the absence of M-cell firing or for weaker stimuli. Ablation of the M-cell, especially the axon initial segment, causes an increase in latency of response to mechano-acoustic stimuli (Liu and Fetcho, 1999; Hecker et al., 2020).

The auditory input received by sensory organs like the inner ear is processed and relayed via hair cell mechanotransduction followed by the ribbon synapses at the base of hair cells (Haddon and Lewis, 1996; Tanimoto et al., 2011; Nicolson, 2017). The afferents directly relay the information to the Mauthner cell as well as several interneurons making a mix of chemical and electrical synapses (Nakajima and Wang, 1974; Moly and Hatta, 2011; Kohashi et al., 2012b; Lacoste et al., 2014). However, it remains unknown if the sensory input is directly received by the spiral fiber neurons in the hindbrain.



The Mauthner cell escape circuit in larval zebrafish.

Spiral fiber neurons are excitatory interneurons present in the rhombomere 3 and make direct connections at the contralateral M-cell axon hillock via chemical and electrical synapses (Nakajima, 1974; Scott et al., 1994; Lacoste et al., 2014; Hale et al., 2016; Marsden et al., 2018a). The spiral fiber junction at the M-cell is rich in connexin-35 and, therefore gap junctions mediating fast responses via M-cell in response to acoustic stimuli (Jabeen and Thirumalai, 2013). There are several other excitatory and inhibitory interneurons which provide input to the M-cell in turn regulating its activity tuned to the stimulus context and intensity. It has been shown that the ablation of spiral fiber neurons causes abolition of short latency escape responses in zebrafish (Lacoste et al., 2014). Feedforward excitatory input from spiral fiber neurons is essential for the Mauthner cells to elicit fast response to an aversive acoustic stimulus, without the involvement of the lateral line (Lacoste et al., 2014).

Other than acoustic input, Mauthner cell also receive visual and tactile sensory input from the optic tectum and lateral line respectively and primarily guide the directional response of Mauthner cells (Zottoli et al., 1987; Lee et al., 1993; Korn and Faber, 2005).

Ultimately, the Mauthner cell executes the escape response by exciting the contralateral myotomes via motor neurons (Fetcho and Faber, 1988; Fetcho, 1991). The M-cell and motor neurons fire almost in parallel, ensuring that the muscle activation is in close coordination with the command from the Mauthner cells. Other than the connections with motor neurons, M-cell also makes connections with pre-motor interneurons in the spinal cord to regulate swimming in zebrafish (Fetcho and Faber, 1988; Fetcho, 1991).

The functions of the various components of the acoustic startle circuit described above have been extensively characterized but there is a scope for investigating the genes responsible for the development of the neurons in this circuit. This chapter describes the role of *fmn2b* in development of the neural circuits underlying acoustic startle in zebrafish.

2.2 Results

2.2.1 *Fmn2b*, the zebrafish ortholog of *Fmn2* has conserved formin homology domains

Zebrafish has two paralogs of *Fmn2*, *fmn2a* and *fmn2b*. Reciprocal BLASTp analysis of the predicted protein sequence of *Fmn2b* revealed that the ortholog *Fmn2b* (E7F517) (UNIPROT) has the highest sequence identity with human *Fmn2* (53.82 % **Figure 2.1A**). *Fmn2a* (X1WC43) (UNIPROT) was found to have considerably less sequence identity with human *Fmn2* (44.75 %). While *Fmn2a* has a characteristic FH2 domain, the FH1 domain is truncated to 33 amino acids. Further, mRNA corresponding to *fmn2a* was expressed at very low levels in zebrafish larvae with no detectable signal in the nervous system up to 96 hpf (data not shown). Therefore, *fmn2b* was considered to be the functional ortholog of Formin-2 in zebrafish. High amino acid sequence similarity was observed between the human (Q9NZ56), mouse (Q9JL04), chick (NP_001317992) and zebrafish *Fmn2* (E7F517) orthologs with the C-terminal FH1, FH2 and FSI domains showing ~70% similarity (**Figure 2.1A, A'**).

2.2.2 *Fmn2b* is expressed in the zebrafish nervous system

The expression pattern of *fmn2b* mRNA in zebrafish across developmental stages (**Figure 2.1 B-J**) was observed using whole mount *in situ* hybridization. The *fmn2b* mRNA was found to be maternally deposited, as seen in 1 cell stage zebrafish embryos, and the expression persisted till 3 hours post fertilization (hpf). There was no discernible *fmn2b* mRNA expression at stages from 6 hpf to 18 hpf. The mRNA expression reappeared in the telencephalon/forebrain at 24 hpf (**Figure 2.1 H**). At stages 48 hpf onwards, the expression extends to the diencephalon/midbrain, the rhombencephalon/hindbrain, the spinal cord and the retinal ganglion cells (RGC) layer of the eye. Similar expression pattern is observed at 96 hpf (**Figure 2.1I-J**). In line with previous studies showing the expression of *fmn2* in the nervous system of human, mice (Leader and Leder, 2000), and chick (Sahasrabudhe et al., 2016), *fmn2* mRNA is also enriched in the zebrafish nervous system.

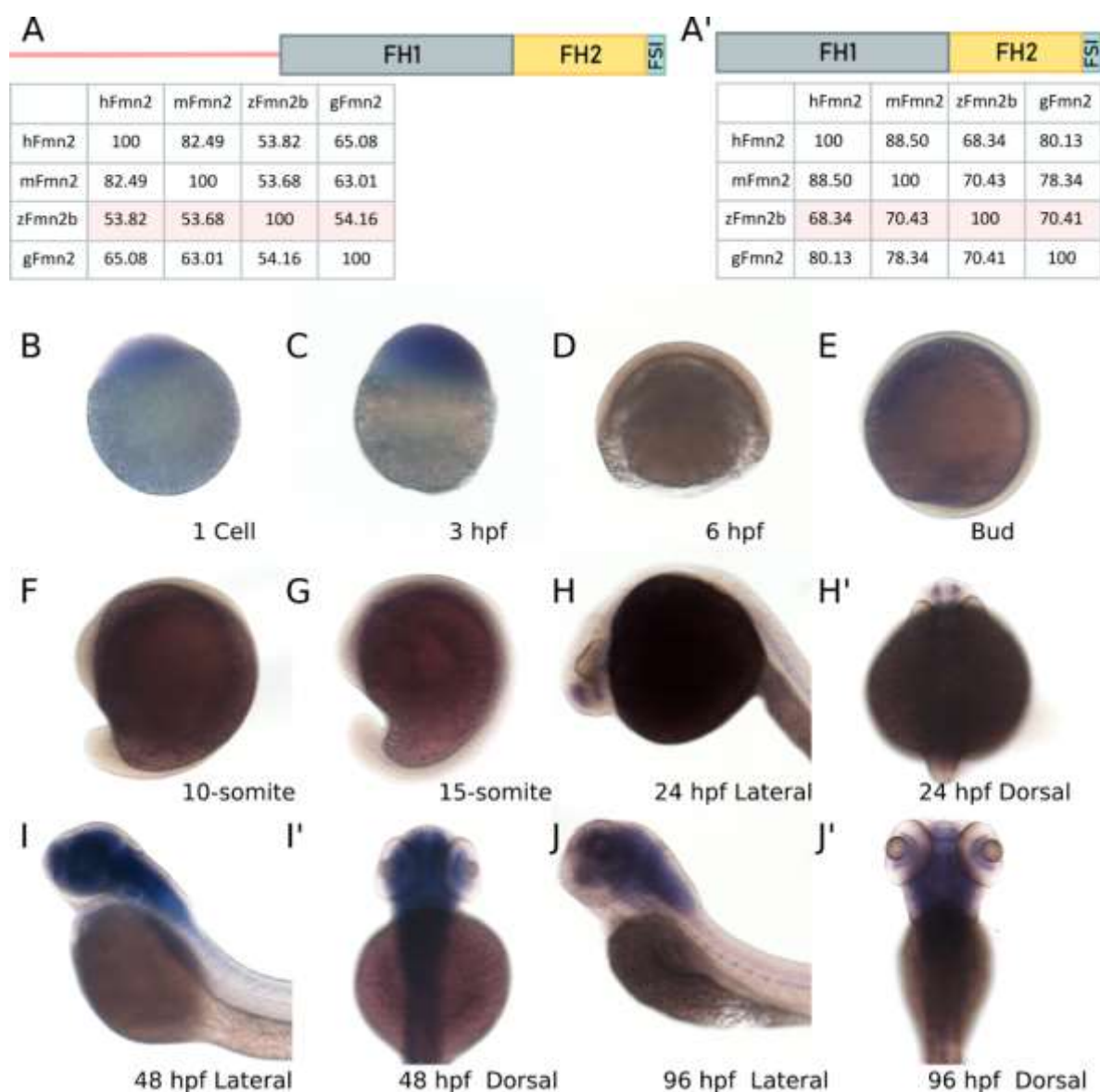


Figure 2.1 *fmn2b* mRNA is maternally deposited and enriched in the zebrafish nervous system

Amino acid sequence alignments were obtained using EMBL Clustal Omega for human Fmn2 (hFmn2), mouse Fmn2 (mFmn2), zebrafish Fmn2b (zFmn2) and chicken Fmn2 (gFmn2) to compare conservation of sequence across vertebrate species. Percent identity matrices are shown for comparison of full length Fmn2 and the functional domains of Fmn2 across species. **A)** Full length zFmn2 showed 53.82%, 53.68% and 54.16% sequence similarity for human, mouse and chicken Fmn2 respectively. **A')** On comparing the functional domains of Fmn2, namely Formin Homology 1 (FH1), Formin Homology 2 (FH2) and Formin Spire Interaction domain (FSI), 68.34%, 70.43% and 70.41% sequence similarity with human, mouse and chicken Fmn2, was found. **B-J)** Representative images of whole mount mRNA in situ hybridization showing the *fmn2b* mRNA expression pattern in the developing zebrafish embryo. *fmn2b* mRNA can be found in **B)** 1 cell stage and **C)** 3 hpf embryos suggesting maternal deposition. The mRNA expression is negligible during **D)** 6 hpf, **E)** bud stage, **F)** 10-somite and **G)** 15 somite embryos. *fmn2b* mRNA expression is regained in **H)** 24 hpf embryos and continues to be expressed until 96 hpf (**I-J')**.

2.2.3 Morpholino mediated knockdown of Fmn2b

To test the contribution of Fmn2b in development of the nervous system, two antisense morpholinos, one translation blocking (MO TB Fmn2b) and one splice blocking (MO SB Fmn2b) were designed (Reagents and Procedures). The MO TB Fmn2b morpholino targets the first exon and the MO SB Fmn2b blocks splicing at the boundary of the fifth exon and intron (**Figure 2.2 A**).

The splice blocking morpholino would result in a truncated protein devoid of the characteristic functional FH1, FH2 and FSI domains and the translation blocking morpholino would cause depletion of the protein levels *in vivo*. To test the extent of knockdown by MO SB Fmn2b, RT-PCR was performed to ensure incorporation of the intron after exon 5 causing incorporation of a stop codon in the translation frame (**Figure 2.2 B**). In 48 hpf MO SB Fmn2b morphants, majority of the *fmn2b* mRNA was present in the splice-blocked form evident from the 550 bp amplicon corresponding to inclusion of the intron between exons 5 and 6, as compared to the spliced version with an expected amplicon size of 251 bp (**Figure 2.2 B**).

The embryos injected at 1 cell stage with morpholinos against *fmn2b* mRNA exhibited morphological defects like shortening of body length, swim bladder deflation, otolith defects, cardiac edema and axial curvature (**Figure 2.2 C, D**). These were excluded from further experiments. The larvae with no visible morphological defects similar to the control morphants were used.

2.2.4 Assessment of behavioural defects using automated acoustic stimulus delivery and high-speed video recording

To evaluate the effect of Fmn2 knockdown on behaviour, the responses of control and *fmn2b* morphants was observed in response to manual tapping of the dish containing the larvae. In this preliminary experiment, uncoordinated locomotion was exhibited by *fmn2b* morphants. For better resolution of these behavioural defects, high speed video recording was employed and the response of morphants to mechano-acoustic stimuli was recorded. In this assay, 96 hpf morphants were head restrained and given a tap on the dish in which they were housed and their response was measured by tracking the movement of their tails. The response of the morphants was recorded at 640 fps using a high-speed video recording camera (AVT Pike, F-032B). The taps were delivered at an

interval of 10 seconds controlled by an Arduino UNO microprocessor and powered by a DC power supply (Figure 2.3). The automated acoustic stimulus delivery setup allowed high speed recording, delivery of intensity-controlled stimulus and feedback information integration into the recorded video timestamp to mark the advent of stimulus (Figure 2.3).

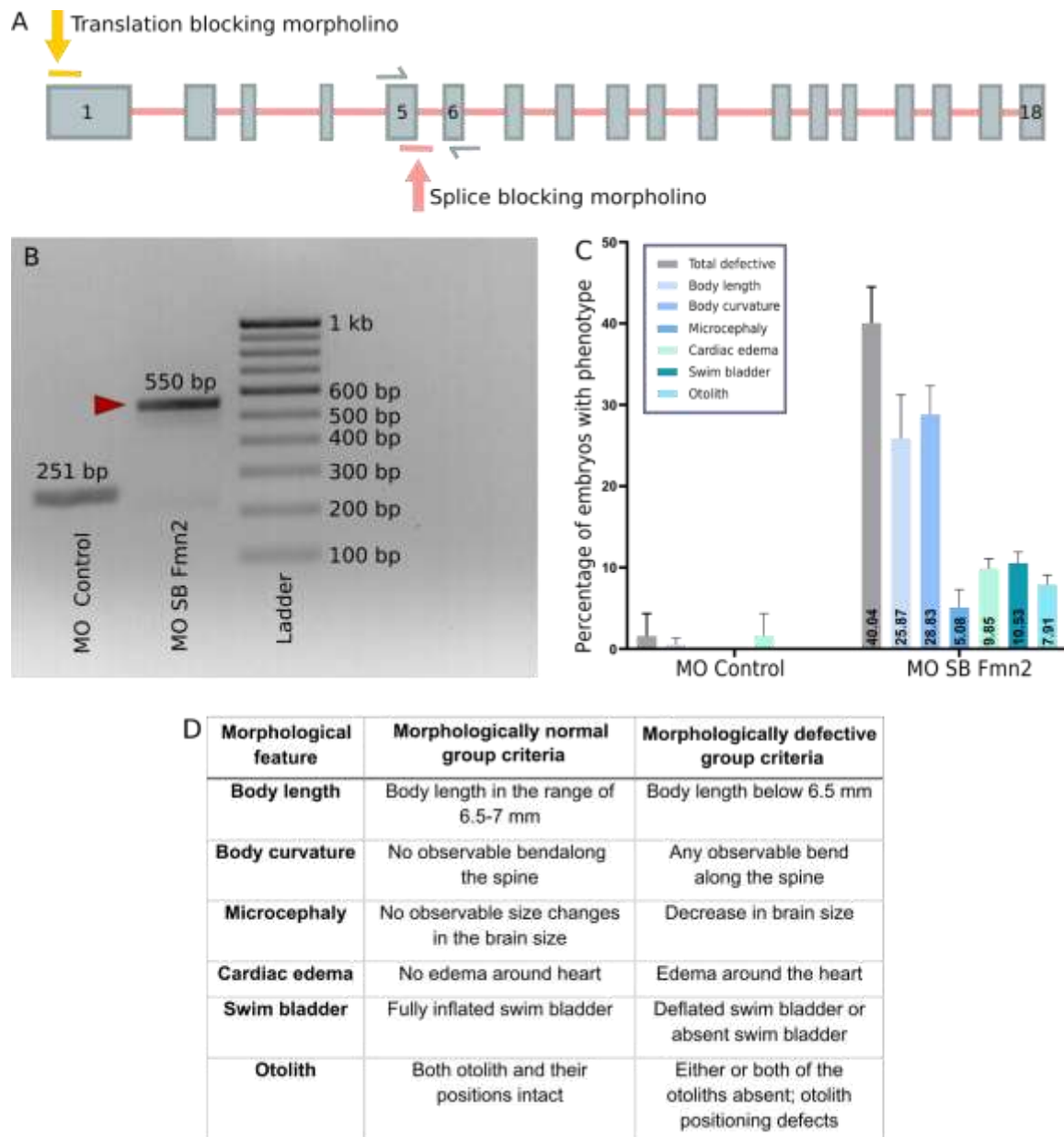


Figure 2.2 Morpholino design, validation, and assessment of morphological defects in morphants.

A) Schematic showing target regions for the two morpholinos used in the experiments. MO TB Fmn2b targets exon 1 to block translation. MO SB Fmn2b targets the exon 5 – intron 5 boundary to cause retention of intron 5 between exons 5 and 6, leading to the occurrence of a premature

stop codon. Both morpholinos ensure that the functional domains are not translated in Fmn2b morphants. B) Validation of knockdown by MO SB Fmn2b morpholino was done using RT-PCR on cDNA obtained from MO Control and MO SB Fmn2b injected embryos. The amplification of a 550 bp amplicon from MO SB Fmn2b morphants cDNA corresponds to inclusion of intron 5 because of efficient splice blocking by the morpholino C) Graph summarizing morphological defects in Fmn2b morphants injected with 2 ng of MO SB Fmn2b. The percentage of embryos showing the various defects are indicated at the bottom of each bar corresponding to the defect. A total of 40.04% embryos in the morphant population showed defects spanning from a few or all of the defects listed. Each bar represents the percentage of embryos exhibiting that morphological defect. Morphologically aberrant embryos often exhibited multiple defects together. D) Table enlisting the parameters used to distinguish between morphologically aberrant and normal embryos. These parameters were used for classification of both morphant and crispant populations.

The tap strength using the piston was controlled by varying the input voltage on the variable power supply. For all the experiments, tap strength corresponding to 13 volts was used. This tap strength was optimized to achieve about 95% responsiveness in the control zebrafish larvae. The responsiveness of the Fmn2b morphants (injected with 2 ng/embryo MO SB Fmn2b) to the same mechano-acoustic stimulus was comparable (94%) to the control animals.

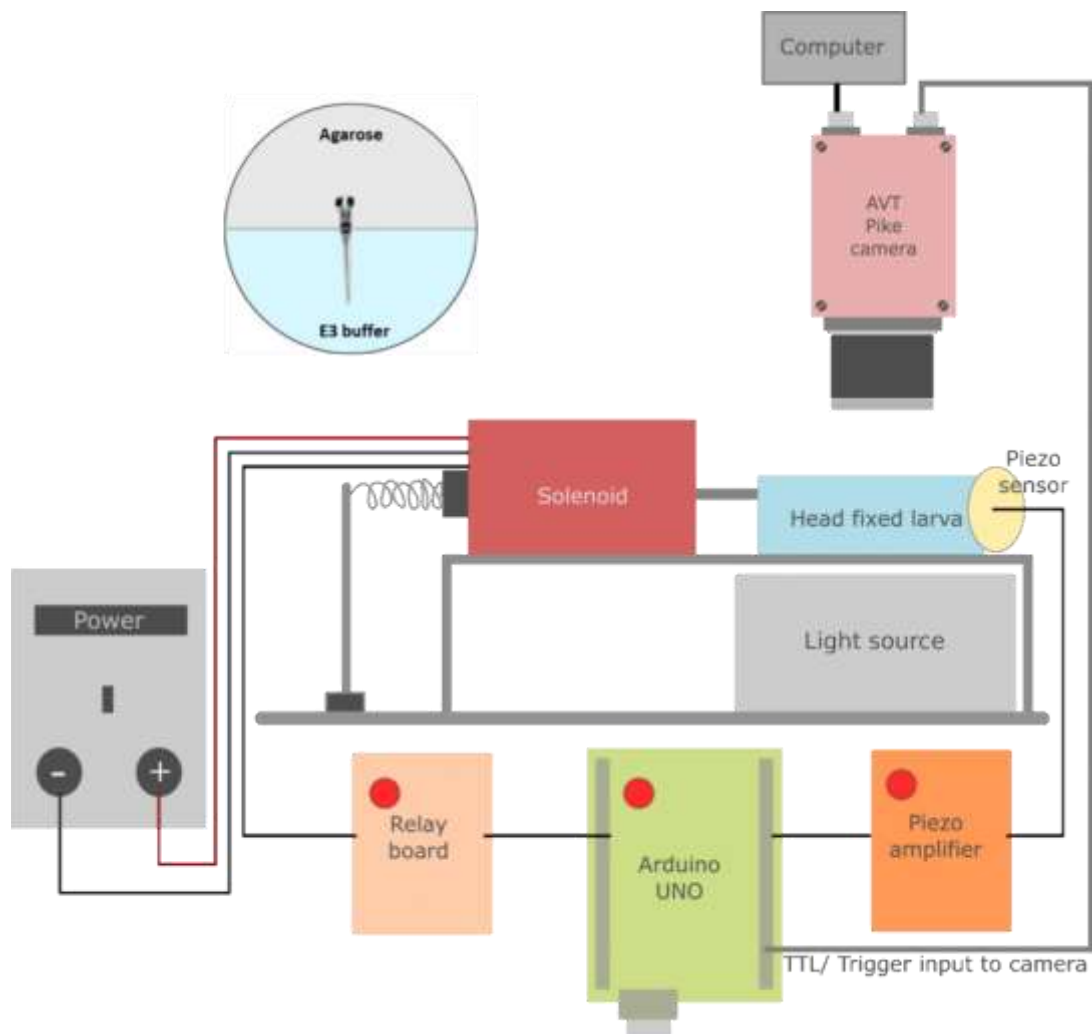


Figure 2.3 Automated acoustic stimulus delivery apparatus with feedback loop. Schematic describing the setup used to deliver acoustic stimulus to zebrafish larvae with their heads embedded in low melt point agarose and their tails freed to record swimming.

The recorded videos were analyzed using a custom written python program to extract timestamp and the body axis coordinates after skeletonizing the shape of the fish (**Figure 2.4**). The software was developed in collaboration with Dr Tomin K James, IISER Pune. The output from the custom python software included the following parameters, as mentioned below:

Latency to first movement: Time taken by the fish to initiate movement post stimulus delivery, marked by an angle change greater than five degrees.

C-bend Max: Maximum angle of C-bend escape (with respect to the head restrained segment)

Latency to C-bend Max: Time taken by the fish to reach the maximum C-bend escape angle, calculated by subtracting latency to first movement from the total time taken to reach maximum angle.

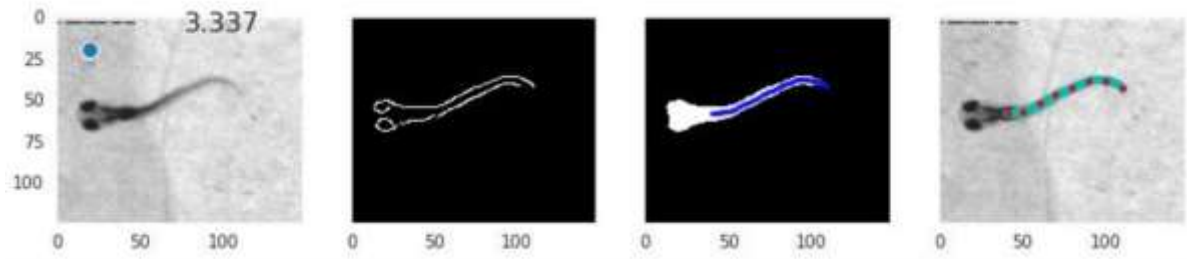


Figure 2.4 Schematic showing representative snapshots from the custom written software for zebrafish tail tracking.

The quantified output was plotted using Estimation statistics. Briefly, the median difference comparisons against the control morpholino (MO Control) are shown in the Cumming estimation plots. The raw data was plotted on the upper axes as individual dots. The vertical gapped lines summarize the median \pm standard deviation for each group. On the lower axes, median differences were plotted as bootstrap sampling distributions obtained by resampling the data 5000 times. The median difference was depicted as a dot for respective groups as compared to the shared control. The 95% confidence interval was indicated by the ends of the vertical error bars (**Figure 2.5 B-F**).

2.2.5 Fmn2b morphants exhibit a delay in initiating the escape response

Zebrafish larvae respond to acoustic stimulus by swimming away from the perceived source. The nature of response in terms of initiation, speed and strength is dependent on the stimulus. Some stimuli warrant a quick response while for others a slow but sustained response is adequate. Acoustic stimulus is associated with a predatory threat for zebrafish larvae due to which they respond with short latencies for potent obnoxious stimuli. The setup described above was used to test the response of Fmn2b morphants to acoustic stimulus and the videos acquired were processed using the custom python software for tail tracking.

The Fmn2b morphants showed an increased latency to first movement (11.54 msec; [9.36,13.38]; n=120; **Figure 2.5 B**) in response to the mechano-acoustic stimulus as compared to the control morphants (6.74 msec; [5.39,9.06]; n=126; **Figure 2.5 B**). To ensure that the morpholino's effect was specific to Fmn2b, mouse Fmn2-GFP (mFmn2-GFP) mRNA, which is resistant to the anti-zebrafish Fmn2b morpholino, was co-injected along with the Fmn2b morpholino. The increased latency could be rescued in Fmn2b morphant larvae co-injected with mFmn2-GFP mRNA (5.16 msec; [4.03,6.29]; n=83; **Figure 2.5 B**). Previous reports implicate Mauthner cells (M-cell) in mediating short latency (SLC; <13 msec) escapes in response to mechano-acoustic stimuli (Lacoste et al., 2014). Whereas, long latency escapes are generally non-Mauthner mediated responses. The latencies to the first movement were classified as short latency C-bend (SLC; <13 msec) and long latency C-bend events (LLC; 13-26 msec). Of the total number of events, there was a decrease in the fraction of SLC versus LLC responses in Fmn2b morphants. In morphants co-injected with mFmn2-GFP mRNA, the fraction of events showing SLC responses was greater than LLC responses as seen in control morphants (**Figure 2.5 C, D**).

However, the latency to achieve maximum C-bend escape angle (**Figure 2.5 E**) and the maximum escape angle (**Figure 2.5 F**) were comparable between the control morphants, the Fmn2b morphants and the Fmn2b morphants co-injected with mouse *fmn2* mRNA.

Hence, Fmn2b knockdown increased the latency to respond to mechano-acoustic stimuli even though the responsiveness and the ability to elicit an escape response remains uncompromised. These results suggest a specific and perhaps localized defect in the mechano-acoustic response circuitry.

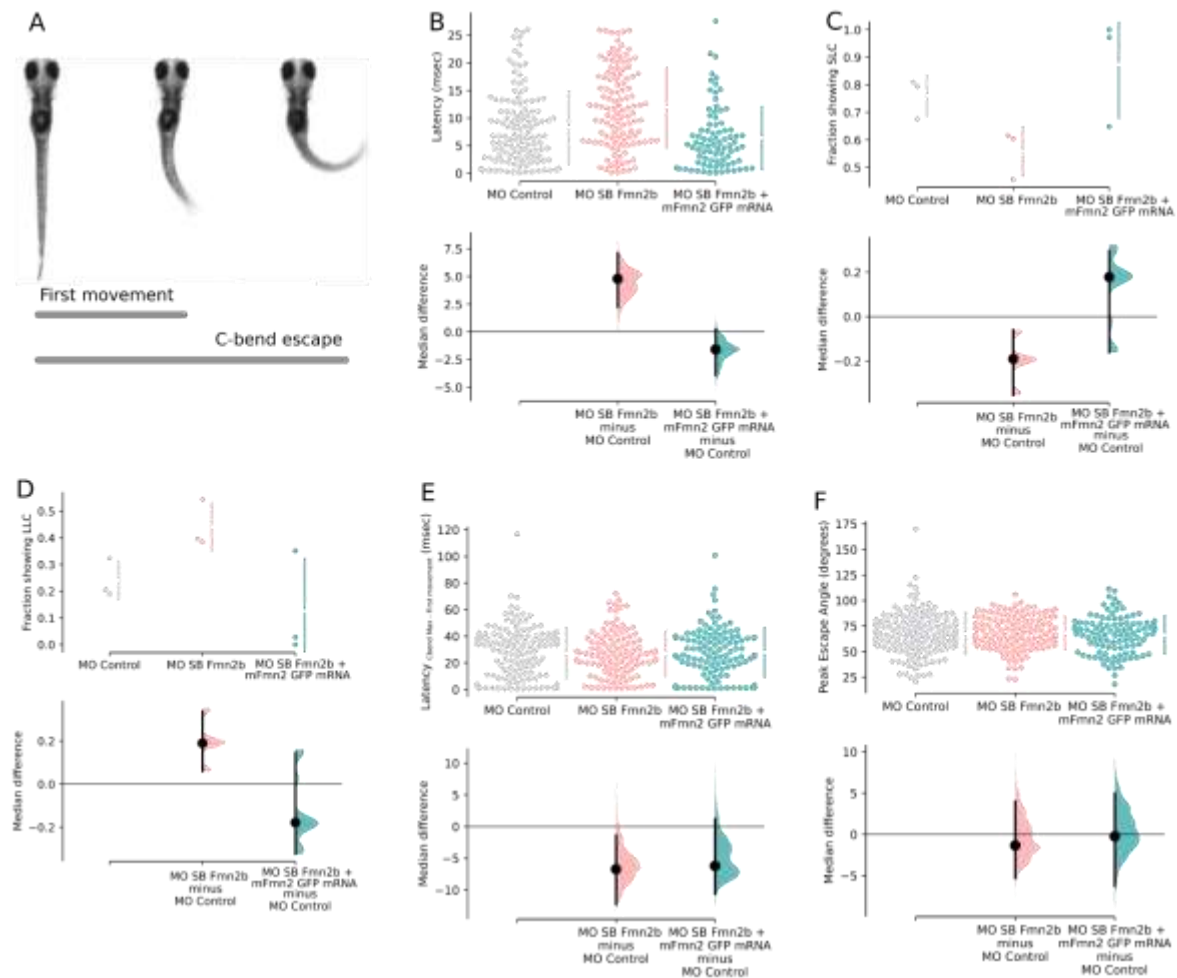


Figure 2.5 Fmn2b knockdown increased the latency to respond to mechano-acoustic stimulus

A) Schematic describing the movements qualifying as the first movement for latency calculation and maximum C-bend for the escape response following the mechano-acoustic stimulus. B) Latency to first movement (msec) is plotted in this graph. The unpaired median difference between MO Control (n=126) and MO SB Fmn2b (n=120) is 4.8 [95.0%CI 2.23, 7.1]. The p-value of the two-sided permutation t-test on the median differences is 0.0. The unpaired median difference between MO Control and MO SB Fmn2b + mFmn2-GFP mRNA (n=83) is -1.58 [95.0%CI -3.89, 0.232]. The p-value of the two-sided permutation t-test on the median differences is 0.081. C) Values calculated for the fraction of the population (n=3) showing Short Latency C bend response (SLC) (< 13 msec) are plotted in this graph. The unpaired median difference between MO Control and MO SB Fmn2b is -0.201 [95.0%CI -0.308, -0.107]. The p-value of the two-sided permutation t-test is 0.0. The unpaired median difference between MO Control and MO SB Fmn2b + mFmn2-GFP mRNA is 0.114 [95.0%CI -0.151, 0.266]. The p-value of the two-sided permutation t-test is 0.357. D) Values calculated for the fraction of the population (n=3) showing Long Latency C bend response (LLC) (13-26 msec) are plotted in this graph. The unpaired median difference between MO Control and MO SB Fmn2b is 0.201 [95.0%CI 0.104, 0.303]. The p-value of the two-sided permutation t-test is 0.0. The unpaired median difference between MO Control and MO SB Fmn2b + mFmn2-GFP mRNA is -0.114 [95.0%CI -0.276, 0.111]. The p-value of the two-sided permutation t-test is 0.29. E) The difference of time taken to achieve the maximum C-bend angle and the latency to first movement for each trial is plotted in this graph. The unpaired

median difference between MO Control and MO SB Fmn2b is -6.71 [95.0%CI -12.2, -1.4]. The p-value of the two-sided permutation t-test is 0.0526. The unpaired median difference between MO Control and Rescue is -6.2 [95.0%CI -10.6, 1.17]. The p-value of the two-sided permutation t-test is 0.152. F) This graph shows the maximum angle (C-bend max) attained during the escape response. The unpaired median difference between MO Control and MO SB Fmn2b is -1.34 [95.0%CI -5.31, 4.0]. The p-value of the two-sided permutation t-test is 0.694. The unpaired median difference between MO Control and Rescue is -0.235 [95.0%CI -6.26, 4.98]. The p-value of the two-sided permutation t-test is 0.875. For all the estimation statistics analysis, the effect sizes and CIs are reported as effect size [CI width lower bound; upper bound].

2.2.6 Fmn2b depletion does not affect the sensory components of the acoustic startle circuit

The acoustic startle response is essential for the survival of zebrafish larvae in terms of reacting to the environment efficiently and reliably. The behavioural deficits observed in Fmn2b morphants could arise from one or more components of the acoustic startle circuit. Different components of the acoustic startle circuit were systematically evaluated to identify the origins of the delay in the initiation of the C-bend escape in Fmn2b morphants. M-cells receive auditory input from the inner ear hair cells, relayed by the statoacoustic ganglion (SAG) (Whitfield et al., 2002; Medan and Preuss, 2014). Evaluation of the otic vesicle and the otoliths did not reveal any anatomical or structural defects. The structural integrity of the inner ear hair cells responsible for the mechanotransduction of the acoustic cues, was probed using the Tg(*brn3c*:GAP43-GFP) line. This line labels a subset of the hair cells in the inner ear and lateral line neuromasts (Xiao et al., 2005b). Microscopic analysis of kinocilia and hair cell bundles of the inner ear cristae revealed no significant differences between control and Fmn2b morphants (**Figure 2.6 A-D**). Uptake of the lipophilic dye FM 4-64 was used to evaluate the functional activity of the inner ear hair cells (Pacentine and Nicolson, 2019). These experiments indicated that activity-dependent vesicle recycling was comparable between control and Fmn2b morphants (**Figure 2.6 E, F**) and suggested that the synaptic activity at the hair cell ribbon synapses is mostly unaffected in the Fmn2b morphants.

The next component of the acoustic startle circuit tested was the Statoacoustic ganglion (SAG) which connects the inner ear hair cells to the M-cell. SAG was also found to be structurally unperturbed as evident in 96 hpf morphants immunostained with anti-neurofilament 3A10 antibody (**Figure 2.7 A, B**).

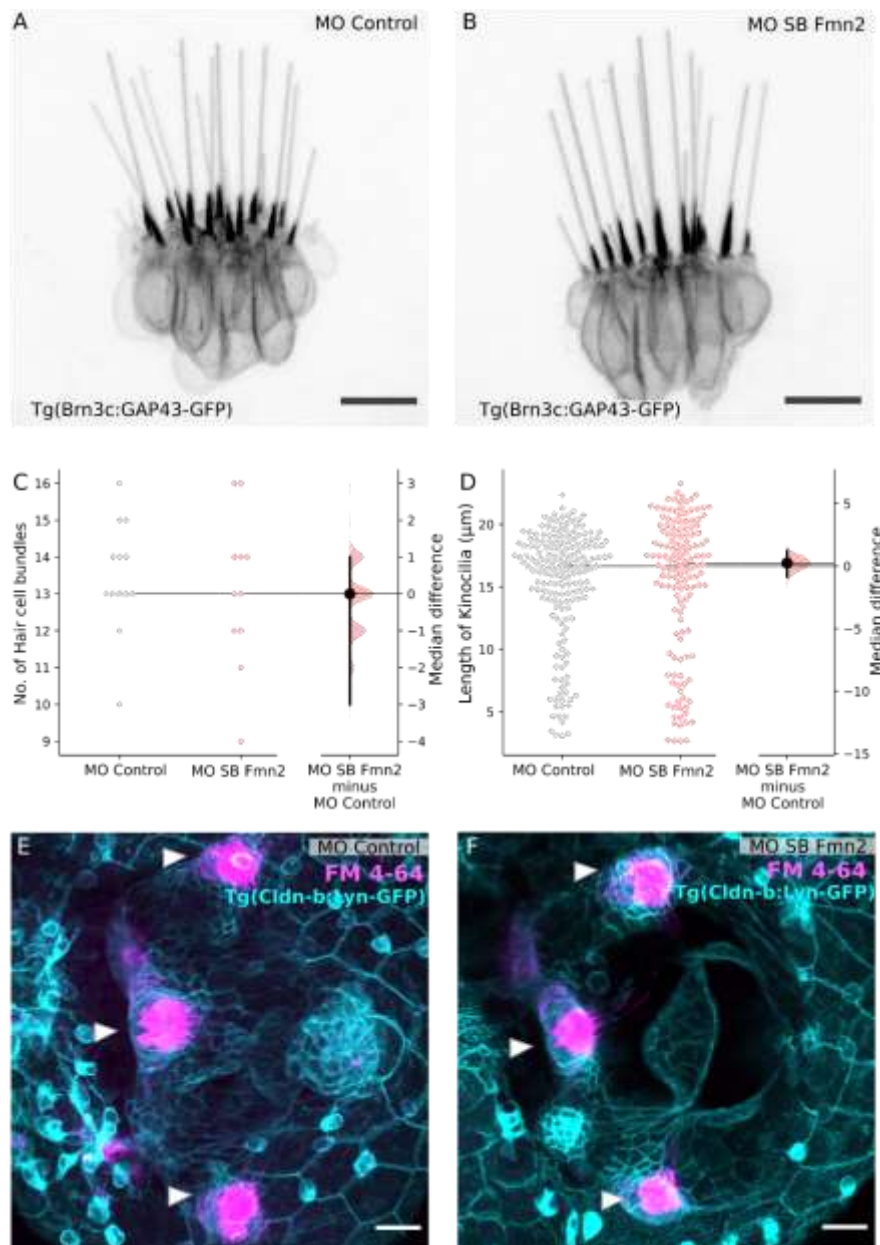


Figure 2.6 Sensory components of the acoustic startle circuit are not affected in *Fmn2b* morphants

Hair cells of the lateral crista of the zebrafish inner ear are visualized using the Tg (*brn3c*:GAP43-GFP) line in 96 hpf larvae with **A)** 2 ng MO Control and **B)** 2 ng MO SB *Fmn2b* cytoplasmic injections. Scale bar is equivalent to 10 μ m. **C)** Quantification of the number of hair cell bundles with a kinocilium is depicted in the Gardner-Altman plot. The unpaired median difference between MO Control and MO SB *Fmn2b* is 0.0 [95.0%CI -3.0, 1.0]. The p-value of the two-sided permutation t-test is 0.687. **D)** Quantification of kinocilia length in the lateral crista hair cells is shown in the Gardner-Altman plot. The unpaired median difference between MO Control and MO SB *Fmn2b* is 0.247 [95.0%CI -0.851, 1.25]. The p-value of the two-sided permutation t-test is 0.663. For all the estimation statistics analysis, the effect sizes and CIs are reported as effect size [CI width lower bound; upper bound]. Representative images for FM-4-64 dye uptake assay in the inner ear of 96 hpf **E)** control morphants and **F)** *Fmn2b* morphants, done in the background of Tg(*cldnb*:lyn-GFP) to mark the inner ear boundary. Scale bar is equivalent to 20 μ m.

Further, the reticulospinal neurons in the hindbrain of 4 dpf morphants were labelled using TMR Dextran to assess the integrity of the M-cell and its homologs MiD2cm and MiD3cm. The M-cell and its homologs, primarily responsible for regulating acoustic startle responses were found to be intact in Fmn2b morphants (Figure 2.7 C, D). Immunostaining of 48 hpf morphants was performed using another anti-neurofilament antibody RMO-44 which has better reactivity than 3A10 for hindbrain cell bodies. The cell bodies and axonal tracts of reticulospinal neurons were comparable between the control and Fmn2b morphants (**Figure 2.7 E, F**).

In conclusion, the sensory components of the acoustic startle circuit providing input to the M-cell are unaffected by Fmn2b knockdown. This observation is consistent with the unaffected responsiveness to mechano-acoustic stimuli in Fmn2b morphants. Therefore, the behavioural phenotype of increased latency is caused by deficits in the neural circuit downstream of the statoacoustic ganglion. The reticulospinal neuron cell bodies including the M-cell and its homologs were found to be intact in Fmn2b morphants. The next step was to probe the inputs to the M-cell in the zebrafish hindbrain in detail.

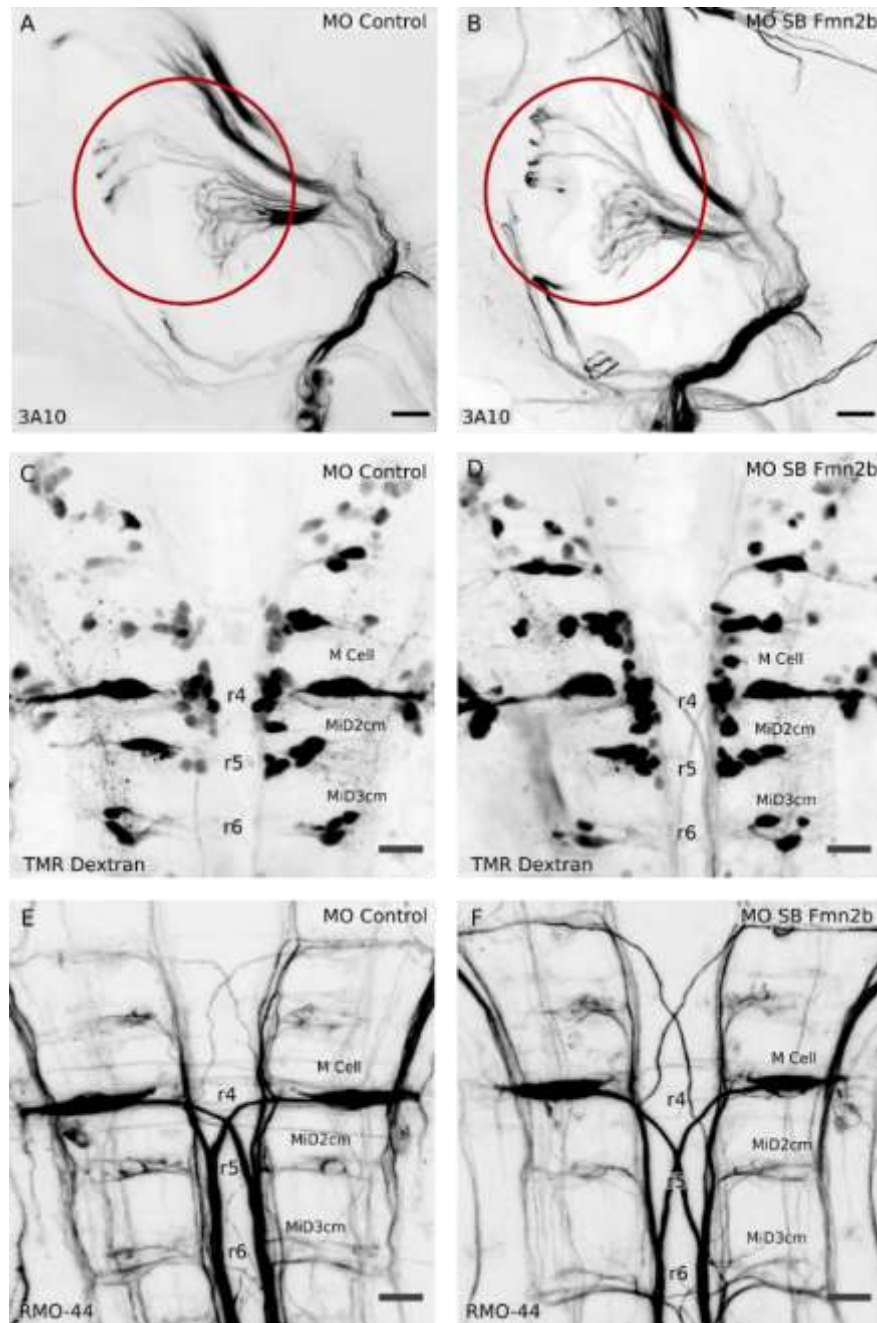


Figure 2.7 The Statoacoustic ganglion (SAG) relaying sensory information and the hindbrain reticulospinal neurons are not affected in Fmn2b morphants

Whole mount immunostaining with anti-neurofilament antibody 3A10 was used to visualize the Statoacoustic ganglion connecting to the M-cells in 96 hpf larvae with **A)** 2 ng MO Control and **B)** 2 ng MO SB Fmn2b cytoplasmic injections. Scale bar is equivalent to 20 μ m. Retrograde labelling of reticulospinal neurons using Tetramethylrhodamine Dextran (TMR Dextran) in 96 hpf **C)** 2 ng MO Control injected embryos and **D)** 2 ng MO SB Fmn2b injected embryos. The M-cell and its homologs, MiD2cm and MiD3cm are intact in Fmn2b morphants. The cell bodies of the reticulospinal neurons stained with RMO-44 antibody in 48 hpf morphants are intact in the **E)** control and **F)** Fmn2b morphants. Scale bar is equivalent to 20 μ m.

2.2.7 The development of Spiral fiber tracts in the hindbrain is regulated by Fmn2b

The M-cell is known to receive inputs from excitatory as well as inhibitory interneurons (Korn and Faber, 2005) to achieve modular fine-tuning of responses to a variety of stimuli. The increase in the response latency in Fmn2b morphants suggests possible defects in the hindbrain circuits involving the M-cells. To assess the state of neuronal connectivity in the hindbrain, the axonal tracts in 96 hpf morphants were visualized using the anti-neurofilament antibody 3A10. Majority of the axonal tracts in the hindbrain, including the M-cell and its homologs, remain unaffected in Fmn2b morphants. However, the spiral fiber tracts in rhombomere 3 were absent. Spiral fiber neurons are commissural interneurons innervating the M-cell axon hillock (Scott et al., 1994; Lorent et al., 2001; Gyda et al., 2012; Lacoste et al., 2014; Liu and Hale, 2017). They have been described earlier to provide excitatory feedforward input to the M-cells and regulate the escape response in larval zebrafish (Lacoste et al., 2014).

The axonal tracts in the hindbrain of 96 hpf embryos were visualized using the 3A10 antibody. About 48% of the MO SB Fmn2b morphants (n=31) showed absence of spiral fiber tracts, whereas none of the control morphants (n=27) showed the defect. The defects were rescued by co-injecting mFmn2-GFP mRNA along with MO SB Fmn2b. The phenotype was rescued in 95% (n=40) of the morpholino and mFmn2-GFP mRNA co-injected embryos (**Figure 2.8 A-D**).

The phenotype was also recapitulated by the MO TB Fmn2b morpholino. In the embryos injected with a 2 ng dose of MO TB *Fmn2b* morpholino at 1-cell stage, 36% of the embryos showed absence of spiral fiber tracts (**Figure 2.9 A**). Further, yolk injections of higher doses (4 ng and 8 ng) of the MO TB Fmn2b caused similar spiral fiber tract development defects (**Figure 2.9 B**), suggesting a dose dependent effect of Fmn2b knockdown of spiral fiber tract development.

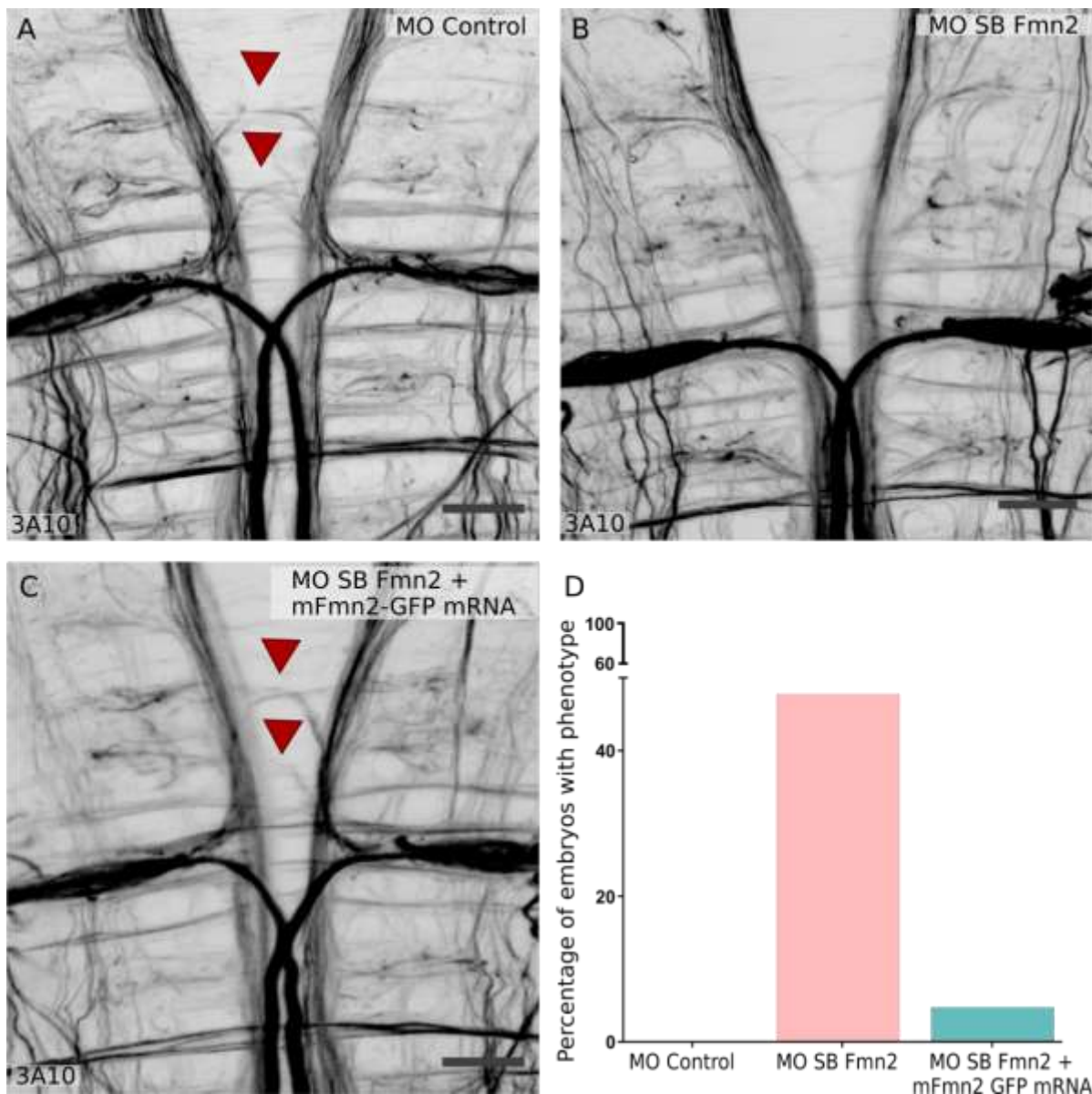


Figure 2.8 Morpholino mediated Fmn2b knockdown impairs axonal outgrowth in the spiral fiber tracts. Whole mount immunostaining using anti-neurofilament antibody 3A10 stains axons in 96 hpf zebrafish hindbrain (A-C). A) Spiral fiber tracts are marked with red arrowheads in control morphants. B) Fmn2b knockdown using splice blocking morpholino (MO SB Fmn2b; 2 ng/embryo injected in the cytoplasm) reveals defects in the spiral fiber tract outgrowth. C) The phenotype in Fmn2b morphants could be rescued by injection of 300 pg mFmn2-GFP mRNA in the MO SB Fmn2b injected embryos at 1 cell stage. Scale bar is equivalent to 20 μ m. D) A total of 48% Fmn2b morphants (n=31) show the absence of spiral fiber tracts as compared to none in the control morphants (n=27). Whereas, only 5% of the embryos rescued with mFmn2-GFP mRNA (n=40) showed the defects. Scale bar is equivalent to 20 μ m.

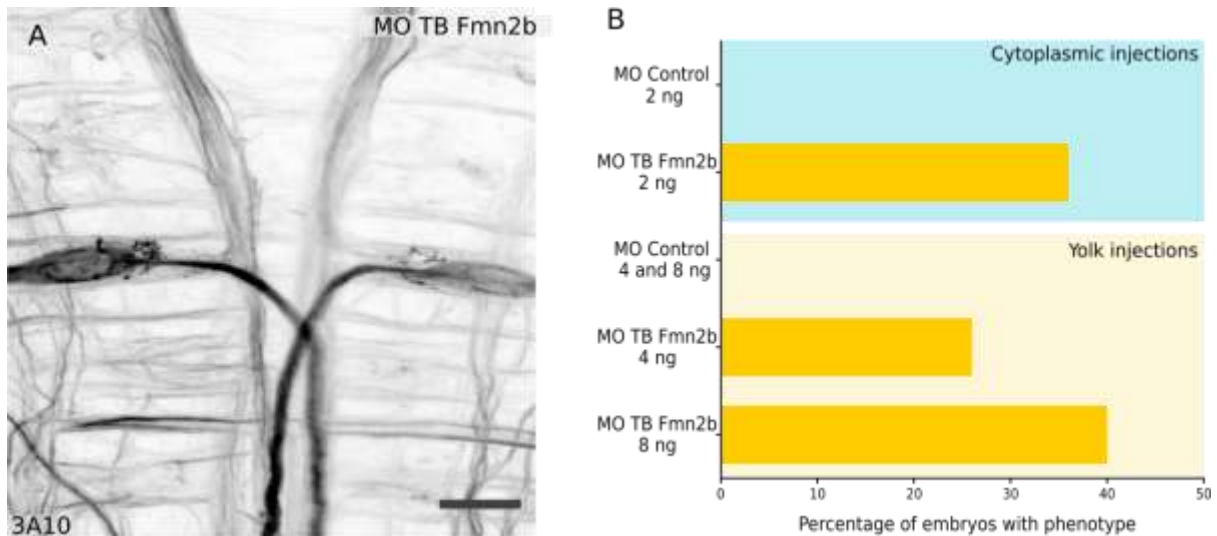


Figure 2.9 The translation blocking morpholino recapitulates the spiral fiber neuron defect in *Fmn2b* morphants. **A)** Whole mount immunostaining using 3A10 antibody of 96 hpf *Fmn2b* morphants injected with 2 ng MO TB *Fmn2b* phenocopies the splice blocking *Fmn2b* morphant defects. Scale bar is equivalent to 20 μ m. **B)** Quantification of cytoplasmic injections of 2 ng MO TB *Fmn2b* and yolk injections of higher doses (4 ng and 8 ng) of MO TB *Fmn2b*. Both cause the spiral fiber neuron outgrowth defect in a dose dependent manner.

2.2.8 *Spiral fiber tracts show outgrowth defects in *Fmn2b* crispants*

Over the past years, there have been concerns regarding the specificity and off-target effects of morpholinos. With the advent of genome editing techniques employing the CRISPR-Cas9 system in zebrafish, the validation of morphant phenotypes with F0 injection of sgRNAs and Cas9 to achieve biallelic mutations is gaining traction (Jao et al., 2013; Shah et al., 2016; Liu et al., 2019). The embryos were injected with two sgRNAs targeting the exon1 of *fmn2b* along with Cas9 mRNA to investigate if knockdown of *Fmn2b* using CRISPR-Cas9 based mosaic indels would phenocopy the defects in spiral fiber tract development observed upon morpholino-based knockdown. The design and validation of the sgRNAs is outlined in Chapter 3. The indels caused by the two sgRNAs are summarized in **Figure 2.10**.

3A10 immunostaining revealed dose-dependent spiral fiber tract defects in the crispants as shown in **Figure 2.11**. In the group which received a 30 pg dose of sgRNAs (n=25), 40% of the embryos had no spiral fiber tracts while another 44% had either only one spiral fiber tract or significant thinning of the tracts. In the group injected with the 100 pg sgRNA dose (n=28), 67.85% of the embryos showed absence of both the spiral fiber

tracts while another 32.15% either lacked one tract or had thin tracts. At this dose, no larvae had intact spiral fiber tracts (Figure 2.11).

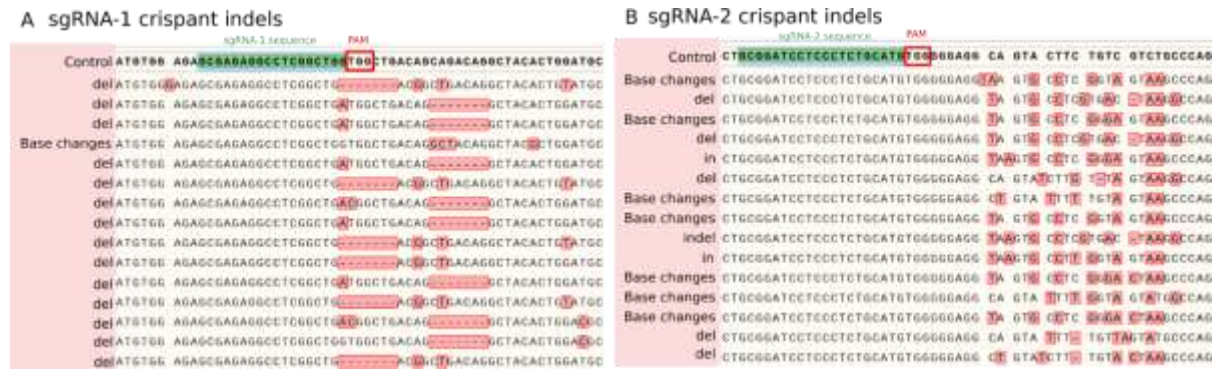


Figure 2.10 Summary of indels and base changes generated in *Fmn2b* crispants

Out of 15 randomly chosen crispants injected with sgRNA-1, sgRNA-2 and Cas9 mRNA, **A)** 93.3% embryos exhibited indels at the sgRNA-1 locus and **B)** 53.3% embryos showed indels at the sgRNA-2 locus on exon 1 of *fmn2b*. Remaining larvae also exhibited base changes at the both the loci. in: insertion; del: deletion.

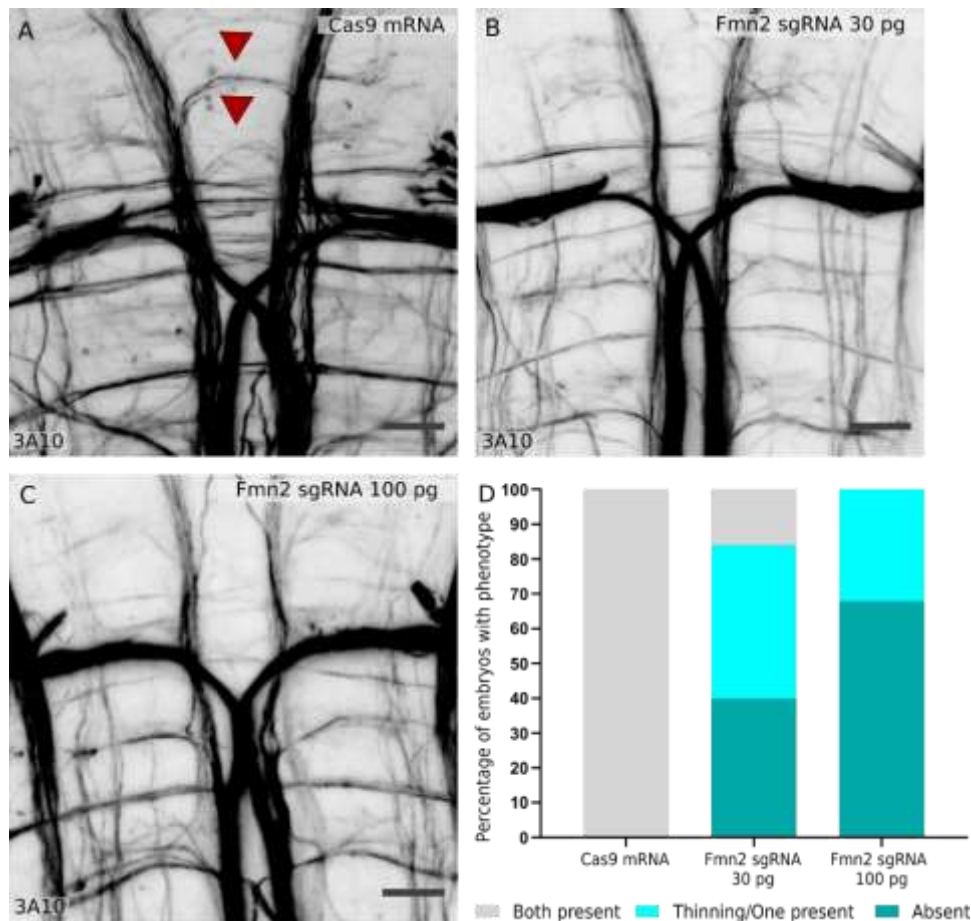


Figure 2.11 *Fmn2b* crispants show impaired axonal outgrowth in the spiral fiber tracts

A) Spiral fiber neurons marked with red arrowheads in embryo injected with Cas9 mRNA. **B)** Fmn2b knockdown using 30 pg dose of each of the two sgRNAs against fmn2b causes defects in the outgrowth of the spiral fiber tracts in Fmn2b crispants. **C)** Fmn2b knockdown using 100 pg dose of each of the two sgRNAs against fmn2b causes defects in the outgrowth of the spiral fiber tracts in Fmn2b crispants. Scale bar is equivalent to 20 μ m. **D)** Quantification of the phenotype reveals that Fmn2b crispants injected with 30 pg sgRNAs and Cas9 mRNA (n=25) show absence of both the spiral fiber tracts in 40% embryos and thinning or absence of only one tract in 44% embryos, as compared to no defects observed in the group injected with the Cas9 mRNA only (n=27). Fmn2b crispants injected with 100 pg sgRNAs and Cas9 mRNA (n=28) show an increase in the severity of the phenotype with 67.85% embryos showing absence of both tracts, 32.15% showing thinning or single tract and no embryos with both the spiral fiber tracts intact.

Representative micrographs depicting the axon thinning and presence of single spiral tract are shown in **Figure 2.12 A-C**. The dose dependent prevalence of the spiral fiber tract development defect reinforces the requirement of Fmn2b in the development of spiral fiber neuron tracts. As seen in morphants, 30-40% of the Fmn2b crispants also showed morphological defects like, curved body axis, shorter body lengths, cardiac edema, microcephaly, deflated swim bladder and otolith defects (**Figure 2.12 D**).

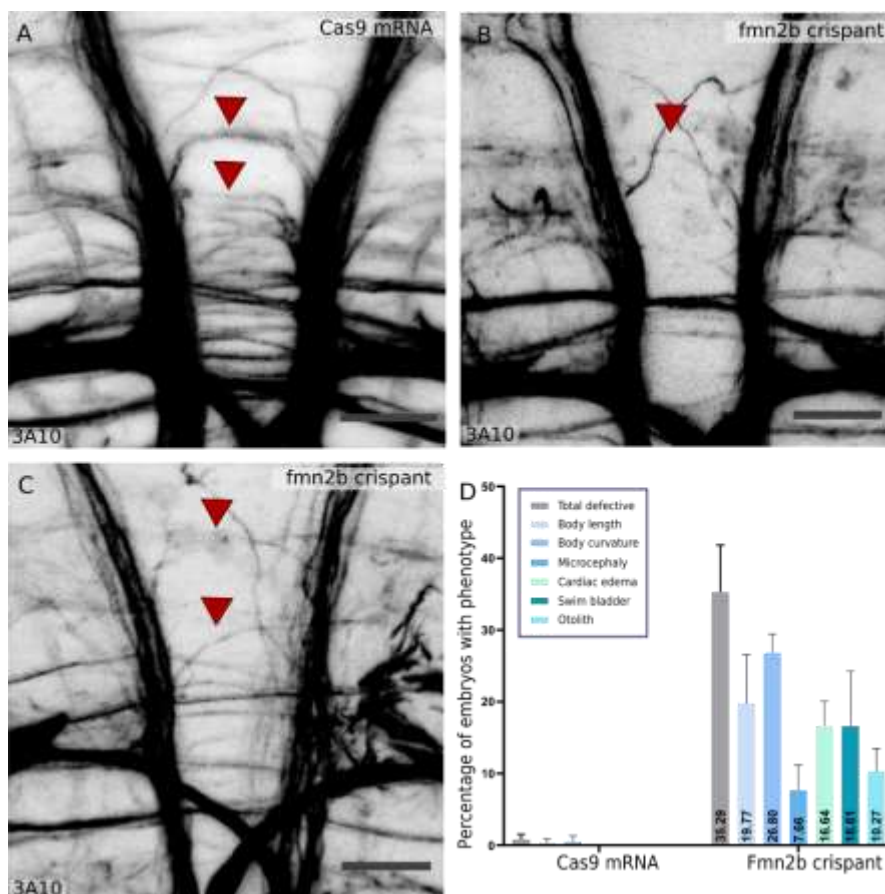


Figure 2.12 Spiral fiber tract and morphological defects in Fmn2b crispants

Representative micrographs showing the **A)** absence of only one tract and **B)** thinning of the spiral fiber tract in Fmn2b crispants as compared to **C)** embryos injected with only Cas9 mRNA. **D)** Quantification of morphological defects in Fmn2b crispants injected with 100 pg each of sgRNA1 and sgRNA2 along with 300 pg of Cas9 mRNA at 96 hpf. The parameters used for classification of morphologically aberrant embryos were the same as in Figure 2.2 D.

These results implicate Fmn2b in the development of the spiral fiber neuron tracts that are necessary for the efficient and reliable execution of the M-cell mediated C-bend escape response. The increase in latency to respond to mechano-acoustic stimulus in Fmn2b morphants can be attributed to the lack of innervation of the M-cells by excitatory spiral fiber neurons.

2.3 Discussion

The zebrafish *fmn2* ortholog, *fmn2b* was identified to be located on chromosome 12. The three key functional protein domains at the C-terminus (FH1, FH2 and FSI domains) that define the fly, chick, mouse and humans orthologs of Fmn2 (Higgs, 2005; Breitsprecher and Goode, 2013) were found to be highly conserved in zebrafish. *fmn2b* mRNA is enriched in the developing zebrafish nervous system though the expression pattern is dynamic during early development. *fmn2b* mRNA is maternally deposited in embryos but disappears after 3 hpf. Robust expression of *fmn2b* mRNA in the nervous system resumes by 24 hpf and persists till 96 hpf (**Figure 2.1**). The spatiotemporal expression pattern coincides with neuronal development in the zebrafish embryo.

Behavioural analysis using an automated stimulus delivery setup and high-speed recording revealed a specific function of Fmn2b in the acoustic startle response. The responsiveness of Fmn2b and control morphants were comparable and indicated that sensory perception was unaffected. However, Fmn2b knockdown increased the latency to respond; the proportion of fast responses decreased while the long latency escape responses increased (**Figure 2.5**).

The inner ear hair cells (**Figure 2.6**) and the statoacoustic ganglion (**Figure 2.7**) were found to be unaffected by Fmn2b depletion. Strikingly, the spiral fiber neurons, which provide excitatory input to the M-cells and form synaptic terminals at the M-cell axon hillock fail to extend their tracts across the midline (**Figure 2.8**). Thus the observed deficits in behaviour are likely due to the absence of spiral fiber neuron innervation resulting in the failure of the command neuron-like M-cells to reach the excitatory threshold (Lacoste et al., 2014). Both the behavioural (**Figure 2.5**) and the neuro-anatomical phenotypes in Fmn2b morphants could be rescued by co-injection of mFmn2-GFP mRNA (**Figure 2.8**). This result underscores the evolutionarily conserved function of Fmn2 from teleosts to mammals. The spiral fiber outgrowth defect was recapitulated by another morpholino MO TB Fmn2b and in F0 *fmn2b* crispants (**Figure 2.9, Figure 2.11**).

Previous studies have highlighted the role of spiral fiber neurons in regulating the fast escape responses in response to mechano-acoustic stimuli (Lorent et al., 2001; Lacoste et al., 2014; Hale et al., 2016; Marsden et al., 2018b). Spiral fiber neurons directly respond to mechano-acoustic stimuli and relay the information to the M-cells, which also receive

direct sensory inputs (Lacoste et al., 2014). In a separate study, the absence of spiral fiber neurons along with other hindbrain commissures caused locomotor defects in *space cadet* mutants (Lorent et al., 2001) later characterized as a mutation in the retinoblastoma-1 (Rb1) gene (Gyda et al., 2012). These studies indicate that the spiral fiber neurons are indispensable for the initiation of a robust startle escape response (Hale et al., 2016). The convergent circuit design in zebrafish hindbrain, where spiral fiber neurons help M-cells reach the excitatory threshold, ensures a speedy and reliable response to a potentially noxious stimulus. The excitability of M-cells decides the further course of action for the animal within the specific context. Zebrafish need the M-cells and two segmental homologs, MiD2cm and MiD3cm, to elicit an effective, fast escape response in zebrafish (Liu and Fetcho, 1999; Kohashi and Oda, 2008). In *Fmn2b* morphants, the M-cells fail to receive inputs from the spiral fiber neurons and exhibit a delay but eventually elicit an escape response. It is likely that MiD2cm and MiD3cm neurons, which also receive the auditory input from the statoacoustic ganglion, are recruited in *Fmn2b* morphants to produce an escape response with increased latency. In addition to the overall increase in latency in *Fmn2b* morphants, the shift towards majority LLC responses in *Fmn2b* morphants instead of SLC responses implies the involvement of M-cell homologs in the absence of spiral fiber excitation of the M-cell. While the possibility of further deficits downstream of the M-cell homologs cannot be ruled out, the *Fmn2b* morphants can still execute C-bend escapes with no significant changes in the maximum bending angle in response to mechano-acoustic stimuli. Therefore, the absence of M-cell innervation by the spiral fiber neurons are the primary reason for the behavioural deficits in *Fmn2b* morphants.

Given the broad expression of the *fmn2b* mRNA in the developing and adult zebrafish nervous system, it is interesting to note that the defects due to *Fmn2b* knockdown are confined to the development of a small population of hindbrain excitatory interneurons, the spiral fiber neurons. Spiral fiber neurons are late pioneering neurons which complete axonogenesis around 72 hpf (Lorent et al., 2001). The developmental timing of axonal outgrowth in this neuronal population and protein perdurance from the maternal *fmn2b* mRNA may render spiral fiber neurons, especially sensitive to morpholino-mediated knockdown. There is a notable expression of *fmn2b* mRNA in the retinal ganglion cells of the eye and the spinal cord of zebrafish larvae. However, the role of *Fmn2b* in development of other neural circuits in zebrafish remains untested.

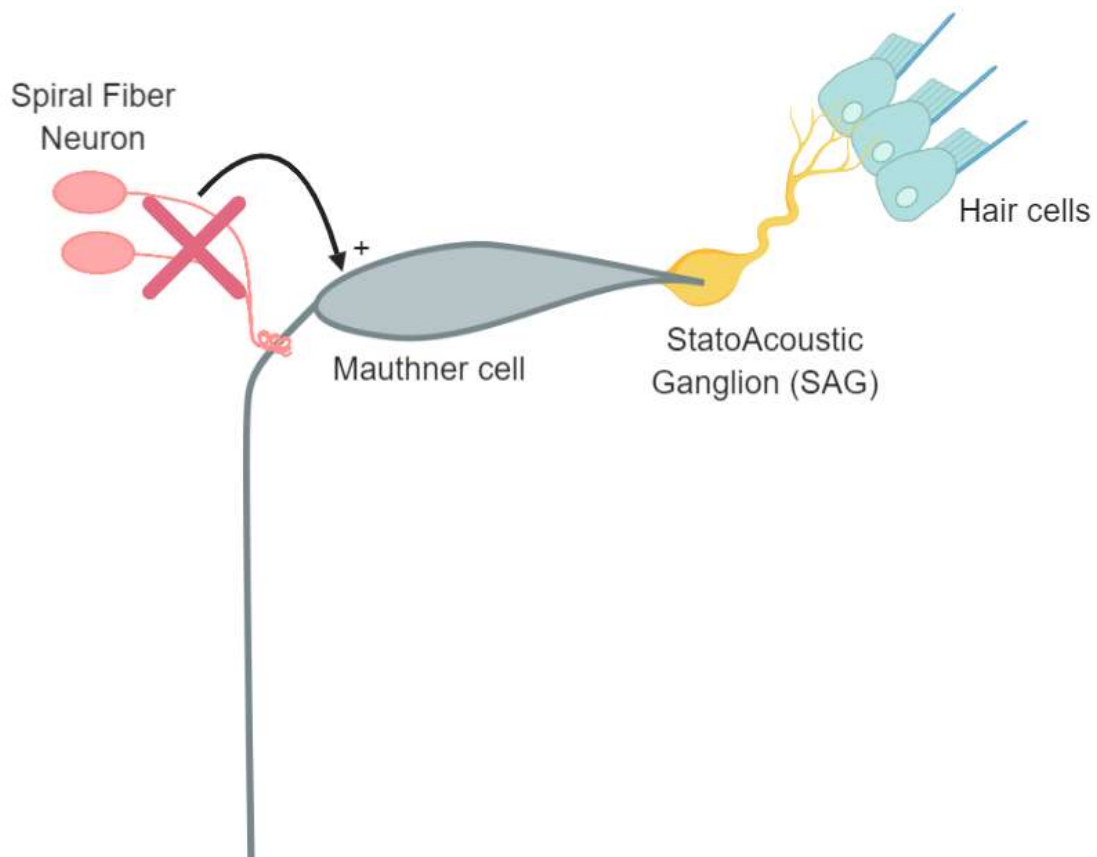
Fmn2b morphants and crispants show partial penetrance of the defects presented. The quantification of morphological defects, spiral fiber neuron defects and the consequent latency defects show a near bi-modal distribution. Embryos were PTU treated to remove pigmentation prior to antibody staining. PTU treated embryos were not used for behaviour experiments. This experiment design did not allow me to do a one-to-one correlation of the neuroanatomical defects in each of the individual embryos corresponding to the behavioural deficits. The lack of one-to-one correlation however can be compensated by the similar trends in the quantification of defects observed.

Fmn2 has previously been shown to be necessary for the axonal outgrowth of spinal neurons in developing chick embryos (Sahasrabudhe et al., 2016; Ghate et al., 2020). Therefore, axonal outgrowth defects of the spiral fiber neurons in zebrafish might be responsible for loss of synaptic connectivity with the M-cells. However, it remains possible that there are additional deficits in neuronal differentiation or specification in the *Fmn2b* morphants.

Both *Fmn2b* morphants and crispants show defects in the development of the spiral fiber tract. Given the mosaic nature of F0 CRISPR-Cas9 mediated knockout, the thinning of the axonal tract upon *Fmn2b* knockdown supports our speculation of axonal outgrowth defect in spiral fiber neurons. The dose dependent effect of the sgRNAs on spiral fiber tract development further strengthens our claim that the spiral fiber neurons have axonal outgrowth defects.

However, it remains to be tested if in addition to outgrowth defects, *Fmn2b* morphants have neural differentiation or specification defects. Previous studies show that *Fmn2* has a synergistic effect on Filamin-a (*Flna*) and causes neurodevelopmental defects in *Fmn2* and *Flna* double knockout mice. On its own, *Fmn2* null allele does not cause neurodevelopmental defects, neural differentiation defects or apoptotic phenotypes in *Fmn2* single knockout mice (Lian et al., 2016). In zebrafish *Fmn2b* morphants, the cell bodies of the reticulospinal neurons in the hindbrain labelled by TMR Dextran retrograde labelling and RMO-44 immunostaining are intact in the *Fmn2b* morphants. This indicates that *Fmn2*, consistent with the findings in primary neuron cultures, is more likely to be involved in the axon outgrowth of spiral fiber neuron tracts and not in the specification or differentiation of the neurons.

The molecular mechanism mediating Fmn2b dependent axonal outgrowth in zebrafish is not known. In chick spinal neurons, Fmn2 mediates growth cone motility by regulating the cell-matrix adhesions necessary to generate traction forces (Sahasrabudhe et al., 2016; Ghate et al., 2020). A recent study implicates Fmn2b in regulating growth cone microtubule dynamics in zebrafish Rohon-Beard neurons (Kundu et al., 2021) and highlights another mechanism mediating outgrowth and pathfinding. Further studies in zebrafish, involving *in vivo* imaging of cytoskeletal dynamics, can pave the way for mechanistic insights into Fmn2 function in intact animals.



In conclusion, Fmn2b was found to mediate the development of the spiral fiber neuron pathway conveying indirect excitatory inputs to the command neuron-like M-cells. The loss of this specific regulatory unit is manifested in a delay in initiating fast escape reflexes in response to mechano-acoustic stimuli, a behaviour of significant survival value. Apart from identifying a novel function for Fmn2 in the development of hindbrain commissural circuitry, our findings highlight the utility of models bridging subcellular functions of Fmn2 identified in cultured neurons to circuit development and associated behavioural consequences.

3

Generation and characterization of *fmn2b* CRISPR mutants

3.1 Introduction

Loss of function is a powerful tool to dissect the function of genes in a biological process. There are several methods to achieve the knockdown of a protein. In this thesis, injection of just fertilized zebrafish embryos with antisense morpholinos and Cas9 endonuclease along with gene targeting short guide RNAs (sgRNAs) have been used to analyze the role of *Fmn2b* in the development of neural circuits.

Loss of function mediated by morpholinos in zebrafish has been an important tool to study gene function but admittedly has its limitations (Eisen and Smith, 2008; Bill et al., 2009; Stainier et al., 2017). Morpholino mediated knockdown reduces the level of target proteins which may not recapitulate the phenotypes due to complete loss of function. Evaluation of the contribution of maternally deposited gene products is also challenging in morpholino mediated knockdown system. The knockdown is transient, and there is evidence of unintended off-target effects of morpholinos. The advent of genetic engineering tools like Zinc Finger Nucleases (ZFNs), TALENs and especially CRISPR-Cas9 (Hwang et al., 2013; Li et al., 2016; Shah et al., 2016; Varshney et al., 2016; Liu et al., 2019) for zebrafish has made precise gene knockouts increasingly accessible over the years. Genome editing approaches allow making stable mutant lines targeting desired genomic loci and are increasingly being used as the predominant way of gene function analysis by reverse genetics.

To further investigate the role of *fmn2b*, CRISPR-Cas9 based *fmn2b* mutants were generated. The details of the mutant alleles generated, early embryonic phenotypes in *fmn2b* mutants and transgenic reagents created for neural circuit analysis are presented in this chapter.

Note: A part of the work included in this chapter was done in the lab of Dr Shawn Burgess at NHGRI, NIH, USA, under the Genome Editing Techniques Initiative (GETIn) internship awarded to me by DBT, India.

3.2 Results

3.2.1 Design and validation of sgRNAs

The characterized functional domains of Formin-2 across vertebrates, and also Fmn2b in zebrafish, are the Formin Homology 1 (FH1), Formin Homology 2 (FH2) and Formin Spire Interaction (FSI) domains. These three domains are responsible for most cytoskeletal remodelling undertaken by Fmn2 and present on the protein's C-terminal. To investigate the effect of knockout of *fmn2b* in zebrafish larvae, 3 sgRNAs targeting the exons 1 and 3 of *fmn2b* were designed using the [CRISPRscan](#) tool (Giraldez Lab, Yale University) and cross verified for high scores using the [ZebrafishGenomics](#) track (Burgess Lab, NHGRI, NIH) in UCSC genome browser (Figure 3.1 A). Targeting early exons would ensure that the resulting mutant allele would cause exclusion of the functional domains in the mutant Fmn2b protein. The efficiency of each of the sgRNAs to induce indels in the F0 injected embryos was tested using the CRISPR-STAT method (Carrington et al., 2015) (**Figure 3.1B**). Briefly, genomic DNA was extracted from eight embryos collected at random from the injected clutch used for fluorescent PCR. The resulting amplicon flanking the target locus would be labelled with FAM-13 dye at the 3' end (**Figure 3.1C**). The amplicons from wildtype fish were compared to the *fmn2b* crispants (F0 progeny injected with 50 pg sgRNA and 300 pg Cas9 mRNA) using capillary gel electrophoresis with a single base-pair resolution (**Figure 3.1D**). Out of the three sgRNAs tested, sgRNA-1 was the most efficient in inducing somatic mutations in the embryos injected, with sgRNA-2 being the next best in introducing indels at the target site (see Reagents and Procedures for sequence information). Both the sgRNAs were used to test the role of *fmn2b* in developing the spiral fiber tracts in crispants (Chapter 2). Further, sgRNA-1 was chosen for creating stable *fmn2b* knockout lines.

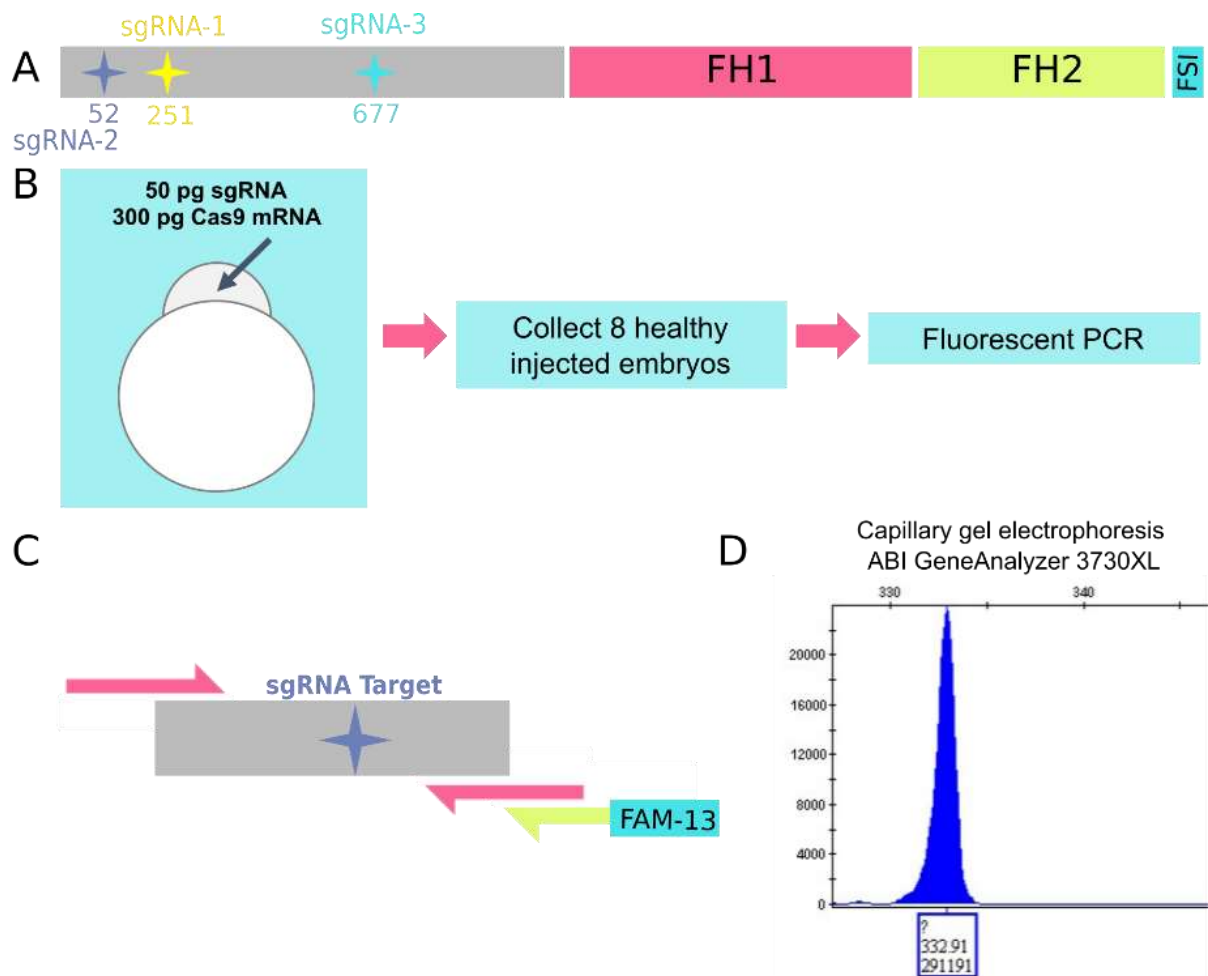


Figure 3.1 Design and validation of sgRNAs against *fmn2b*. **A)** Schematic denoting the Formin homology 1 (FH1), Formin homology 2 (FH2) and Formin Spire interaction (FSI) domains of zebrafish *Fmn2b* (1473 amino acids) and the location of three sgRNAs tested is marked with the corresponding amino acid position. **B)** Schematic showing the experimental workflow for sgRNA testing based on the CRISPR-STAT method. **C)** Schematic of primer design for fluorescent PCR with the overhang primer tagged with FAM-13 dye. **D)** Representative output plot depicting the size and magnitude of a peak from fluorescent PCR corresponding to the wildtype amplicon flanking the sgRNA locus.

3.2.2 Screening potential founder lines with heritable indels

The embryos injected with sgRNA-1 and Cas9 mRNA were raised to adulthood till they achieved sexual maturity. Individual embryos from the injected clutch were outcrossed to a wildtype fish of the opposite sex to obtain eggs that were genotyped using fluorescent PCR. Multiple founder lines with different allelic mutations were identified for *fmn2b* by fluorescent-PCR. Some of the indels introduced by sgRNA-1 in exon 1 of *fmn2b* in the founder zebrafish are summarized in **Table 3-1**. The F1 progeny obtained from the

outcross of these founder lines was raised to adulthood, and the siblings were in-crossed. The F2 progeny thus obtained was grown to sexual maturity and genotyped using the caudal fin clip method and subsequent Sanger sequencing of the genomic locus flanking the sgRNA-1 target to determine whether they were heterozygous or homozygous for the inherited mutant allele.

Table 3-1 Examples of indels from different founder lines (injected with sgRNA-1 and Cas9 mRNA) outcrossed with wildtype fish.

Genotype	Size 1	Height 1	Size 2	Height 2	Size change (bp)	Indel
<i>fmn2b</i> _sgRNA1_WT	332.81	10731				
<i>fmn2b</i> _sgRNA1_1	328.1	11158	332.63	10612	4.53	del
<i>fmn2b</i> _sgRNA1_2	332.64	18044	342.38	19647	9.74	in
<i>fmn2b</i> _sgRNA1_3	325.38	15262	332.64	23476	7.26	del
<i>fmn2b</i> _sgRNA1_4	328.08	22296	332.54	21307	4.46	del
<i>fmn2b</i> _sgRNA1_5	328.09	19875	332.52	17520	4.43	del
<i>fmn2b</i> _sgRNA1_6	328.03	18051	332.57	15442	4.54	del
<i>fmn2b</i> _sgRNA1_7	325.36	26496	332.79	15631	7.43	del
<i>fmn2b</i> _sgRNA1_8	325.3	23818	332.61	14569	7.31	del

The size indicates the amplicon size from the fluorescent PCR, and the height corresponds to the number of amplicons detected in the capillary gel electrophoresis fragment analysis. The size of the amplicon from wildtype fish at the sgRNA-1 locus is 333 bp. The amplicons from the founder fish had a wildtype amplicon and a mutated version. The size difference between the two amplicons was used to determine the indels.

3.2.3 Establishing homozygous mutant lines for *fmn2b*

As shown in Table 3.1, sgRNA-1 caused various indels near the intended target around 753 bp into the *fmn2b* sequence in exon 1, corresponding to the 251st amino acid position in the 1473 amino acid long Fmn2b protein sequence. Two alleles causing a 7 bp

(*fmn2b*^{Δ7/Δ7}) and 4 bp (*fmn2b*^{Δ4/Δ4}) deletion respectively were selected and maintained as homozygous mutants (Figure 3.2 A-B''). The deletions cause a premature stop codon to occur downstream at 299th and 300th amino acid, respectively in the *fmn2b*^{Δ7/Δ7} and *fmn2b*^{Δ4/Δ4} mutants (Figure 3.2 C). Homozygous mutants were in-crossed to obtain heteroallelic homozygous mutants with one each of the two alleles and henceforth, denoted as *fmn2b*^{Δ4/Δ7}.

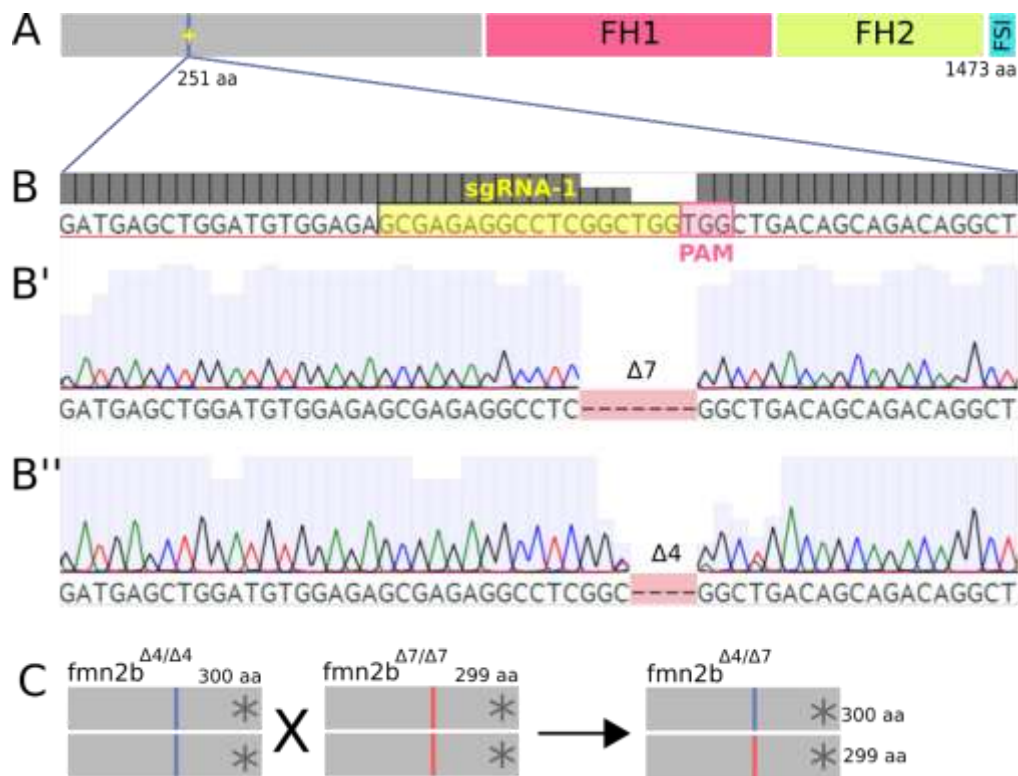


Figure 3.2 Generation of *fmn2b* CRISPR mutants. A) Schematic marking the site of *fmn2b* sgRNA-1. B) Genomic locus from *fmn2b* exon 1 starting from 720 bp (corresponding to 240th amino acid). The sgRNA sequence is highlighted in yellow, followed by the PAM sequence in pink. Representative chromatograms of amplicons sequenced from homozygous CRISPR mutants for *fmn2b* show two alleles with a 7 bp and a 4 bp deletion respectively. These two alleles are denoted as *fmn2b*^{Δ7/Δ7} and *fmn2b*^{Δ4/Δ4}. C) Schematic outlining the generation of *fmn2b* heteroallelic homozygous mutants.

3.2.4 Early developmental phenotypes in *fmn2b* CRISPR mutants

Generation of *fmn2b* knockout lines allowed the investigation of the role of *fmn2b* in early development and the neuronal development of zebrafish embryos. The heterozygous (*fmn2b*^{+/^{Δ7}) and heteroallelic homozygous (*fmn2b*^{Δ4/Δ7}) *fmn2b* mutants showed significant mortality as compared to *fmn2b*^{+/+} embryos during early development. In the}

fmn2b^{+/ Δ 7} population, 14% of the embryos did not survive by 24 hpf, whereas in the *fmn2b* ^{Δ 4/ Δ 7} population, 17% of the embryos died within the first 24 hours of development (Figure 3.3 A). Early mortality of *fmn2b* mutants implicates the involvement of *fmn2b* in oocyte and early embryonic development as previously reported in mice and humans (Leader et al., 2002; Ryley et al., 2005; Dumont et al., 2007; Schuh and Ellenberg, 2008; Mogessie and Schuh, 2017). In addition to the early mortality observed in *fmn2b* mutants, the surviving population exhibits morphological defects similar to *fmn2b* morphants and crispants showed in Chapter 2. Around 25% of the surviving population showed one or more of the morphological defects like shortening of body length, increased axial curvature, microcephaly, cardiac edema, deflated swim bladder and malformed otoliths. The morphological defects were negligible in the wildtype population. Around 17% of the *fmn2b* mutants showed body length and curvature defects, 12% had microcephaly, and <5% showed cardiac edema, swim bladder deflation and otolith defects (Figure 3.3 B). Despite the early embryonic mortality and morphological defects, around 50-60% of the total clutch from *fmn2b* homozygous mutants survived to become adults. The homozygous *fmn2b* mutants were able to reproduce, and the obtained clutch from F1, F2 and F3 progeny of *fmn2b* homozygous mutant in-crosses showed a similar trend of mortality and morphological defects.

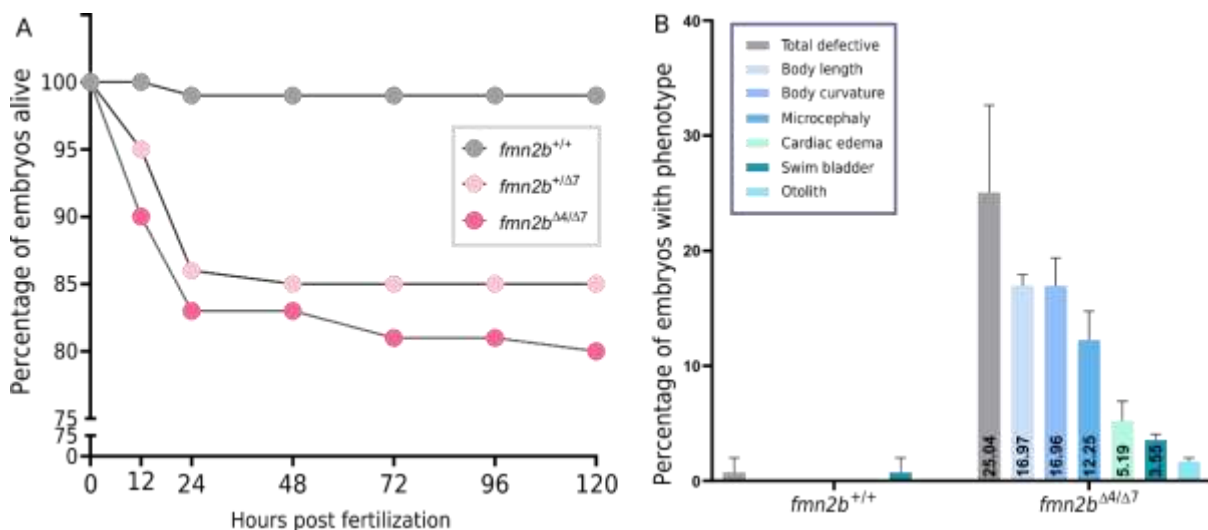


Figure 3.3 Mortality and morphological defects in *fmn2b* mutants. A) Graph plotting the percentage of embryos alive at the end of the indicated time post fertilization. B) Graph plotting the percentage of embryos with the indicated morphological defects.

Further characterization of the early developmental defects was done by microscopic analysis of *fmn2b* mutants. Live imaging of developing *fmn2b* mutant embryos revealed a non-uniform appearance of the yolk as compared to wildtype embryos. The yolk of *fmn2b* mutants had clump-like structures throughout the yolk (**Figure 3.4 A, B**). These clumps persisted in the yolk of the developing embryo till 24-72 hpf, contingent on their survival. Most of the embryos with the yolk defects did not survive beyond 24 hpf suggesting a potential role of yolk defects in early mortality.

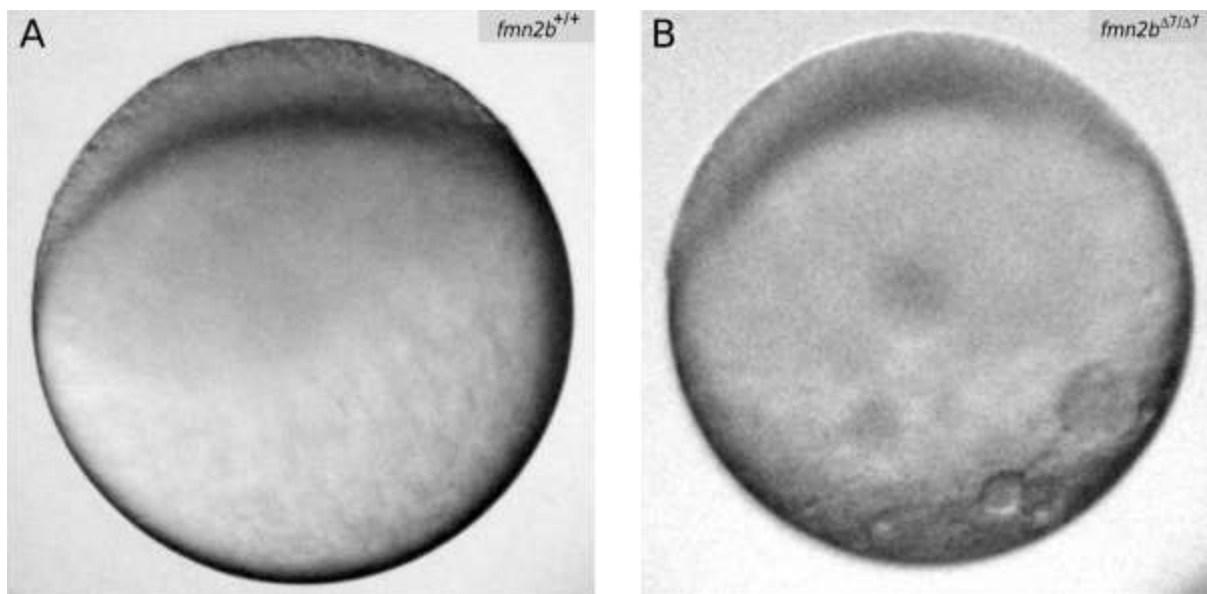


Figure 3.4 Defects in yolk architecture of 5 hpf A) *fmn2b*^{+/+} and B) *fmn2b*^{Δ4/Δ7} embryos.

3.2.5 Generating reagents to visualize neuronal populations in *fmn2b* mutants

The *fmn2b* mutants recapitulate the early developmental defects observed in the *fmn2b* morphants and crispants. To look at the effect of *fmn2b* knockout on the development of neural circuits, the *fmn2b* mutants were crossed to transgenic lines labelling the motor neurons (*Tg(mnx1:GFP)*) and a subset of Retinal Ganglionic cell (RGC) neurons (*Tg(brn3c:GAP43-GFP)*). The phenotypes observed in motor neuron development are presented in Chapter 4, and the defects underlying the visual processing neural circuits are presented in Chapter 5. The details of the crosses to achieve labelling of motor neurons and RGCs in *fmn2b* mutants using the transgenes mentioned above is shown in **Figure 3.5** below.

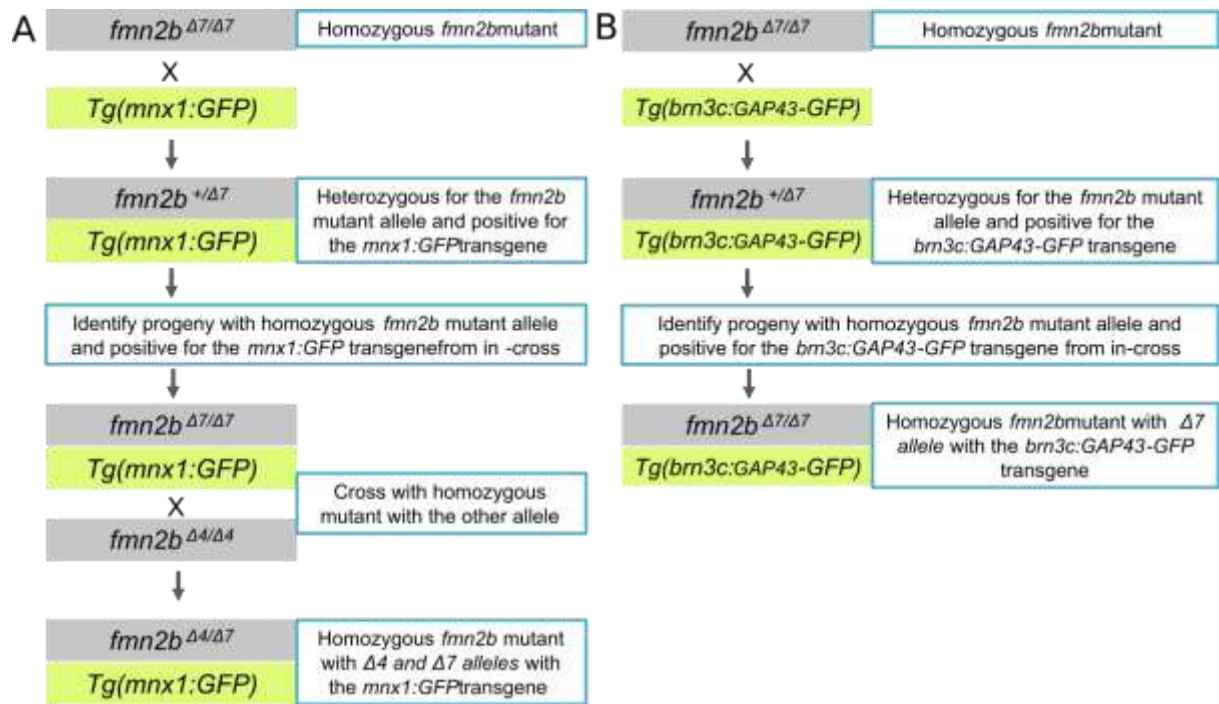


Figure 3.5 A) Schematic depicting the workflow for generating *fmn2b* CRISPR mutants in *Tg(mnx1:GFP)* background to label motor neurons. B) Schematic depicting the workflow for generating *fmn2b* CRISPR mutants in *Tg(brn3c:GAP43-GFP)* background to label a subset of Retinal Ganglionic Cell projections to the optic tectum.

3.3 Discussion

Two mutant alleles were successfully generated targeting the exon 1 of *fmn2b*. The *fmn2b^{Δ4/Δ4}* and *fmn2b^{Δ7/Δ7}* alleles cause a premature stop codon to occur at the 300th and 299th amino acid position, respectively ensuring that the functional domains of *Fmn2b*, FH1, FH2 and FSI are not translated in the *fmn2b* mutants. Despite recent advances in improvement of specificity of Cas9 nucleases, the possibility of off-target mutations in CRISPR-Cas9 mutants remains likely. Multiple mutant alleles of the desired genetic locus are compared to ensure the specificity of the mutation on gene function. But this does not ensure absence of any off-target effects. For the *fmn2b* mutants generated, *fmn2b^{Δ4/Δ4}* and *fmn2b^{Δ7/Δ7}* mutant alleles were crossed and screened to obtain *fmn2b^{Δ4/Δ7}* embryos which are homozygous for mutations in exon 1 and will make a transcript with a premature stop codon from both the gene copies. But, the *fmn2b^{Δ4/Δ7}* embryos will be heterozygous for any unintended off-target mutations that persisted even after wildtype outcrossing. Moreover, the phenotypes were comparable in the *fmn2b^{Δ4/Δ4}*, *fmn2b^{Δ7/Δ7}* and *fmn2b^{Δ4/Δ7}* embryos implicating *fmn2b* in the observed defects in mutants.

The early mortality and morphological defects observed in *fmn2b* mutants point to a non-neuronal role of *fmn2b* in embryonic development. One possibility is that the actin cytoskeleton of the yolk required for proper transport of nutrients to the developing embryo is rendered dysfunctional due to the absence of maternally deposited *fmn2b* transcripts. The *Drosophila* ortholog of Formin-2, Cappuccino (Capu), is required for building the actin mesh throughout the oocyte, and its absence causes premature cytoplasmic streaming (Manseau and Schüpbach, 1989; Emmons et al., 1995; Dahlgaard et al., 2007; Yoo et al., 2015). It will be interesting if similar defects are observed in the *fmn2b* zebrafish mutants and are potentially responsible for the yolk defects and early mortality. Quantification of early mortality in *fmn2b* morphants and crispants could not exclude any artefacts of injection stress to the embryos. However, the *fmn2b* morphants and crispants consistently showed increased mortality compared to the wildtype injected group. Overall, the questions surrounding the pleiotropic functions of *fmn2b* remain unanswered. The *fmn2b* mutants generated here will serve as an essential tool to study the neuronal and non-neuronal role of *fmn2b* in development. This line of investigation segregating the neuronal and non-neuronal contribution of *fmn2b* would benefit from conditional *fmn2b* mutants with spatiotemporal control of *fmn2b* knockout in zebrafish.

In this regard, the reagents for neuron-specific and heat shock mediated knockout of zebrafish have also been made.

As discussed earlier, as many as eleven identified formins are present in zebrafish, with the functional FH1 and FH2 domains but differing in the composition of the N-terminal or presence of other regulatory domains. There is a high likelihood of redundancy in the function of formins, especially the closely related formins. Despite maternal deposition and extensive expression of *fmn2b* mRNA in the nervous system, the *fmn2b* mutants (and morphants and crispants) are not lethal. It remains to be tested if other formins cooperate to take over the functions of the missing formins in the system. In zebrafish, the closest relative of *fmn2b* is its paralog *fmn2a*. Although *fmn2a* has remarkably low expression in the developing zebrafish and no expression in the nervous system, it will be interesting to note if *fmn2a* is upregulated in the absence of *fmn2b* or if the phenotypes observed in *fmn2b* mutants are exacerbated in the *fmn2b* and *fmn2a* double mutant.

4

Motor neuron outgrowth is regulated by Fmn2b

4.1 Introduction

Motor neurons are the final, executory neurons underlying most motor behaviours performed by zebrafish during development and throughout their lifespan. The motor neurons receive synaptic inputs from reticulospinal neurons, including the Mauthner cell and a plethora of interneurons which regulate their function in response to stimuli (Bernhardt et al., 1990; Hale et al., 2001; McLean and Fetcho, 2008). The cell bodies of the motor neurons are located in the ventral spinal cord, from where the axons emerge and take restricted trajectories and make unique arborization patterns innervating specific muscle targets (Myers, 1985; Eisen et al., 1986; Eisen, 1991). Zebrafish have two types of motor neurons, primary and secondary, present on both sides of the spinal cord. The axial muscles in zebrafish are organized in myotomes spanning the dorsal, medial and ventral regions on both sides and receive projections from three primary motor neurons and several secondary motor neurons per hemisegment (Myers, 1985).

4.1.1 Birth and outgrowth of motor neurons

On either side of the spinal cord, three subtypes of primary motor neurons are present, easily identified from their morphology and muscle target (Stifani, 2014). The three types of primary motor neurons are Caudal Primary (CaP), Middle Primary (MiP) and Rostral Primary (RoP) motor neurons, named after the relative position of their cell bodies in the spinal cord (Myers et al., 1986). Primary motor neurons are born 9-10 hours post fertilization, and the axonogenesis starts ventrally around 18 hpf. CaP motor neurons are the first to extend their axons, followed by MiP and RoP neurons (Eisen et al., 1986; Myers et al., 1986; Westerfield, 1992). The axons of each motor neuron follow a stereotypical pathway and project to unique fast-twitch muscle fibers needed for their respective function (Eisen et al., 1986; Westerfield et al., 1986; Kuwada et al., 1990a). Pathfinding by the primary motor neuron growth cones is dependent on interactions with the environment, not the adjacent motor neurons and does not follow a preset temporal pattern (Eisen et al., 1986; Myers et al., 1986).

Secondary motor neurons are born 5-6 hours after the primary motor neurons and begin axonogenesis hours later, independent of the pioneering neurons. On average, secondary motor neuron growth cones exit the spinal cord around 26-27 hours (Myers et al., 1986). Compared to primary motor neurons, the secondary motor neurons have smaller cell

bodies, and their arborization fields are smaller (Pike et al., 1992; Westerfield, 1992; Beattie et al., 1997; Menelaou and Svoboda, 2009).

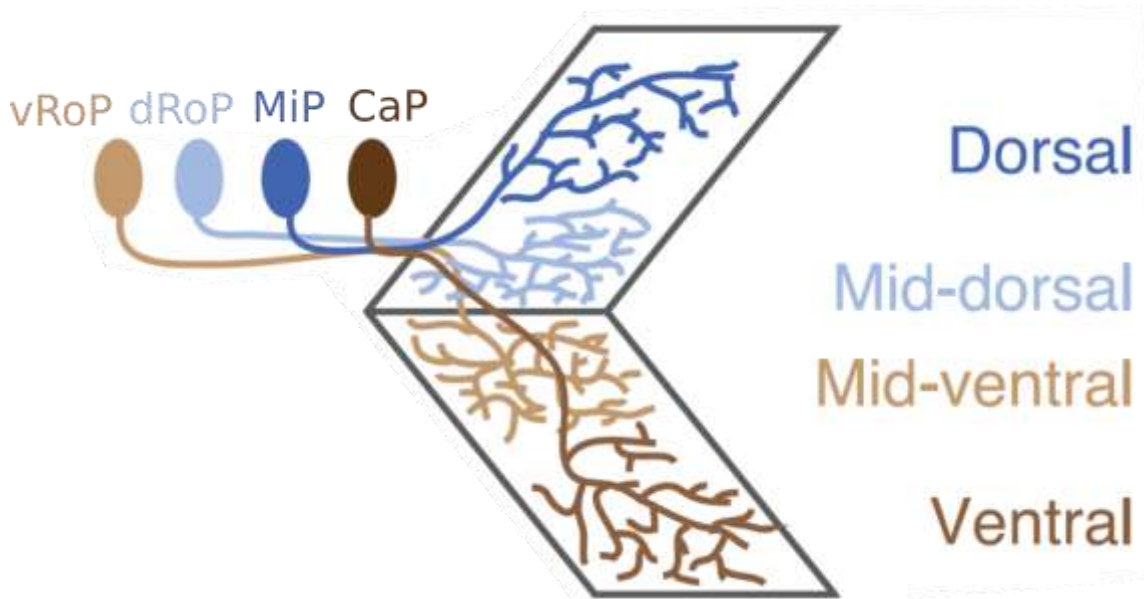


Figure 4.I.1. Schematic showing the innervation pattern of the CaP, vRoP, dRoP and MiP motor neurons onto the myotome (Bagnall and McLean, 2014)

4.1.2 Pathway selection by motor neurons

The initial trajectory of the CaP, MiP and RoP axons is common till the choice point marked by the horizontal myoseptum. After reaching this choice point, axons of each of the primary motor neurons migrate in different directions. CaP axons continue to extend ventrally and occupy the ventral most musculature. MiP axons take an about-turn and migrate towards the dorsal muscle. RoP axons exit the horizontal myoseptum laterally and primarily project to the mid-dorsal and mid-ventral region (Myers, 1985; Eisen et al., 1986, 1989; Myers et al., 1986; Kuwada et al., 1990b; Eisen, 1991). Recently, studies have identified two types of RoP neurons, dorsal RoP (dRoP) and ventral RoP (vRoP) neurons, which project to the mid-dorsal and mid-ventral regions, respectively (Bagnall and McLean, 2014; Bello-Rojas et al., 2019). Each of the primary and secondary motor neurons occupies a distinctive position as they innervate the target muscles. These territories form structurally and functionally distinct motor units, which can help the fish execute motor behaviours requiring varied speed and force (Bagnall and McLean, 2014; Bello-Rojas et al., 2019). The development of identified motor neurons is independent of the trajectories and temporal development of other motor neurons. There is no effect of

ablation of pioneer motor neurons on the ability of the follower motor neurons to follow the stereotyped pathway and innervate target musculature. (Eisen et al., 1989).

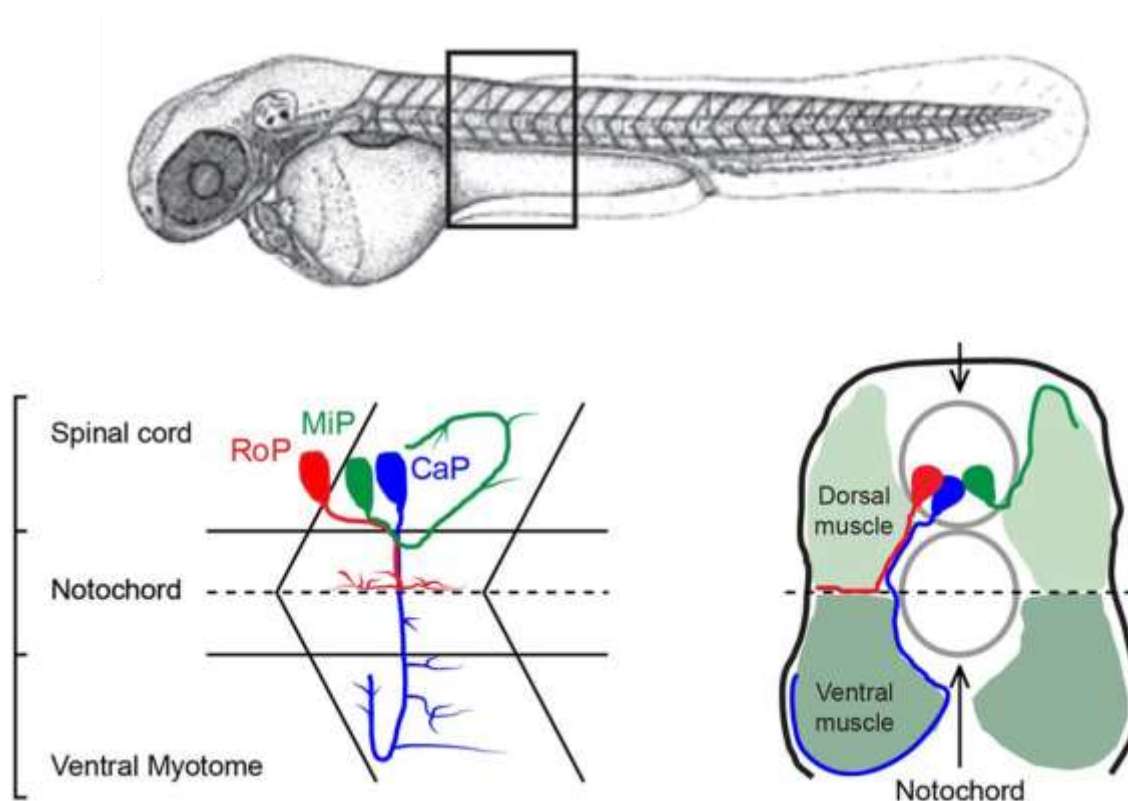


Figure 4.I.2. Schematic showing the lateral and section view of the zebrafish spinal cord and the relative placement of the primary motor neurons. The horizontal myoseptum acts as a spatial marker to provide a choice point for the CaP, MiP and RoP motor neurons to change their trajectories (Issa et al., 2012)

4.1.3 Cytoskeletal proteins in neuronal morphogenesis and branching

Outgrowth and branching of neurons require active cytoskeletal remodelling of the actin and microtubule cytoskeleton, employing many cytoskeletal proteins (Kessels et al., 2011; Kalil and Dent, 2014; Coles and Bradke, 2015; Kawabata Galbraith and Kengaku, 2019). Branch maturation and stability are aided by microtubule innervation (Lasser et al., 2018). Different types of neurons make diverse branched structures suited to their function (Kalil and Dent, 2014). Actin remodelling protein, Cordon Bleu (Cobl), an actin nucleator, is critical for branching of dendritic structures in hippocampal and Purkinje neurons (Ahuja et al., 2007; Haag et al., 2012). The kinesin adaptor, Calsyntenin-1 (Clstn-1), regulates the branching of the peripheral Rohon Beard (RB) neurons via endosomal traffic control (Ponomareva et al., 2014). Microtubule severing proteins like Fidgetin like-1 and Fidgetin like-2 are implicated in the negative regulation of motor neuron branching

in zebrafish (Fassier et al., 2018). Knockdown of Atlastin, a dynamin superfamily of large GTPases, leads to motor neuron pathfinding defects and reduction in zebrafish larval motility and upregulation of BMP signalling (Fassier et al., 2010). Kinesin-12 knockdown causes a decrease in the velocity of sensory and motor neuron growth cones during early development in zebrafish (Xu et al., 2014). Myosin phosphatase activity is required for preventing excessive branching of CaP motor neurons (Bremer and Granato, 2016). The depletion of Dynactin subunit 1a (Dctn1) causes motor neuron pathfinding defects, neuromuscular instability and locomotion defects in zebrafish and aged mice (Yu et al., 2018; Bercier et al., 2019). Among actin-binding proteins, the role of Profilin in motor neuron outgrowth and branching has been characterized extensively. Profilin 1 (Pfn1) regulates the polymerization of actin in coordination with formins via their FH1 domains (Katoh and Katoh, 2004; Paul and Pollard, 2008; Funk et al., 2019). Mutations in Pfn1 cause familial amyotrophic lateral sclerosis in humans and mice (Wu et al., 2012; Yang et al., 2016; Brettle et al., 2019). Pfn1 is also required for motor neuron outgrowth in *Drosophila* (Wills et al., 1999).

The function of the formin class of actin and microtubule remodelling proteins in axonal branching *in vivo* remains elusive. Few reports characterize the role of Dishevelled associated activator of morphogenesis (Daam) formins in *Drosophila* axonal growth (Matussek et al., 2008; Prokop et al., 2011) and Daam1a in habenular morphogenesis and IPN connectivity in zebrafish (Colombo et al., 2013). Another study identified Formin-3 (Form3) in the maintenance of complex dendritic arbors of nociceptive sensory neurons in *Drosophila* via microtubule stabilization and adequate organelle trafficking (Das et al., 2017).

However, there are hardly any reports about the role of formins, particularly in motor neuron development. Previous reports show the requirement of Fmn2 in outgrowth and pathfinding (Sahasrabudhe et al., 2016; Ghate et al., 2020; Kundu et al., 2021) and axonal branching (Kundu et al., 2020) in chick spinal primary neurons. The following section presents the role of the zebrafish ortholog of Formin-2, Fmn2b, in regulating motor neuron outgrowth and branching *in vivo* and the consequent effects on motor behaviour.

4.2 Results

4.2.1 *fmn2b* mRNA is expressed in the spinal cord of zebrafish embryos

In addition to the expression in the central nervous system, *fmn2b* mRNA is also expressed in the spinal cord 48 hpf onwards (**Figure 4.1** A, B). One of the major classes of neurons in the spinal cord is motor neurons. The motor neurons have predetermined trajectories as their axons exit from the cell bodies located in the spinal cord and reach their respective targets across the myotome. Given the expression of *fmn2b* mRNA in the spinal cord, *fmn2b* mutants described in the previous chapter were used to observe any motor behavioural deficits.

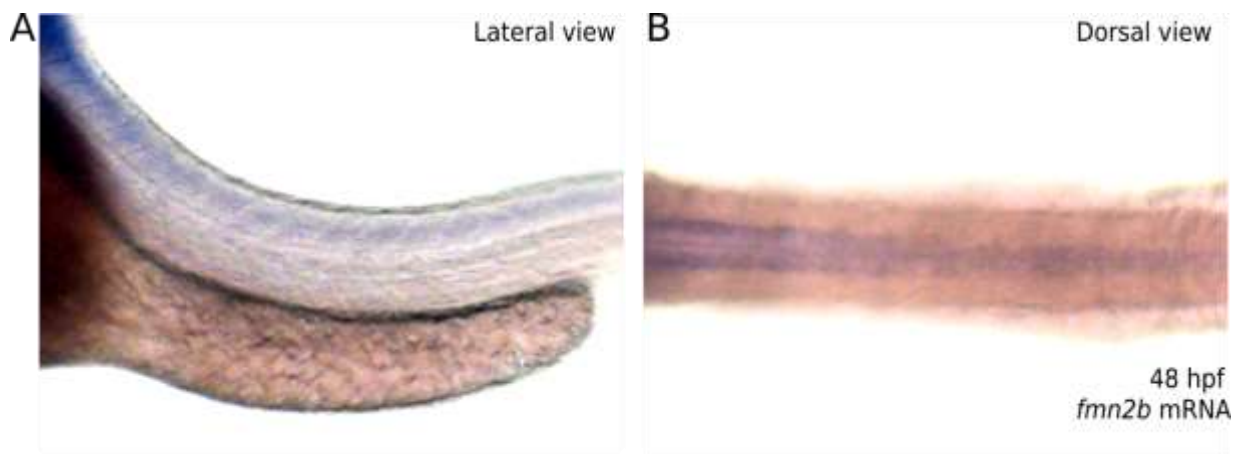


Figure 4.1 *fmn2b* mRNA is expressed in the spinal cord of zebrafish embryos A) Lateral and B) dorsal of 60 hpf embryo showing *fmn2b* mRNA expression in the spinal cord.

4.2.2 *fmn2b* mutants exhibit defects in Spontaneous Tail Coiling (STC) and Touch Evoked Escape Response (TEER)

The first motor behaviour to appear in the developing zebrafish embryo is the spontaneous tail coiling which starts around 17 hpf and persists till 27 hpf (Saint-Amant and Drapeau, 1998; Brustein et al., 2003). This time window coincides with the outgrowth and pathfinding of primary motor neurons (Myers et al., 1986). On comparing 22 hpf wild-type (*fmn2b*^{+/+}) and *fmn2b* mutant (*fmn2b*^{A4/Δ7}) embryos, it was observed that the frequency of spontaneous tail coiling was reduced in *fmn2b*^{A4/Δ7} embryos ($3.168 \pm 0.314 \text{ min}^{-1}$) as compared to the *fmn2b*^{+/+} embryos ($5.003 \pm 0.203 \text{ min}^{-1}$) (**Figure 4.2** A). The maximum amplitude of tail coiling did not change significantly in the *fmn2b*^{A4/Δ7}

embryos (**Figure 4.2 B**). The decrease of coiling frequency but not the magnitude of coiling indicates that the defects are likely due to motor neuron development or NMJ defects rather than loss of muscle integrity.

As the embryo develops, the motor neurons start executing touch evoked escape responses beginning at 48 hpf, manifested as quick C-bend escapes followed by swimming bouts. In touch evoked escape response (TEER) assay performed with 60 hpf embryos, the distance covered by the *fmn2b^{A4/Δ7}* embryos (13.55 ± 1.06 mm) and the average speed of movement across the swim bout (34.26 ± 2.785 mm/s) was severely reduced as compared to the distance covered (65.31 ± 4.93 mm) and swim speed (84.37 ± 3.253) of *fmn2b^{+/+}* embryos (**Figure 4.2 C, D, E**). However, the maximum instantaneous speed attained by an embryo during the entire swim bout was not significantly different between *fmn2b^{+/+}* (199.5 ± 7.039 mm/s) and *fmn2b^{A4/Δ7}* embryos (183.2 ± 6.245 mm/s) (**Figure 4.2 F**). This observation suggests that the motor defects in *fmn2b^{A4/Δ7}* embryos at 24 hpf and 60 hpf could arise from abnormal motor neuron development or innervation of the muscles and not due to defects in the muscle architecture or activity. The comparable maximum instantaneous speed of *fmn2b^{+/+}* and *fmn2b^{A4/Δ7}* embryos supports that the muscles remain largely unaffected upon *fmn2b* knockout. Therefore, *fmn2b* mutants have motor deficits manifested as reduced spontaneous tail coiling and reduced distance travelled and average speed in TEER assay.

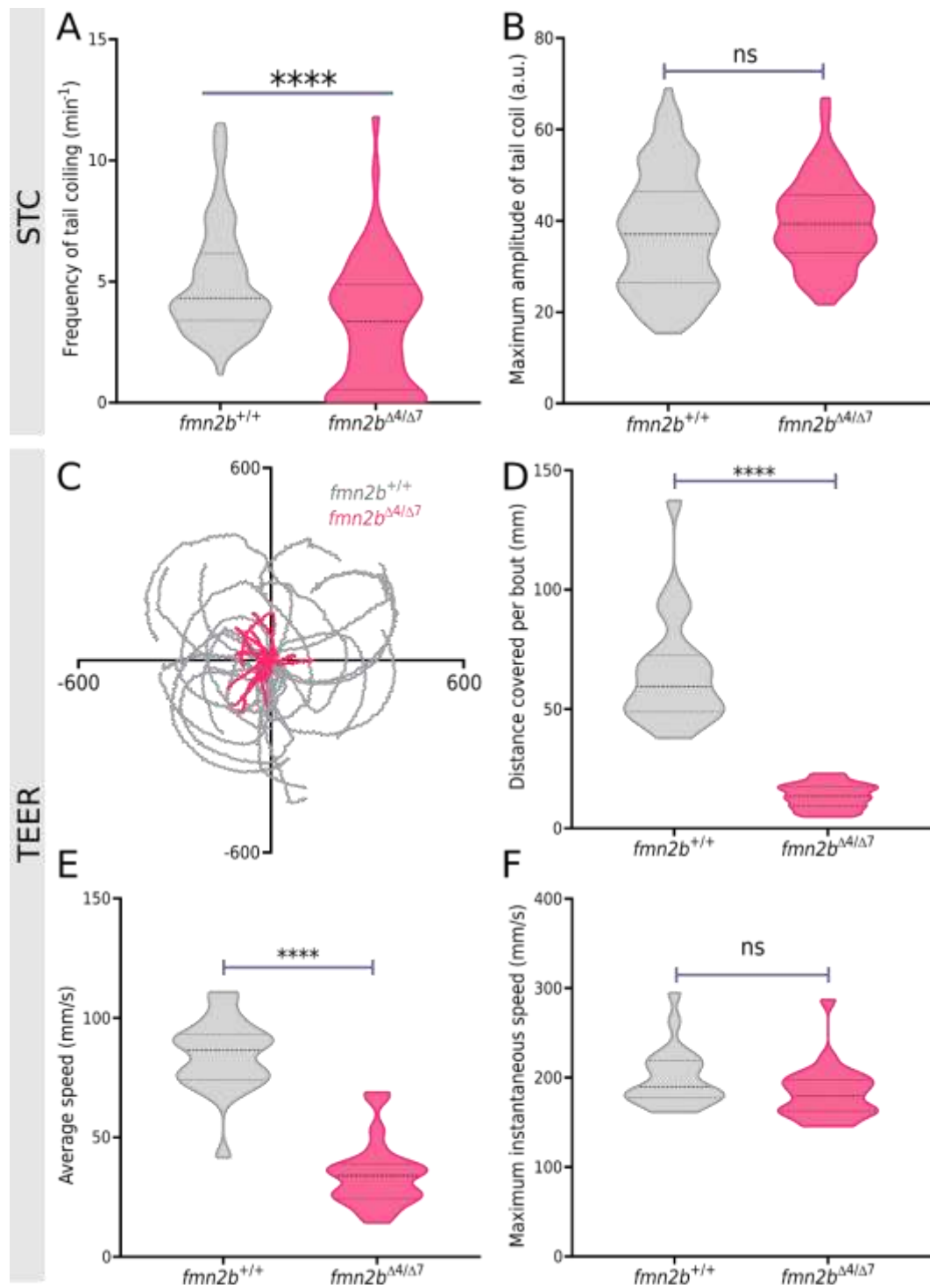


Figure 4.2 *fmn2b* mutants exhibit motor defects. **A)** Spontaneous tail coiling (STC) frequency and **B)** maximum amplitude of tail coiling in 22 hpf – 26 hpf *fmn2b*^{+/+} (n=121) and *fmn2b*^{Δ4/Δ7} (n=68) embryos. **C)** Trajectories of 2 dpf *fmn2b*^{+/+} (n=22) and *fmn2b*^{Δ4/Δ7} (n=24) embryos in Touch Evoked escape response (TEER), re-centered at a common origin for representation. The X and Y axes in the plot correspond to the pixel values corresponding to coordinates of the fish from consecutively acquired frames. Quantification of **D)** distance covered per swim bout, **E)** average speed during the swim bout, and **F)** maximum instantaneous swimming speed of 2dpf *fmn2b*^{+/+} (n=22) and *fmn2b*^{Δ4/Δ7} (n=24) embryos in response to a tactile stimulus. (**** p-value <0.0001; ns- not significant; Mann-Whitney U test)

4.2.3 *fmn2b* mRNA is expressed in the motor neurons of zebrafish embryos

To explicitly test the expression of *fmn2b* mRNA in the motor neurons, wild-type *Tg(mnx1:GFP)* embryos labelling the motor neurons were used to check the expression of *fmn2b* in the GFP positive motor neurons by RT-PCR. Briefly, 24 hpf and 60 hpf *Tg(mnx1:GFP)* embryos were treated with trypsin to obtain a single cell suspension, from which motor neurons were isolated using Fluorescence-activated cell sorting (FACS) (Figure 4.3 A). RT-PCR was performed on cDNA extracted from sorted motor neurons labelled by *mnx1:GFP* using primers against β 2-actin (*actb2*) control (1153 bp) and *fmn2b* N-terminal (408 bp) from 24 hpf and 60 hpf embryos, respectively. RT-PCR confirmed the presence of *fmn2b* transcript in motor neurons in 24 hpf and 60 hpf embryos (Figure 4.3 B).

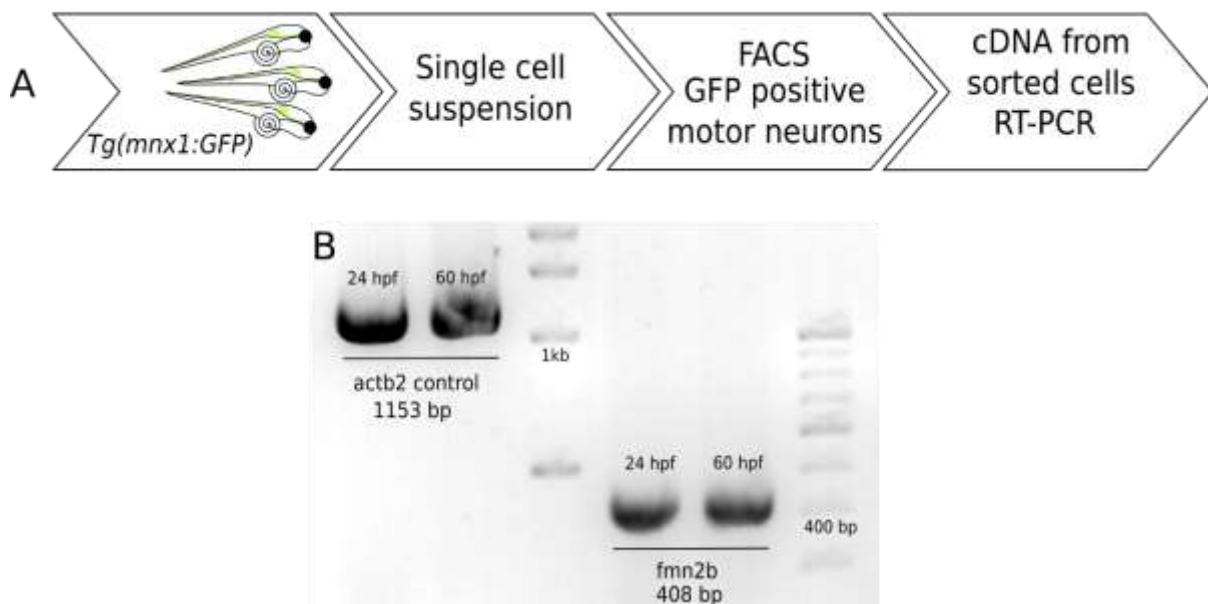


Figure 4.3 *fmn2b* is expressed in the motor neurons of zebrafish embryos. **A)** Schematic for cell sorting of motor neurons from wild-type *Tg(mnx1:GFP)* embryos and RT-PCR. **B)** Gel showing bands for amplified β 2-actin (*actb2*) control and *fmn2b* N-terminal from cDNA obtained from FACS sorted motor neurons (*mnx1:GFP* positive cells) in 24 hpf and 60 hpf wild-type *Tg(mnx1:GFP)* embryos.

4.2.4 *CaP* motor neuron growth cone translocation is slower in *fmn2b* mutants

To test the hypothesis that the behavioural defects in *fmn2b* mutants arise due to motor neuron morphogenesis defects, the *fmn2b*^{Δ4/Δ7} mutant line was crossed to *Tg(mnx1:GFP)* to obtain homozygous mutants for *fmn2b* in the transgenic background labelling motor neurons (Figure 3.5 A). Using the *fmn2b* mutant line with motor neurons labelled with GFP under the *mnx1* promoter, the developing motor neurons were observed from 22 hpf to 26 hpf. The growth cones of the pioneering caudal primary (CaP) motor neurons were tracked using the Manual Tracking ImageJ plugin, and the average translocation speed was calculated. The *fmn2b*^{Δ4/Δ7} embryos showed slow outgrowth of the CaP neurons (Figure 4.4 A, B). The growth cone translocation speed of *fmn2b*^{Δ4/Δ7} embryos ($22.1 \pm 1.575 \mu\text{m/h}$) was slower than the *fmn2b*^{+/+} embryos ($28.34 \pm 1.962 \mu\text{m/h}$) (Figure 4.4 C).

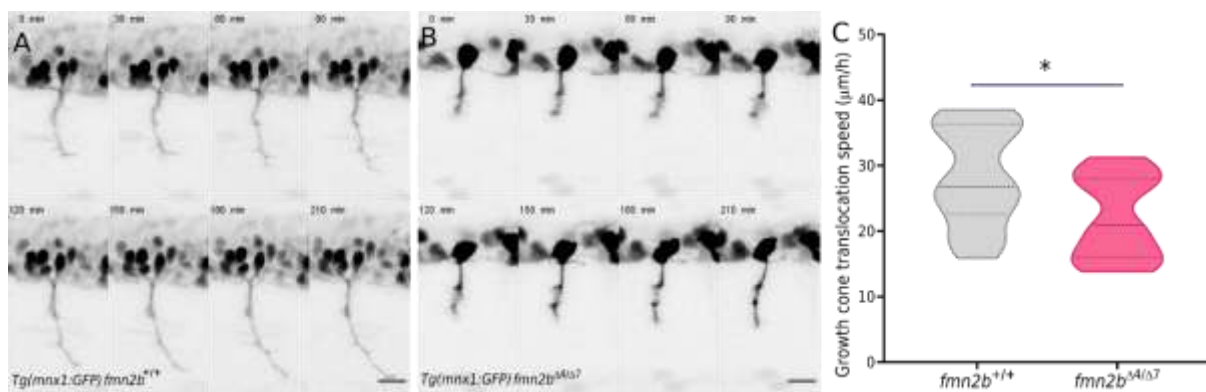


Figure 4.4 *fmn2b* is required for motor neuron growth cone translocation

A) Representative montages of live imaging of growth cone translocation in *fmn2b*^{+/+} and **B)** *fmn2b*^{Δ4/Δ7} embryos in the background of *Tg(mnx1:GFP)* during the time period of 22 hpf to 26 hpf. **C)** Quantification of motor neuron growth cone translocation speed in *fmn2b*^{+/+} (n=15 growth cones; N=3 embryos) and *fmn2b*^{Δ4/Δ7} (n=16 growth cones; N=4 embryos). (* p-value = 0.0298; Mann-Whitney U test) Scale bar is equivalent to 20 μm .

4.2.5 Primary motor neuron outgrowth and branching defects in *fmn2b* mutants

In addition to the slow outgrowth of CaP motor neurons in *fmn2b* mutants, the collateral branches extended by the motor neurons at 24 hpf and 60 hpf were observed using the *fmn2b* mutant line *fmn2b*^{Δ4/Δ7} in the background of the transgenic line *Tg(mnx1:GFP)*. The embryos were mounted laterally to image the motor neurons using a 25X oil immersion (NA 0.8) objective in a Zeiss LSM780 microscope. After the images were acquired, the motor neuron fascicle length and the number of branches normalized to the fascicle length, i.e., the branch density, were quantified using the NeuronJ plugin in ImageJ. At 24 hpf, 100% of the hemisegments had the CaP motor neuron soma present in

fmn2b^{+/+} as well *fmn2b*^{A4/Δ7} embryos. Representative micrographs showing the effect of *fmn2b* knockout on motor neurons labelled with *mnx1:GFP* are presented for 24 hpf (**Figure 4.5 A, B**) and 60 hpf (**Figure 4.6 A, B**) embryos. The branch density along the fascicle length (**Figure 4.5 E**) and the length of the fascicle (**Figure 4.5 F**) extended by the primary motor neurons at 24 hpf was found to be reduced in *fmn2b*^{A4/Δ7} embryos. Similarly, 60 hpf *fmn2b*^{A4/Δ7} embryos showed a reduction in the outgrowth of the primary and secondary motor neuron axons measured by the fascicle length (**Figure 4.6 F**) and reduction in the density (**Figure 4.6 E**) of collateral branches along the fascicle. The functional domains FH1 and FH2, characteristic of Formin-2, are conserved across vertebrates (**Figure 2.1 A**). To assess if the expression of exogenous Fmn2 could rescue the outgrowth and branching defects, full-length mouse Fmn2 (*mFmn2*) mRNA tagged with mCherry was injected in the *fmn2b*^{A4/Δ7} mutant embryos at the 1-cell stage. The branch density and fascicle length defects were rescued in 24 hpf (**Figure 4.5 E, F**) and 60 hpf (**Figure 4.6 E, F**) mutant embryos.

The FH2 domain of formins is required for F-actin nucleation, a principal function of formins (Goode and Eck, 2007; Quinlan et al., 2007; Yoo et al., 2015). To test the role of actin nucleating activity of Fmn2b in motor neuron branching, an F-actin nucleation dead version of mFmn2 with a point mutation converting the Isoleucine at 1226 amino acid position to Alanine (Quinlan et al., 2007; Roth-Johnson et al., 2014; Kundu et al., 2020), mFmn2-I1226A was used. The mRNA for mFmn2-I1226A tagged with mCherry was injected in the *fmn2b*^{A4/Δ7} embryos, and the motor neuron development was analyzed. Representative micrographs showing the effect of injection of full length and nucleation dead mFmn2 on *fmn2b* mutants are presented for 24 hpf (**Figure 4.5 C, D**) and 60 hpf (**Figure 4.6 C, D**) embryos. The 24 hpf (**Figure 4.5 E, F**) and 60 hpf (**Figure 4.6 E, F**) mutant embryos injected with the *mFmn2-I1226A* mRNA continued to exhibit the outgrowth and branching defects similar to the *fmn2b*^{A4/Δ7} embryos. Rescue of phenotype exhibited by the *fmn2b*^{A4/Δ7} mutants by full-length mFmn2 but not the nucleation dead version, mFmn2-I1226A points towards the conserved function of Fmn2 in motor neuron development. It highlights the significance of the nucleation activity of Fmn2 in the outgrowth and branching of motor neurons. The branching defects observed in *fmn2b* mutants are also recapitulated in Fmn2b morphants, where they show a reduction in branch density as well as fascicle length at 24 hpf and 60 hpf (data not shown).

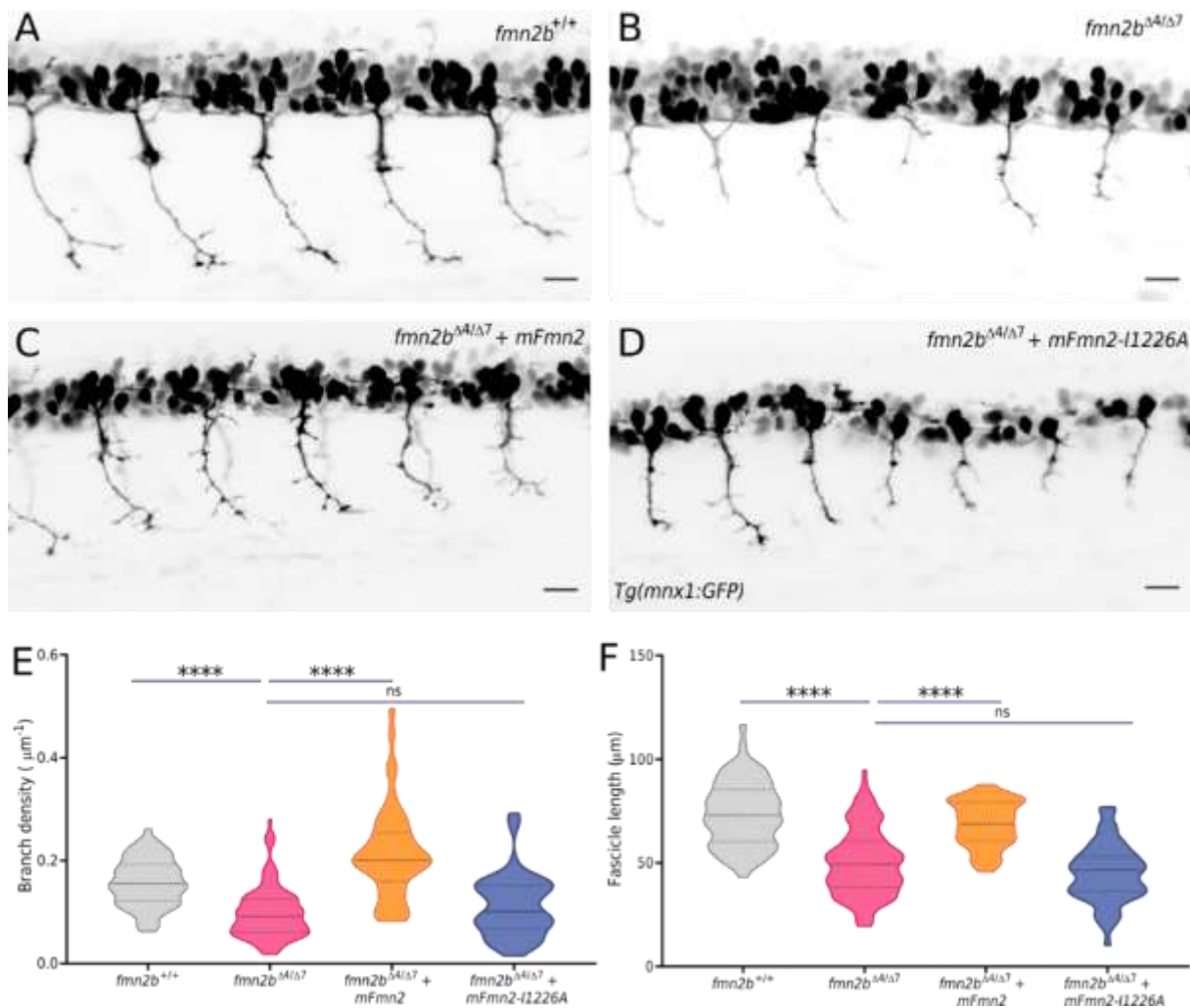


Figure 4.5 Outgrowth and branching defects in 24 hpf *fmn2b* mutants

Representative micrographs of motor neurons labelled by Tg(mnx1:GFP) in 24 hpf old **A)** *fmn2b*^{+/+} and **B)** *fmn2b* ^{$\Delta 4/\Delta 7$} embryos. Representative micrographs of motor neurons labelled by Tg(mnx1:GFP) in 24 hpf old *fmn2b* ^{$\Delta 4/\Delta 7$} mutant embryos injected at 1-cell stage with **C)** full-length mouse Fmn2 (mFmn2) mRNA and **D)** nucleation dead version, mFmn2-I1226A mRNA. **E)** Quantification of branch density (number of branches per fascicle normalized to the fascicle length) along the fascicle extended by motor neurons per myotome hemisegment in *fmn2b*^{+/+} ($0.1571 \pm 0.005 \mu\text{m}^{-1}$; n=70 hemisegments) and *fmn2b* ^{$\Delta 4/\Delta 7$} embryos ($0.0981 \pm 0.005 \mu\text{m}^{-1}$; n=118 hemisegments). The defects were rescued in *fmn2b* ^{$\Delta 4/\Delta 7$} embryos injected with mFmn2 mRNA ($0.2139 \pm 0.012 \mu\text{m}^{-1}$; n=51 hemisegments) but not in the embryos injected with mFmn2-I1226A mRNA ($0.111 \pm 0.007 \mu\text{m}^{-1}$; n=63 hemisegments). **F)** Quantification of fascicle length extended by motor neurons per myotome hemisegment in *fmn2b*^{+/+} ($68.97 \pm 1.55 \mu\text{m}$; n=70 hemisegments) and *fmn2b* ^{$\Delta 4/\Delta 7$} embryos ($44.98 \pm 1.756 \mu\text{m}$; n=118 hemisegments). The defects were rescued in *fmn2b* ^{$\Delta 4/\Delta 7$} embryos injected with mFmn2 mRNA ($73.7 \pm 1.86 \mu\text{m}$; n=51 hemisegments) but not in the embryos injected with mFmn2-I1226A mRNA ($73.7 \pm 1.86 \mu\text{m}$; n=63 hemisegments). (**** p-value <0.0001; ns - not significant; Kruskal Wallis test followed by Dunn's post-hoc analysis) Scale bar is equivalent to 20 μm .

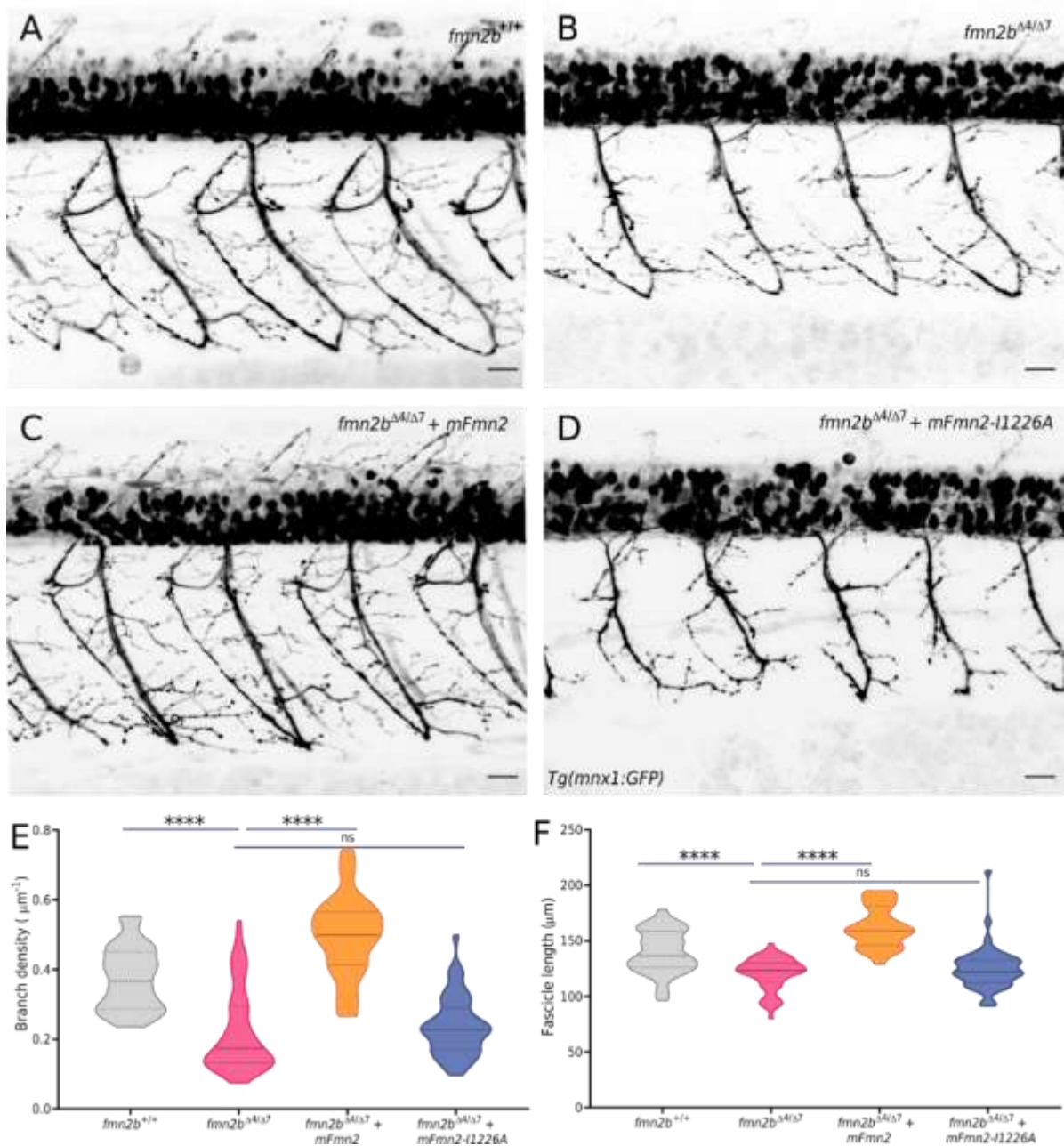


Figure 4.6 Outgrowth and branching defects in 60 hpf *fmn2b* mutants

Representative micrographs of motor neurons labelled by Tg(mnx1:GFP) in 60 hpf old **A)** *fmn2b*^{+/+} and **B)** *fmn2b*^{Δ4/Δ7} embryos. Representative micrographs of motor neurons labelled by Tg(mnx1:GFP) in 24 hpf old *fmn2b*^{Δ4/Δ7} mutant embryos injected at 1-cell stage with **C)** full-length mouse Fmn2 (mFmn2) mRNA and **D)** nucleation dead version, mFmn2-I1226A mRNA. **E)** Quantification of branch density (number of branches per fascicle normalized to the fascicle length) along the fascicle extended by motor neurons per myotome hemisegment in *fmn2b*^{+/+} ($0.3746 \pm 0.014 \mu\text{m}^{-1}$; n=37 hemisegments) and *fmn2b*^{Δ4/Δ7} embryos ($0.2211 \pm 0.015 \mu\text{m}^{-1}$; n=57 hemisegments). The defects were rescued in *fmn2b*^{Δ4/Δ7} embryos injected with mFmn2 mRNA ($0.4955 \pm 0.021 \mu\text{m}^{-1}$; n=30 hemisegments) but not in the embryos injected with mFmn2-I1226A mRNA ($0.2369 \pm 0.012 \mu\text{m}^{-1}$; n=48 hemisegments). **F)** Quantification of fascicle length extended

by motor neurons per myotome hemisegment in *fmn2b*^{+/+} ($139.6 \pm 3.21 \mu\text{m}$; n=37 hemisegments) and *fmn2b* ^{$\Delta 4/\Delta 7$} embryos ($120.4 \pm 1.94 \mu\text{m}$; n=57 hemisegments). The defects were rescued in *fmn2b* ^{$\Delta 4/\Delta 7$} embryos injected with mFmn2 mRNA ($162.7 \pm 3.38 \mu\text{m}$; n=30 hemisegments) but not in the embryos injected with mFmn2-I1226A mRNA ($124.7 \pm 2.81 \mu\text{m}$; n=48 hemisegments). (**** p-value <0.0001; ns - not significant; Kruskal Wallis test followed by Dunn's post-hoc analysis) Scale bar is equivalent to 20 μm .

4.2.6 Rostral Primary (RoP) motor neuron development is compromised in *fmn2b* mutants

Despite slower outgrowth rates and reduced branching in *fmn2b* ^{$\Delta 4/\Delta 7$} embryos, CaP neurons eventually reach their target and innervate the ventral musculature in the zebrafish flank. On the contrary, another class of primary motor neurons, the Rostral primary (RoP) motor neurons, typically project to the mid-dorsal and mid-ventral musculature (Bagnall and McLean, 2014; Bello-Rojas et al., 2019), are affected in *fmn2b* ^{$\Delta 4/\Delta 7$} embryos. The position of the RoP and MiP cell bodies are also predetermined and are usually found adjacent to the CaP and VaP cell body cluster in the spinal cord. The cell bodies of primary motor neurons are distinctly recognizable at 24 hpf. The *fmn2b* mutants exhibited defects in the development of the RoP neurons. To quantify these defects, the myotome hemisegments with or without the defect were counted, and the percentage of hemisegments with or without the defect was plotted.

On examining the 24 hpf embryos, the RoP cell body was missing in *fmn2b* mutants. Compared to 2.5% of the hemisegments quantified in *fmn2b*^{+/+} embryos, 46.87% of the hemisegments in *fmn2b* ^{$\Delta 4/\Delta 7$} embryos did not have the RoP cell body. In the *fmn2b* ^{$\Delta 4/\Delta 7$} embryos injected with mFmn2 mRNA, only 2.85% of hemisegments had missing RoP soma, whereas 43.75% of the hemisegments in mutant embryos injected with the mFmn2-I1226A mRNA continued to show loss of RoP soma (**Figure 4.9**).

At 60 hpf, the RoP motor neurons failed to innervate their target in the mid-dorsal and mid-ventral musculature. Two major types of defects were observed, absence of RoP outgrowth and stalling of RoP at the choice point near the horizontal myoseptum (HMS), where the RoP axons take a sharp lateral turn.

In the *fmn2b* mutant embryos, 91.3% of the hemisegments analyzed showed little to no lateral innervation. Of these, 44.35% of the hemisegments showed defasciculated axons near the

near the horizontal myoseptum, which acts as a choice point for RoP axons to turn laterally. The laterally. The hemisegments with defasciculated axons were classified as stalled RoP axons. axons. Similar defects in RoP-like secondary motor neurons have been reported to occur due to due to depletion of Kif1b and Fidgetin like-1 in zebrafish (Fassier et al., 2018; Atkins et al., 2019). al., 2019). However, 46.95% of hemisegments had no RoP innervation altogether and were were classified as RoP absent. Only 8.7% of hemisegments showed the stereotypical RoP innervation and were classified as RoP present. In the *fmn2b^{+/+}* embryos, only a minor fraction, fraction, 3.15% of the hemisegments quantified, showed RoP stalling defects, and the rest had had stereotypical innervation by the RoP neurons. The RoP stalling and outgrowth defects were defects were rescued by injecting full-length *mFmn2* mRNA with only 10.16% hemisegments hemisegments with RoP stalling and 8.47% hemisegments with RoP outgrowth defects. On the On the other hand, RoP defects persisted in the *fmn2b^{Δ4/Δ7}* embryos injected with *mFmn2-I1226A* *mFmn2-I1226A* mRNA, with 18.3% of hemisegments having stalled RoP axons 81.7 without RoP without RoP innervation (**Figure 4.9 RoP soma are affected in *fmn2b* mutants at 24 hpf**

Representative micrographs of motor neurons labelled by Tg(mnx1:GFP) in 24 hpf **A)** *fmn2b^{+/+}* and **B)** *fmn2b^{Δ4/Δ7}* embryos. Representative micrographs of motor neurons labelled by Tg(mnx1:GFP) in 24 hpf old *fmn2b^{Δ4/Δ7}* mutant embryos injected at 1-cell stage with **C)** full-length mouse Fmn2 (mFmn2) mRNA and **D)** nucleation dead version, mFmn2-I1226A mRNA. The red arrowheads point towards the RoP soma. **E)** Bar graph summarizing the percentage of embryos with defects in RoP soma in 24 hpf *fmn2b^{+/+}* (n=18) and *fmn2b^{Δ4/Δ7}* embryos (n=23). The defects were rescued in *fmn2b^{Δ4/Δ7}* embryos injected with mFmn2 mRNA (n=12) but not in the embryos injected with mFmn2-I1226A mRNA (n=10). **F)** Violin plots depicting the variation in data summarized in the bar graphs for 24 hpf embryos. (**** p-value <0.0001; ns - not significant; Kruskal Wallis test followed by Dunn's post-hoc analysis) Scale bar is equivalent to 20 μm.

Figure 4.10).

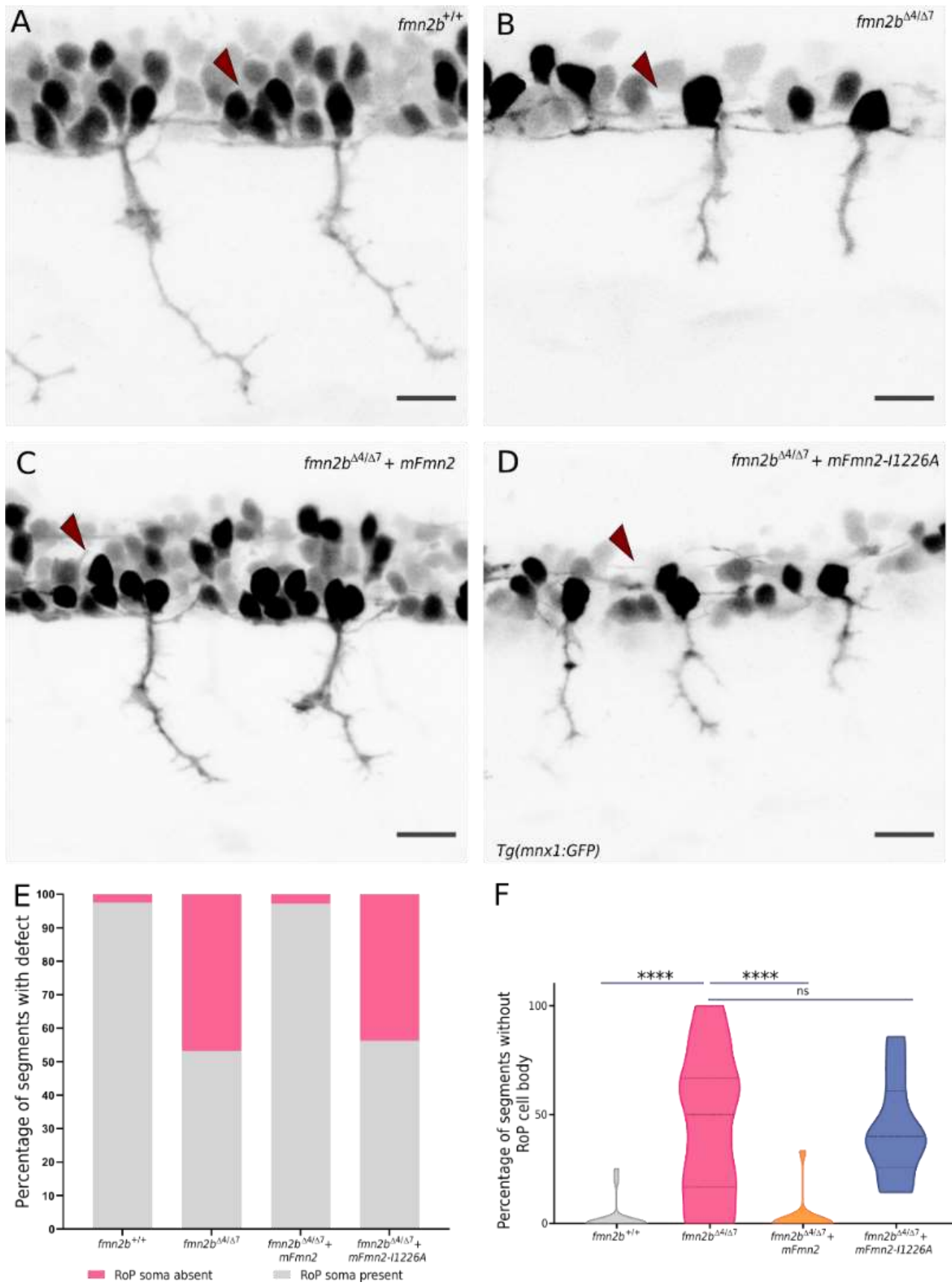


Figure 4.7 RoP soma are affected in *fmn2b* mutants at 24 hpf (continued on next page)

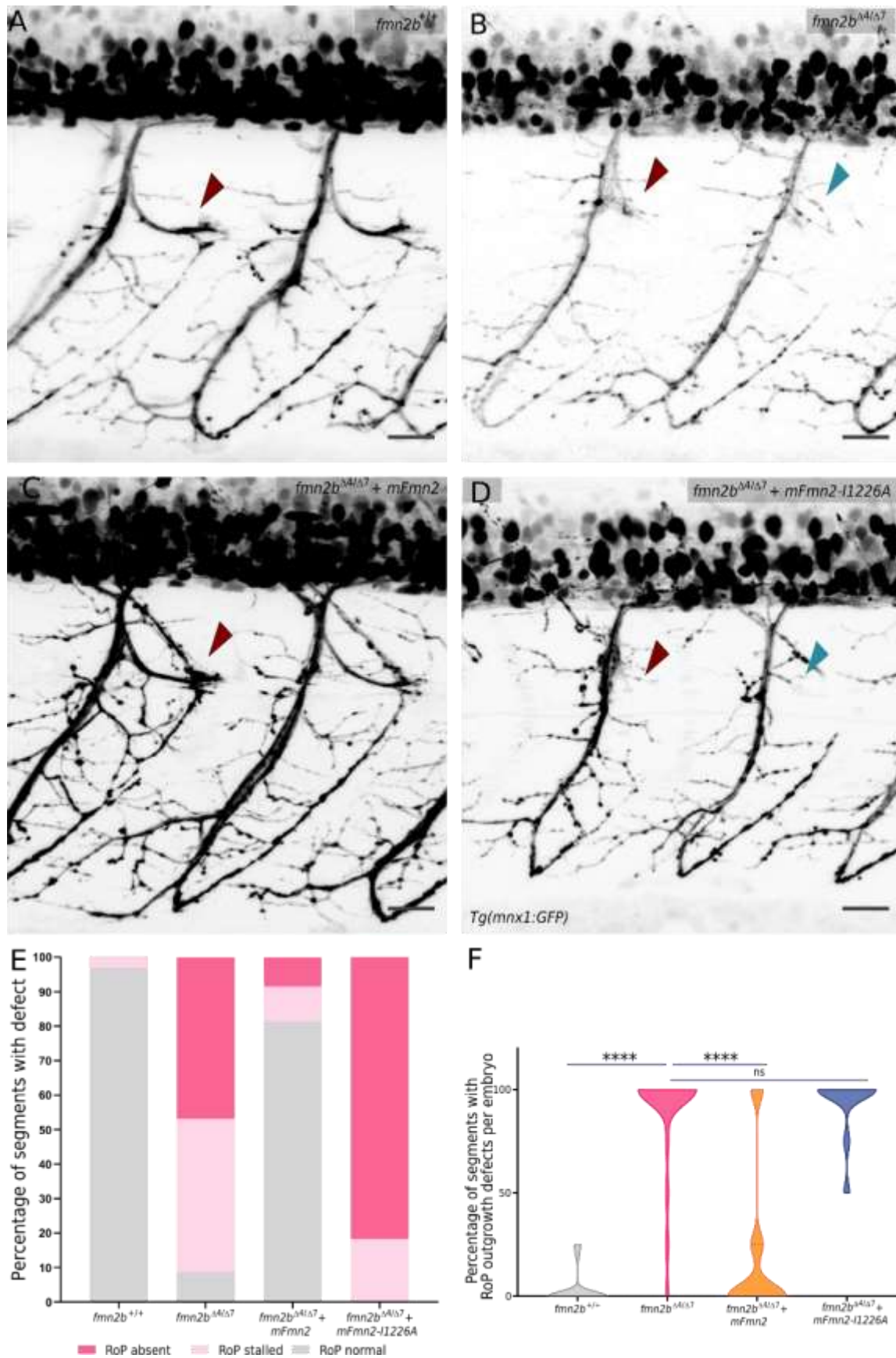


Figure 4.8 Lateral innervation of the myotome by RoP is affected in *fmn2b* mutants at 60 hpf (continued on next page)

Figure 4.9 RoP soma are affected in *fmn2b* mutants at 24 hpf

Representative micrographs of motor neurons labelled by Tg(mnx1:GFP) in 24 hpf **A)** *fmn2b*^{+/+} and **B)** *fmn2b*^{Δ4/Δ7} embryos. Representative micrographs of motor neurons labelled by Tg(mnx1:GFP) in 24 hpf old *fmn2b*^{Δ4/Δ7} mutant embryos injected at 1-cell stage with **C)** full-length mouse *Fmn2* (mFmn2) mRNA and **D)** nucleation dead version, mFmn2-I1226A mRNA. The red arrowheads point towards the RoP soma. **E)** Bar graph summarizing the percentage of embryos with defects in RoP soma in 24 hpf *fmn2b*^{+/+} (n=18) and *fmn2b*^{Δ4/Δ7} embryos (n=23). The defects were rescued in *fmn2b*^{Δ4/Δ7} embryos injected with mFmn2 mRNA (n=12) but not in the embryos injected with mFmn2-I1226A mRNA (n=10). **F)** Violin plots depicting the variation in data summarized in the bar graphs for 24 hpf embryos. (**** p-value <0.0001; ns - not significant; Kruskal Wallis test followed by Dunn's post-hoc analysis) Scale bar is equivalent to 20 μm.

Figure 4.10 Lateral innervation of the myotome by RoP is affected in *fmn2b* mutants at 60 hpf

Representative micrographs of motor neurons labelled by Tg(mnx1:GFP) in 60 hpf **A)** *fmn2b*^{+/+} and **B)** *fmn2b*^{Δ4/Δ7} embryos. Representative micrographs of motor neurons labelled by Tg(mnx1:GFP) in 60 hpf old *fmn2b*^{Δ4/Δ7} mutant embryos injected at 1-cell stage with **C)** full-length mouse *Fmn2* (mFmn2) mRNA and **D)** nucleation dead version, mFmn2-I1226A mRNA. The red arrowheads point towards the stalled RoP, and the blue arrowheads point towards no RoP outgrowth. **E)** Bar graphs summarizing the percentage of embryos with defects in RoP axon outgrowth in 60 hpf *fmn2b*^{+/+} (n=22) and *fmn2b*^{Δ4/Δ7} embryos (n=26). The defects were rescued in *fmn2b*^{Δ4/Δ7} embryos injected with mFmn2 mRNA (n=14) but not in the embryos injected with mFmn2-I1226A mRNA (n=13). **F)** Violin plots depicting the variation in data summarized in the bar graphs for 60 hpf embryos. (**** p-value <0.0001; ns - not significant; Kruskal Wallis test followed by Dunn's post-hoc analysis) Scale bar is equivalent to 20 μm.

4.2.7 The muscle structure is not affected in *fmn2b* mutants

The motor defects seen in *fmn2b* mutants can be attributed to the motor neurons' outgrowth and branching defects. Further, phalloidin staining was done with 60 hpf embryos to label the muscle actin to visualize muscle integrity. The *fmn2b*^{+/+} and *fmn2b*^{Δ4/Δ7} embryos had comparable muscle architecture observed by phalloidin staining (**Figure 4.11**). This observation supports the earlier findings in touch evoked escape response assay where the maximum instantaneous speed was unaffected in *fmn2b*^{Δ4/Δ7} embryos. So far, the defects seen in motor behaviours can be explained by decreased arborization and, therefore, innervation of the muscles by primary and secondary motor neurons in 24 hpf and 60 hpf *fmn2b* mutants despite the muscle structure is unaffected. This apart, the *fmn2b* mutants were next screened for any defects at the level of the neuromuscular junctions formed by the motor neurons.

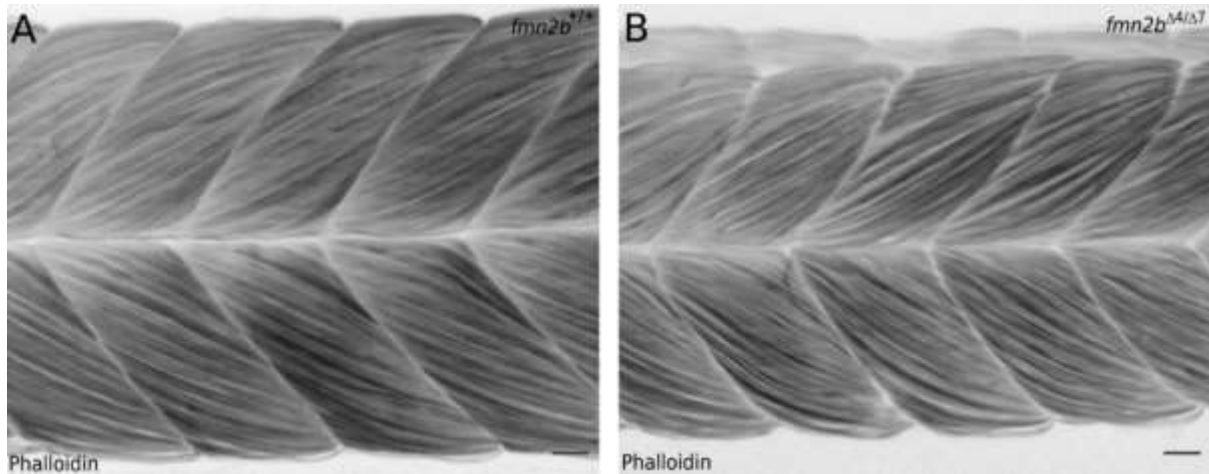


Figure 4.11 Muscle integrity in *fmn2b* mutants

Representative micrographs of 60 hpf **A)** *fmn2b*^{+/+} (n=10) and **B)** *fmn2b*^{Δ4/Δ7} (n=10) embryos stained with Alexa fluor 568 tagged phalloidin to label the muscle structure. Scale bar is equivalent to 20 μm.

4.2.8 Coverage of NMJ synapses in *fmn2b* mutants

Primary motor neurons innervate fast-twitch muscles and form functional synapses by 48 hpf. The motor deficits seen in *fmn2b* mutants in touch evoked escape response assay could be due to defects at the level of NMJ synapses. Double immunostaining of whole-mount 60 hpf embryos with *znp-1* antibody (presynaptic marker) and α-bungaratoxin (post-synaptic marker) marks engaged NMJ synapses. Synapses with colocalized *znp-1* and α-bungaratoxin labelling were quantified using the SynapCountJ plugin in Fiji. SynapCountJ quantifies the synapses co-labelled with presynaptic and postsynaptic markers across the neuronal arbor traces made using the NeuronJ plugin. The number of synapses obtained from SynapCountJ was normalized to the area of the myotome corresponding to one somite and the length of the arbor traced.

The *fmn2b*^{Δ4/Δ7} embryos were found to have reduced coverage of synapses per myotome (**Figure 4.12 C**). Still, the number of synapses normalized to the arbor length was found to be comparable in the *fmn2b*^{+/+} and *fmn2b*^{Δ4/Δ7} embryos. This result is consistent with previous observations of reduced branching density of motor neurons. However, the normalized number of synapses made by the motor neurons, albeit with reduced branching density, is not affected in *fmn2b* mutants (**Figure 4.12 D**). Therefore, *fmn2b* mutants have fewer NMJ synapses due to inadequate arborization of the primary motor

neurons, but the ability of NMJ synapse formation is not significantly affected. The NMJ defects corroborate with the locomotor defects seen in *fmn2b* mutants caused due to a decrease in the total number of synapses per myotome, leading to insufficient activation of the myotome.

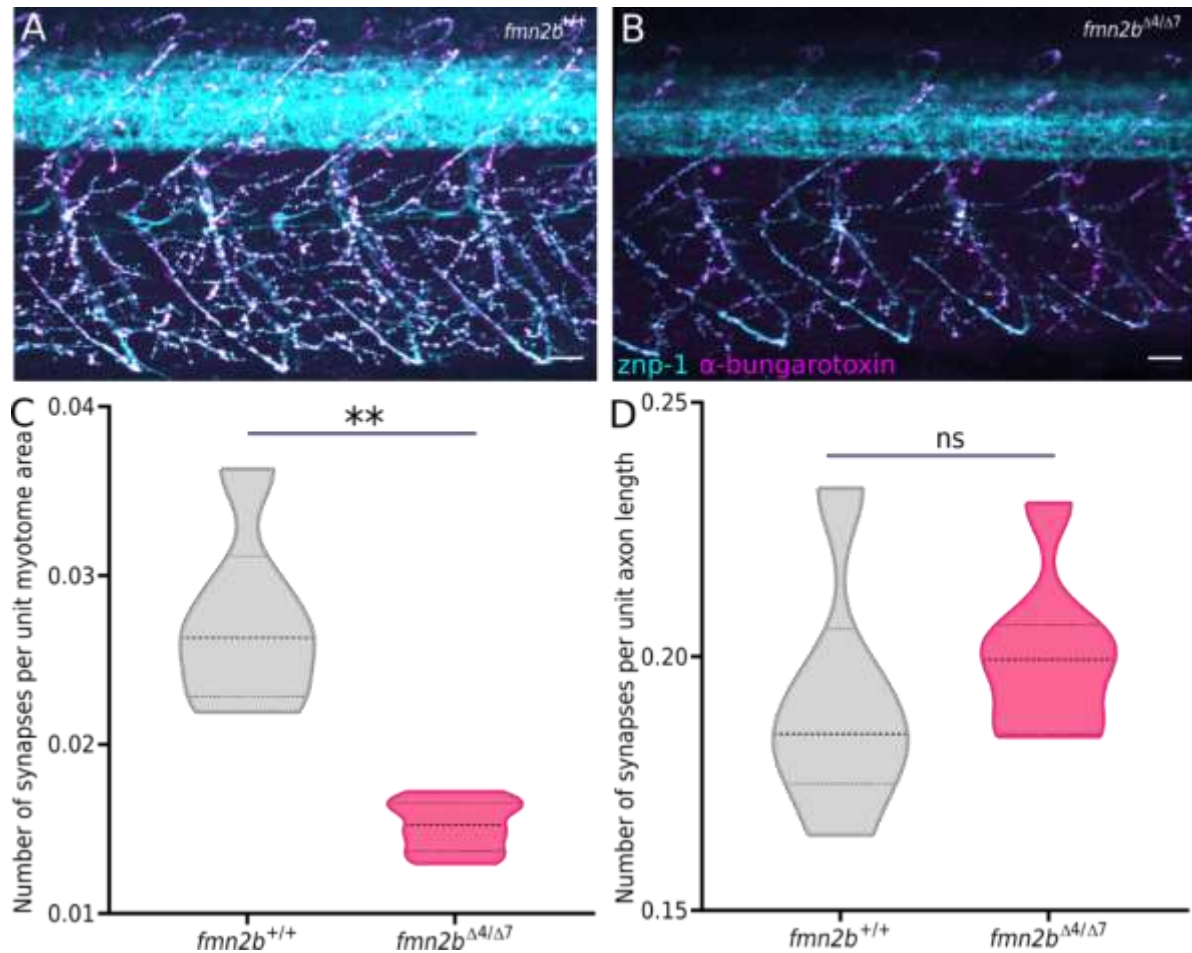


Figure 4.12 Synapse coverage in *fmn2b* mutants

Representative micrographs of 60 hpf **A)** *fmn2b*^{+/+} (n=6) **B)** *fmn2b*^{Δ4/Δ7} embryos (n=7) costained with znp-1 antibody and α-bungaratoxin. Quantification of colocalization of znp-1 and α-bungaratoxin in NMJ structures of 60 hpf embryos. **C)** Number of synapses per unit myotome area in *fmn2b*^{+/+} (0.0272 ± 0.002 ; n=6) and *fmn2b*^{Δ4/Δ7} embryos (0.01521 ± 0.0005 ; n=7, **p-value=0.0012). **D)** Number of synapses per unit axon length in *fmn2b*^{+/+} (0.1903 ± 0.009 ; n=6) and *fmn2b*^{Δ4/Δ7} embryos (0.2001 ± 0.005 ; n=7). (ns- not significant; Mann Whitney U test) Scale bar is equivalent to 20 μm.

4.2.9 Effect of overexpression of *Fmn2* in motor neurons

The role of *fmn2b* in motor neuron development has been established by observing *fmn2b* mutants, where the loss of *Fmn2b* in motor neurons causes a reduction in outgrowth and branching. Overexpression of mouse *Fmn2* was done in wildtype embryos to test the phenotypes in the *Fmn2* gain of function context. The embryos overexpressing m*Fmn2* show increased branching, but overexpression of the nucleation dead m*Fmn2*-I1226A did not cause any significant changes and was comparable to the wild-type embryos (**Figure 4.13** A, B, E, F). The branch density was found to be increased in m*Fmn2* mRNA injected embryos at 24 hpf, and 60 hpf but not in m*Fmn2*-I1226A mRNA injected group (**Figure 4.13** C, G). Interestingly, in 24 hpf embryos, the fascicle length was not significantly different in embryos overexpressing m*Fmn2* but found to be decreased in embryos overexpressing m*Fmn2*-I1226A. In 60 hpf embryos, the fascicle length was slightly increased in the m*Fmn2* overexpression group but remain unaffected in the m*Fmn2*-I1226A overexpression group (**Figure 4.13** D, H).

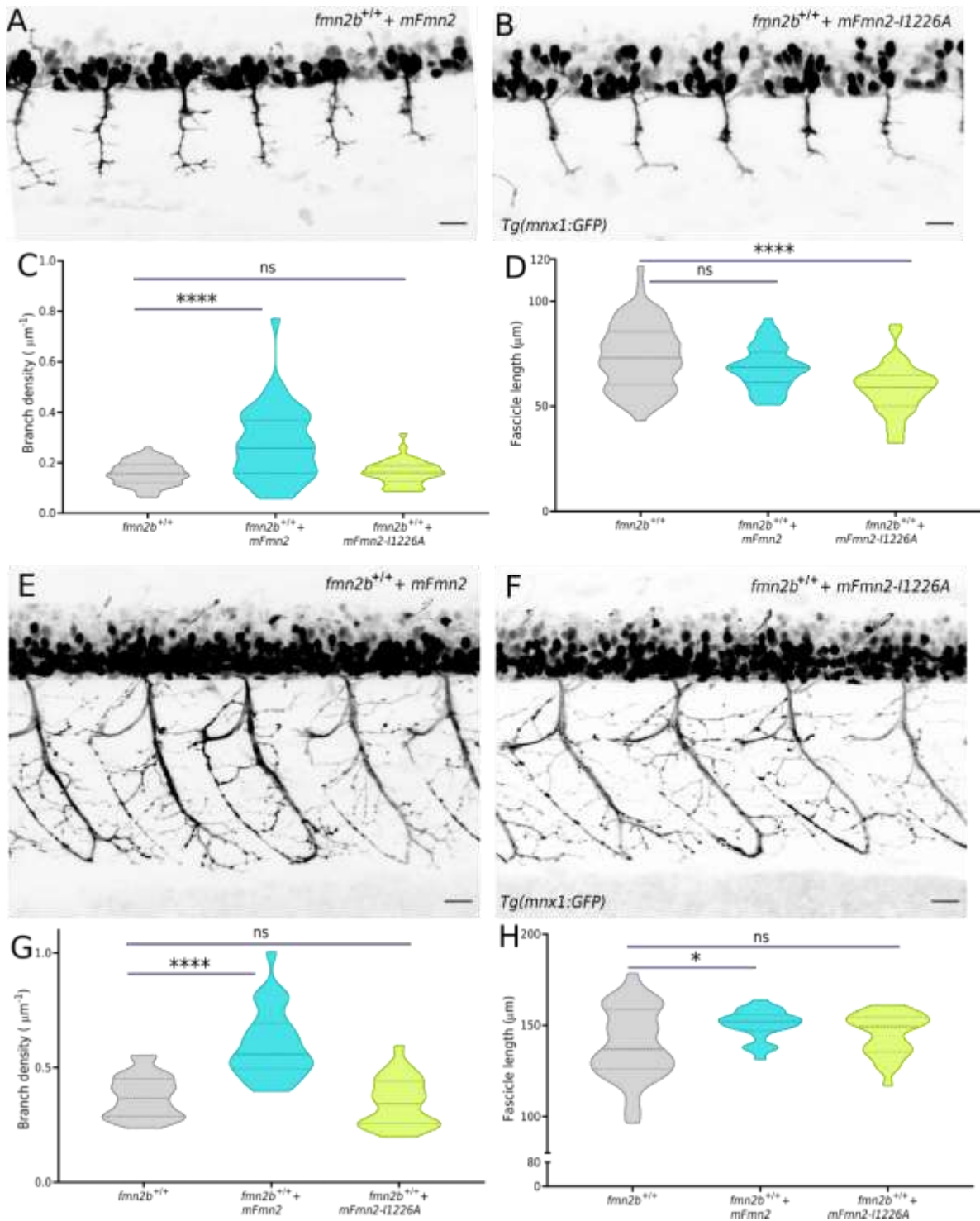


Figure 4.13 Outgrowth and branching phenotypes upon overexpression of mouse Fmn2 in wild-type embryos

Representative micrographs of motor neurons labelled by Tg(mnx1:GFP) in 24 hpf old *fmn2b^{+/+}* embryos injected with **A**) mFmn2 mRNA and **B**) mFmn2-I1226A mRNA. **C**) Quantification of branch density (number of branches per fascicle normalized to the fascicle length) along the fascicle extended by motor neurons per myotome hemisegment in *fmn2b^{+/+}* embryos injected with mFmn2 mRNA ($0.2728 \pm 0.0217 \mu\text{m}^{-1}$; $n=40$ hemisegments) and mFmn2-I1226A mRNA ($0.1617 \pm 0.007 \mu\text{m}^{-1}$; $n=40$ hemisegments). **D**) Quantification of fascicle length extended by

motor neurons per myotome hemisegment in *fmn2b^{+/+}* embryos injected with mFmn2 mRNA ($73.7 \pm 1.86 \mu\text{m}$; n=40 hemisegments) and mFmn2-I1226A mRNA ($68.3 \pm 1.603 \mu\text{m}$; n=40 hemisegments). Representative micrographs of motor neurons labelled by Tg(*mnx1*:GFP) in 60 hpf old *fmn2b^{+/+}* embryos injected with **E)** mFmn2 mRNA and **F)** mFmn2-I1226A mRNA. **G)** Quantification of branch density (number of branches per fascicle normalized to the fascicle length) along the fascicle extended by motor neurons per myotome hemisegment in 60 hpf *fmn2b^{+/+}* embryos injected with mFmn2 mRNA ($0.599 \pm 0.027 \mu\text{m}^{-1}$; n=28 hemisegments) and mFmn2-I1226A mRNA ($0.3481 \pm 0.02 \mu\text{m}^{-1}$; n=28 hemisegments). **H)** Quantification of fascicle length extended by motor neurons per myotome hemisegment in 60 hpf *fmn2b^{+/+}* embryos injected with mFmn2 mRNA ($150.4 \pm 1.536 \mu\text{m}$; n=28 hemisegments) and mFmn2-I1226A mRNA ($145 \pm 2.18 \mu\text{m}$; n=28 hemisegments). (**** p-value <0.0001; * p-value = 0.0175; ns - not significant; Kruskal Wallis test followed by Dunn's post-hoc analysis) Scale bar is equivalent to 20 μm .

However, quantification of RoP soma and RoP axon outgrowth phenotypes in the *fmn2b^{+/+}* embryos overexpressing mFmn2 and mFmn2-I1226A did not reveal any significant changes (**Figure 4.14 A-H**).

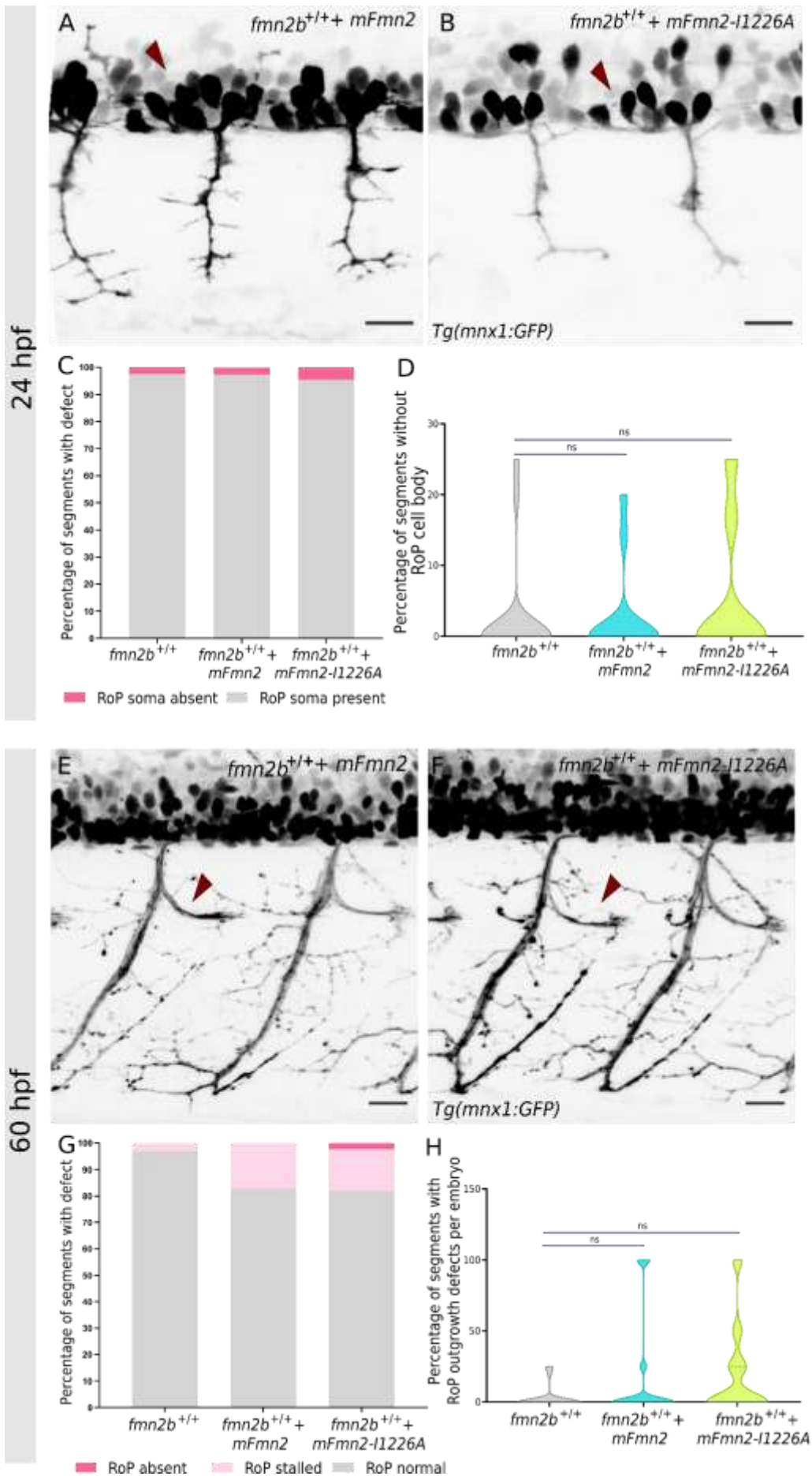


Figure 4.14 RoP development is not affected by overexpression of Fmn2 in wild-type embryos

Representative micrographs of motor neurons labelled by Tg(mnx1:GFP) in 24 hpf old *fmn2b^{+/+}* embryos injected with **A**) mFmn2 mRNA and **B**) mFmn2-I1226A mRNA. Red arrowhead points towards the RoP soma. Representative micrographs of motor neurons labelled by Tg(mnx1:GFP) in 60 hpf old *fmn2b^{+/+}* embryos injected with **E**) mFmn2 mRNA and **F**) mFmn2-I1226A mRNA. Red arrowhead points towards the RoP outgrowth. **C**) Bar graphs summarizing the percentage of embryos with defects in RoP cell body in 24 hpf *fmn2b^{+/+}* (n=18). No defects were observed in *fmn2b^{+/+}* embryos injected with mFmn2 mRNA (n=13) and mFmn2-I1226A mRNA (n=16). **G**) Bar graphs summarizing the percentage of embryos with defects in RoP axon outgrowth in 60 hpf *fmn2b^{+/+}* (n=22). No defects were observed in *fmn2b^{+/+}* embryos injected with mFmn2 mRNA (n=13) and mFmn2-I1226A mRNA (n=11). Violin plots depicting the variation in data summarized in the bar graphs for **D**) 24 hpf embryos and **H**) 60 hpf embryos. (ns- not significant; Kruskal Wallis test followed by Dunn's post-hoc analysis) Scale bar is equivalent to 20 μ m.

4.3 Discussion

In zebrafish, motor neuron development follows a preset spatiotemporal pattern, causing the emergence of some of the earliest behaviours in the zebrafish embryo. The role of *fmn2b* in the outgrowth and branching of motor neurons and the associated motor behaviours has been described in this chapter. The expression of *fmn2b* mRNA in the spinal cord paved the way for the hypothesis that *fmn2b* could be required in motor neuron development (**Figure 4.1**). The presence of *fmn2b* transcripts specifically in motor neurons expressing *mnx1:GFP* strengthened this hypothesis (**Figure 4.3**).

The *fmn2b* mutants show defects in motor behaviours during early development. Spontaneous tail coiling frequency was reduced in 22-26 hpf *fmn2b* mutant embryos and touch evoked swimming was affected in 60 hpf *fmn2b* mutants. The behavioural defects were corroborated by outgrowth and branching defects in motor neurons (**Figure 4.2**).

Live imaging of 22-26 hpf *fmn2b*^{+/+} and *fmn2b*^{A4/Δ7} embryos in the background *Tg(mnx1:GFP)* revealed that the growth cone translocation speed of CaP motor neurons is decreased in *fmn2b*^{A4/Δ7} embryos (**Figure 4.4**). The delayed outgrowth of CaP motor neurons at this early stage pointed towards a potential role of *fmn2b* in the further development of motor neurons. Recent studies in chick spinal neurons implicate Fmn2 in growth cone translocation (Sahasrabudhe et al., 2016; Ghate et al., 2020). Fmn2 is shown to regulate growth cone motility by acting as a molecular clutch and stabilizing point contacts in migrating neurons. Therefore, the slow growth cone translocation speeds observed in zebrafish CaP neurons could be attributed to the requirement of Fmn2 in exerting traction force at the adhesion sites for adequate motility (Sahasrabudhe et al., 2016; Ghate et al., 2020). Another aspect to consider is the microtubule deregulation caused due to Fmn2 knockdown, as reported previously in the growth cones of chick spinal neurons. Microtubules' innervation of growth cone filopodia provides directionality and stability to the branches (Kundu et al., 2020). Microtubule dynamics visualized using EB3 comets in zebrafish Rohon Beard (RB) neurons revealed that Fmn2 knockdown causes a reduction in stability of microtubule innervation and therefore underscore its requirement in microtubule regulation *in vivo* (Kundu et al., 2021). The experiments in this study showing EB3 labelling and visualization in zebrafish RB neurons were performed by me and are discussed briefly in the future directions. Similar experiments could provide insights regarding the role of cytoskeletal dynamics in motor

neuron development. Growth cone motility requires coordinated actin and microtubule rearrangements in response to the guidance cues in which formins play an active role (Fernández-Barrera and Alonso, 2018; Kawabata Galbraith and Kengaku, 2019). These observations are worth investigating in the context of motor neuron development defects in *fmn2b* mutants.

Motor neurons develop in two distinct phases in zebrafish embryos. Primary motor neurons are the first to be born, undergo axonogenesis and start innervating the target muscle fibers by 24 hpf to form transient synapses. On the other hand, secondary motor neurons extend their axons only after 26 hpf and form synapses by 60 hpf (Myers et al., 1986). The experiments done in this chapter were performed at 24 hpf and 60 hpf to selectively look at primary motor neurons at 24 hpf and collectively look at primary and secondary motor neurons at 60 hpf. In addition, the 60 hpf embryos have elaborate branching and fully functional NMJ synapses made by all the classes of primary motor neurons, CaP, MiP and RoP, allowing characterization of *fmn2b* in outgrowth, branching and synapse formation in motor neurons.

The behaviour defects are corroborated by outgrowth and branching defects in motor neurons of *fmn2b*^{Δ4/Δ7} embryos. In 24 hpf *fmn2b* mutant embryos, branch density along the fascicle extended by CaP, MiP and RoP and the fascicle length itself was reduced, suggesting a decrease in the innervation of the intended fast muscle fibers. The decreased branching is manifested as the reduction in spontaneous tail coiling frequency. Further, the branch density and fascicle outgrowth phenotypes are rescued by the expression of mouse Fmn2 in the *fmn2b* mutants. However, the nucleation dead version of mouse Fmn2 could not rescue the defects (**Figure 4.5**).

Similarly, the 60 hpf *fmn2b*^{Δ4/Δ7} embryos have reduced branch density and fascicle outgrowth compared to wild-type embryos and are likely to be causing the reduction in speed and distance covered by *fmn2b* mutants. The motor neuron branching and outgrowth defects in 60 hpf *fmn2b* mutants could be rescued by full-length mFmn2 but not the nucleation dead version, mFmn2-I1226A (**Figure 4.6**). The rescue of phenotypes in the *fmn2b* mutants by mouse Fmn2 suggests a conserved role of Formin-2 in motor neuron development across vertebrates.

The RoP soma and RoP outgrowth were severely affected in *fmn2b* mutants. At 24 hpf, multiple hemisegments in *fmn2b* mutants did not have RoP soma at its characteristic position in the spinal cord (**Figure 4.9**). The role of Fmn2 in the regulation of differentiation or specification of progenitors is not formally tested despite several studies indirectly indicating pathways involving Fmn2 in cell differentiation. In a recent report, Fmn2 has been shown to cause neural progenitor differentiation defects Fmn2 and Flna double knockout mice in a synergistic manner (Lian et al., 2016). However, this hypothesis has not been formally tested in zebrafish. The absence of RoP soma in zebrafish *fmn2b* mutants shown here hints at a possible role of *fmn2b* in neural progenitor specification or differentiation. The RoP soma were seen in the expected location in *fmn2b*^{A4/Δ7} embryos injected with mFmn2 mRNA, but the injection of mFmn2-I1226A mRNA could not rescue the defect. It is interesting to note that the F-actin nucleating activity of Fmn2 is required for the differentiation of motor neuron progenitors or their specification. These results open up new possibilities to uncover the mechanistic role of Fmn2 in neural development.

In wild-type zebrafish embryos, the lateral projections from RoP motor neurons and follower follower secondary motor neurons begin outgrowth later than CaP and MiP neurons (Kuwada, (Kuwada, 1993; Liu et al., 2016). In 60 hpf *fmn2b* mutants, the side branches of RoP motor neurons innervating the horizontal myoseptum were either not observed or appeared to be stalled at the choice point, i.e., the horizontal myoseptum (**Figure 4.9 RoP soma are affected in *fmn2b* mutants at 24 hpf**

Representative micrographs of motor neurons labelled by Tg(mnx1:GFP) in 24 hpf **A)** *fmn2b*^{+/+} and **B)** *fmn2b*^{A4/Δ7} embryos. Representative micrographs of motor neurons labelled by Tg(mnx1:GFP) in 24 hpf old *fmn2b*^{A4/Δ7} mutant embryos injected at 1-cell stage with **C)** full-length mouse Fmn2 (mFmn2) mRNA and **D)** nucleation dead version, mFmn2-I1226A mRNA. The red arrowheads point towards the RoP soma. **E)** Bar graph summarizing the percentage of embryos with defects in RoP soma in 24 hpf *fmn2b*^{+/+} (n=18) and *fmn2b*^{A4/Δ7} embryos (n=23). The defects were rescued in *fmn2b*^{A4/Δ7} embryos injected with mFmn2 mRNA (n=12) but not in the embryos injected with mFmn2-I1226A mRNA (n=10). **F)** Violin plots depicting the variation in data summarized in the bar graphs for 24 hpf embryos. (**** p-value <0.0001; ns - not significant; Kruskal Wallis test followed by Dunn's post-hoc analysis) Scale bar is equivalent to 20 μm.

Figure 4.10). RoP-like secondary motor neurons, which follow the same trajectory as RoP primary motor neurons, have previously shown pathfinding and stalling defects at the horizontal myoseptum in Fidgetin like-1 and Kif1b mutants (Fassier et al., 2018; Atkins

et al., 2019). Similarly, the stalling of RoP axons appears as defasciculation of axons in *fmn2b* mutants implicating Fmn2b in axonal pathfinding in response to guidance cues at the choice point. The absence of RoP outgrowth could also be because of the lack of RoP soma, as observed in 24 hpf mutants. This caused a noticeable reduction in the innervation of the mid-dorsal and mid-ventral region of the myotome. The RoP may be more severely affected than the CaP neurons due to their late axonogenesis concomitant with the pleiotropic function and late expression of *fmn2b* in the spinal cord at 48 hpf.

Axonal outgrowth and branching relies on coordinated actin and microtubule dynamics and is further regulated by extrinsic cues (Ketschek and Gallo, 2010; Gallo, 2011, 2016; Coles and Bradke, 2015; Ketschek et al., 2015; Armijo-Weingart and Gallo, 2017; Menon and Gupton, 2018). Cytoskeletal proteins like Arp2/3, Rho family GTPases, Drebrin, WVE-1/WAVE regulatory complex (WRC) and septins have been shown to regulate actin cytoskeleton required for adequate axonal branching (Spillane et al., 2011; Hu et al., 2012; Chia et al., 2014; Spillane and Gallo, 2014; Ketschek et al., 2016; Balasanyan et al., 2017). In addition, the F-actin nucleation activity of formins has recently been implicated in the maintenance of actin trails and patches necessary for axon branching (Ganguly et al., 2015; Kundu et al., 2020). Abrogation of F-actin nucleation activity of Fmn2 can be achieved by mutating the Isoleucine residue at 1226 amino acid position to Alanine (Quinlan et al., 2007; Roth-Johnson et al., 2014; Kundu et al., 2020). Remarkably, the failure of mFmn2-I1226A in rescuing the defects underscores the significance of the actin nucleating activity of Fmn2b in motor neuron outgrowth and branching consistent with reports from primary neuronal cultures of chick spinal cord reported previously (Kundu et al., 2020). Therefore, the motor neuron development in zebrafish is dependent on the F-actin nucleation activity of Fmn2b.

Analysis of NMJ synapses using znp-1 and α -bungarotoxin double staining in *fmn2b* mutants showed no changes in the number of synapses along the total length of the motor neuron branches. Still, it showed a reduction in the total number of synapses when normalized to the area of the target myotome. This observation suggests that the primary role of Fmn2b is in regulating motor neuron branching and not in the formation of NMJ synapses. The behavioural defects in *fmn2b* mutants are likely due to the muscles not receiving sufficient input due to inadequate branching (**Figure 4.12**).

Intriguingly, the overexpression of mouse Fmn2 in *fmn2b*^{+/+} (wild-type) embryos causes opposite effects compared to *fmn2b* knockout manifested as hyperbranching. Although, the nucleation dead version of mFmn2 does not cause any changes, again pointing towards the involvement of actin nucleation activity of Fmn2. Fmn2 knockout and overexpression are similar in spinal neuron cultures from chick embryos, bolstering the role that *fmn2b* plays in neuronal outgrowth and branching.

In a recent study, prolonged exposure of zebrafish larvae to strong and variable water currents caused upregulation of Fmn2b, as observed in a proteomic screen (Langebeck-Jensen et al., 2019). The rapid upregulation of Fmn2b in response to environmental stressors involving swimming and force generation in larvae with pre-established motor neural circuits invoke the possible involvement of *fmn2b* in neuronal plasticity. It will be interesting to note if the upregulation of Fmn2b upon exposure to strong water flow causes any changes in the motor neuron branching or their functional activity.

Mutations in human Fmn2 have been reported to cause sensory process dysfunction (Marco et al., 2018). Although indirectly, the role of Fmn2 in sensorimotor integration could be tested in future to obtain insights regarding the sensory processing and integration defects seen in humans with mutations in Fmn2. This apart, there is increasing evidence to suggest the need for adequate cytoskeletal dynamics in health and disease concerning motor neurons. Amyotrophic Lateral Sclerosis (ALS) and Spinal Muscular Atrophy (SMA) are genetic diseases affecting motor neurons with several cytoskeletal proteins implicated in their pathology. Proteins like Pfn1, which work with close cooperation from formins, are very well characterized in the pathogenesis of familial ALS (Wu et al., 2012). However, the role of formins in motor neuron degeneration or motor neuron disease pathogenesis is not characterized. The anatomical and behavioural defects related to motor neurons observed in *fmn2b* mutants present a unique opportunity to test the role of formins in disease progression of neuropathies, including but not limited to ALS and SMA.

In conclusion, this is new evidence supporting the notion that *fmn2b*, particularly its actin nucleating activity, has a critical role in regulating motor neuron development and associated motor behaviours.

5

Role of Fmn2b in development of visual circuits

5.1 Introduction

The retinal ganglion cells (RGCs) relay visual information from the eyes to the contralateral optic tectum in a topographic manner. In zebrafish, the visual connections start forming between 3 and 5 dpf and remain plastic throughout the life span of zebrafish (Stuermer, 1988; Hutson and Chien, 2002b; Kita et al., 2015). RGCs are midline crossing neurons that make an elaborate arbor onto the contralateral side of the optic tectum in the developing zebrafish embryo. RGCs are late pioneering neurons that start outgrowth around 34-36 hpf, form the optic nerve, crossing the optic chiasma to reach the tectum by 46-48 hpf and make first functional connections in the optic tectum by 72 hpf (Stuermer, 1988; Kita et al., 2015). RGCs defasciculate into branches predestined to their final targets in the optic tectum based on their relative position in the retina (Mumm et al., 2006; Scott and Baier, 2009). The arborization is followed by activity-dependent pruning of the connections made previously to accommodate visual experience-dependent plasticity (Hua et al., 2005; Mumm et al., 2006; Avitan et al., 2017; Xie et al., 2019). Therefore, RGCs are an interesting population of neurons for investigating the role of *fmn2b* mediated outgrowth and development because they are midline crossing and late pioneering neurons, like the spiral fiber neurons in the hindbrain. The requirement of active remodelling of the branched structures of the RGC arbor would require dynamic cytoskeletal remodelling, making the role of *fmn2b* in RGC development particularly exciting. The information relayed by the RGCs to the tectum needs further processing, which is undertaken by various tectal neurons dependent on the stimulus (Scott and Baier, 2009; Nevin et al., 2010; Kita et al., 2015).

One such group of neurons is the commissures connecting the two optic tecta in zebrafish, akin to the superior colliculus in mammals (Gebhardt et al., 2019). The function of Intertectal neurons (ITNs), previously termed as Intertectal commissures (ITCs) (Wilson et al., 1990), has recently been characterized in zebrafish in mediating relay of visual information between the two optic tecta enabling binocular vision (Gebhardt et al., 2019). The ITNs receive the retinotectal inputs from the contralateral RGCs and do not require the ipsilateral connectivity to achieve binocular vision integration during prey capture (Gebhardt et al., 2019). The ITNs are also late pioneering commissural neurons and present an opportunity to study the role of *Fmn2b* in their development.

The data presented in this chapter is from preliminary experiments suggesting a potential role of Fmn2b in the development of neural circuits underlying vision in zebrafish. The leads presented in this chapter need to be systematically tested along with the consequences of abnormalities in the neural circuits on behaviour.

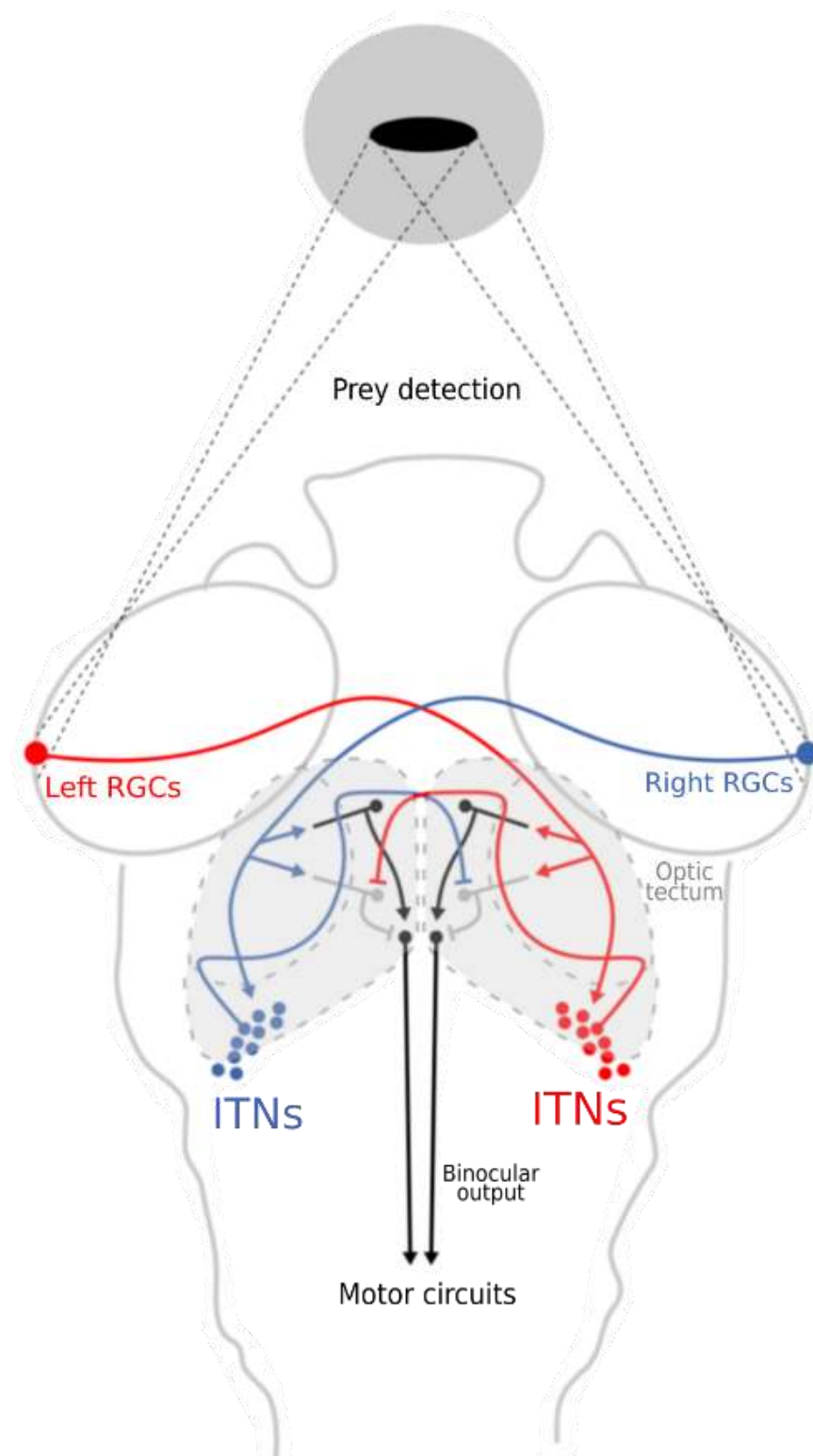


Figure 5.I.1. Schematic showing the RGCs, ITNs and optic tectum in a zebrafish larva (adapted from (Gebhardt et al., 2019))

5.2 Results

5.2.1 Expression of *fmn2b* mRNA in the Retinal Ganglionic Cell layer in zebrafish

The expression of *fmn2b* mRNA is broadly seen in the central nervous system, including the spinal cord. Interestingly, *fmn2b* mRNA was also seen to be expressed in the retinal ganglionic cell layer of zebrafish embryos from 24 hpf up to 96 hpf (Figure 5.1 A-D). The micrographs in **Figure 5.1** show *fmn2b* expression restricted to the RGC layer. They marked expression in the optic nerve of 96 hpf embryos, pointing towards a specific function of *fmn2b* in RGC neuron development.

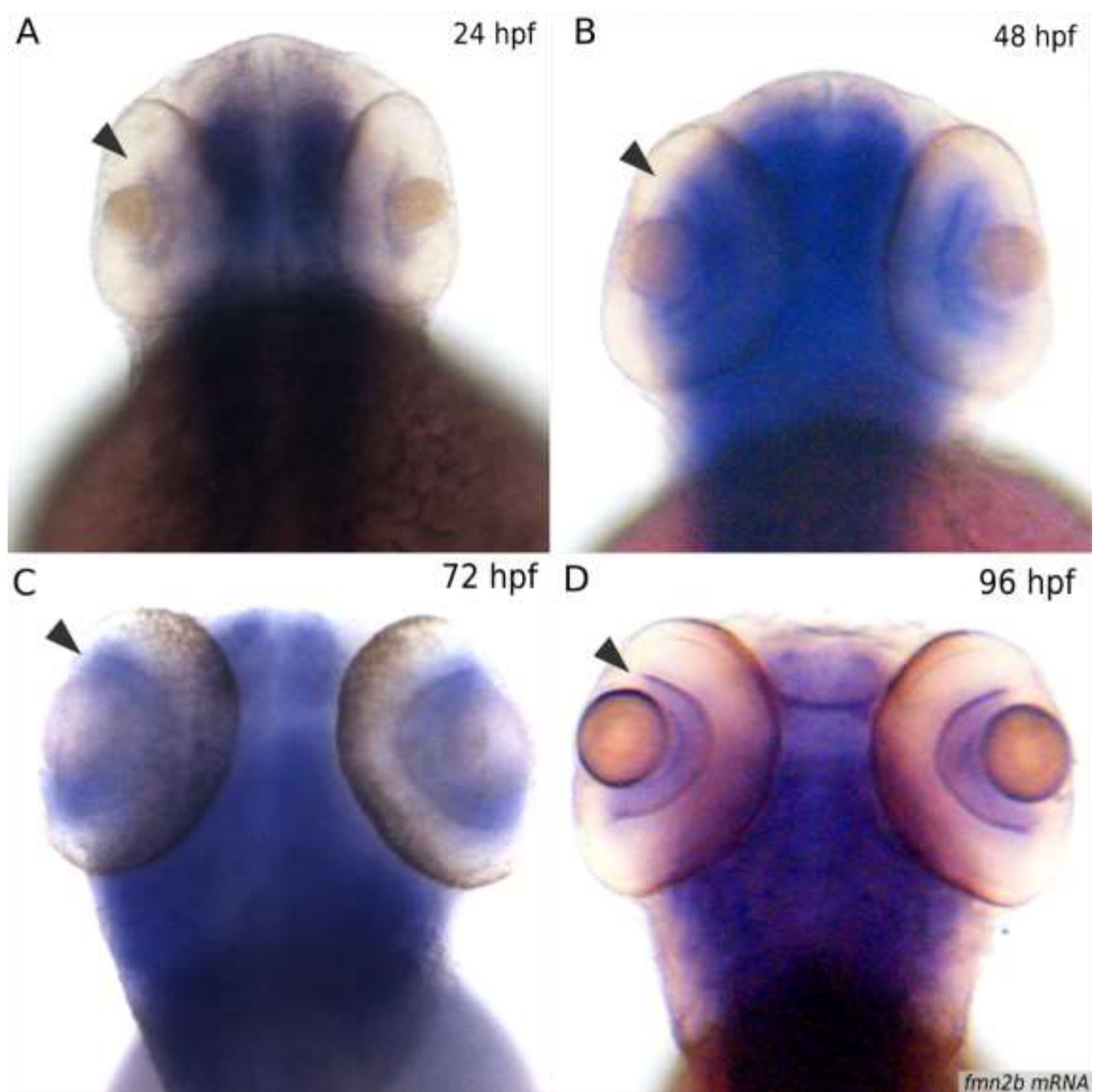


Figure 5.1 Expression of *fmn2b* mRNA in RGC layer of A) 24 hpf B) 48 hpf C) 72 hpf and D) 96 hpf embryos. The arrowhead points towards the RGC layer.

5.2.2 *fmn2b* mutants show thinning of the optic nerve

Fmn2 is involved in outgrowth and pathfinding of commissural neurons in chick spinal cord *in ovo* (Sahasrabudhe et al., 2016) and zebrafish commissural interneuron, spiral fiber neuron *in vivo* (Chapter 2). Whole mount immunostaining using anti-acetylated tubulin antibody was done with *fmn2b*^{+/+} and *fmn2b*^{Δ7/Δ7} embryos to label axonal tracts at 48 hpf stage. The optic nerve labelled by acetylated tubulin was found to be thinner in the *fmn2b*^{Δ7/Δ7} embryos. The anterior and post-optic commissures also appeared thinner in the *fmn2b*^{Δ7/Δ7} embryos. The thinning of one of the earliest axonal tracts indicate that *fmn2b* is necessary in axonogenesis. The thinning of the tracts could be due to outgrowth or differentiation defects in the respective neuronal cell bodies but remains to be tested (Figure 5.2).

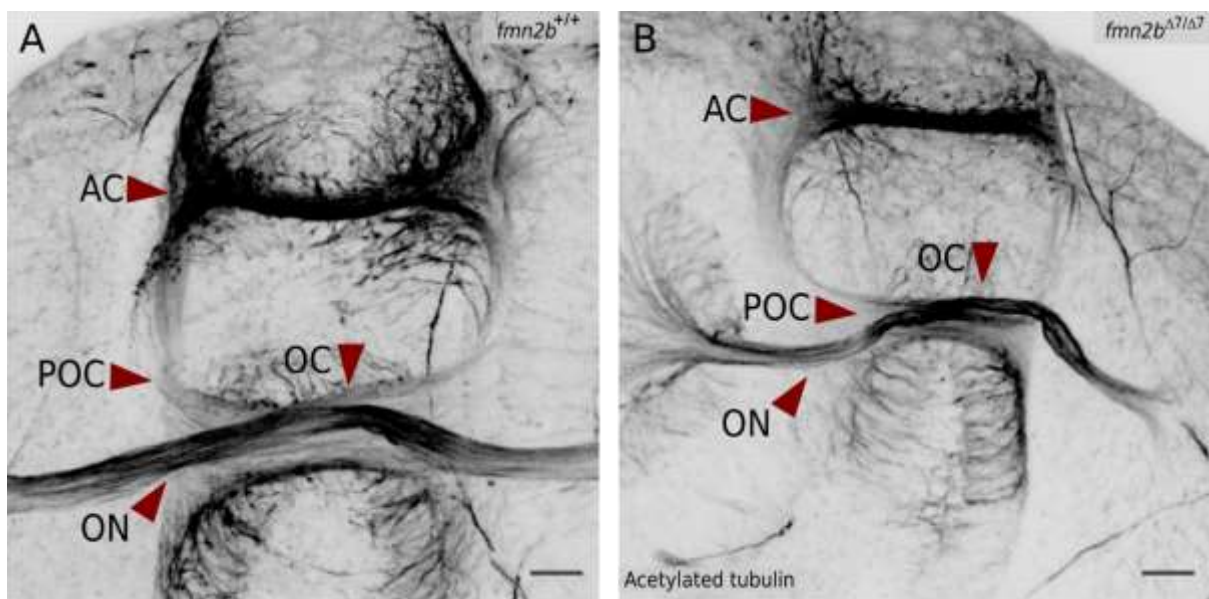


Figure 5.2 Optic nerve thinning in *fmn2b* mutants. A) *fmn2b*^{+/+} embryos B) *fmn2b*^{Δ7/Δ7} embryos. AC: Anterior Commissure, POC: Post-optic Commissure, OC: Optic chiasma, ON: Optic nerve. Scale bar is 20 μ m.

5.2.3 Arborization of Retinal Ganglionic cell (RGC) axons is reduced in the optic tectum of *fmn2b* mutants

The *Tg(brn3c:GAP43-GFP)* line labels a subpopulation of RGC neurons allowing live imaging of axonal outgrowth and arborization of the retinotectal projections (Xiao et al., 2005a). As described in Chapter 3, the *fmn2b*^{Δ7/Δ7} embryos were crossed to the *Tg(brn3c:GAP43-GFP)* line and screened for embryos homozygous for the *fmn2b* mutant allele and expressing GFP in the RGC subpopulation. These embryos were used to investigate the role of *fmn2b* in RGC development. The RGCs visualized at 4 dpf in *fmn2b*^{+/+} embryos appeared to have formed the characteristic arborization pattern onto the optic tectum (**Figure 5.3 A**). However, the arborization of RGCs was severely reduced in the *fmn2b*^{Δ7/Δ7} embryos (**Figure 5.3 B**). Further, live imaging experiments need to be done to track the development of RGCs starting at 48 hpf up to 120 hpf and beyond. Similar defects in RGC arborization were observed in *fmn2b* morphants (data not shown).

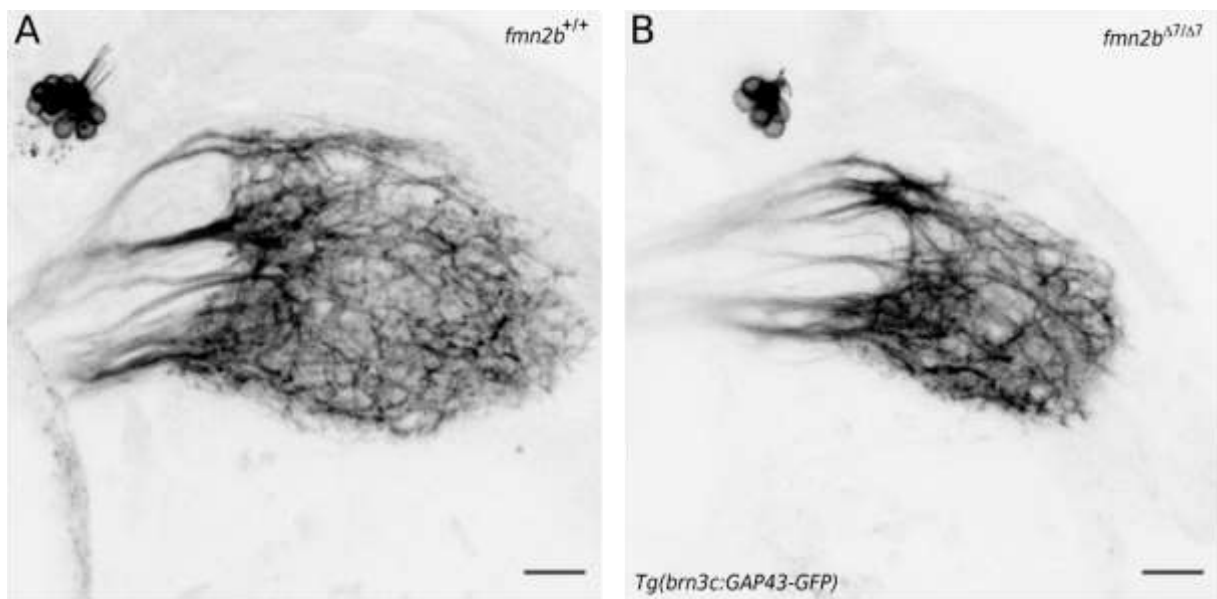


Figure 5.3 RGC arborization in **A)** *fmn2b*^{+/+} embryos **B)** *fmn2b*^{Δ7/Δ7} embryos visualized with the *Tg(brn3c:GAP43-GFP)* line. Scale bar is 20 μm. Lateral view.

5.2.4 The outgrowth of Intertectal neurons (ITNs) is affected in *fmn2b* mutants

RGCs are first-order neurons that project to the optic tectum. Inadequate retinotectal innervation could lead to defects in the downstream neurons. There are several types of

neurons in the tectum that perform various visual processing tasks dependent on the visual input. ITNs are responsible for binocular vision by relaying the visual information regarding small moving objects received via the RGCs to the contralateral tectum. Immunostaining of 96 hpf embryos with an antibody against acetylated tubulin revealed outgrowth defects in the inter-tectal neurons (ITNs) in *fmn2b*^{Δ7/Δ7} embryos (**Figure 5.4 A-C**). The number of Intertectal neuron tracts was reduced in both the heterozygous and the homozygous *fmn2b* mutants (**Figure 5.4 D**). The role of Fmn2 in growth cone motility as observed in *fmn2b* mutants (Chapter 4) and chick spinal neurons (Sahasrabudhe et al., 2016; Ghate et al., 2020) could explain the ITN tract outgrowth defects. Similar defects in the ITN neurons were observed in *fmn2b* morphants (data not shown).

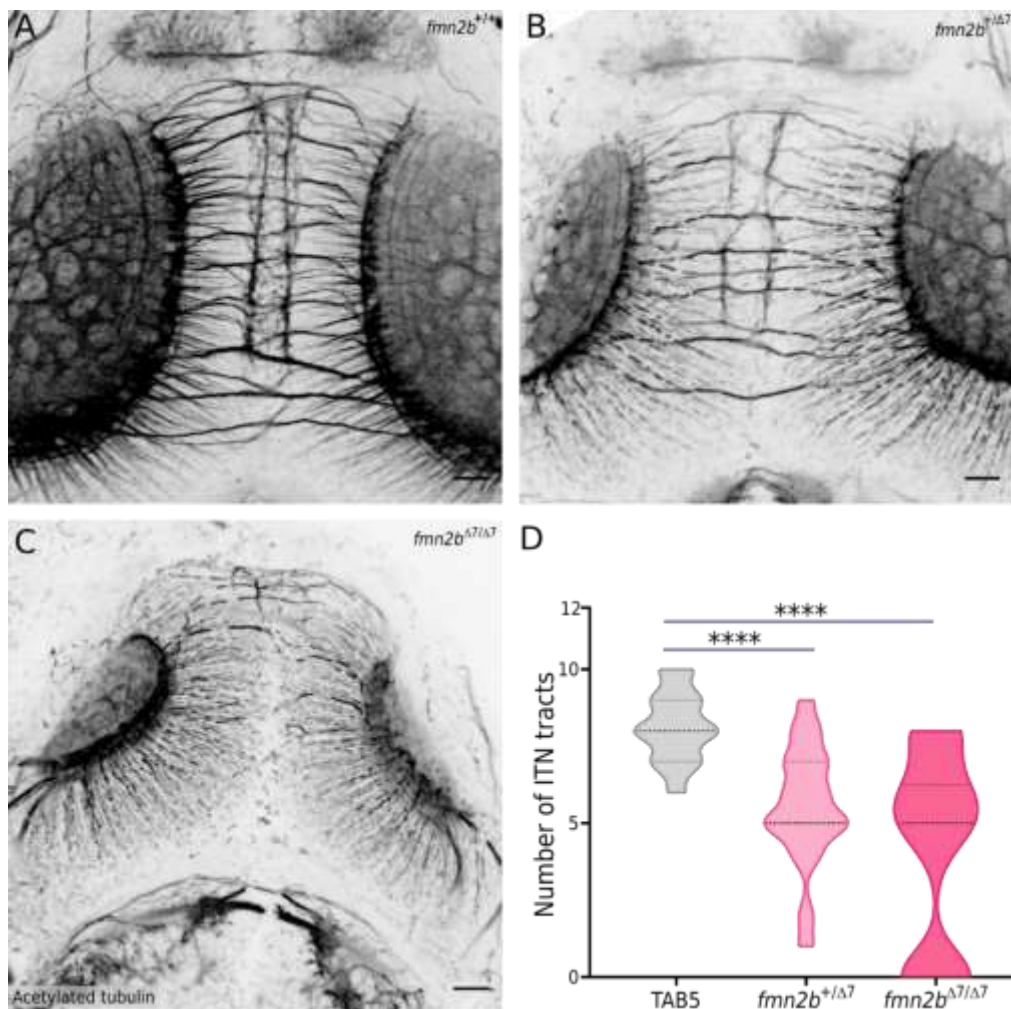


Figure 5.4 Intertectal neurons (ITNs) connecting the two optic tecta visualized by anti-acetylated tubulin immunostaining in A) *fmn2b*^{+/+} embryos (n=14), B) *fmn2b*^{+/Δ7} embryos (n=19) and C) *fmn2b*^{Δ7/Δ7} embryos (n=26) D) Quantification of number of ITN tracts per embryo. Scale bar is 20 μm. (** p-value <0.0001; Kruskal Wallis test followed by Dunn's post-hoc analysis)**

5.3 Discussion

In the *in situ* hybridization experiments, a prominent signal of *fmn2b* mRNA could be seen in the RGC layer (**Figure 5.1**) across developmental stages. To pinpoint the defects at the level of the neural circuits associated with visual processing in the *Fmn2* morphants, Retinal ganglionic cells (RGCs) were visualized using the *Tg(brn3c:GAP43-GFP)* line in the *fmn2b* mutant background. The *fmn2b* mutants showed arborization defects at 96 hpf (**Figure 5.3**). Further, immunostaining with the anti-acetylated tubulin antibody revealed thinning of the optical nerve, post-optic commissure (**Figure 5.2**) and outgrowth defects in the Intertectal neuron (ITNs) in *fmn2b* mutants (**Figure 5.4**). The ITNs are a unique set of commissural neurons connecting the two optic tecta and help with the inter-hemispheric relay of visual information (Gebhardt et al., 2019). Selective branching is imperative for initial pathfinding and arborization in the zebrafish retinotectal projections (Chalmers et al., 2016). Given the involvement of *Fmn2* in outgrowth, pathfinding and branching shown in chick spinal neurons (Sahasrabudhe et al., 2016; Kundu et al., 2020) and zebrafish motor neurons (Chapter 4), the role of *fmn2b* in RGC and ITN development needs to be investigated further. Rescue experiments remain to be done to see if *Fmn2* expression in the *fmn2b* mutants can reverse the phenotypes. Additionally, the consequence of RGC and ITN defects combined on the visual acuity of *fmn2b* morphants should be tested in future.

6

Future Directions

The work presented in this thesis underscores the role of *Fmn2b* in regulating outgrowth, pathfinding and branching of neurons to aid in establishing precise neuronal connectivity eventually. The requirement of *Fmn2b* in the development of the excitatory interneuron, spiral fiber neuron in the acoustic startle circuit and the consequent role in mediating short latency escape responses is highlighted (Chapter 2). Generation of transgenic CRISPR mutants (Chapter 3) allowed for detailed characterization of motor neuron development and motor behaviours in *fmn2b* mutants (Chapter 4). Preliminary leads suggest that *Fmn2b* could be involved in the development of neural circuits underlying visual acuity (Chapter 5). Nevertheless, there is more that remains to be explored. Some of the future directions that could be explored are outlined here.

6.1 Behavioural characterization of *fmn2b* mutants

This thesis focuses on neural circuits and the underlying behaviours in embryonic or larval zebrafish. Predominantly, the effect of *Fmn2b* depletion on acoustic startle and locomotor behaviours has been shown. However, other neural circuits could be affected, causing behavioural deficits in *fmn2b* mutants. One example is the visual processing circuits that need to be studied in more detail and quantification of any defects caused in the visual acuity of *fmn2b* mutants in the context of prey capture.

Behaviour abnormalities in the *fmn2b* mutants can be explicitly screened for cognitive abnormalities. Loss of *Fmn2* has been shown to cause intellectual disability and age-related dementia in *Fmn2* null mice (Perrone et al., 2012; Law et al., 2014; Agís-Balboa et al., 2017; Anazi et al., 2017; Marco et al., 2018; Gorukmez et al., 2020). Larval, juvenile and adult zebrafish mutants can be used to assess the effect of *Fmn2b* depletion in social interactions, learning and memory. **Figure 6.1**

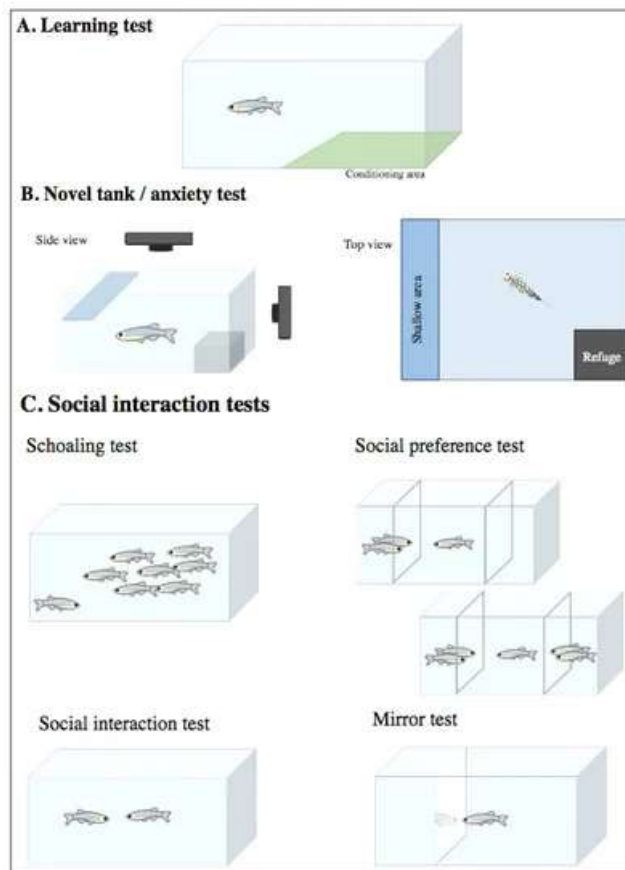


Figure 6.1 Behavior assays for adult zebrafish. (A) Conditioned place preference (CPP) test (B) Novel tank test to assess anxiety and fear (C) Social interaction tests like schooling, social preference for conspecific fish and mirror tests. Image reproduced from (Vaz et al., 2019)

6.2 Functional imaging of the neural circuits in *fmn2b* mutants

Depleting *Fmn2b* in developing zebrafish embryos either by transient knockdown by morpholinos or by CRISPR-Cas9 mediated mutagenesis causes neuro-anatomical defects in various neural circuits outlined in this thesis. Although many components of the affected neural circuits do not exhibit structural defects, their function may be compromised in *fmn2b* mutants. The absence of innervation from the inadequately developed neurons like spiral fiber tracts, primary motor neurons, and intertectal neurons is bound to affect their downstream targets. Furthermore, the structural defects seen in these neurons could be accompanied by changes in the activity of neurons upstream or downstream in the neural circuit. To address this, functional imaging of neural circuits using genetically encoded calcium indicators or calcium responsive dye injections in *fmn2b* mutants could be done in future.

6.3 Molecular mechanisms underlying outgrowth defects due to *Fmn2* depletion

Outgrowth defects are common in both *Fmn2b* morphants and mutants. Previous work in primary cell cultures and *in ovo* experiments using chick spinal cord implicate *Fmn2* in axonal outgrowth, mechanotransduction, growth cone turning, pathfinding and branching. The investigation of the molecular mechanism behind these defects revealed that the F-actin nucleating activity by the FH2 domain, actin-microtubule crosstalk by the FSI domain and the molecular clutch activity of *Fmn2* in growth cone motility are important (Sahasrabudhe et al., 2016; Ghate et al., 2020; Kundu et al., 2020, 2021). However, the consequences of depletion of *Fmn2* on subcellular cytoskeletal dynamics *in vivo* remains largely unknown.

A recent effort in this direction was made by visualizing the EB3 (End Binding 3) comet dynamics to test the effect of *fmn2b* depletion on Rohon Beard (RB) sensory neurons in zebrafish (Kundu et al., 2021). RB neurons are sensory neurons innervating the muscles and skin of zebrafish and have extensive branches (Liu and Halloran, 2005; Umeda and Shoji, 2017). I tested the role of *fmn2b* in maintaining microtubule dynamics in the growth cones of RB neurons by expressing EB3-GFP under the *ngn1* promoter in collaboration with Tanushree Kundu (Kundu et al., 2021). The *fmn2b* morphants showed increased growth speeds and decreased track lifetimes for the EB3 comets in the RB neuron growth cones compared to the control morphants. **Figure 6.2**

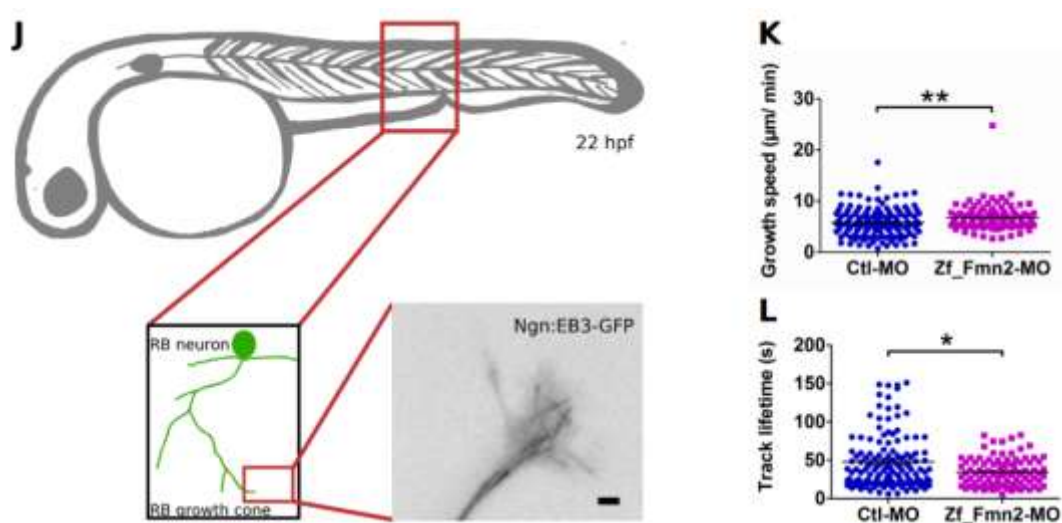


Figure 6.2 EB3 dynamics in zebrafish RB neurons are affected by *Fmn2b* knockdown. Image reproduced from (Kundu et al., 2021). **J**) Schematic showing the location of RB neurons in the zebrafish embryo at 22 hpf. The inset shows EB3 comets in a peripheral RB growth cone *in vivo*.

Scatter plot showing **K)** Growth speed and **L)** Track lifetime of EB3 comets in RB growth cones *in vivo*.

In future, subcellular imaging of tagged actin and microtubule cytoskeleton *in vivo* will provide insights into the mechanistic function of Fmn2b in the development of neural circuits. Further, the *fmn2b* mutants reported in this thesis will serve as an essential tool to investigate subcellular cytoskeletal dynamics and can be expanded to test the domain-specific activities of Fmn2b. In particular, the cytoskeletal dynamics can be visualized by labelling subcellular actin and microtubules in motor neurons *in vivo* to test their spatiotemporal organization in *fmn2b* mutants causing the outgrowth and branching defects.

6.4 The outgrowth defects could be due to loss of progenitors

Another aspect that is less studied is the role of Fmn2 in the differentiation and specification of progenitors. A report from mice shows that the Fmn2 null mice do not show microcephaly or gross morphological defects unless in the context of Flna and Fmn2 double knockout (Lian et al., 2016). On the contrary, *fmn2b* mutants and morphants consistently show morphological defects during early development, including but not limited to microcephaly. A preliminary experiment was done with *fmn2b* mutants generated in Chapter 3, to stain the nuclei with DAPI. The *fmn2b* mutants showed decrease and disorganization of the nuclei in the retina and the central nervous system (Figure F.2). The involvement of Fmn2b in neural progenitor differentiation or specification could be tested by doing EdU pulse treatment across developmental stages coinciding with the birth of neurons being tested and co-labelling of progenitor population using suitable molecular markers. This would allow marking the progenitor pool in a specific neuronal population. For example, retinal progenitor pool can be labelled around 26-28 hpf by EdU pulse and co-stained with a neuronal marker (HuC) or RGC marker (*atoh7*) at a later stage to assess the status of differentiation in the retina (Hu and Easter, 1999). A similar approach can be taken for other neurons affected in *fmn2b* mutants like the motor neurons and intertectal neurons. **Figure 6.3**

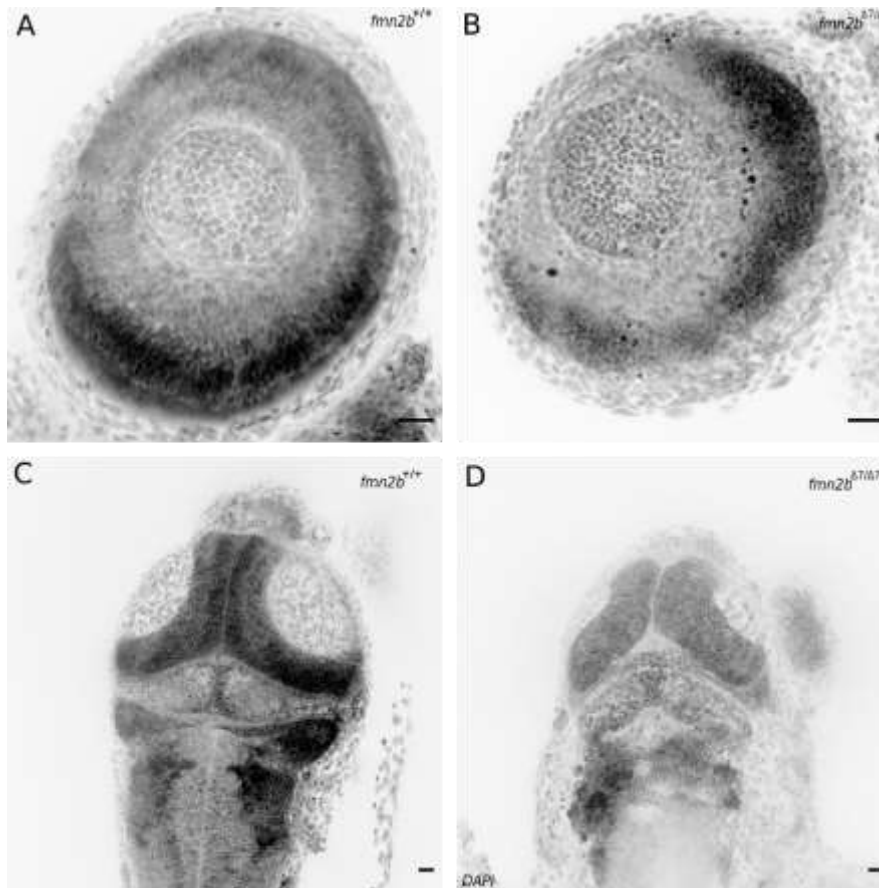


Figure 6.3 Representative micrographs of DAPI stained **retina** of **A)** *fmn2b*^{+/+} embryos **B)** *fmn2b*^{Δ7/Δ7} embryos. Representative micrographs of **dorsal view** of DAPI stained **C)** *fmn2b*^{+/+} embryos **D)** *fmn2b*^{Δ7/Δ7} embryos. Scale bar is 20 μm.

6.5 Delineating the function of *fmn2b* in neuronal vs non-neuronal development

The *Fmn2b* loss-of-function models described in this thesis do not specifically target the nervous system. The effect of *Fmn2b* depletion in morphants and CRISPR mutants is seen in neuronal as well as non-neuronal tissues. To delineate the function of *Fmn2b* and specifically test its role in the nervous system, I designed conditional knockout strategies to express a combination of sgRNAs and Cas9 in a spatiotemporally controlled manner which is outlined below. Briefly, plasmid constructs, as shown below, were made in a backbone containing Tol2 ITR sites to enable Tol2 transposase mediated transgenesis. The idea is to differentially express Cas9-(2A)-GFP (2A: self-cleaving peptide) under HuC (pan-neuronal) or Hsp70 (Heat shock inducible) promoters. Similarly, sgRNAs multiplexed by HH and HDV self-cleaving ribozymes could also be expressed under the U6 (ubiquitous), HuC or Hsp70 promoters. Transgenesis of these constructs is aided by

transgenesis markers like Lens-Cerulean (LC), Lens-mCherry (LM) and *cmlc2*:GFP (CG). Intersectional expression of Cas9 and sgRNA in a tissue-specific or developmental stage-specific manner will allow conditional knockout of *fmn2b* as required. **Figure 6.4**

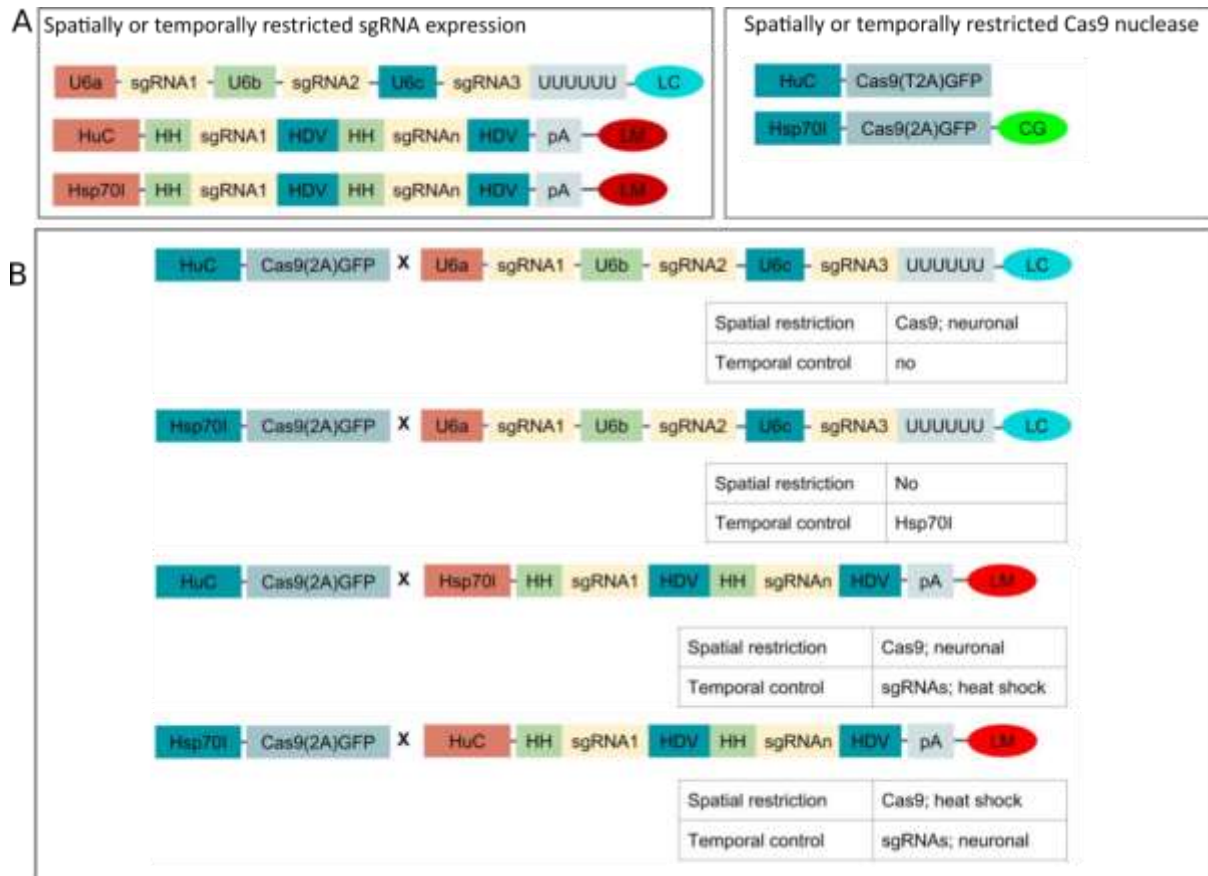


Figure 6.4 Schematic showing the plasmid constructs for the conditional knockout. A) Constructs for sgRNA and Cas9 expression. **B)** Possible combinations of expression of Cas9 and sgRNAs using the conditional knockout constructs.

In addition to making conditional knockouts, the neural circuit specific role of *Fmn2b* in morphogenesis and associated behaviour can be assessed by restricted expression of mouse *Fmn2* in neurons affected in morphants and/or mutants. Neuron specific expression can be achieved by driving the expression of mouse *Fmn2* under the *hcrtr* promoter that can be obtained from (Tg(-6.7FRhcrtr:gal4VP16)) to selectively label spiral fiber neurons (Lacoste et al., 2014). Similarly, the specific role of *Fmn2b* in motor neuron development and motor activity can be investigated using the *mxn1* promoter specific for motor neurons driving the expression of mouse *Fmn2*.

6.6 Compensation by other formins

The loss of Fmn2b results in early mortality and embryonic developmental defects in both morphants and mutants, pointing towards a significant role of Fmn2b in development. Despite 40% of the *fmn2b* mutant progeny exhibiting mortality or gross morphological defects, around 50-60% of the population survives to become adults suggesting the *fmn2b* depletion phenotypes have partial penetrance. There are fifteen classes of formins with overlapping spatiotemporal expression and function (Higgs, 2005; Breitsprecher and Goode, 2013; Kawabata Galbraith and Kengaku, 2019). The expression of multiple formins in the nervous system and their temporal overlap begs the question of functional redundancy, which remains unexplored.

Due to genome duplication in teleosts, most genes have two paralogs in zebrafish. The role of Fmn2a, the paralog of Fmn2b in zebrafish, has not been tested in the context of neurodevelopment or embryogenesis. There was no tangible expression of *fmn2a* mRNA in the zebrafish nervous system, as seen by *in situ* hybridization experiments. More experiments are needed to assess the expression of *fmn2a* in zebrafish in non-neuronal tissues and if the expression changes upon *fmn2b* knockout. Expression levels of formins that are found to be expressed in the nervous system and are phylogenetically related to Fmn2b should also be checked in *fmn2b* mutants to investigate the functional redundancy of formins. Phylogenetic analysis of formins in zebrafish shows the following tree. The closest relatives of Fmn2b are Fmn2a, Fmn1. The next set of formins that were closely related in the phylogenetic analysis were Fhod1, Fhod3a and Fhod3b. These preliminary leads could be followed to compare the relative expression of these formins in wildtype fish and *fmn2b* mutants in a tissue-specific and developmental stage-dependent manner. **Figure 6.5**

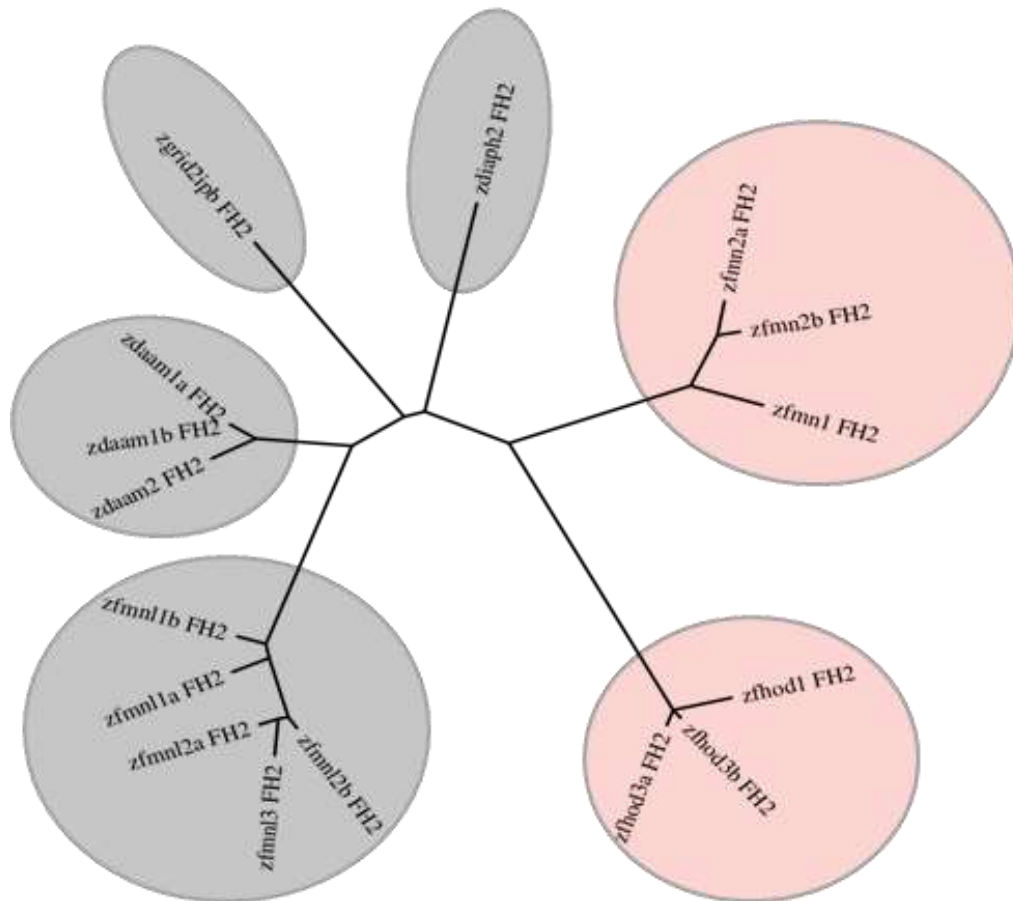


Figure 6.5 Phylogenetic analysis of formins expressed in the zebrafish nervous system. The formins under the pink bubble are the closest relatives of the zebrafish *fmn2b*.

In conclusion, the work presented in the thesis opens up many possibilities for testing the role of *fmn2b* in neural development beyond locomotor neural circuits. Given the contribution of Fmn2 in neurodevelopmental disorders, *fmn2b* mutants could be used to model neurodevelopmental disorders and motor neuron diseases. The *fmn2b* mutants will be a valuable tool to dissect the molecular function of Fmn2b using subcellular cytoskeletal imaging in a neuron-specific manner. Unlike transient knockdown, genetic null mutants of *fmn2b* will aid characterization of neural circuits and associated behaviours in larval and adult zebrafish.

7

Reagents and Procedures

7.1 Zebrafish maintenance and procedures

Locally sourced wildtype strain of zebrafish was used in all the experiments. Adult zebrafish were raised in a recirculating aquarium system (Techniplast) at 28.5 °C under a 14-hour light and 10-hour dark cycle. Embryos were collected and raised in E3 buffer (5 mM NaCl, 0.33 mM MgSO₄, 0.17 mM KCl, 0.33 mM CaCl₂, 5 % Methylene Blue) at 28.5 °C and used at different stages as previously described (Kimmel et al., 1995). All the protocol concerning zebrafish handling, maintenance, breeding and manipulations have been cleared by the Institute Animal Ethics Committee (IAEC), IISER Pune. The following transgenic zebrafish lines were used: *Tg(cldn-b:Lyn-GFP)* (Haas and Gilmour, 2006), *Tg(brn3c:GAP43-GFP)* (Xiao et al., 2005b) and *Tg(mnx1:GFP)*.

7.2 Whole mount in situ hybridization

Total RNA was isolated from 48 hpf wildtype embryos using the RNeasy mini kit (Qiagen) and reverse transcribed using the SuperScript IV RT Kit (ThermoFisher) to obtain cDNA. The cDNA was amplified for a 366 bp long gene specific region of *Fmn2* corresponding the 5' UTR and exon 1 flanked with T7 and T3 promoter sequences in the antisense and sense direction respectively. Primer sequences are given in the table below.

Fmn2b_5'_T3	GCAATTAACCCTCACTAAAGGGATGCGTTGTTGTGTTTGTG
Fmn2b_5'_T7	TAATACGACTCACTATAGGGGCTCTCGCTGTCTGATGAAG

The amplified product was purified and used as the template for in vitro transcription of antisense and sense probes against *Fmn2* mRNA. Zebrafish embryos ranging from 1 cell stage to 96 hpf were used for whole mount in situ hybridization experiments as described previously (Thisse and Thisse, 2008). BM Purple was used as a chromogenic substrate for detection.

7.3 Isolation of motor neurons from transgenic embryos, FACS, RT-PCR

Single cell suspension was made from 200 *Tg(mnx1:GFP)* embryos as previously described (Bresciani et al., 2018). Briefly, the embryos were dissociated by trypsinization and filtering through a 70 µm sieve to obtain single cell suspension in 1X DMEM containing 10% FBS. The cells were sorted using a BD Biosciences fluorescence-activated

cell sorting (FACS) equipment selecting cells expressing GFP, i.e., the motor neurons. RNA was extracted using Qiagen RNeasy Kit and cDNA was prepared using the SuperScript IV RT Kit (ThermoFisher). The cDNA was used for amplifying *fmn2b* transcripts in the *mnx1* positive motor neurons. Primers and PCR protocol used to test the presence of *fmn2b* transcripts in motor neurons tagged by *Tg(mnx1:GFP)* were the same as the ones used for amplification of ISH probes from cDNA.

7.4 Morpholino and RNA injections

Two morpholinos targeting *fmn2b* were obtained from Gene Tools. The splice blocking morpholino targets the intron between exons 5 and 6 and ensures the inclusion of a stop codon in the translation frame. The translation blocking morpholino binds early on in the first exon. The control morpholino targets the beta-thalassemia causing mutation in the human beta-globin gene. The control morpholino has no reported off-target effects and is used as a negative control. The sequences of the morpholinos used are given below.

MO Control	5'-CCTCTTACCTCAGTTACAATTTATA-3'
MO SB Fmn2b	5'-ACAGAAGCGGTCATTACTTTTTGGT-3'
MO TB Fmn2b	5'-ATGAGCGGCGGCGGTTTCAAGCCAT-3'

All experiments were done by injecting 2 nl volume of the MO Control and MO SB *fmn2b* (1 ng/nl; 2 ng per embryo) in the cytoplasm of the 1-cell stage embryos. For MO TB *fmn2b* dose dependence, 4 ng/embryo and 8 ng/embryo doses of the morpholino were injected in the yolk of embryos in addition to the cytoplasmic injection of 2 ng/embryo. The injection volume was calibrated at 2 nl per embryo for each needle before injection. Post injections, embryos were washed and raised in E3 buffer (supplemented with methylene blue) at 28.5 °C till the desired developmental stage with regular cleaning. For immunostaining and live imaging experiments, the buffer was supplemented with 0.003% Phenylthiourea (PTU; Sigma) to remove pigmentation from the skin. For rescue experiments, capped mRNA was synthesized using the SP6 mMessage mMachine RNA synthesis kit (Ambion) from pCS2-mFmn2-GFP plasmid (provided by Prof. Philip Leder, Harvard Medical School). After purification using RNeasy MinElute Cleanup Kit (Qiagen), 300 pg of mFmn2-GFP capped RNA was co-injected with MO SB *Fmn2b* morpholino per embryo.

7.5 Validation of splice blocking morpholino

The splice blocking morpholino MO SB Fmn2 was validated by RT-PCR. Total RNA isolated from morpholino injected 48 hpf embryos (RNeasy mini kit, Qiagen) was reverse transcribed using the SuperScript IV RT Kit (ThermoFisher). The cDNA obtained was amplified by the following primers flanking the intron between exon 5 and 6. Primer sequences are given below.

MOSBFmn2_RT_FWD	5'-TCTGTTTGCATTGGGAGC-3'
MOSBFmn2_RT_REV	5'-CTTGGTCTTTGACCTGCTGAT-3'

In control morphants, the expected amplicon size is 251 bp whereas in Fmn2 morphants the amplicon size was expected and found to be 550 bp due to blocked splicing of the intron between exons 5 and 6.

7.6 sgRNA and Cas9 preparation and injections for crispants and CRISPR mutants

Two sgRNAs targeting exon 1 of *fmn2b* were designed as previously described (Varshney et al., 2016). sgRNAs were designed as oligonucleotides with a T7 promoter upstream and annealed to obtain DNA template for *in vitro* transcription using T7 HiScribe kit (NEB). Cas9 mRNA was synthesized using the T3 mMessage mMachine RNA synthesis kit (Ambion) from pT3TS-nCas9n plasmid (provided by Dr. Shawn Burgess, NHGRI, NIH). After purification of the sgRNAs and Cas9 mRNA, 300 pg of Cas9 mRNA was injected as control.

Name	Genomic location	Sequence
Fmn2b_sgRNA 1	12:47451436-47451459 (+)	5'-GGGCGAGAGGCCTCGGCTGG-3'
Fmn2b_sgRNA 2	12:47450847-47450870 (-)	5'-GCGGATCCTCCCTCTGCATG-3'
Fmn2b_sgRNA 3	12:47471895-47471918 (-)	5'-GGACGCTCGAGTGACGGCGG-3'

CRISPR Cas9 based mutagenesis

To generate *fmn2b* CRISPR mutants, the following strategy based on previous work was followed (Carrington et al., 2015; Varshney et al., 2015, 2016).

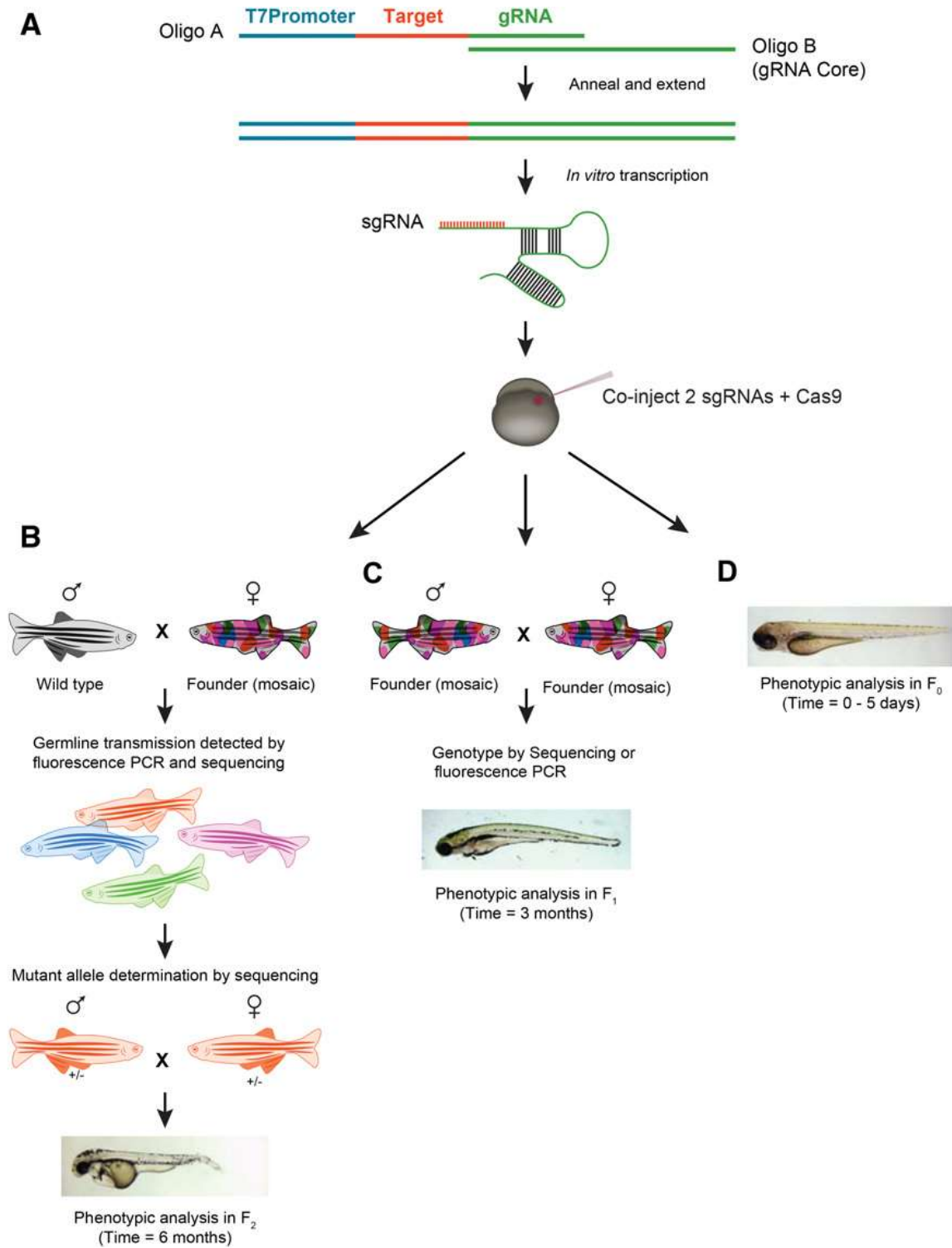


Figure RP.1. Schematic outlining the mutagenesis strategy. (Varshney et al., 2015)

7.7 F0 sgRNA injection and analysis in *fmn2b* crispants

To generate crispants, 30 pg or 100 pg of both sgRNAs were injected along with the Cas9 mRNA. Sequences for the sgRNAs are given below. We injected Cas9 mRNA with or without the two sgRNAs (sgRNA-1 and sgRNA-2 together) at the 1 cell stage. To ascertain the activity of the sgRNAs, we extracted the genomic DNA from 24 hpf crispants using a modified HotSHOT protocol for zebrafish (Meeker et al., 2007). The genomic DNA from the Cas9 mRNA only control (n=8) and the crispants (n=15) was used for amplifying the region flanking each of the sgRNA loci by PCR and Sanger sequencing was performed on the amplicons. We observed mutations in all the crispant embryos that were sequenced. Out of the 15 embryos, 93.3% crispants showed indels at the sgRNA-1 locus and 53.3% crispants showed indels at the sgRNA-2 locus. Furthermore, all the remaining crispants without indels also showed base changes with some of them causing premature stop codons to occur. The Cas9 mRNA only control showed no indels or base changes at both the sgRNA loci. This suggests that the two sgRNAs injected in the crispants cause indels or premature stop codons in a substantial fraction of the population potentially causing frameshift mutations and therefore, a truncated protein.

7.8 Genotyping *fmn2b* crispants and CRISPR mutants

Genotyping for *fmn2b* crispants and CRISPR mutants was done in two ways. The crispants were genotyped using Sanger sequencing to visualize indels created in the F0 injected zebrafish embryos. For identifying founder lines for *fmn2b* mutants, fluorescent PCR was performed and analyzed by capillary gel electrophoresis using the ABI GeneAnalyzer 3730XL, as previously described (Carrington et al., 2015; Varshney et al., 2015, 2016). Identification of homozygous mutant lines was also done using Sanger sequencing. Primer sequences for sanger sequencing of genomic DNA amplicons from crispants are as follows:

Fmn2b_PCR_F_sgRNA1	AAGCGTAAGAACCAGAATAAGC
Fmn2b_PCR_R_sgRNA1	TCATCCGAATGGCTTGC
Fmn2b_PCR_F_sgRNA2	GAGTGTGCAGGAAGATGC
Fmn2b_PCR_R_sgRNA2	GTGACGAAGGAGAGGTACAG
Fmn2b_PCR_F_sgRNA3	AAGAAGCCCACTGTCACG

7.9 Whole mount immunostaining

PTU treated embryos were collected at desired stages and fixed in 4% formaldehyde overnight at 4°C. The fixed embryos were stained as described earlier (Hatta, 1992) using 3A10 (DSHB) (1:50) antibody in blocking buffer. The larvae were washed with PBS-triton (0.5%) followed by blocking in 5% BSA. For RMO-44 immunostaining, embryos at the desired stage were fixed using 2% Trichloroacetic acid (TCA) at room temperature for 3 hours, washed with PBS followed by acetone permeabilization for 30 minutes at -20°C. The embryos were then washed with distilled water, incubated in blocking buffer for 1 hour and transferred to RMO-44 (1:100) and incubated at room temperature for 12 hours. The larvae were then stained with anti-mouse AlexaFluor-568/488 (1:200) overnight at 4°C in blocking buffer.

For acetylated tubulin staining, embryos were fixed in Dent's fixative (80% Methanol and 80% DMSO) at RT for 4 hours. The embryos were rehydrated through a methanol/PBS gradient and permeabilized with Proteinase K (10 mg/ml – 40 mg/ml depending on the stage of embryos 1dpf to 4 dpf) for 10-20 minutes. After washing with 0.5% PBS-Triton, embryos were fixed in 4% PFA for 20 minutes at RT, washed again with 0.5% PBS-Triton for 10 minutes and incubated in blocking buffer. Blocked embryos were incubated in anti-acetylated antibody (1:1000) in blocking buffer at 4°C overnight. The larvae were then stained with anti-mouse AlexaFluor-568/488 (1:200) overnight at 4°C in blocking buffer. For staining actin structures, embryos were fixed in 4% PFA at 4°C overnight and washed with 0.5% PBS-Triton. The fixed embryos were permeabilized with 2% PBS-Triton for 2 hours at room temperature and then incubated in Phalloidin Alexa Fluor 568 diluted 1:50 in 2% PBS Triton overnight at 4 °C in dark. After extensive washing with PBS-triton (0.5%), the embryos were cleared in 50% glycerol and mounted dorsal side down on a glass bottom petri dish using low gelling agarose (Sigma).

7.10 FM 4-64 labelling

To label the hair cells of the inner ear cristae, 1 nl solution of 3 µM FM 4-64 (Molecular Probes, Invitrogen) dissolved in DMSO was injected in the otic cavity of 96 hpf zebrafish

embryos mounted laterally in low gelling agarose (Sigma). The injected embryos were removed from the gel using E3 buffer and imaged within 1 hour of injections.

7.11 TMR Dextran labelling

Retrograde labelling of the reticulospinal neurons was done using Tetramethylrhodamine Dextran (TMR Dextran) (3000 MW) by microinjection of three pulses of 1 nl each in the ventral side of the spinal cord of 3 dpf zebrafish larvae mounted in 1% low gelling agarose. The injected larvae were allowed to recover in E3 medium overnight at 28°C and fixed with 4% PFA at 4dpf for 3 hours at room temperature. The fixed larvae were cleared using 50% glycerol and mounted in a coverslip sandwich for imaging.

7.12 Neuromuscular junction labelling and quantification

For neuromuscular junction staining of embryos, znp-1 antibody (DSHB; 1:100) and Tetramethyl Rhodamine labelled α -bungarotoxin (Invitrogen; 1:200) were used as pre-synaptic and post-synaptic markers respectively. Whole mount immunostaining procedures described in previous section were followed as described. The synapses were counted using the SynapCountJ plugin after making the traces of arbors in NeuronJ plugin in Fiji.

7.13 Fluorescence microscopy, live imaging and mounting procedure

All the microscopic imaging was performed on the inverted LSM 780 confocal microscope (Zeiss) with a 25x oil immersion objective (NA 1.4).

The growth cone of motor neurons was visualized using the *Tg(mnx1:GFP)* in wildtype or mutant background by mounting the live embryos laterally in 0.5% low melt point agarose (Sigma) in a coverslip bottom 35 mm petri plate. The embryos were imaged starting at 22 hpf for 4-6 hours every 3 minutes. The growth cone translocation was analyzed using the Manual tracking plugin in Fiji to track the movement of the leading edge across time. The coordinates obtained were analyzed using the ibidi Chemotaxis tool to calculate the average growth cone translocation speed.

7.14 Behaviour experiment set up and behaviour analysis

7.14.1 Automated acoustic startle assay

We designed a behavioural assay as described previously (Lacoste et al., 2014) to screen larvae based on their response to a mechano-acoustic stimulus. The control and Fmn2b morphants were anaesthetized using 0.03% tricaine (MS-222, Sigma), head-restrained using 1% low gelling agarose and their tails were suspended in E3 buffer, in a 35 mm petri dish. All the fish were habituated for 30 minutes in the behaviour room maintained at a temperature of 27°C. Individual dishes containing one larva were placed and taped onto the behavioural setup, as shown in Figure 2 A. Up to 6 taps were delivered using a 14 V DC solenoid (obtained from a local store) to the dish at an interval of 10 seconds at an intensity corresponding to 14 V from a power supply. The setup comprises of an automated stimulus delivery control unit (Arduino), a solenoid with a piston driven by a variable power supply, a piezo sensor (SparkFun) to detect the stimulus, and a feedback TTL pulse to the camera to mark the reception of the stimulus. This allowed precise marking of the stimulus delivery directly onto the images acquired using a high-speed video camera (AVT Pike, F-032B) at 640 fps. The secure image signature (SIS) feature of the camera was used to put a time-stamp on individual frames acquired.

7.14.2 Analysis of tail movement using a custom Python software

The recordings were analyzed using a custom-written Python program to extract the time-stamp, time of stimulus delivery and skeletonizing the fish to obtain coordinates of a spline curve fit to the fish shape in every frame. The skeleton was segmented into 20 points, and the last five points were used for further calculations. The program calculates the tail angle from last five points on the fish skeleton with respect to the restrained head segment. An event qualifies as an escape response if the angle crosses a threshold of 60 degrees from the rest position (Lacoste et al., 2014). The following parameters have been quantified, as mentioned below:

Latency to first movement: Time taken by the fish to initiate movement post stimulus delivery, marked by an angle change greater than five degrees.

C-bend Max: Maximum angle of C-bend escape (with respect to the head restrained segment)

Latency to C-bend Max: Time taken by the fish to reach the maximum C-bend escape angle, calculated by subtracting latency to first movement from the total time taken to reach maximum angle.

Spontaneous tail coiling (STC) assay

Embryos (22-24 hpf) within their chorions were transferred to a 35 mm petri plate containing E3 buffer at of 28.5°C. A video camera (AVT Pike, F-032B) was used to record the spontaneous tail coiling behaviour of the embryos for a time period of 3 minutes at 15 fps. The videos were processed and analysed using a MATLAB script ZebraSTM published previously (González-Fraga et al., 2019).

7.14.3 Touch evoked escape response (TEER) assay

60 hpf zebrafish embryos were housed in a 35 mm petri plate containing pre-warmed E3 buffer at 28.5 °C. A tuberculin needle was repurposed by attaching a soft nylon fiber in front of the syringe holding the needle, to deliver tactile stimuli to zebrafish embryos. A soft touch was delivered to the head of the zebrafish once and their behaviour was recorded using a high-speed video camera (AVT Pike F-032B) at 208 fps. The videos obtained were analyzed using the Manual tracking plugin in Fiji to mark the trajectories of the zebrafish embryos upon receiving the tactile stimulus. The tracks were further analyzed using the ibidi Chemotaxis tool to calculate the distance travelled and average speed. The maximum instantaneous speed was calculated manually from the coordinates obtained from the manual tracking output.

7.15 Figures and Statistical analysis

All the analysis was performed in a genotype blinded manner. The images were processed in Fiji and assembled as figure panels using Inkscape. The data for all measurements are represented as (median; [95% confidence intervals]; number of events) for Chapter 2 in the results section. For Chapters 3, 4 and 5, the data was represented as (mean \pm SEM). Data obtained from various experiments were analyzed using an **estimation statistics** approach (Ho et al., 2019) and the median difference values and respective permutation test p-values are indicated in the figure legends. All data points have been presented as a swarm plot for individual values displaying the underlying distribution. The effect size is presented as a bootstrap 95% confidence

interval (95% CI) below the swarm plots showing the median differences obtained by resampling the data 5000 times. The plots were generated using the web application available at <https://www.estimationstats.com/#/>. The Violin plots were plotted in GraphPad Prism 8 and indicated statistical tests were performed using GraphPad Prism 8.

8

References

- Agís-Balboa RC et al. (2017) Formin 2 links neuropsychiatric phenotypes at young age to an increased risk for dementia. *EMBO J* 36:2815–2828.
- Ahuja R, Pinyol R, Reichenbach N, Custer L, Klingensmith J, Kessels MM, Qualmann B (2007) Cordon-Bleu Is an Actin Nucleation Factor and Controls Neuronal Morphology. *Cell* 131:337–350.
- Almuqbil M, Hamdan FF, Mathonnet G, Rosenblatt B, Srour M (2013) De novo deletion of FMN2 in a girl with mild non-syndromic intellectual disability. *Eur J Med Genet* 56:686–688.
- Amsterdam A, Burgess S, Golling G, Chen W, Sun Z, Townsend K, Farrington S, Haldi M, Hopkins N (1999) A large-scale insertional mutagenesis screen in zebrafish. *Genes Dev* 13:2713–2724.
- Anazi S et al. (2017) Expanding the genetic heterogeneity of intellectual disability. *Hum Genet* 136:1419–1429.
- Armijo-Weingart L, Gallo G (2017) It takes a village to raise a branch: Cellular mechanisms of the initiation of axon collateral branches. *Mol Cell Neurosci* 84:36–47.
- Atkins M, Gasmi L, Bercier V, Revenu C, Del Bene F, Hazan J, Fassier C (2019) FIGNL1 associates with KIF1B β and BICD1 to restrict dynein transport velocity during axon navigation. *J Cell Biol* 218:3290–3306.
- Avitan L, Pujic Z, Mólter J, Van De Poll M, Sun B, Teng H, Amor R, Scott EK, Goodhill GJ (2017) Spontaneous Activity in the Zebrafish Tectum Reorganizes over Development and Is Influenced by Visual Experience. *Curr Biol* 27:2407–2419.e4.
- Bagnall MW, McLean DL (2014) Modular Organization of Axial Microcircuits in Zebrafish. *Science (80-)* 343:197–200.
- Baier H, Klostermann S, Trowe T, Karlstrom RO, Nüsslein-Volhard C, Bonhoeffer F (1996) Genetic dissection of the retinotectal projection. *Development* 123:415–425.
- Bak M, Fraser SE (2003) Axon fasciculation and differences in midline kinetics between pioneer and follower axons within commissural fascicles. *Development* 130:4999–5008.

- Balasanayan V, Watanabe K, Dempsey WP, Lewis TL, Trinh LA, Arnold DB (2017) Structure and Function of an Actin-Based Filter in the Proximal Axon. *Cell Rep* 21:2696–2705.
- Beattie CE, Hatta K, Halpern ME, Liu H, Eisen JS, Kimmel CB (1997) Temporal separation in the specification of primary and secondary motoneurons in zebrafish. *Dev Biol* 187:171–182.
- Bello-Rojas S, Istrate AE, Kishore S, McLean DL (2019) Central and peripheral innervation patterns of defined axial motor units in larval zebrafish. *J Comp Neurol* 527:2557–2572.
- Bercier V, Hubbard JM, Fidelin K, Durooure K, Auer TO, Revenu C, Wyart C, Del Bene F (2019) Dynactin1 depletion leads to neuromuscular synapse instability and functional abnormalities. *Mol Neurodegener* 14:1–22.
- Bernhardt RR, Chitnis AB, Lindamer L, Kuwada JY (1990) Identification of spinal neurons in the embryonic and larval zebrafish. *J Comp Neurol* 302:603–616.
- Bill BR, Petzold AM, Clark KJ, Schimmenti L a, Ekker SC (2009) A primer for morpholino use in zebrafish. *Zebrafish* 6:69–77.
- Bonner J, Letko M, Nikolaus OB, Krug L, Cooper A, Chadwick B, Conklin P, Lim A, Chien C Bin, Dorsky RI (2012) Midline crossing is not required for subsequent pathfinding decisions in commissural neurons. *Neural Dev* 7:18.
- Breitsprecher D, Goode BL (2013) Formins at a glance. *J Cell Sci* 126:1–7.
- Bremer J, Granato M (2016) Myosin phosphatase Fine-tunes Zebrafish Motoneuron Position during Axonogenesis. *PLoS Genet* 12:1006440.
- Bresciani E, Broadbridge E, Liu PP (2018) An efficient dissociation protocol for generation of single cell suspension from zebrafish embryos and larvae. *MethodsX* 5:1287–1290.
- Brettle M, Stefen H, Djordjevic A, Fok SYY, Chan JW, van Hummel A, van der Hoven J, Przybyla M, Volkerling A, Ke YD, Delerue F, Ittner LM, Fath T (2019) Developmental Expression of Mutant PFN1 in Motor Neurons Impacts Neuronal Growth and Motor Performance of Young and Adult Mice. *Front Mol Neurosci* 12:231.
- Brustein E, Saint-Amant L, Buss RR, Chong M, McDearmid JR, Drapeau P (2003) Steps

- during the development of the zebrafish locomotor network. *J Physiol Paris* 97:77–86.
- Burgess H a., Granato M (2008) The neurogenetic frontier-lessons from misbehaving zebrafish. *Briefings Funct Genomics Proteomics* 7:474–482.
- Burgess HA, Johnson SL, Granato M (2009) Unidirectional startle responses and disrupted left-right co-ordination of motor behaviors in *robo3* mutant zebrafish. *Genes, Brain Behav* 8:500–511.
- Campellone KG, Welch MD (2010) A nucleator arms race: Cellular control of actin assembly. *Nat Rev Mol Cell Biol* 11:237–251.
- Carrington B, Varshney GK, Burgess SM, Sood R (2015) CRISPR-STAT: An easy and reliable PCR-based method to evaluate target-specific sgRNA activity. *Nucleic Acids Res* 43:e157.
- Chalmers K, Kita EM, Scott EK, Goodhill GJ (2016) Quantitative Analysis of Axonal Branch Dynamics in the Developing Nervous System. *PLoS Comput Biol* 12:1004813.
- Chia PH, Chen B, Li P, Rosen MK, Shen K (2014) Local F-actin network links synapse formation and axon branching. *Cell* 156:208–220.
- Coles CH, Bradke F (2015) Coordinating Neuronal Actin-Microtubule Dynamics. *Curr Biol* 25:R677–R691.
- Colombo A, Palma K, Armijo L, Mione M, Signore IA, Morales C, Guerrero N, Meynard MM, Pérez R, Suazo J, Marcelain K, Briones L, Härtel S, Wilson SW, Concha ML (2013) Daam1a mediates asymmetric habenular morphogenesis by regulating dendritic and axonal outgrowth. *Dev* 140:3997–4007.
- Dahlgaard K, Raposo AASF, Niccoli T, St Johnston D (2007) Capu and Spire Assemble a Cytoplasmic Actin Mesh that Maintains Microtubule Organization in the *Drosophila* Oocyte. *Dev Cell* 13:539–553.
- Das R, Letcher JM, Harris JM, Foldi I, Nanda S, Bobo HM, Mihály J, Ascoli GA, Cox DN (2017) Formin3 regulates dendritic architecture via microtubule stabilization and is required for somatosensory nociceptive behavior. *bioRxiv:227348*.
- Dickson BJ (2002) Molecular mechanisms of axon guidance. *Science* (80-) 298:1959–

1964.

- Dumont J, Million K, Sunderland K, Rassinier P, Lim H, Leader B, Verlhac M-H (2007) Formin-2 is required for spindle migration and for the late steps of cytokinesis in mouse oocytes. *Dev Biol* 301:254–265.
- Dutta P, Maiti S (2015) Expression of multiple formins in adult tissues and during developmental stages of mouse brain. *Gene Expr Patterns* 19:52–59.
- Eisen JS (1991) Motoneuronal development in the embryonic zebrafish. In: *Development*, pp 141–147. The Company of Biologists.
- Eisen JS, Myers PZ, Westerfield M (1986) Pathway selection by growth cones of identified motoneurons in live zebra fish embryos. *Nature* 320:269–271.
- Eisen JS, Pike SH, Debu B (1989) The growth cones of identified motoneurons in embryonic zebrafish select appropriate pathways in the absence of specific cellular interactions. *Neuron* 2:1097–1104.
- Eisen JS, Smith JC (2008) Controlling morpholino experiments: don't stop making antisense. *Development* 135:1735–1743.
- Emmons S, Phan H, Calley J, Chen W, James B, Manseau L (1995) cappuccino, a *Drosophila* maternal effect gene required for polarity of the egg and embryo, is related to the vertebrate limb deformity locus. *Genes Dev* 9:2482–2494.
- Fassier C, Fréal A, Gasmi L, Delphin C, Ten Martin D, De Gois S, Tambalo M, Bosc C, Mailly P, Revenu C, Peris L, Bolte S, Schneider-Maunoury S, Houart C, Nothias F, Larcher J-C, Andrieux A, Hazan J (2018) Motor axon navigation relies on Fidgetin-like 1-driven microtubule plus end dynamics. *J Cell Biol* 217:1719–1738.
- Fassier C, Hutt JA, Scholpp S, Lumsden A, Giros B, Nothias F, Schneider-Maunoury S, Houart C, Hazan J (2010) Zebrafish atlastin controls motility and spinal motor axon architecture via inhibition of the BMP pathway. *Nat Neurosci* 13:1380–1387.
- Fernández-Barrera J, Alonso MA (2018) Coordination of microtubule acetylation and the actin cytoskeleton by formins. *Cell Mol Life Sci* 75:3181–3191.
- Fetcho J, Faber D (1988) Identification of motoneurons and interneurons in the spinal network for escapes initiated by the mauthner cell in goldfish. *J Neurosci* 8:4192–

4213.

Fetcho JR (1991) Spinal network of the Mauthner cell. *Brain Behav Evol* 37:298–316.

Fidelin K, Djenoune L, Stokes C, Prendergast A, Gomez J, Baradel A, Del Bene F, Wyart C (2015) State-dependent modulation of locomotion by GABAergic spinal sensory neurons. *Curr Biol* 25.

Flynn KC (2013) The cytoskeleton and neurite initiation. *Bioarchitecture* 3:86–109.

Flynn KC, Bradke F (2020) Role of the cytoskeleton and membrane trafficking in axon–dendrite morphogenesis. In: *Cellular Migration and Formation of Axons and Dendrites*, pp 21–56. Elsevier.

Funk J, Merino F, Venkova L, Heydenreich L, Kierfeld J, Vargas P, Raunser S, Piel M, Bieling P (2019) Profilin and formin constitute a pacemaker system for robust actin filament growth. *Elife* 8.

Gallo G (2011) The cytoskeletal and signaling mechanisms of axon collateral branching. *Dev Neurobiol* 71:201–220.

Gallo G (2016) Coordination of the axonal cytoskeleton during the emergence of axon collateral branches. *Neural Regen Res* 11:709–711.

Ganguly A, Tang Y, Wang L, Ladtschik K, Loi J, Dargent B, Leterrier C, Roy S (2015) A dynamic formin-dependent deep F-actin network in axons. *J Cell Biol* 210:401–417.

Gebhardt C, Auer TO, Henriques PM, Rajan G, Duroure K, Bianco IH, Del Bene F (2019) An interhemispheric neural circuit allowing binocular integration in the optic tectum. *Nat Commun* 10:1–12.

Ghate K, Mutalik SP, Sthanam LK, Sen S, Ghose A (2020) Fmn2 Regulates Growth Cone Motility by Mediating a Molecular Clutch to Generate Traction Forces. *Neuroscience* 448:160–171.

González-Fraga J, Dipp-Alvarez V, Bardullas U (2019) Quantification of Spontaneous Tail Movement in Zebrafish Embryos Using a Novel Open-Source MATLAB Application. *Zebrafish* 16:214–216.

Goode BL, Eck MJ (2007) Mechanism and Function of Formins in the Control of Actin

- Assembly. *Annu Rev Biochem* 76:593–627.
- Goodhill GJ, Faville R a, Sutherland DJ, Bicknell B a, Thompson AW, Pujic Z, Sun B, Kita EM, Scott EK (2015) The dynamics of growth cone morphology. *BMC Biol* 13:1–18.
- Gordon-Weeks PR, Fournier AE (2014) Neuronal cytoskeleton in synaptic plasticity and regeneration. *J Neurochem* 129:206–212.
- Gorukmez O, Gorukmez O, Ekici A (2020) A Novel Nonsense FMN2 Mutation in Nonsyndromic Autosomal Recessive Intellectual Disability Syndrome. *Fetal Pediatr Pathol*.
- Granato M, Nüsslein-Volhard C (1996) Fishing for genes controlling development. *Curr Opin Genet Dev* 6:461–468.
- Granato M, van Eeden FJ, Schach U, Trowe T, Brand M, Furutani-Seiki M, Haffter P, Hammerschmidt M, Heisenberg CP, Jiang YJ, Kane D a, Kelsh RN, Mullins MC, Odenthal J, Nüsslein-Volhard C (1996) Genes controlling and mediating locomotion behavior of the zebrafish embryo and larva. *Development* 123:399–413.
- Gyda M, Wolman M, Lorent K, Granato M (2012) The Tumor Suppressor Gene Retinoblastoma-1 Is Required for Retinotectal Development and Visual Function in Zebrafish Link BA, ed. *PLoS Genet* 8:e1003106.
- Haag N, Schwintzer L, Ahuja R, Koch N, Grimm J, Heuer H, Qualmann B, Kessels MM (2012) The actin nucleator Cobl is crucial for purkinje cell development and works in close conjunction with the F-actin binding protein Abp1. *J Neurosci* 32:17842–17856.
- Haas P, Gilmour D (2006) Chemokine Signaling Mediates Self-Organizing Tissue Migration in the Zebrafish Lateral Line. *Dev Cell* 10:673–680.
- Haddon C, Lewis J (1996) Early ear development in the embryo of the Zebrafish, *Danio rerio*. *J Comp Neurol* 365:113–128.
- Haffter P, Granato M, Brand M, Mullins MC, Hammerschmidt M, Kane D a, Odenthal J, van Eeden FJ, Jiang YJ, Heisenberg CP, Kelsh RN, Furutani-Seiki M, Vogelsang E, Beuchle D, Schach U, Fabian C, Nüsslein-Volhard C (1996) The identification of genes with unique and essential functions in the development of the zebrafish, *Danio rerio*.

Development 123:1–36.

Hale ME, Katz HR, Peek MY, Fremont RT (2016) Neural circuits that drive startle behavior, with a focus on the Mauthner cells and spiral fiber neurons of fishes. *J Neurogenet* 30.

Hale ME, Ritter D a., Fetcho JR (2001) A confocal study of spinal interneurons in living larval zebrafish. *J Comp Neurol* 437:1–16.

Hatta K (1992) Role of the floor plate in axonal patterning in the zebrafish CNS. *Neuron* 9:629–642.

Hecker A, Schulze W, Oster J, Richter DO, Schuster S (2020) Removing a single neuron in a vertebrate brain forever abolishes an essential behavior. *Proc Natl Acad Sci U S A* 117:3254–3260.

Higgs DM, Radford CA (2013) The contribution of the lateral line to “hearing” in fish. *J Exp Biol* 216:1484–1490.

Higgs HN (2005) Formin proteins: A domain-based approach. *Trends Biochem Sci* 30:342–353.

Ho J, Tumkaya T, Aryal S, Choi H, Claridge-Chang A (2019) Moving beyond P values: data analysis with estimation graphics. *Nat Methods* 16:565–566.

Hu J, Bai X, Bowen JR, Dolat L, Korobova F, Yu W, Baas PW, Svitkina T, Gallo G, Spiliotis ET (2012) Septin-driven coordination of actin and microtubule remodeling regulates the collateral branching of axons. *Curr Biol* 22:1109–1115.

Hu M, Easter J (1999) Retinal neurogenesis: The formation of the initial central patch of postmitotic cells. *Dev Biol* 207:309–321.

Hua JY, Smear MC, Baier H, Smith SJ (2005) Regulation of axon growth in vivo by activity-based competition. *Nature* 434:1022–1026.

Hubbard JM, Böhm UL, Prendergast A, Tseng P-EB, Newman M, Stokes C, Wyart C (2016) Intraspinal Sensory Neurons Provide Powerful Inhibition to Motor Circuits Ensuring Postural Control during Locomotion. *Curr Biol* 26:2841–2853.

Hutson LD, Chien C Bin (2002a) Wiring the zebrafish: Axon guidance and synaptogenesis.

- Curr Opin Neurobiol 12:87–92.
- Hutson LD, Chien CB (2002b) Wiring the zebrafish: Axon guidance and synaptogenesis. Curr Opin Neurobiol 12:87–92.
- Hwang WY, Fu Y, Reyon D, Maeder ML, Tsai SQ, Sander JD, Peterson RT, Yeh J-RJ, Joung JK (2013) Efficient genome editing in zebrafish using a CRISPR-Cas system. Nat Biotechnol 31:227–229.
- Issa F a, O'Brien G, Kettunen P, Sagasti A, Glanzman DL, Papazian DM (2011) Neural circuit activity in freely behaving zebrafish (*Danio rerio*). J Exp Biol 214:1028–1038.
- Issa FA, Mock AF, Sagasti A, Papazian DM (2012) Spinocerebellar ataxia type 13 mutation that is associated with disease onset in infancy disrupts axonal pathfinding during neuronal development. DMM Dis Model Mech 5:921–929.
- Jabeen S, Thirumalai V (2013) Distribution of the gap junction protein connexin 35 in the central nervous system of developing zebrafish larvae. Front Neural Circuits 7.
- Jao LE, Wente SR, Chen W (2013) Efficient multiplex biallelic zebrafish genome editing using a CRISPR nuclease system. Proc Natl Acad Sci U S A 110:13904–13909.
- Jontes JD, Buchanan J, Smith SJ (2000) Growth cone and dendrite dynamics in zebrafish embryos: early events in synaptogenesis imaged in vivo. Nat Neurosci 3:231–237.
- Kalil K, Dent EW (2014) Branch management: mechanisms of axon branching in the developing vertebrate CNS.
- Kalueff A V et al. (2013) Towards a comprehensive catalog of zebrafish behavior 1.0 and beyond. Zebrafish 10:70–86.
- Karlstrom RO, Trowe T, Klostermann S, Baier H, Brand M, Crawford a D, Grunewald B, Haffter P, Hoffmann H, Meyer SU, Müller BK, Richter S, van Eeden FJ, Nüsslein-Volhard C, Bonhoeffer F (1996) Zebrafish mutations affecting retinotectal axon pathfinding. Development 123:427–438.
- Katoh M, Katoh M (2004) Characterization of FMN2 gene at human chromosome 1q43. Int J Mol Med 14:469–474.
- Kawabata Galbraith K, Kengaku M (2019) Multiple roles of the actin and microtubule-

- regulating formins in the developing brain. *Neurosci Res* 138:59–69.
- Kerstein PC, Nichol RH, Gomez TM (2015) Mechanochemical regulation of growth cone motility. *Front Cell Neurosci* 9:244.
- Kessels MM, Schwintzer L, Schlobinski D, Qualmann B (2011) Controlling actin cytoskeletal organization and dynamics during neuronal morphogenesis. *Eur J Cell Biol* 90:926–933.
- Ketschek A, Gallo G (2010) Nerve Growth Factor Induces Axonal Filopodia through Localized Microdomains of Phosphoinositide 3-Kinase Activity That Drive the Formation of Cytoskeletal Precursors to Filopodia. *J Neurosci* 30:12185–12197.
- Ketschek A, Jones S, Spillane M, Korobova F, Svitkina T, Gallo G (2015) Nerve growth factor promotes reorganization of the axonal microtubule array at sites of axon collateral branching. *Dev Neurobiol* 75:1441–1461.
- Ketschek A, Spillane M, Dun XP, Hardy H, Chilton J, Gallo G (2016) Drebrin coordinates the actin and microtubule cytoskeleton during the initiation of axon collateral branches. *Dev Neurobiol* 76:1092–1110.
- Kida YS, Sato T, Miyasaka KY, Suto A, Ogura T (2007) Daam1 regulates the endocytosis of EphB during the convergent extension of the zebrafish notochord. *Proc Natl Acad Sci U S A* 104:6708–6713.
- Kimmel CB, Ballard WW, Kimmel SR, Ullmann B, Schilling TF (1995) Stages of embryonic development of the zebrafish. *Dev Dyn* 203:253–310.
- Kinkhabwala A, Riley M, Koyama M, Monen J, Satou C, Kimura Y, Higashijima S-I, Fetcho J (2011) A structural and functional ground plan for neurons in the hindbrain of zebrafish. *Proc Natl Acad Sci U S A* 108:1164–1169.
- Kita EM, Scott EK, Goodhill GJ (2015) Topographic wiring of the retinotectal connection in zebrafish. *Dev Neurobiol* 75:542–556.
- Knafo S, Wyart C (2018) Active mechanosensory feedback during locomotion in the zebrafish spinal cord. *Curr Opin Neurobiol* 52:48–53.
- Kohashi T, Nakata N, Oda Y (2012a) Effective sensory modality activating an escape triggering neuron switches during early development in zebrafish. *J Neurosci*

32:5810–5820.

Kohashi T, Nakata N, Oda Y (2012b) Effective sensory modality activating an escape triggering neuron switches during early development in zebrafish. *J Neurosci* 32:5810–5820.

Kohashi T, Oda Y (2008) Initiation of Mauthner- or non-Mauthner-mediated fast escape evoked by different modes of sensory input. *J Neurosci* 28:10641–10653.

Korn H, Faber DS (2005) The Mauthner cell half a century later: A neurobiological model for decision-making? *Neuron* 47:13–28.

Krainer EC, Ouderkirk JL, Miller EW, Miller MR, Mersich AT, Blystone SD (2013) The multiplicity of human formins: Expression patterns in cells and tissues. *Cytoskeleton* 70:424–438.

Kundu T, Das SS, Kumar DS, Sewatkar LK, Ghose A (2020) Antagonistic activities of Fmn2 and ADF regulate axonal F-actin patch dynamics and the initiation of collateral branching. *bioRxiv:2020.11.16.384099*.

Kundu T, Dutta P, Nagar D, Maiti S, Ghose A (2021) Coupling of dynamic microtubules to F-actin by Fmn2 regulates chemotaxis of neuronal growth cones. *J Cell Sci*.

Kuwada JY (1993) Pathway selection by growth cones in the zebrafish central nervous system. *Perspect Dev Neurobiol* 1:195–203.

Kuwada JY, Bernhardt RR, Chitnis AB (1990a) Pathfinding by identified growth cones in the spinal cord of zebrafish embryos. *J Neurosci* 10:1299–1308.

Kuwada JY, Bernhardt RR, Nguyen N (1990b) Development of spinal neurons and tracts in the zebrafish embryo. *J Comp Neurol* 302:617–628.

Lacoste AMB, Schoppik D, Robson DN, Haesemeyer M, Portugues R, Li JM, Randlett O, Wee CL, Engert F, Schier AF (2014) A Convergent and Essential Interneuron Pathway for Mauthner-Cell-Mediated Escapes. *Curr Biol*:1526–1534.

Lai S-L, Chan T-H, Lin M-J, Huang W-P, Lou S-W, Lee S-J (2008) Diaphanous-Related Formin 2 and Profilin I Are Required for Gastrulation Cell Movements Heisenberg C-P, ed. *PLoS One* 3:e3439.

- Lam P, Mangos S, Green JM, Reiser J, Huttenlocher A (2015) In Vivo Imaging and Characterization of Actin Microridges Weaver AM, ed. PLoS One 10:e0115639.
- Langebeck-Jensen K, Shahar OD, Schuman EM, Langer JD, Ryu S (2019) Larval Zebrafish Proteome Regulation in Response to an Environmental Challenge. *Proteomics* 19:1900028.
- Lasser M, Tiber J, Lowery LA (2018) The role of the microtubule cytoskeleton in neurodevelopmental disorders. *Front Cell Neurosci* 12:165.
- Law R et al. (2014) Biallelic truncating mutations in FMN2, encoding the actin-regulatory protein formin 2, cause nonsyndromic autosomal-recessive intellectual disability. *Am J Hum Genet* 95:721–728.
- Leader B, Leder P (2000) Formin-2, a novel formin homology protein of the cappuccino subfamily, is highly expressed in the developing and adult central nervous system.
- Leader B, Lim H, Carabatsos MJ, Harrington A, Ecsedy J, Pellman D, Maas R, Leder P (2002) Formin-2, polyploidy, hypofertility and positioning of the meiotic spindle in mouse oocytes. *Nat Cell Biol* 4:921–928.
- Lee RKK, Eaton RC (1991) Identifiable Retidospinal Neurons of the Adult Zebrafish , *Brachydanw rerio*. 3432.
- Lee RKK, Eaton RC, Zottoli SJ (1993) Segmental Arrangement of Reticulospinal Neurons in the Goldfish Hindbrain. 556.
- Lewis TL, Courchet J, Polleux F (2013) Cellular and molecular mechanisms underlying axon formation, growth, and branching. *J Cell Biol* 202:837–848.
- Li M, Zhao L, Page-McCaw PS, Chen W (2016) Zebrafish Genome Engineering Using the CRISPR–Cas9 System. *Trends Genet* 32:815–827.
- Lian G, Dettenhofer M, Lu J, Downing M, Chenn A, Wong T, Sheen V (2016) Filamin A- and formin 2-dependent endocytosis regulates proliferation via the canonical wnt pathway. *Dev* 143:4509–4520.
- Lian G, Sheen VL (2015) Cytoskeletal proteins in cortical development and disease: Actin associated proteins in periventricular heterotopia. *Front Cell Neurosci* 9:1–13.

- Liu K, Petree C, Requena T, Varshney P, Varshney GK (2019) Expanding the CRISPR toolbox in zebrafish for studying development and disease. *Front Cell Dev Biol* 7:13.
- Liu KS, Fetcho JR (1999) Laser ablations reveal functional relationships of segmental hindbrain neurons in zebrafish. *Neuron* 23:325–335.
- Liu LYM, Lin MH, Lai ZY, Jiang JP, Huang YC, Jao LE, Chuang YJ (2016) Motor neuron-derived *Thsd7a* is essential for zebrafish vascular development via the Notch-dll4 signaling pathway. *J Biomed Sci* 23:1–11.
- Liu Y, Halloran MC (2005) Development/Plasticity/Repair Central and Peripheral Axon Branches from One Neuron Are Guided Differentially by Semaphorin3D and Transient Axonal Glycoprotein-1.
- Liu YC, Hale ME (2017) Local Spinal Cord Circuits and Bilateral Mauthner Cell Activity Function Together to Drive Alternative Startle Behaviors. *Curr Biol* 27.
- Lorent K, Liu KS, Fetcho JR, Granato M (2001) The zebrafish space cadet gene controls axonal pathfinding of neurons that modulate fast turning movements. *Development* 128:2131–2142.
- Lowery LA, Van Vactor D (2009) The trip of the tip: understanding the growth cone machinery. *Nat Rev Mol Cell Biol* 10:332–343.
- Luo L (2002) Actin Cytoskeleton regulation in neuronal morphogenesis and structural plasticity. *Annu Rev Cell Dev Biol* 18:601–636.
- Manseau LJ, Schüpbach T (1989) cappuccino and spire: two unique maternal-effect loci required for both the anteroposterior and dorsoventral patterns of the *Drosophila* embryo. *Genes Dev* 3:1437–1452.
- Marco EJ, Aitken AB, Nair VP, da Gente G, Gerdes MR, Bologlu L, Thomas S, Sherr EH (2018) Burden of de novo mutations and inherited rare single nucleotide variants in children with sensory processing dysfunction. *BMC Med Genomics* 11:50.
- Marín O, Gleeson JG (2011) Function follows form: Understanding brain function from a genetic perspective. *Curr Opin Genet Dev* 21:237–239.
- Marques JC, Lackner S, Félix R, Orger MB (2018) Structure of the Zebrafish Locomotor Repertoire Revealed with Unsupervised Behavioral Clustering. *Curr Biol* 28:181-

195.e5.

- Marsden KC, Jain RA, Wolman MA, Echeverry FA, Nelson JC, Hayer KE, Miltenberg B, Pereda AE, Granato M (2018a) A *Cyfp2*-Dependent Excitatory Interneuron Pathway Establishes the Innate Startle Threshold. *Cell Rep* 23:878–887.
- Marsden KC, Jain RA, Wolman MA, Miltenberg B, Pereda AE, Correspondence MG, Echeverry FA, Nelson JC, Hayer KE, Granato M, Purpura DP (2018b) A *Cyfp2*-Dependent Excitatory Interneuron Pathway Establishes the Innate Startle Threshold. *Cell Rep* 23:878–887.
- Matussek T, Gombos R, Szécsényi A, Sánchez-Soriano N, Czibula Á, Pataki C, Gedai A, Prokop A, Raskó I, Mihály J (2008) Formin Proteins of the DAAM Subfamily Play a Role during Axon Growth. *J Neurosci* 28:13310 LP – 13319.
- Mcarthur KL, Chow DM, Fetcho JR (2020) The Zebrafish in Biomedical Research: Biology, Husbandry, Diseases, and Research Applications.
- McLean DL, Fetcho JR (2008) Using imaging and genetics in zebrafish to study developing spinal circuits in vivo. *Dev Neurobiol* 68:817–834.
- Medan V, Preuss T (2014) The Mauthner-cell circuit of fish as a model system for startle plasticity. *J Physiol Paris* 108:129–140.
- Meeker ND, Hutchinson SA, Ho L, Trede NS (2007) Method for isolation of PCR-ready genomic DNA from zebrafish tissues. *Biotechniques* 43:610–614.
- Menelaou E, Svoboda KR (2009) Secondary motoneurons in juvenile and adult zebrafish: Axonal pathfinding errors caused by embryonic nicotine exposure. *J Comp Neurol* 512:305–322.
- Menon S, Gupton S (2018) Recent advances in branching mechanisms underlying neuronal morphogenesis .
- Mogessie B, Schuh M (2017) Actin protects mammalian eggs against chromosome segregation errors. *Science* (80-) 357.
- Moly PK, Hatta K (2011) Early glycinergic axon contact with the Mauthner neuron during zebrafish development. *Neurosci Res* 70:251–259.

- Mumm JS, Williams PR, Godinho L, Koerber A, Pittman AJ, Roeser T, Chien C-B, Baier H, Wong ROL (2006) In vivo imaging reveals dendritic targeting of laminated afferents by zebrafish retinal ganglion cells. *Neuron* 52:609.
- Muñoz-Lasso DC, Romá-Mateo C, Pallardó F V., Gonzalez-Cabo P (2020) Much More Than a Scaffold: Cytoskeletal Proteins in Neurological Disorders. *Cells* 9:358.
- Myers PZ (1985) Spinal motoneurons of the larval zebrafish. *J Comp Neurol* 236:555–561.
- Myers PZ, Eisen JS, Westerfield M (1986) Development and Axonal Outgrowth of Identified Motoneurons in the Zebrafish.
- Nakajima Y (1974) Fine structure of the synaptic endings on the Mauthner cell of the goldfish. *J Comp Neurol* 156:375–402.
- Nakajima Y, Wang DW (1974) Morphology of afferent and efferent synapses in hearing organ of goldfish. *J Comp Neurol* 156:403–416.
- Nakayama H, Oda Y (2004) Common Sensory Inputs and Differential Excitability of Segmentally Homologous Reticulospinal Neurons in the Hindbrain. *J Neurosci* 24:3199–3209.
- Nevin LM, Robles E, Baier H, Scott EK (2010) Focusing on optic tectum circuitry through the lens of genetics. *BMC Biol* 8:126.
- Nicolson T (2017) The genetics of hair-cell function in zebrafish. *J Neurogenet* 31:102–112.
- Nicolson T, Rüscher A, Friedrich RW, Granato M, Ruppertsberg JP, Nüsslein-Volhard C (1998) Genetic analysis of vertebrate sensory hair cell mechanosensation: The zebrafish circler mutants. *Neuron* 20:271–283.
- Nüsslein-Volhard C (2012) The zebrafish issue of *Development*. *Development* 139:4099–4103.
- Odenthal J, Haffter P, Vogelsang E, Brand M, van Eeden FJ, Furutani-Seiki M, Granato M, Hammerschmidt M, Heisenberg CP, Jiang YJ, Kane D a, Kelsh RN, Mullins MC, Warga RM, Allende ML, Weinberg ES, Nüsslein-Volhard C (1996) Mutations affecting the formation of the notochord in the zebrafish, *Danio rerio*. *Development* 123:103–115.

- Pacentine I V, Nicolson T (2019) Subunits of the mechano-electrical transduction channel, *Tmc1/2b*, require *Tmie* to localize in zebrafish sensory hair cells.
- Paul A, Pollard T (2008) The Role of the FH1 Domain and Profilin in Formin-Mediated Actin-Filament Elongation and Nucleation. *Curr Biol* 18:9–19.
- Peleg S, Sananbenesi F, Zovoilis A, Burkhardt S, Bahari-Javan S, Agis-Balboa RC, Cota P, Wittnam JL, Gogol-Doering A, Opitz L, Salinas-Riester G, Dettenhofer M, Kang H, Farinelli L, Chen W, Fischer A (2010) Altered histone acetylation is associated with age-dependent memory impairment in mice. *Science* (80-) 328:753–756.
- Perrone MD, Rocca MS, Bruno I, Faletra F, Pecile V, Gasparini P (2012) De novo 911 Kb interstitial deletion on chromosome 1q43 in a boy with mental retardation and short stature. *Eur J Med Genet* 55:117–119.
- Phng LK, Gebala V, Bentley K, Philippides A, Wacker A, Mathivet T, Sauter L, Stanchi F, Belting HG, Affolter M, Gerhardt H (2015) Formin-mediated actin polymerization at endothelial junctions is required for vessel lumen formation and stabilization. *Dev Cell* 32:123–132.
- Pike SH, Melancon EF, Eisen JS (1992) Pathfinding by zebrafish motoneurons in the absence of normal pioneer axons. *Development* 114:825–831.
- Pinto CS, Khandekar A, Bhavna R, Kiesel P, Pigo G, Sonawane M (2019) Microridges are apical epithelial projections formed of F-actin networks that organize the glycan layer. *Sci Rep* 9:1–16.
- Ponomareva OY, Holmen IC, Sperry AJ, Eliceiri KW, Halloran MC (2014) Calsyntenin-1 Regulates Axon Branching and Endosomal Trafficking during Sensory Neuron Development & In Vivo; *J Neurosci* 34:9235 LP – 9248.
- Prokop A, Sanchez-Soriano N, Goncalves-Pimentel C, Molnar I, Kalmr T, Mihaly J (2011) DAAM family members leading a novel path into formin research. *Commun Integr Biol* 4:538–542.
- Pruyne D, Evangelista M, Yang C, Bi E, Zigmond S, Bretscher A, Boone C (2002) Role of formins in actin assembly: Nucleation and barbed-end association. *Science* (80-) 297:612–615.

- Quinlan ME, Hilgert S, Bedrossian A, Mullins RD, Kerkhoff E (2007) Regulatory interactions between two actin nucleators, Spire and Cappuccino. *J Cell Biol* 179:117–128.
- Ravanelli AM, Klingensmith J (2011) The actin nucleator Cordon-bleu is required for development of motile cilia in zebrafish. *Dev Biol* 350:101–111.
- Roth-Johnson EA, Vizcarra CL, Bois JS, Quinlan ME (2014) Interaction between microtubules and the drosophila formin cappuccino and its effect on actin assembly. *J Biol Chem* 289:4395–4404.
- Ryley DA, Wu H-H, Leader B, Zimon A, Reindollar RH, Gray MR (2005) Characterization and mutation analysis of the human FORMIN-2 (FMN2) gene in women with unexplained infertility. *Fertil Steril* 83:1363–1371.
- Sahasrabudhe A, Ghatge K, Mutalik S, Jacob A, Ghose A (2015) Formin-2 regulates stabilization of filopodial tip adhesions in growth cones and affects neuronal outgrowth and pathfinding in vivo. *Development:dev*.130104-.
- Sahasrabudhe A, Ghatge K, Mutalik S, Jacob A, Ghose A (2016) Formin 2 regulates the stabilization of filopodial tip adhesions in growth cones and affects neuronal outgrowth and pathfinding in vivo. *Dev* 143:449–460.
- Saint-Amant L, Drapeau P (1998) Time course of the development of motor behaviors in the zebrafish embryo. *J Neurobiol* 37:622–632.
- Santos-Ledo A, Jenny A, Marlow FL (2013) Comparative gene expression analysis of the *fmln* family of formins during zebrafish development and implications for tissue specific functions. *Gene Expr Patterns* 13:30–37.
- Schier a. F, Joyner a. L, Lehmann R, Talbot WS (1996) From screens to genes: Prospects for insertional mutagenesis in zebrafish. *Genes Dev* 10:3077–3080.
- Schönichen A, Geyer M (2010) Fifteen formins for an actin filament: A molecular view on the regulation of human formins. *Biochim Biophys Acta - Mol Cell Res* 1803:152–163.
- Schuh M, Ellenberg J (2008) A New Model for Asymmetric Spindle Positioning in Mouse Oocytes. *Curr Biol* 18:1986–1992.

- Schweitzer J, Becker T, Lefebvre J, Granato M, Schachner M, Becker CG (2005) Tenascin-C is involved in motor axon outgrowth in the trunk of developing zebrafish. *Dev Dyn* 234:550–566.
- Scott EK, Baier H (2009) The cellular architecture of the larval zebrafish tectum, as revealed by Gal4 enhancer trap lines. *Front Neural Circuits* 3:13.
- Scott JW, Zottoli SJ, Beatty NP, Korn H (1994) Origin and function of spiral fibers projecting to the goldfish Mauthner cell. *J Comp Neurol* 339:76–90.
- Severi KE, Portugues R, Marques JC, O'Malley DM, Orger MB, Engert F (2014) Neural Control and Modulation of Swimming Speed in the Larval Zebrafish. *Neuron* 83:692–707.
- Shah AN, Davey CF, Whitebirch AC, Miller AC, Moens CB (2016) Rapid Reverse Genetic Screening Using CRISPR in Zebrafish. *Zebrafish* 13:152–153.
- Sillar KT (2009) Escape Behaviour: Reciprocal Inhibition Ensures Effective Escape Trajectory. *Curr Biol* 19:R697–R699.
- Spillane M, Gallo G (2014) Involvement of Rho-family GTPases in axon branching. *Small GTPases* 5.
- Spillane M, Ketschek A, Jones SL, Korobova F, Marsick B, Lanier L, Svitkina T, Gallo G (2011) The actin nucleating Arp2/3 complex contributes to the formation of axonal filopodia and branches through the regulation of actin patch precursors to filopodia. *Dev Neurobiol* 71:747–758.
- Stainier DYR, Raz E, Lawson ND, Ekker SC, Burdine RD, Eisen JS, Ingham PW, Schulte-Merker S, Yelon D, Weinstein BM, Mullins MC, Wilson SW, Ramakrishnan L, Amacher SL, Neuhauss SCF, Meng A, Mochizuki N, Panula P, Moens CB (2017) Guidelines for morpholino use in zebrafish. *PLoS Genet* 13:e1007000.
- Stewart WJ, Nair A, Jiang H, Mchenry MJ (2014) Prey fish escape by sensing the bow wave of a predator. *1:4328–4336*.
- Stifani N (2014) Motor neurons and the generation of spinal motor neuron diversity. *Front Cell Neurosci* 8:293.
- Stuermer C a (1988) Retinotopic organization of the developing retinotectal projection

- in the zebrafish embryo. *J Neurosci* 8:4513–4530.
- Sullivan L (1896) The tall office building artistically considered. *Lippincott's Mag*:403–409.
- Sun H, Al-Romaih KI, MacRae CA, Pollak MR (2014) Human kidney disease-causing INF2 mutations perturb Rho/Dia signaling in the glomerulus. *EBioMedicine* 1:107–115.
- Swain GP, Snedeker JA, Ayers J, Selzer ME (1993) Cytoarchitecture of Spinal-Projecting Neurons in the Brain of the Larval Sea Lamprey. *J Neurosci* 13:210:194–210.
- Szikora S, Földi I, Tóth K, Migh E, Vig A, Bugyi B, Maléth J, Hegyi P, Kaltenecker P, Sanchez-Soriano N, Mihaly J (2017) The formin DAAM is required for coordination of the actin and microtubule cytoskeleton in axonal growth cones. *J Cell Sci* 130:2506–2519.
- Tanimoto M, Ota Y, Inoue M, Oda Y (2011) Origin of Inner Ear Hair Cells: Morphological and Functional Differentiation from Ciliary Cells into Hair Cells in Zebrafish Inner Ear. *J Neurosci* 31:3784–3794.
- Tessier-Lavigne M, Goodman CS (1996) The molecular biology of axon guidance. *Science* (80-) 274:1123–1133.
- Thisse B, Thisse C (2005) High Throughput Expression Analysis of ZF-Models Consortium Clones. ZFIN Direct Data Submission. High Throughput Expr Anal ZF-Models Consort Clones ZFIN Direct Data Submission Available at: <http://zfin.org>.
- Thisse C, Thisse B (2008) High-resolution in situ hybridization to whole-mount zebrafish embryos. *Nat Protoc* 3:59–69.
- Thurston SF, Kulacz WA, Shaikh S, Lee JM, Copeland JW (2012) The Ability to Induce Microtubule Acetylation Is a General Feature of Formin Proteins. *PLoS One* 7:e48041.
- Umeda K, Shoji W (2017) From neuron to behavior: Sensory-motor coordination of zebrafish turning behavior. *Dev Growth Differ* 59:107–114.
- Varshney GK, Carrington B, Pei W, Bishop K, Chen Z, Fan C, Xu L, Jones M, LaFave MC, Ledin J, Sood R, Burgess SM (2016) A high-throughput functional genomics workflow based on CRISPR/Cas9-mediated targeted mutagenesis in zebrafish. *Nat Protoc* 11:2357–2375.

- Varshney GK, Pei W, Lafave MC, Idol J, Xu L, Gallardo V, Carrington B, Bishop K, Jones M, Li M, Harper U, Huang SC, Prakash A, Chen W, Sood R, Ledin J, Burgess SM (2015) High-throughput gene targeting and phenotyping in zebrafish using CRISPR/Cas9. *Genome Res* 25:1030–1042.
- Vaz R, Hofmeister W, Lindstrand A (2019) Zebrafish models of neurodevelopmental disorders: Limitations and benefits of current tools and techniques. *Int J Mol Sci* 20:1296.
- Westerfield M (1992) Motor axon pathfinding. *2*:28–30.
- Westerfield M, McMurray J V., Eisen JS (1986) Identified motoneurons and their innervation of axial muscles in the zebrafish. *J Neurosci* 6:2267–2277.
- Whitfield TT, Riley BB, Chiang M-Y, Phillips B (2002) Development of the Zebrafish Inner Ear.
- Wills Z, Marr L, Zinn K, Goodman CS, Van Vactor D (1999) Profilin and the Abl tyrosine kinase are required for motor axon outgrowth in the *Drosophila* embryo. *Neuron* 22:291–299.
- Wilson SW, Ross LS, Parrett T, Easter SS (1990) The development of a simple scaffold of axon tracts in the brain of the embryonic zebrafish, *Brachydanio rerio*.
- Wu CH et al. (2012) Mutations in the profilin 1 gene cause familial amyotrophic lateral sclerosis. *Nature* 488:499–503.
- Xiao T, Roeser T, Staub W, Baier H (2005a) A GFP-based genetic screen reveals mutations that disrupt the architecture of the zebrafish retinotectal projection. *Development* 132:2955–2967.
- Xiao T, Roeser T, Staub W, Baier H, Nüsslein-Volhard C, Bonhoeffer F (2005b) A GFP-based genetic screen reveals mutations that disrupt the architecture of the zebrafish retinotectal projection. *Development* 132:2955–2967.
- Xie J, Jusuf PR, Bui B V., Goodbourn PT (2019) Experience-dependent development of visual sensitivity in larval zebrafish. *Sci Rep* 9:1–11.
- Xu M, Liu D, Dong Z, Wang X, Wang X, Liu Y, Baas PW, Liu M (2014) Kinesin-12 influences axonal growth during zebrafish neural development. *Cytoskeleton* 71:555–563.

- Yamada K, Ono M, Bensaddek D, Lamond AI, Rocha S (2013a) FMN2 is a novel regulator of the cyclin-dependent kinase inhibitor p21. *Cell Cycle* 12:2348–2354.
- Yamada K, Ono M, Perkins ND, Rocha S, Lamond AI (2013b) Identification and Functional Characterization of FMN2, a Regulator of the Cyclin-Dependent Kinase Inhibitor p21. *Mol Cell* 49:922–933.
- Yang C, Danielson EW, Qiao T, Metterville J, Brown RH, Landers JE, Xu Z (2016) Mutant PFN1 causes ALS phenotypes and progressive motor neuron degeneration in mice by a gain of toxicity. *Proc Natl Acad Sci U S A* 113:E6209–E6218.
- Yoo H, Roth-Johnson EA, Bor B, Quinlan ME (2015) *Drosophila* Cappuccino alleles provide insight into formin mechanism and role in oogenesis. *Mol Biol Cell* 26:1875–1886.
- Yu J, Lai C, Shim H, Xie C, Sun L, Long CX, Ding J, Li Y, Cai H (2018) Genetic ablation of dynactin p150Glued in postnatal neurons causes preferential degeneration of spinal motor neurons in aged mice. *Mol Neurodegener* 13.
- Zeller J, Granato M (1999) diwanka in motor axon migration.
- Zottoli SJ, Hordes AR, Faber DS (1987) Localization of optic tectal input to the ventral dendrite of the goldfish Mauthner cell. *Brain Res* 401:113–121.